Structural, microstructural and thermo-physical properties of alkaline earth based phospo-silicate glass/glass-ceramics

By

Kuldeep Sharma

(PHYS01200904002)

Bhabha Atomic Research Centre, Mumbai

Under the guidance of

Prof. G. P. Kothiyal

A thesis submitted to the
Board of Studies in Physical Sciences
In partial fulfillment of requirements
for the Degree of

DOCTOR OF PHILOSOPHY

of

HOMI BHABHA NATIONAL INSTITUTE

February, 2013

Homi Bhabha National Institute

Recommendations of the Viva Voce Committee

As members of the Viva Voce Committee, we certify that we have read the dissertation prepared by **Kuldeep Sharma** entitled “**Structural, microstructural and thermo-physical properties of alkaline earth based phospo-silicate glass/glass-ceramics**” and recommend that it may be accepted as fulfilling the thesis requirement for the award of Degree of Doctor of Philosophy.

Gautam Kumar Dey

Chairman - Dr. G. K. Dey **Date:** 3/4/2014

Guide / Convener – Dr. G. P. Kothiyal **Date:** 3.4.2014

Shiv Kumar

Member Dr. S. K. Gupta **Date:** 3.4.2014

Member Prof. D Bahadur **Date:** 3 4.2014

External Examiner Prof. S. Murugavel **Date:** 3.4.2014

Final approval and acceptance of this thesis is contingent upon the candidate’s submission of the final copies of the thesis to HBNI.

Certificate

I hereby certify that I have read the thesis prepared under my direction. All the suggestions made by the referees in evaluation report have been incorporated. Therefore, I recommend that this thesis may be accepted as fulfilling the requirement for the Degree of Doctor of Philosophy.

Date: 03-04-2014
Place: Trombay

Dr. G. P. Kothiyal
(Guide)

STATEMENT BY AUTHOR

This dissertation has been submitted in partial fulfillment of requirements for an advanced degree at Homi Bhabha National Institute (HBNI) and is deposited in the Library to be made available to borrowers under rules of the HBNI.

Brief quotations from this dissertation are allowable without special permission, provided that accurate acknowledgement of source is made. Requests for permission for extended quotation from or reproduction of this manuscript in whole or in part may be granted by the Competent Authority of HBNI when in his or her judgment the proposed use of the material is in the interests of scholarship. In all other instances, however, permission must be obtained from the author.

Kuldeep Sharma

DECLARATION

I, hereby declare that the investigation presented in the thesis has been carried out by me. The work is original and has not been submitted earlier as a whole or in part for a degree / diploma at this or any other Institution / University.

Kuldeep Sharma

DEDICATED

TO

MY PARENTS

Acknowledgements

I wish to take this privilege to place on record in a very special and distinctive manner, an expression of deep sense of gratitude and indebtedness to my research guide, **Dr. G P Kothiyal**, Former Head, Glass and Advanced Ceramics Division (BARC), Mumbai for his excellent guidance during the thesis work.

It gives me pleasure to record my sincere thanks to **Prof. L Montagne**, Université Lille Nord de France-UMR, for his guidance, support and immeasurable help to carry out different experiments at his place during my visit to his lab under Indo-French centre of promotion of advanced research project IFCPAR-4008-1.The financial support for this visit is gratefully acknowledged. I also thank **Prof. G K Dey**, **Prof. S K Gupta**, **Prof. D Bahadur** (**Doctoral committee**) for their suggestions and guidance during the course of the work. I also thank **Dr. M G Krishnan,** Head, Glass and Advanced Materials Division and Director, Materials Group for their support and encouragement.

I gratefully acknowledge the help of **Shri. M R Singh, Dr. S M Yusuf**, **Dr. Bhushan**, **Dr. C L Prajapat, Dr. S Bhattacharya, Dr Jagannath, Dr. M N Deo, Dr. Sudhanshu Saxena, Dr. P K Sharma, Shri Sher Singh Meena and Mr. Anupam Dixit** for carrying out different experiments. I express my sincere thanks to all my colleagues in erstwhile Glass and Advanced Ceramics Division and now Glass and Advanced Materials Division for their encouragement, cooperation, support and help in various stages of the thesis work. I wish to thank all **my friends** for their constant encouragement and support throughout the period of work. Finally, I convey my heartfelt gratitude to **my parents and family members** who have always inspired me and without their constant support and encouragement, this work would not have reached the present stage.

Contents Page

2.3.5 Magnetic

2.3.6 Seal Fabrication

2.3.7 Testing of seals

Chapter 3

3.3 Results and discussion

3.3.3 Structural measurements

3.3.5 in-vitro studies

Chapter 4

4.3 Results and discussion

4.3.2 Structural studies

4.3.5 in-vitro studies

Chapter 5

5.3 Results and discussion

Homi Bhabha National Institute

Ph. D. PROGRAMME

1. Name of the Student: **Kuldeep Sharma**

2. Name of the Constituent Institution: **Bhabha Atomic Research Centre Mumbai**

3. Enrolment No. : **PHYS01200904002**

4. Title of the Thesis: **Structural, microstructural and thermo-physical properties of alkaline earth based phospo-silicate glass/glass-ceramics.**

5. Board of Studies: **Physical Sciences**

SYNOPSIS

Glasses are defined as the materials having no long range order and exhibit glass-transition behaviour [1,2]. These materials possess certain useful properties like thermo-physical, optical, mechanical etc [3-4]. Further, the controlled crystallization in glasses yields glass-ceramics, which exhibit improved thermo-mechanical, biocompatibility, wetting and optical properties [5-7]. The specific property of glass-ceramics can be controlled, for example, thermal expansion coefficient (TEC) can be fine tuned by controlling the amount, nature and morphology of the phases crystallized. Based on the property induced in the glass-ceramics, these have been found useful for biomedical applications, as sealants for high temperature applications, among others [8-10].

Phosphate based silicate glasses are studied as potential candidates as implant material for human body because of their bioactivity [33-35]. A bioactive glass-ceramic forms a biologically active hydroxyapatite layer on its surface that permits bonding with bone and soft tissues. Hench [36] reported the first bioactive glass having composition (wt %) 45%

SiO_2, 24.5% Na_2O, 24.5% CaO and 6% P_2O_5 commonly known as 45S5 and concluded that addition of alumina tends to decrease the bioactivity of these glasses. Kokubo et al. [43] studied the SiO_2–CaO–P_2O_5–MgO glass systems and developed the apatite and wollastonite glass-ceramics in glass containing (wt %) 4.6MgO- 44.7CaO-34 SiO_2-16.2 P_2O_5- 0.5CaF_2. Oliveira et al. [44] reported that the glasses with increased surface activity can be developed by replacing calcium oxide by magnesium oxide in the (mol%) 31SiO_2–11P_2O_5–(58-x)CaO–xMgO series. Ebisawa et al [45] reported an improvement in response of ferromagnetic glasses with addition of small amount of P_2O_5. In-vitro/vivo study on ZnO containing bioglass/glass-ceramic has shown that ZnO can be used to modify the surface properties, which in turn have stimulatory effect on bone formation [46, 47]. Thus, the bioactive response of the glass/glass-ceramics can be optimized by controlling the glass phases in the glass-ceramics, which can be modified by varying the alkaline earths like CaO, MgO and ZnO in glass matrix.

A number of glass systems belonging to BaO-Al_2O_3-SiO_2 with different modifiers like CaO, SrO and formers such as B_2O_3 and P_2O_5 have been studied for sealing application [52-59, 68, 76-78]. But major problem with barium alumino silicate based sealant materials is degradation of seals due to formation of $BaCrO_4$. Thus, in order to avoid this, SrO based glasses have been studied. Tiwari et al. [189] reported good bonding of SrO and ZnO based silicate glasses with Crofer-22 APU, which is used as interconnect in SOFC. Ojha et al. [190] studied the SrO and La_2O_3 based Al_2O_3-B_2O_3-SiO_2 glasses and reported that SrO modified the network and resulted in change in thermo-physical properties. Wang et al. [191] prepared La_2O_3-Al_2O_3-B_2O_3-SiO_2 glasses free of alkaline earth metals and found a decrease in softening temperature of glasses with addition of La_2O_3. However, P_2O_5 based glasses have been less investigated as compared to silicate glasses. Phosphate based glass exhibit insufficient durability for sealing, nevertheless, addition of silica can increase the stability of phosphate in the glass [192]. Of course, there is still a need to reduce the softening temperature (T_s), so that seals can be prepared at relatively lower temperatures (1000°C). It is also desirable to match the TEC ($12\times10^{-6}\,{}^{o}C^{-1}$) with the metallic interconnects of SOFCs.

This thesis covers work carried out on the preparation, thermo-physical, structural and microstructural properties of two different glass systems having different amount of P_2O_5; namely (i) CaO-SiO_2-P_2O_5 with different additives (ii) BaO-SrO-SiO_2-P_2O_5 based glasses/glass-ceramics. In addition, to demonstrate the applicability of these materials, specific properties related to bio and bonding behaviour are also investigated. The calcium phospho-silicate glass/glass-ceramics with different additives like iron oxide, ZnO and Ag are investigated as prospective bio-materials. As mentioned before, desired surface response of the glass/glass-ceramics can be obtained by varying the composition of alkaline earths like CaO and MgO in glass matrix. The addition of modifiers in glasses will result in breaking of Si–O–Si bonds creating non-bridging oxygen groups (Si–O–NBO). This facilitates the formation of Si–OH functional groups on the surface, which improve the surface response. Introduction of iron oxide, zinc oxide and Ag in glasses is expected to modify the local structure of the glass, consequently material response and behaviour will be affected. Therefore, the effect of addition of Fe_2O_3, ZnO and Ag on structural and microstructural properties of glass/glass-ceramics are investigated. Further the work is also pursued to evaluate the materials in-vitro i.e. in simulated body fluid (SBF) and bovine serum albumin (BSA). Glass-ceramics containing Ag are studied for antibacterial activity against Escherichia coli (E. coli).

Silicate glasses containing SrO and BaO with different modifiers are studied for bonding/sealing applications. For effective bonding, it is required that coefficient of thermal expansion of sealant is as close to that of metallic interconnect. As the thermo-physical properties of glass and glass-ceramics depend on the composition, different glasses are prepared with varying amount of P_2O_5 and V_2O_5 content. Since the major requirements of sealing material for SOFC application is good gas tightness at the high operating temperature (600-800°C), sealant materials are tested for adherence and stability at high temperature.

This thesis comprises of eight chapters that are arranged as follows.

Chapter 1: *Introduction*

This chapter describes an introduction to glasses and glass-ceramics in general. An overview of different applications and advantages of glass/glass-ceramics with respect to application related properties are discussed. Subsequently, reported work on bio-glass/ glass-ceramics and sealant materials for SOFC is discussed. The limitations of the existing research and the need for the new materials are discussed. Finally, the scope of present thesis and different investigated properties are discussed.

Chapter 2: *Experimental Techniques*

In this chapter, details of preparation and characterization techniques used in present work are given along with basic principles, their merits/demerits etc. The melt quench method remains the most commonly employed technique for bulk glass preparation. The crystallization behaviour of glasses is studied using differential thermal analysis (DTA).

Based on the DTA data, glasses are crystallized and the crystalline phases are identified by X-ray diffraction (XRD).

Thermal expansion coefficient, glass transition temperature (T_g) and softening temperature (T_{ds}) of the glass and glass-ceramic samples are measured using a Setaram 92-12 thermo mechanical analyzer (TMA). In addition to XRD, Raman and FTIR spectroscopy are also used to characterize the glasses and glass-ceramics. MAS-NMR spectroscopy technique is useful in probing the immediate environment of the atoms in the glasses. In order to mimic the molecular motion of liquids, the solid samples are spun rapidly at an angle of 54.7^o called 'magic angle' with respect to the applied field direction, which allows the considerable improvement in the resolution of the NMR spectra of solid samples. However, quadrupolar broadening cannot be removed by MAS-NMR. This effect is reduced by using high static magnetic field B^0.

SEM is employed to examine the morphology of crystalline phases in the glass-ceramics. Bio-glass/glass-ceramics surfaces are investigated after different time of immersion in SBF and BSA, using scanning electron microscopy (SEM), X-ray photoelectron spectroscopy (XPS) and secondary ion mass spectroscopy (SIMS) techniques.

Magnetic response of glass-ceramics samples was measured at room temperature, with $|H| \leq 5$ kOe using SQUID magnetometer (Quantum Design – MPMS5). Mössbauer spectra have been obtained using a spectrometer (Nucleonix Systems Pvt. Ltd., Hyderabad, India) operated in constant acceleration mode (triangular wave) in transmission geometry. Mössbauer spectra were fitted by a WinNormos fit programme.

The glasses used for sealing applications are studied using Hot Stage Microscopy to find out maximum shrinkage temperature and flow temperature. Subsequently, the procedures used for seal fabrication are discussed and seals are tested for bonding integrity using leak testing on a vacuum and over pressure testing set up.

Chapter 3: ***Structural, microstructural and in-vitro studies of calcium silico-phosphate glass/ glass-ceramics containing iron oxide***

In this chapter, preparation and results on structural, micro-structural and magnetic properties of glass/glass-ceramics with nominal composition $34SiO_2$-(45-x)CaO-$16P_2O_5$-4.5 MgO-$0.5CaF_2$ –xFe_2O_3 (where x = 5, 10, 15, 20 wt %) have been discussed. Fraction of non bridging oxygen first increases with an increase in iron oxide content upto 15 wt% and then decreases with further increase in iron oxide content to 20 wt. %. This suggests that iron oxide behaves as a network modifier at low concentration and stabilizes the glass network at higher content. The glass-ceramics exhibit an increase in the formation of magnetite phase with an increase in iron oxide, however, at higher iron oxide content fraction of non-bridging decreases, which influences the bioactive response. The studies in BSA have shown the glass-ceramics containing 15 and 20 wt% iron oxide show better adsorption of BSA implying good biocompatibility.

Chapter 4: ***Structural, microstructural and in-vitro studies of calcium silico-phosphate glass/ glass-ceramics containing iron oxide and zinc oxide***

This chapter has been devoted to the studies carried out on glass/glass-ceramics containing iron and zinc oxide. The glass and glass-ceramics with composition $25SiO_2$-$50CaO$-$15P_2O_5$-$(10-x)Fe_2O_3$-$xZnO$ (where x = 0-5) mol % has been prepared. Addition of ZnO modifies the local environment in glass, which influences the structural, magnetic and microstructural properties. Fraction of non-bridging oxygen decreases with an increase in zinc oxide content. Magnetic studies revealed the relaxation of magnetic particles and an increase in saturation magnetization with addition of 2 mol % ZnO. Addition of ZnO also results in a decrease in strength of dipolar interaction. In-vitro studies in SBF have shown the formation of Ca-P rich layer on the glass-ceramics when immersed in SBF, implying the bioactive nature of the samples. Surface morphology of glass-ceramics samples in BSA after different time of immersion revealed the formation of Si–OH functional groups. Absorption of BSA takes place by interaction with silanol groups present on the surface. Incorporation of ZnO leads to formation of strong glass network, thereby adhesion of BSA decreases with an increase in ZnO content.

Chapter 5: ***Studies of calcium silico-phosphate glass-ceramics containing iron oxide, zinc oxide and Ag***

In this chapter, structural and magnetic properties of glass/glass-ceramic containing iron, zinc oxide and Ag are discussed. The glass/glass-ceramics with $25SiO_2$-$(50-x)CaO$-$15P_2O_5$-$8Fe_2O_3$-$2ZnO$-xAg (where x = 0, 2 and 4 mol %) are prepared. Magnetic properties in spinel like phase depend on the arrangement of Fe^{2+} and Fe^{3+} ions in the spinel lattice. Isomer shift values obtained by Mössbauer spectroscopy suggest that Fe^{3+} ions are in octahedral co-ordinations. Magnetization improved with an increase in Ag content up to 4 mol% which is attributed to improvement and attainment of maximum magnetic ordering. Antibacterial response of Ag containing glass-ceramics samples is studied against E. coli and found to depend on Ag ions concentration in the glass matrix. The glass-ceramic containing 4% Ag showed complete inhibition of bacterial growth at a concentration of 10% (w/v). However, the glass-ceramic containing 2% Ag showed the similar effect at 20% (w/v).

Chapter 6: ***Studies on barium alumino strontium silicate (BASP) glass/glass-ceramics containing P_2O_5***

In this chapter, barium strontium silicate based glasses are investigated as potential sealants for solid oxide fuel cells. As mentioned earlier phosphate based glasses exhibit insufficient durability for sealing applications, but addition of silica can increase the stability. Thus, a series of glasses have been formulated with small amount of P_2O_5. Since addition of P_2O_5 in alumino-silicate glasses scavenges the modifier cations and increase the network polymerisation, hence P_2O_5 is added in the form of $Ba_3(PO_4)_2$ to a base glass composition. The effect of $Ba_3(PO_4)_2$ incorporation on thermo-physical, structural and sealing characteristics of a glass of composition (mol%) $30SiO_2$-$20SrO$-$30BaO$-$10B_2O_3$-$5La_2O_3$-$5Al_2O_3$ is studied. The glasses are characterized for structural features with XRD and solid-state NMR. Seals of glasses with Crofer- 22 APU metallic alloy are made, and the microstructure and interface of seals are investigated. Interfaces of seals reveal good bonding with Crofer-22 APU, which did not deteriorate even after heat treatment at 800°C for 500h. The glasses show the development of Ba_2SiO_4, $BaAl_2Si_2O_8$, and Sr_2SiO_4 crystalline phases upon heat treatment at 800°C, which are not found to be detrimental for high temperature sealing applications. The glass composition formulated by addition of 1 mol% $Ba_3(PO_4)_2$ has shown good thermal and sealing characteristics, while further increase of $Ba_3(PO_4)_2$ to 2 mol% leads to increased crystallization tendency.

Chapter 7: ***Studies on barium alumino strontium silicate glass/glass-ceramics containing V_2O_5 and P_2O_5***

Effects of addition of V_2O_5 and P_2O_5 to barium strontium silicate based glasses are discussed in this chapter. V_2O_5 acts as modifier and thus results in a decrease in glass-transition and softening temperature of glasses. The addition of V_2O_5 is likely to reduce the glass surface tension, which may result in good sealing with metallic interconnect. A series of glasses have been prepared with nominal composition $27SiO_2$-$23SrO$-$32BaO$-$4Al_2O_3$-$10B_2O_3$-$(4-x)$ P_2O_5-xV_2O_5 where x=0-4 mol%. Crystallization kinetics and thermo-physical properties of glasses (Tg, Ts and TEC) have been studied. The glasses are characterized for structural features with XRD and solid-state NMR. NMR measurements indicate that ^{29}Si forms mainly Q^2 structure units. The glass samples do not show major structural changes when P_2O_5 is replaced with V_2O_5. The change in thermo-physical properties is due to variation in strength of bonds in the network. Seals with Crofer-22 plates have been made around 975-1000°C and interfaces of seals reveals inter-diffusion of ions at the interface. The interfaces show good bonding when tested upto 1500 h at 800ºC. The seals are also attempted with Haynes metal using a novel idea with a groove of about 0.5mm deep at the surface. Seals are tested for hermeticity at high operating temperatures (800ºC) using pressure difference technique. The seals are found hermetic even after 15 heating and cooling cycles, implying the efficient sealing of the material with metal.

Chapter 8: ***Summary and Conclusions***

The chapter summarizes the work carried out in the thesis and discusses the scope for further extension of the work reported here.

In conclusion, we have investigated a few alkaline earth based silicate glass/glass-ceramics having different amount of P_2O_5 for different applications. In the case of bio-glass/glass-ceramics, it is found that the addition of iron oxide and zinc oxide modifies the structure. Iron oxide behaves as network modifier at low concentration and stabilizes the glass network at higher content. ZnO behaves as a structural modifier and stabilizes the network when its content increases. Crystallization of glasses produced nanometer size crystallites of calcium phosphate, hematite and magnetite, which were evenly dispersed in the glassy silica matrix. In-vitro studies in SBF, has shown the formation of bioactive layer after different time of immersion. The adhesion of polymer has been seen on the glass-ceramics when immersed in BSA, implying good biocompatibility. However, polymeric adhesion decreases with addition of ZnO. Thus, these materials thus exhibited the property, which can be exploited to bind specific proteins on the surface for magnetic drug targeting or polymer detection and separation.

In a novel idea, sealing glasses have been formulated by the combined addition of P_2O_5 and BaO [$Ba_3(PO_4)_2$], to avoid the negative effect of P_2O_5 on sealing properties of glass. The positive effect of $Ba_3(PO_4)_2$ incorporation on thermo-physical properties is demonstrated by the decrease in softening temperature, enabling the seal fabrication (with Crofer-22APU) below 1000°C. Moreover, crystalline phases and TEC are found stable and compatible for sealing applications. Other glasses containing both V_2O_5 and P_2O_5 have been studied. V_2O_5 addition results in a decrease in glass-transition and softening temperature of glasses. Glass compositions studied show the desired thermo-physical properties (TEC and Tg) for effective sealing for high temperature application.

The chapter is concluded by bringing out the future scope of the research work related to the topic of the thesis.

List of Publications

a. Paper in Journals

1. **K. Sharma**, G. P. Kothiyal, L. Montagne, F. Mayer, B. Revel, Int. J. Hydrogen Energy **38 (2013) 15542**.
2. **K Sharma**, S Bhattacharya, K G Bhushan, G P Kothiyal, J. Non-Cryst. Solids***, 376 (2013) 221.***
3. G. P. Kothiyal, M. Goswami, Babita Tiwari, **K. Sharma**, A. Ananthanarayanan, Lionel Montagne, J. Adv. Ceram. 1(2)(2012)110.
4. **K. Sharma**, G. P. Kothiyal, L. Montagne, F. Mayer, B. Revel, Int. J. Hydrogen Energy 37 (2012) 11360.
5. **K. Sharma**, M. N Deo, G. P Kothiyal, J. Non-Cryst. Solids 358 (2012) 1886.
6. **K. Sharma**, Sher Singh Meena, Sudhanshu Saxena, S. M. Yusuf, A. Srinivasan, G. P. Kothiyal, Mater. Chem. Phy. 133 (2012) 144.
7. **K. Sharma**, S. Bhattacharya, C. Murali, G. P. Kothiyal, App. Surf. Sci. 258 (2012) 2356.
8. G. P. Kothiyal, **K. Sharma**, A. Srinivasan, ***Springer Conference Series*** (2012) *597.*
9. **K. Sharma**, A. Dixit, S. Bhattacharya, Jagannath, G. P. Kothiyal, App. Surf. Sci. 256 (2010) 3107.
10. **K. Sharma**, Sher Singh, C. L. Prajapat, S. Bhattacharya, Jagannath, M. R. Singh, S. M. Yusuf, G. P. Kothiyal. J. Magn. Magn. Mater. 321(2009)3821.
11. **K. Sharma**, A. Dixit, Sher Singh, C. L. Prajapat, S. Bhattacharya, Jagannath, M. R Singh, S. M. Yusuf, P. K. Sharma, A. K. Tyagi, G. P. Kothiyal, J. Mater. Sci. Eng.-C 29(2009)2226.
12. G. P. Kothiyal, A. Arvind, R. Kumar, A. Dixit, **Kuldeep Sharma**, Madhumita Goswami, J. Phy. Conf. Series-2009. IOP Conf. Series: Mater. Sci. Eng. 2 (2009) 012005.

b. Paper in Conference/Symposium Proceedings

1. **K. Sharma**, A. Ananthanarayanan, G. P. Kothiyal, L. Montagne, F. O. Mear, G. Tricot, and B. Revel , European Fuel Cell - Piero Lunghi Conference & Exhibition, December 14-16, 2011, Rome, Italy

2. L. Montagne, F. Méar, S. Castanie, **K. Sharma**, G. P. Kothiyal, ICONSAT, January 21-26, 2012, Hyderabad, India.
3. **K. Sharma,** A. Dixit, A. Arvind, G. P. Kothiyal, Symposium on synthesis and Characterization of Glass and Glass-ceramics, July 7-8, 2010, CMET-Pune.
4. **K. Sharma,** Jagannath, C. Murali, G. P. Kothiyal, Symposium on synthesis and Characterization of Glass and Glass-ceramics, July 7-8, 2010, CMET-Pune.
5. **K. Sharma,** A. Dixit, Sher Singh Meena, S. M. Yusuf, A. Srinivasan, G. P. Kothiyal, Symposium on synthesis and Characterization of Glass and Glass-ceramics, July 7-8, 2010, CMET-Pune.
6. G. P. Kothiyal, Madhumita Goswami, **K. Sharma,** Shobha Shingaravelan, Anupam Dixit, Arvind A, National Seminar on Advanced Applications of Glasses, Mar 22-23, 2010, VNIT, Nagpur.
7. **K. Sharma**, S. Bhattacharya, M. N. Deo, G. P. Kothiyal, Proceeding of the International Conference on Advances in Electron Microscopy and related Techniques, (EMSI-10), Mar 8-10, 2010, BARC, Mumbai.
8. G. P. Kothiyal, Madhumita Goswami, **Kuldeep Sharma**, S. Bhattacharya, Arvind A., Proceeding of the International Conference on Advances in Electron Microscopy and related Techniques, (EMSI-10), Mar 8-10, 2010, BARC, Mumbai.
9. **K. Sharma,** A. Dixit, Sher Singh Meena, C. L. Prajapat, S. Bhattacharya, M. N. Deo, G. P. Kothiyal, Proceeding of the International Conference on Nano-science and Technology(ICONSAT-10), Feb 17-19, 2010.
10. G. P. Kothiyal, **K. Sharma,** R. K. Singh, A. Srinivasan, Theme Symposium on Advanced Ceramic Materials-Monoliths to Composites, Feb 9-11, 2010, Sardar Patel University, Vallabh Vidyanagar, Gujarat.
11. **K. Sharma,** A. Sarkar, S. Bhattacharya, G. P. Kothiyal, Proceeding of DAE Solid State Physics Symposium (DAE SSPS-2009), 54 (2009) 513.
12. **K . Sharma**, A. Dixit, Sher Singh Meena, S. Bhattacharya, M. N. Deo, G. P. Kothiyal. (ISNM-2009) at K. M. V. Jalandhar (28-29 Oct, 2009).

List of Figures

List of Tables

Chapter 1

Introduction

This chapter describes an introduction to glasses in general. The conditions of glass formation and role of different components in the glass stucture are presented. Subsequently, reported work in the area of bio-glass/glass-ceramics and sealant materials is discussed.

1.1 General introduction

1.2 Definition of glass

1.3 Conditions for glass formation

1.4 Major components of glass

1.5 Types of glasses

1.6 Structural aspect of glasses

1.7 Introduction to present work

1.1 General introduction

Glass is a fascinating material as it plays an important role in many specialized applications [1, 2]. It is possible to make glasses over a wide range of compositions [3]. The use of glass has a long history beginning with the making of knives and other implements from obsidian, a naturally occurring glass, by primitive man [4]. During last five decades, rapid advancements in the understanding of glass science have helped in developing glass and glass-ceramics with improved properties and new functionalities. Some of the recent developments in the field of glass have lead to various technological applications, which include glass fiber reinforcement of cement as a new building material, substrates for microelectronics circuitry in the form of semiconducting glasses, nuclear waste immobilization and specific bio-medical applications.

In addition to scientific interest, many industries such as automobiles, architecture, data transmission, display technology etc. depend greatly upon glasses. ***Table 1.1*** lists some of the applications of various kinds of glasses. For many of these applications it is difficult to find another material which combines the functionality, cost and ease of manufacturing of glass. Crystallization in glasses is usually deleterious to some applications, such as displays or waste immobilization [6]. However, controlled crystallization of glasses can result in a kind of polycrystalline material possessing improved properties [7]. Glass-ceramics by definition are the products of controlled crystallization of glasses. In a sense therefore, glass-ceramics are a composite of a crystalline phase embedded in a glassy matrix. Although the French chemist Réamur had conceived the idea of a dense crystalline material formed by the crystallization of glass in the 18th century, it was Donald Stookey who first perfected the production of glass-ceramics in the 1950 [8]. As a result of improved thermo-physical and chemical properties, they find application in a number of sectors such as cookware, sealants etc. [9-11]. Controlling the nature and morphology of the crystallized phases can allow fine control over properties such as thermal expansion coefficient (TEC).

Table 1.1. *Some glasses and their applications.*

Glass	Application
Soda-Lime-Silicate	Glazing, Packaging
Borosilicate	High temperature applications, pharmacy
Alumino-Silicates	Reinforcing Fibres
Lead Silicate	Shielding, Tableware, high pressure sealing
Silica	Optical Fibres
Chalcogenides	IR optics
Bioglass	Bio-medical

1.2 What is glass?

Glass is commonly defined as an inorganic product of fusion, which is cooled to a rigid condition without crystallizing. However, more generally glass can be defined as an amorphous solid, completely lacking in long range periodic atomic structure and exhibiting a region of glass transition behaviour [1]. However, the ‘glassy’ state is not unique and it depends upon the thermal history of the melt [2]. Thus, a material, inorganic, organic, or metallic, formed by any technique and which exhibits glass transition behaviour can be termed as a glass.

Glass transition behaviour can be discussed on the basis of changes in either enthalpy or volume with the temperature. When a molten material is cooled, depending on the cooling rate crystallization may take place at or just below the melting point T_m or the melt may be cooled to the temperature below T_m without crystallization (supercooling). This will accompany with increase in the viscosity. These changes are schematically represented in

Fig. 1.1. The crystallization process is manifested by a sudden change in the volume at the melting point, whereas the glass transition is characterized by a gradual change in the slope. The temperature range over which the slope change occurs is called the glass transition range and the point of intersection of the tangents drawn on both solid and liquid side of the curve (***Fig.1.1.***) is known as glass transition temperature (T_g). The glass transition is continuous as the slope gradually changes over the region.

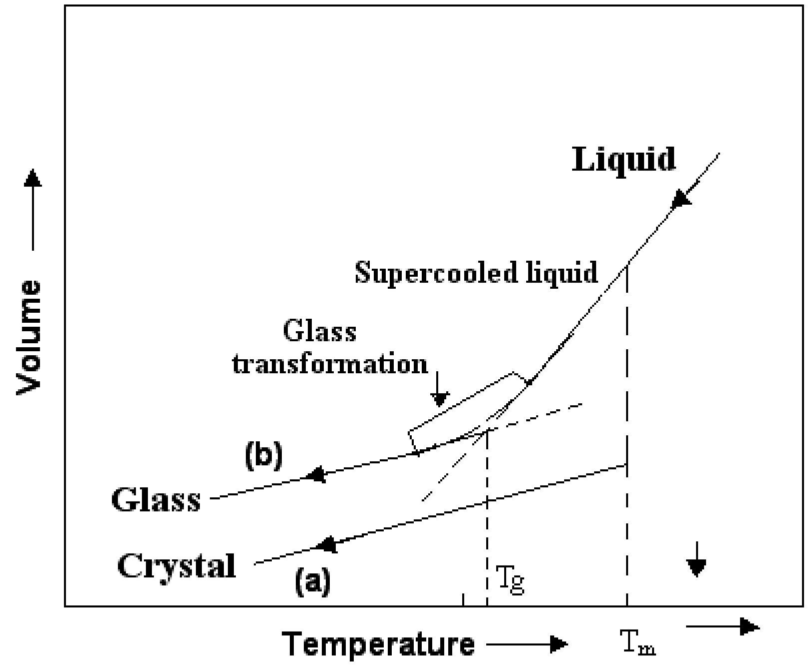

Fig.1.1. *Temperature dependence of volume of a melt when cooled.*

The phenomenon of glass transition is not thoroughly understood [12]. Many theories have been suggested based on a single property/ parameter, which characterize the glass. However, these theories have been successful only to a limited extent as the glass transition is a function of many parameters like heat capacity, bulk compressibility, thermal conductivity, melting temperature, cooling/quenching rate etc., for a particular glass. Normally differential scanning calorimetry (DSC), differential thermal analysis (DTA), dialatometric measurements etc., are used for measuring the glass transition temperatures.

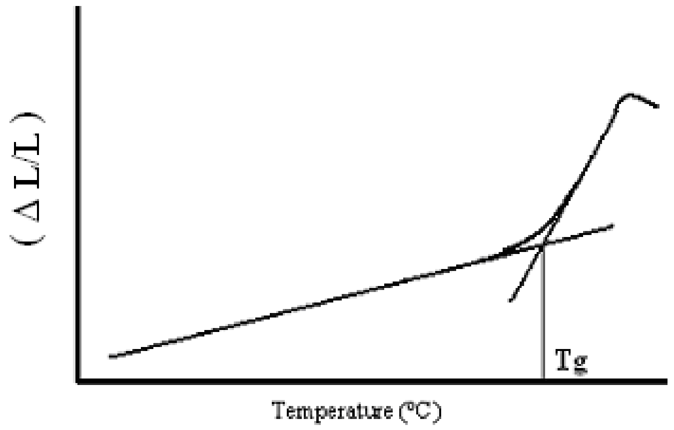

Fig.1.2. Representative pattern of a graph showing change in length as a function of temperature.

Fig.1.2. shows a typical curve of change in length per unit length (ΔL/L) versus temperature obtained when a glass is subjected to dialatometric measurement. The extrapolation method is used for obtaining the values of glass transition temperature (T_g).

1.3. Conditions for glass formation

The first significant attempt to explain the glass formation in certain oxides was made by Zachariasen [13] in 1932, based on the continuous random network formation theory. He suggested that the crystalline and the glassy forms of an oxide should have the same type of oxygen polyhedra joined in a similar way except that in glassy phase there is a change of bond angles and bond lengths. Further, the network should be sufficiently flexible to incorporate the disorder, which is the characteristic of the glassy phase and the internal energy of both the crystalline and glassy phase should be comparable. From this condition, he derived four rules for oxide structure that allow one to choose those oxides that tend to form glasses. These rules were remarkably successful in predicting new glass forming oxides as well as including such oxides known at that time of their formulation. The rules derived by him are summarized below.

1) An oxygen atom is linked to not more than two glass forming atoms.

2) The co-ordination number of the glass forming atoms is small.

3) The oxygen polyhedra shares corners with each other not edges or faces.

4) The polyhedra are linked in a three dimensional network.

Oxides A_2O and AO where A is a meal atom, do not satisfy the rules. Oxides A_2O_3 satisfy rules 1, 3 and 4 if the oxygen atoms from triangles around each A atom. AO_2 or A_2O_3 satisfy these rules, if the oxygen atom form tetrahedra around each A. Higher co-ordination is apparently excluded by the rule 2. From these considerations, Zachariasen concluded that following oxides should be glass formers; B_2O_3, SiO_2, GeO_2, P_2O_5, As_2O_5, P_2O_3, As_2O_3, Sb_2O_3,V_2O_5, Sb_2O_5, Nb_2O_5 and Ta_2O_5. At the time of Zachariasen, B_2O_3, SiO_2, GeO_2, P_2O_5, As_2O_5 and As_2O_3 were used for making the glasses but later, glasses of several other oxides as mentioned above have been prepared. Thus, Zachariasen rules are very accurate in predicting glass formation in these oxides.

However, on the basis of this simple model, glass formation in the non-oxide system could not be explained. A number of theories have been suggested by different authors [14-16] based on different criteria like bond strength between the constituent elements and their electro negativity values etc. These theories were found to be applicable only to certain specific systems. In other words, there is no general rule to predict the glass forming ability in any given system. The prime reason for this is the lack of correlation between the known parameters of the material like composition and structure with the thermodynamic and kinetic parameters, which are difficult to evaluate and depend on the nucleation and crystal growth rates. However, from the structural properties and phase diagrams of existing glass forming systems, few empirical inferences have been drawn to predict whether a material can form the glassy phase or not.

The presence of deep eutectics existing in the phase diagram of certain systems is favourable for glass formation. Many covalent glass-forming systems were found to have large number of stable crystalline polymorphs, which have comparable free energies. Lower coordination number of the constituent elements favors glassy phase formation. Glassy state is a metastable state with respect to the crystalline state of the same composition. This means that the glassy state exists because on cooling the melt below its glass transition temperature, the system does not have time to reach the equilibrium state, having the lowest available free energy, which is nothing but the nucleation of a crystalline phase. For a crystal to nucleate, fluctuations must occur. These will occur more slowly, when the liquid becomes highly viscous, thereby favouring the glassy phase formation [17]. It has also been observed that the more strongly the components in a mixture interact (e.g. the interaction between the solvent and the solute in a solution), the lower will be the activity coefficient of the solvent and hence the freezing point is reduced to a larger extent. More the freezing point decreases, more viscous the liquid becomes, thereby preventing nucleation and favouring glass formation.

1.4. Major components of a glass

Glass is generally composed of different oxides playing different roles. Silicon oxide is the primary glass former. But due to its high melting point (1750^{o}C), oxides of other elements are added to reduce its melting temperature and also enhance the properties of glass as needed. Broadly, these oxides which form the major constituents of a glass are as follows

(a) Network former oxides

These oxides are capable of forming glassy network independently. e.g. SiO_2, B_2O_3, P_2O_5 etc.

(b) Intermediate oxides

These oxides do not form glasses themselves but they take part in the glass network formed by the network formers. e.g. Al_2O_3, MgO, ZnO, PbO.

(c) Network modifiers

These oxides do not form glass network of their own, but they modify network of glass and change the properties of glass drastically. e.g. Na_2O, K_2O, BaO, CaO etc. The other constituents of glass batch are cullets used as auxillary batch ingredient, fluxes like soda ash, potash, lime, boric acid, calcium fluoride etc, which induce rapid chemical activity causing the batch to melt together and form glass, fining agents like arsenic oxide to remove the air bubbles during glass manufacturing and coloring agents like Mn_2O_3, CuO, Cr_2O_3, CeO_2 etc which helps in producing colored glasses.

1.5. Types of glasses

Depending on the network former used, glasses can be classified as silicate, borosilicate, aluminosilicate, borate, phosphate glasses, chalcogenide glasses etc. Glasses can also be categorized depending on its end use as optical glasses, sealing glasses, special application glasses etc. Brief description of some of the glasses is presented in the following section.

1.5.1. *Vitreous silica*

Silica glass is prepared by heating the sand in a refractory metal or graphite crucible at around 2000^{o}C.

1.5.2. Alkali and alkaline earth silicate glasses

A large number of studies have been reported regarding the glass formation, devitrification kinetics, physical properties, structural aspects of alkali and alkaline earth silicate glasses [18, 19]. It has been reported that glasses with low alkali content (less than 5 mol %) are difficult to prepare on account of the high viscosity of their melt and high rate of volatilization of alkali metal oxides at the melting temperature.

1.5.3. Borate glasses

Pure borate glasses without any moisture content are difficult to prepare under normal conditions. Almost water free borate glasses were prepared by Poch [20] by melting ortho boric acid for several hours at a pressure of 1 mm Hg. Glass formation of B_2O_3 with various metal oxides, has been extensively studied and reported some anomalous behavior for these glasses [21, 22].

1.5.4. Borosilicate glasses

Borosilicate glasses have been used for making laboratory apparatus, process plants in chemical industry, high intensity lighting applications etc., and are mainly composed of 70-80% silica, 7-13 % boric oxide with small amounts of alkali and aluminium oxides. For binary SiO_2-B_2O_3 system, the glass formation takes place at relatively high temperature (~1600^{o}C). Generally in borosilicate glasses, small amounts of alkali metal oxides are added for easy glass formation. They have got good chemical durability and high thermal shock resistance. The relative proportions of three and four coordinated boron ions in Na_2O-B_2O_3-SiO_2 glasses were determined by Milber et al [23] using ^{11}B NMR technique. Abe et al [24] further explained various anomalous properties of borosilicate glasses assuming that atomic groups are formed in these glasses consisting of one BO_4 tetrahedron and four BO_3 triangles bonded to this tetrahedron.

1.5.5. Aluminosilicate glasses

These glasses mainly consist upto 20 mole% of Al_2O_3 along with small amounts of calcium oxide, magnesium oxide etc., with silica as major component. Such glasses find wide applications as structural materials for combustion tubes, gauge glasses for high pressure steam boilers and in halogen tungsten lamps capable of operating at temperature as high as 750^{o}C.

1.5.6. Phosphate glasses

Glasses having P_2O_5 as one of the major component are called phosphate glasses. They melt at relatively lower temperature and have got very high thermal expansion coefficient. Moisture sensitiveness of these glasses is a major problem in their applications. However, phosphate glasses having different additives are found to show better stability under ambient conditions and are extensively used for various biomedical, infrared transmission windows, high temperature lighting and sealing applications.

1.5.7. Germanate glasses

Pure GeO_2 readily forms glass. The kinetics of glass formation in germanate, has been extensively studied by Vergano et al [25]. But pure GeO_2 glasses are of little technological importance. GeO_2 along with silica are added to calcium aluminate glasses to extend their optical transmission in far infrared. Similarly in silica based materials, GeO_2 has been added as a minor constituent to improve the refractive index for applications in optical communication.

1.5.8. Aluminate glasses

Although pure Al_2O_3 does not form a glass, it assists the glass formation. Binary and ternary aluminate glasses namely $CaO-Al_2O_3$ and $CaO-MgO-Al_2O_3$ were prepared by Shepherd et al [26] and the glass formation tendency of these compositions has been thoroughly studied by these authors. These compositions melt at relatively high temperatures (~1400°C) with a glass transition temperature around 800°C.

1.5.9. Tellurite Glasses

Tellurite glasses were first prepared and studied by Stanworth in 1952 [27]. The important properties of these glasses are refractive index (2.3) and high thermal expansion coefficient $\approx 25.0 \times 10^{-6}$ /°C. TeO_2 based glasses have also been used in the preparation of transparent glass ceramics. Most of the tellurite glasses have got good stability under ambient conditions.

1.5.10. Vanadate glasses

Pure V_2O_5 melts at around 660°C and forms glass only when it is cooled rapidly. Glass formation between V_2O_5 and a number of oxides like P_2O_5, TeO_2, B_2O_3, GeO_2, BaO, ZnO, CdO, MgO etc., has been investigated by various authors [28-30] and the regions of glass formation and the quenching rate required for the glass formation have been reported.

1.5.11. Chalcogenide glasses

Glasses formed by compounds containing elements of Group V-VI of the periodic table are known as chalcogenide glasses. Amorphous chalcogenide materials can be prepared by a variety of methods. Methods like vapor-quenching techniques produce amorphous materials in the form of thin films over a wide composition range, whereas the melt-quench techniques have been used to make glasses in the bulk form over a limited composition range [31].

1.6. Structural aspect of glasses

The understanding of the nature of the glass has been extended through the development of X-ray diffraction technique. Early investigations showed that the structural unit in crystalline SiO_2 is a tetrahedron consisting of a Si^{4+} ion at the center, with an O^{2-} ion at each of the four corners of the tetrahedron, as shown in ***Fig.1.3***. [32]

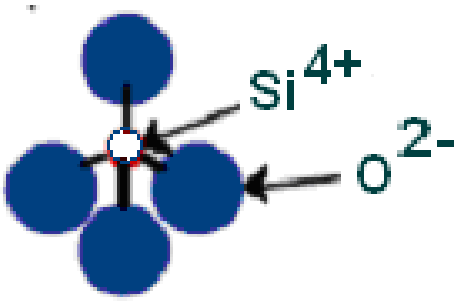

Fig.1.3. *Schematic of structure of a SiO_2 tetrahedron.*

For charge neutralization, each oxygen ion should be bonded directly to two silicon ions, so that the oxygen ions will be shared by two adjacent tetrahedra. In crystals, these structural units are arranged periodically in three dimensions, whereas in glass they are randomly arranged. ***Fig.1.4. (a)*** shows the periodic arrangement of the structural units in crystalline quartz and ***Fig.1.4. (b)*** shows the non periodic arrangement of structural units in glass.

When modifying oxides such as Na_2O and CaO are added to the silica, the ratio of O to Si ions increases. The addition of extra ions breaks the glass network and the network loses its continuity at the points where these particular ions are situated, consequently, the network becomes less rigid. Na and Ca ions accommodate themselves in the spaces resulting from breakage of networks. On account of their smaller sizes, the Na ions are able to pass from one space to another with relatively low energy values so that they retain some degree of mobility even at room temperature. This has a definite influence on some of the properties of glasses like thermal expansion, micro hardness etc.

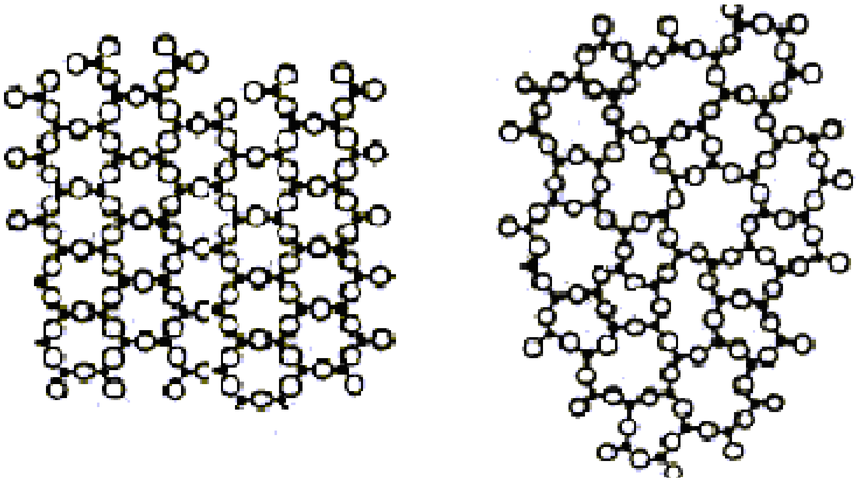

(a) ***(b)***

Fig. 1.4. *Atomic structural representation of (a) crystalline quartz and (b) glass.*

Boron oxide is also a network former like silica. The coordination of the B and O atoms may be either three-fold or four-fold when it is added to silicate glasses. The addition of PbO in silicate glass results in the structural change in glass as it plays a dual role of network modifier as well as network former, depending on its concentration, thereby modifying various thermo-physical and mechanical properties of the glass system. The various physical properties of glasses are correlated with their structural units by different new techniques such as NMR, IR, neutron diffraction etc.

1.7 Introduction to present work

As mentioned before glasses/glass-ceramics are versatile materials and suitable for many applications. In recent years, glass/glass-ceramics have received a lot of importance for biomedical research and applications [33-35]. Materials used for implantology must be biocompatible and preferably bioactive. A bioactive glass-ceramic forms a biologically active hydroxyapatite layer on the surface that permits bonding with bone and soft tissue [36]. Other specific requirements such as Young's Modulus, bending strength etc. may also have to be met depending upon the implantation site.

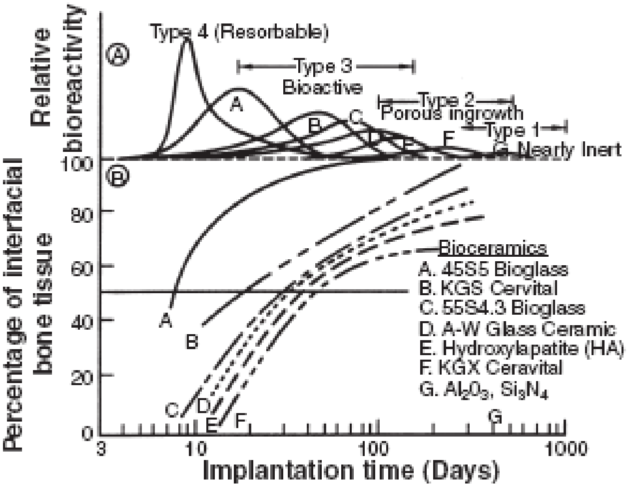

Fig. 1.5. *Bioactivity spectra for various bioceramic implants: (A) relative rate of bioreactivity, (B) percentage of the formation of interfacial bone tissue bonding at an implant interface [36].*

Some of the examples of clinically used glass-ceramics include apatite-wollastonite (A-W) glass- ceramic CERABONE® produced by Nippon Electrical Glass (NEG) Co. Ltd. (Japan) and the machinable mica-apatite glass-ceramics of the BIOVERIT® family manufactured by Vitron Spezialwerkstoffe GmbH (Germany). The BIOVERIT® glass-ceramics are bioactive with the added attraction of easy machinability. The BIOVERIT® family of glass-ceramics has been used in orthopaedic surgery as spacers, in head and neck surgeries and as middle ear implants [37, 38].

If the implant material is toxic then tissue surrounding the implant dies. Alternatively, the material may be non-toxic but bio-inert, causing the formation of a fibrous capsule around the implant. On the other hand, if the material is biologically active, then it will bond with the surrounding tissue and if it is soluble, then it will be eventually replaced by the surrounding tissue. The bio-activity spectra for various materials are presented in ***Fig. 1.5.***

A bioactive glass-ceramic forms a biologically active hydroxyapatite layer on its surface that permits bonding with bone and soft tissues. Hench [36] reported the first bioactive glass having composition (wt %) 45% SiO_2, 24.5% Na_2O, 24.5% CaO and 6% P_2O_5 commonly known as 45S5. The bio-active glasses are different from traditional soda-lime-silica glasses which contain more than 70% of SiO_2 by wt. and do not produce any biological activity for bonding with the bone or tissues upon their implantation. An important characteristic of bio-glass is the time dependent kinetic modification of its surfaces upon implantation in the body. The surface forms a biologically active hydroxy apatite carbonate (HCA) layer which provides bonding interface with the tissues. The bio-active material develops an adherent interface with body tissues which can resist mechanical forces substantially.

Mostly, the bio-active silicate glasses are based upon 45S5 glass as mentioned earlier. Glasses with lower CaO/P_2O_5 ratio than 5:1 do not form interfacial bonds with bones or tissues. It was also mentioned here that the rate of reaction between implant and aqueous solution under physiological condition is very fast if the implant is resorable. However, if the rate of reaction is too slow then the implant is not bioactive. Thus the level of bioactivity of a material is related with time; therefore bio-active implants require a definite incubation period before the bone proliferates and bonds. The duration of incubation period varies considerably with composition.

The specific response of a calcium silico-phosphate glass is shown in ***Fig. 1.6.*** The formation of Ca-P bioactive layer involves several steps and governed by the nucleation and growth of particles at the surface. The specific steps of the reaction are reported by Hench [39].

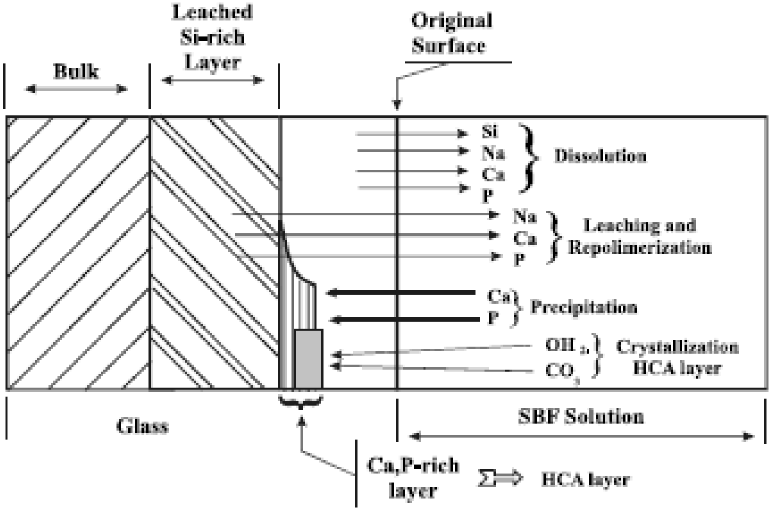

Fig.1.6: *Schematic view of the steps involved in the formation of a hydroxy-apaptite layer [39].*

The formation of hydroxyapatite commences when surface dissolution takes place. In the first stage loss of sodium ions (Na^+) from the surface of the glass takes place via ion exchange with hydrogen (H^+ or H_3O^+). This is followed by the formation and condensation of silanol groups at the surface. Then after Ca^{2+} and PO_4^{3-} groups migrate to the surface through the SiO_2 rich layer forming a CaO-P_2O_5 rich film on top of the SiO_2-rich layer, followed by growth of the amorphous CaO-P_2O_5 rich film by incorporation of soluble calcium and phosphates from the solution. The formation of hydroxyl-apatite layer would then allow the integration of the implant with the surrounding tissue. It must be mentioned that minor changes in glass composition can dramatically alter the bio-activity. Hench has reported that the granules of bio-active glass partially behave as resorbable implant due to an increase in their surface area and stimulate new bone formation [39]. In addition to the bio-active glasses, bio-glass ceramics and composites are also known to form interfacial bond with bones [40- 42]. Kokubo et al. [43] studied the SiO_2–CaO–P_2O_5–MgO glass systems and developed the apatite and wollastonite glass-ceramics in glass containing (wt %) 4.6MgO-44.7CaO-34 SiO_2-16.2 P_2O_5- 0.5CaF_2. Oliveira et al. [44] reported that the glasses with increased surface activity can be developed by replacing calcium oxide by magnesium oxide in the (mol%) $31SiO_2$–$11P_2O_5$–(58-x)CaO–xMgO series. Hench [39] concluded that addition of alumina tends to decrease the bioactivity of these 45S5 bases glasses. Ebisawa et al [45] reported an improvement in response of ferromagnetic glasses with addition of small amount of P_2O_5. In-vitro study on ZnO containing bioglass/glass-ceramic has shown that ZnO can be used to modify the surface properties, which in turn have stimulatory effect on bone formation [46, 47]. Thus, the bioactive response of the glass/glass-ceramics can be optimized by controlling the glass phases in the glass-ceramics, which can be modified by varying the alkaline earths like CaO, MgO and ZnO in glass matrix.

Other promising application of glass/glass-ceramics is as a sealant material for solid oxide fuel cells (SOFCs). SOFCs are electrochemical devices, which convert chemical energy into electric energy. SOFC based power generation presents many advantages, including higher efficiency, lower environmental impact and ability to co-generate heat from the exhaust gas to name a few, as compared to conventional power generation [48-51]. However, in these devices, the most important technological challenge lies in the development of high temperature sealants, which separate the fuel and air and prevent their leakage.

The glass-ceramic used for sealing must show good matching of thermal expansion coefficient (TEC) and low reactivity with other fuel cell components [52-55]. Achieving a sealant that fulfils these conditions is important for long term stability of SOFC stacks. Although some alkali metal containing glasses have been used for sealants in SOFCs, they are generally avoided because they react with other fuel cell components [56–59].

Two important criteria for selection of a suitable glass for sealant are the glass transition temperature (Tg) and the thermal expansion coefficient (TEC) of materials. In glass-ceramics we get the greater range of thermal expansion coefficients, allowing the formation of well matched seals. This can be achieved by careful selection of starting glass composition, nucleants, and the heat treatment schedule employed to crystallize the glass so that specific crystalline phases are formed.

Most of the promising compositions studied for SOFC sealants are barium-containing glass/ glass–ceramics, which have relatively large coefficients of thermal expansion. In the case of barium-containing glass–ceramics for SOFCs, the TEC value increases on crystallization. The coefficients of thermal expansion of $BaO–MgO–SiO_2$ and $BaO–ZnO–SiO_2$ increase with increasing BaO content for constant SiO_2 contents [60].

The crystallization in the glass based sealants cannot be avoided as the sealants are used at higher temperature. Thus, the particular crystalline phases formed in a glass-ceramic are critical, therefore, the crystallization kinetics must also be controlled. The crystallization in barium aluminosilicate glasses is faster than that of the corresponding calcium and magnesium aluminosilicate glasses, which has been attributed to the lower field strength of barium as compared to that of calcium and magnesium [61, 62].

It is also required that the glass should wet the surfaces before crystallization. Crystallization in glass decreases the viscosity of the glass [63, 64]. Further the optimal crystallization rate depends on the flow characteristics of the glass [65, 66]. If the crystallization occurs before complete wetting or sintering, poor adherence or porosity can result. Conversely, insufficient crystallization may lead to inadequate mechanical properties.

The crystallization kinetics can be controlled with the addition of nucleating agents. Control of the crystallization also includes the control of the specific phases formed. Nickel and Cr_2O_3 have been used as nucleating agents. The high activation energy for crystallization with nickel and Cr_2O_3 nucleating agents has been reported and attributed to the more covalent nature of the bonding, which also increases the glass transition temperatures [67].

The glass transition temperature depends on the strength of glass network, which can be modified by addition of different modifiers. It has been seen that nickel, chromium and titanium can be tetrahedrally coordinated and thus act as network formers, whereas zirconia is only stable with higher coordination numbers, and thus will only act as a network modifier [67]. Thus, the titania addition leads to decrease in the coefficient of thermal expansion of magnesium and barium based glasses.

Boron oxide is most commonly added to decrease the viscosity, softening point and glass transition temperature [68, 69] of SOFC glass sealants. However, the effect of boron oxide on the coefficient of thermal expansion can be overcome by adding other component in the glass. Boron oxide also stabilizes the amorphous structure as shown by the increase in activation energy for crystallization with increasing boron content (B/Al ratio) [68]. Aluminium in glass–ceramics can have tetrahedral coordination and replace the silicon in the glass network, but at larger concentrations acts as a network modifier [6]. Zinc and lanthanum are also used to control the viscosity [6, 68]. Lanthanum additions increase both the softening point and the coefficient of thermal expansion [70].

As mentioned before the sealant materials must be chemically compatible with other fuel cell components. The chemical compatibility of glass-ceramic sealants with the yttria-stabilized zirconia electrolyte is generally good. Silicates containing barium, calcium or magnesium have been reported to form adherent and stable interfaces with yttria-stabilized zirconia [71, 74]. Reactions are more prevalent with the interconnect materials, primarily due to chromium, which is typically present in both ceramic and metallic interconnect materials. The interfaces between silicates containing barium, magnesium glasses and chromium forming alloys have been observed to contain $BaCrO_4$ or $MgCrO_4$ [75]. Thus, the improvements in thermal expansion matching provided by barium additions lead to increased reaction with the interconnect material.

In addition to silicates, other systems have also been investigated. Phosphate-based systems have been studied and developed [76–78]. Non-oxide systems synthesized from polymer precursors have been developed [79, 80]. However, the stability of such systems in the oxidizing environment of the SOFC creates an additional challenge for their implementation.

Most of the SOFC sealants reported so far have been based on the alkaline earth alumino-silicate system such as barium alumino-silicate due to good thermal expansion matching and the ability to wet materials such as the interconnect allowing good sealing. While the chemical durability of these glass-ceramics is generally good, it is necessary to further improve the phase stability, crystallization and adhesion behaviour of the glass-ceramic with other SOFC components.

This thesis covers work carried out on the preparation, thermo-physical, structural and microstructural properties of two different glass systems having different amount of P_2O_5; namely (i) CaO-SiO_2-P_2O_5 with different additives (ii) BaO-SrO-SiO_2-P_2O_5 based glasses/glass-ceramics. In addition, to demonstrate the applicability of these materials, specific properties related to bio and bonding behaviour are also investigated. The calcium phospho-silicate glass/glass-ceramics with different additives like iron oxide, ZnO and Ag are investigated as prospective bio-materials. As mentioned before, desired surface response of the glass/glass-ceramics can be obtained by varying the composition of alkaline earths like CaO and MgO in glass matrix. The addition of modifiers in glasses will result in breaking of Si–O–Si bonds creating non-bridging oxygen groups (Si–O–NBO). This facilitates the formation of Si–OH functional groups on the surface, which improve the surface response. Introduction of iron oxide, zinc oxide and Ag in glasses is expected to modify the local structure of the glass, consequently material response and behaviour will be affected. Therefore, the effect of addition of Fe_2O_3, ZnO and Ag on structural and microstructural properties of glass/glass-ceramics is investigated. Further the work is also pursued to evaluate the materials in-vitro i.e. in simulated body fluid (SBF) and bovine serum albumin (BSA). Glass-ceramics containing Ag are studied for antibacterial activity against Escherichia coli (E. coli).

Silicate glasses containing SrO and BaO with different modifiers are studied for bonding/sealing applications. For effective bonding, it is required that coefficient of thermal expansion of sealant is as close to that of metallic interconnect. As the thermo-physical properties of glass and glass-ceramics depend on the composition, different glasses are prepared with varying amount of P_2O_5 and V_2O_5 content. Since the major requirements of sealing material for SOFC application is good gas tightness at the high operating temperature (600-800°C), sealant materials are tested for adherence and stability at high temperature.

Efforts have been made to carry out a systematic study on the said two systems. The account of work has been presented in following eight chapters.

Chapter 1: ***Introduction***

This chapter describes an introduction to glasses and glass-ceramics in general. An overview of different applications and advantages of glass/glass-ceramics with respect to structure related properties are discussed. A summary of the work reported on bio-glass/ glass-ceramics and sealant materials for SOFC is presented. The limitations of the existing research and the need for the new materials are discussed. Finally, the scope of present thesis and different investigated properties are discussed.

Chapter 2: ***Experimental methodology and techniques***

In this chapter, details of preparation and characterization techniques used in present work are given along with basic principles, their merits/demerits etc.

Chapter 3: ***Structural, microstructural and in-vitro studies of calcium silico-phosphate glass/ glass-ceramics containing iron oxide***

In this chapter, preparation and results on structural, micro-structural and magnetic properties of glass/glass-ceramics with nominal composition $34SiO_2$-(45-x)CaO-$16P_2O_5$-4.5 MgO-$0.5CaF_2$ –xFe_2O_3 (where x = 5, 10, 15, 20 wt %) have been discussed. The glass-ceramics exhibited an increase in the formation of magnetite phase with an increase in iron oxide, which induces the magnetic property, however, at higher iron oxide content fraction of non-bridging decreased, which influences the bioactive response.

Chapter 4: ***Structural, microstructural and in-vitro studies of calcium silico-phosphate glass/ glass-ceramics containing iron oxide and zinc oxide***

This chapter has been devoted to the studies carried out on glass/glass-ceramics containing iron and zinc oxide. The glass and glass-ceramics with composition $25SiO_2$-50CaO-$15P_2O_5$-(10-x)Fe_2O_3-xZnO (where x = 0-5) mol % has been prepared. Fraction of non bridging oxygen decreased with an increase in zinc oxide content. Addition of ZnO also results in a decrease in strength of dipolar interaction. Magnetic studies revealed the relaxation of magnetic particles and an increase in saturation magnetization with addition of 2 mol % ZnO. In-vitro studies in SBF have shown the formation of Ca-P rich layer on the glass-ceramics when immersed in SBF, implying the bioactive nature of the samples.

Chapter 5: ***Studies of calcium silico-phosphate glass-ceramics containing iron oxide, zinc oxide and Ag***

In this chapter, structural and magnetic properties of glass/glass-ceramic containing iron, zinc oxide and Ag are discussed. The glass/glass-ceramics with $25SiO_2$-(50-x)CaO-$15P_2O_5$-$8Fe_2O_3$-2ZnO-xAg (where x = 0, 2 and 4 mol %) were prepared and studied. Magnetization improved with an increase in Ag content upto 4 mol% which is attributed to improvement and attainment of maximum magnetic ordering. Antibacterial response of Ag containing glass-ceramics samples was studied against E. coli and found to depend on Ag ions concentration in the glass matrix.

Chapter 6: ***Studies on barium alumino strontium silicate (BASP) glass/glass-ceramics containing P_2O_5***

In this chapter, barium strontium silicate based glasses are investigated as potential sealants for solid oxide fuel cells. The effect of $Ba_3(PO_4)_2$ incorporation on thermo-physical, structural and sealing characteristics of a glass of composition (mol%) $30SiO_2$-20SrO-30BaO-$10B_2O_3$-$5La_2O_3$-$5Al_2O_3$ is studied. The glasses are characterized for structural features with XRD and solid-state NMR. Seals of glasses with Crofer- 22 APU metallic alloy are made, and the microstructure and interface of seals are investigated. The glass composition formulated by addition of 1 mol% $Ba_3(PO_4)_2$ has shown good thermal and sealing characteristics, while further increase of $Ba_3(PO_4)_2$ to 2 mol% leads to increased crystallization tendency.

Chapter 7: ***Studies on barium alumino strontium silicate (BASP) glass/glass-ceramics containing V_2O_5 and P_2O_5***

Effects of addition of V_2O_5 and P_2O_5 to barium strontium silicate based glasses are discussed in this chapter. V_2O_5 acts as modifier and thus results in a decrease in glass-transition and softening temperature of glasses. A series of glasses have been prepared with nominal composition $27SiO_2$-$23SrO$-$32BaO$-$4Al_2O_3$-$10B_2O_3$-(4-x) P_2O_5-xV_2O_5 where x=0-4 mol%. The glasses were characterized for structural features with XRD and solid-state NMR. The glass samples did not show major structural changes when P_2O_5 was replaced with V_2O_5. The change in thermo-physical properties was due to variation in strength of bonds in the network. Seals were made and tested for hermeticity at high operating temperatures (800ºC) using pressure difference technique. The seals were found hermetic even after 15 heating and cooling cycles, implying the efficient sealing of the material with metal.

Chapter 8: ***Summary and future scope***

The chapter summarizes the work carried out in the thesis and discusses the scope for further extension of the work reported here.

Chapter 2

Experimental Methodology and Techniques

Glasses and glass-ceramics can be characterized in terms of various properties such as thermo-physical, mechanical, structural, optical, chemical etc. This chapter presents a very brief overview of the techniques used for characterization of glass/ glass/ceramic samples.

2.1 Introduction

A number of techniques are available for the glass preparation, which depends on the glass system and the end product. An essential prerequisite for glass formation is to establish the processing conditions like cooling rate to be sufficiently high to prevent crystallization. Melt quenching is the widely used for producing bulk glasses, while for the preparation of amorphous thin films, various physical and chemical vapour techniques with appropriate changes are employed.

The experimental sets up used for glass preparation were grinder/mixer (ball mill), calcination furnace, raising/lowering hearth furnace for quenching, annealing furnace etc. For preparation of samples some of the instruments used were precision cutting machine, molding machine, hydraulic press, polisher etc. Thermo-mechanical investigations were carried out by thermo-mechanical analyzer (TMA), differential thermal analyzer/thermogravimetry (DTA/TG), and hot stage microscopy (HSM). The physical properties like density were measured using standard techniques. The samples were characterized for structural features by using X-ray diffraction (XRD), Fourier transform infrared spectroscopy (FTIR) and for microstructural features using scanning electron microscopy (SEM). The samples were also studided for magnetic properties by using using SQUID magnetometer and Mössbauer spectrometer.

2.2 Sample preparation

Glasses were prepared by melt-quench technique. It involves grinding/mixing, calcinations, melting, quenching and annealing. For effective mixing and reaction among different constituents, the reactants were thoroughly ground in a planetary ball mill and then subjected to different heating steps depending on the type of glass, prior to final melting and quenching process. During calcinations, precursors of the constituent elements are converted into their respective oxides. Alumina and platinum crucibles were used for calcinations and melting purposes respectively.

In melt-quench technique the melt is cooled sufficiently fast to preclude nucleation and crystal growth. Rates of cooling required for glassy phase formation are different for different materials. For example, certain good glass formers such as B_2O_3, P_2O_5 etc. will form glassy phase even under conditions of slow cooling (1K/s) whereas to get metallic glass cooling rates of the order of 10^3-10^6 K/s are required [2]. Effective cooling can be achieved by quenching the melt immediately after removing from the furnace in between conducting materials like copper or brass plates or pouring in graphite moulds. Sometime glass is directly poured in chilled water. Most of the glasses based on conventional network formers like B_2O_3, SiO_2, P_2O_5 etc., can be prepared by this method.

Starting charge is usually prepared by weighing the required amount of chemicals. They need not be oxides, but can be nitrates or carbonates. As an example the precursor needed for P_2O_5 is $NH_4H_2PO_4$. Upon heating at 225°C, $NH_4H_2PO_4$ decomposes according to the following reaction:

$$2NH_4H_2PO_4 \rightarrow P_2O_5 + 3H_2O + 2NH_3\uparrow \qquad \textbf{(2.1)}$$

Thus 2 molecules of $NH_4H_2PO_4$ yield one molecule of P_2O_5, knowing the molecular weights of the species involved, we can state that if y g P_2O_5 is needed, it would need **y** x 1.6208g of $NH_4H_2PO_4$. The factor 1.6208 is known as the gravimetric factor. The gravimetric factors can be calculated for other precursors as well. The reaction also illustrates that if the precursors do not decompose properly, gas bubbles may get trapped in the glass, compromising its properties. Therefore the precursors must be thoroughly mixed and calcined. During calcination, carbonates or nitrates are converted into oxides. A measurement of weight loss ascertains proper decomposition of the precursors. Glasses are then melted in various furnaces. A typical glass melting furnace is shown in ***Fig. 2.1.***

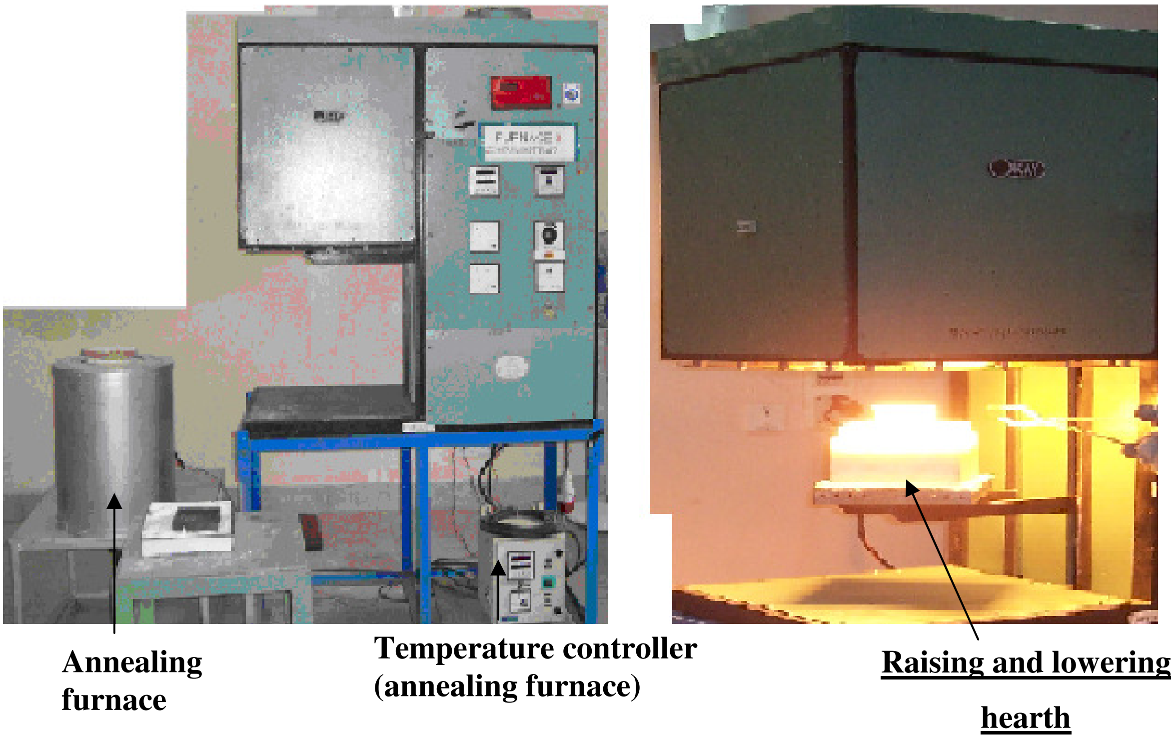

Fig. 2.1. *Typical glass melting raising and lowering hearth furnace.*

In this furnace superkanthal is used as heating elements. The furnace operates up to 1650°C continuously and up to 1700°C for 4hrs. Heating of the charge was carried out at a fast rate in auto control mode till 900^{o}C followed by programmed schedule (150^{o}C/hr) till 1300^{o}C for borate glass and 1550 ^{o}C for silicate glass. The molten glass is kept at dwell time for nearly 2 h followed by pouring in graphite moulds kept in an annealing furnace.

2.2.1 Annealing

When the molten glass is quenched, it develops lot of stresses. These stresses can be nullified by the process called annealing. In this process, the glass is kept at a temperature of 50^{o}C below the glass transition temperature for 4 h to remove the stresses and obtain a stress free glass. For this purpose a precise temperature control furnace was used.

2.2.2 Wafering of glass

For various studies/characterizations, the glass samples are required in regular geometrical shapes. Therefore the prepared glass is cut in different shapes and sizes using a precision cutting machine (BUEHLER ISOMET 4000). The sliced glasses were polished in grinding machine with 200-600 mesh size polishing paper using carborundum and fine alumina powder and then used for characterization. For e.g. for thermal expansion measurements, cylindrical sample of 3-5 mm thickness and less than 9 mm diameter is required, whereas for micro hardness measurements cylindrical sample, with one side fine polished surface was required. For degradation studies, cylindrical sample, both side polished and of known surface area was used.

2.3. Characterization

2.3.1. Density measurements

Density was measured by weighing a suitably selected piece of solid sample in air and dividing this weight by the buoyancy, when the sample is suspended in water. According to Archimedes principle, the buoyancy equals the weight of the displaced fluid, which, for water, equals to the volume. If W_a and W_b are the weights of the specimen in air and in water respectively, then the buoyancy is ($W_a - W_b$) (density of water is 10^3 kg/m^3) and density,

$$\rho = \frac{Wa}{(Wa - Wb)} \tag{2.2}$$

In case sample reacts with water, a suitable inert liquid such as xylene, toluene etc. can be selected as the immersion liquid. The molar volume [81, 82] of the samples can be calculated from the following expression,

$$MolarVolume = \frac{M}{\rho} \tag{2.3}$$

Where, ρ is the density of the sample and M is the molecular weight. In the present measurements, distilled water was used as the immersion fluid and the reported density values are the average of at least three independently measured values.

2.3.2. Thermal characterization

2.3.2.1. Thermal expansion coefficient

Thermo-mechanical analyzer, is used to measure the thermo-physical properties of materials, when subjected to heating /cooling. Linear thermal expansion is measured as the change in length of a material per unit length, subjected to temperature changes. Symbolically represented by $\Delta L/L_0$, where ΔL is the observed change in length ($\Delta L = L_1 - L_O$), and L_1 and L_O are the lengths of the specimen at test temperatures T_1 and reference temperature T_0.

Mean Coefficient of Linear Thermal Expansion

This defines as the linear thermal expansion per unit change in temperature. The mean coefficient of linear thermal expansion (α) is defined as

$$\alpha = \frac{L_1 - L_0}{L_0(T_1 - T_0)} = \frac{\Delta L}{L_0 \Delta T} \qquad \textbf{(2.4)}$$

In present investigation we have used a thermo-mechanical analyzer (TMA –92 Setaram, France) of push rod type as shown in ***Fig. 2.2***.

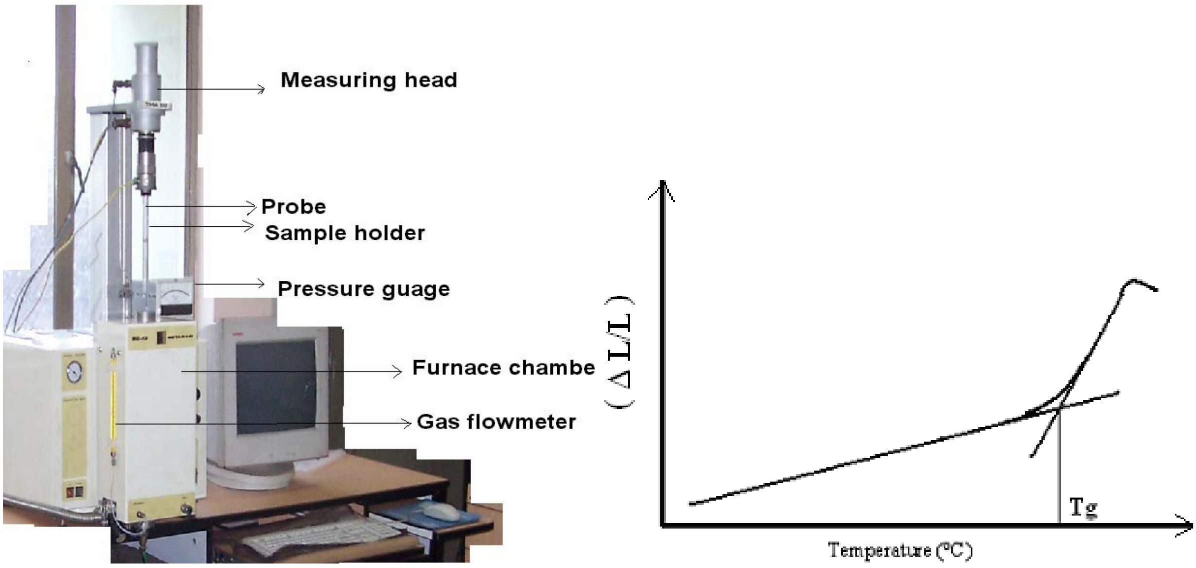

Fig.2.2. *(a) Photograph of TMA instrument and (b) A typical TMA curve of a glass sample.*

The system has quartz sample holder and silica probe which can be used upto 1000°C. For higher temperature, alumina is used. Heating of the sample causes it to expand, pushing the tube and push rod in opposite directions. This movement is sensed by a transducer (LVDT). The temperature of the sample and furnace is measured using chromel-alumel (K-type) thermocouple and Pt-Rh (R type) thermocouple respectively within the accuracy of ±0.01°C. The sample (10 mm in diameter and 5-10 mm in height) is mounted on the quartz sample holder, located inside the measurement chamber. The chamber is evacuated to 10^{-3} mbar and then flushed with high-purity argon. The argon flow rate is maintained at 40 liters per minute and the sample is heated at 10 K min^{-1}, under a constant load of 5 g, for the thermal expansion measurements. All the measurements are carried out in flowing argon atmosphere with a constant flow rate of 40-50 liters per minute. The average value of the thermal expansion coefficient is estimated by measuring the change in the length of the sample between 30 and 300ºC. The glass transition temperature is determined from the intersection of the linear portions of this curve, which are extrapolated from the temperature regions below and above the glass transition temperature.

2.3.2.2. Differential thermal analysis (DTA)

This is based on differential thermal behaviour of a sample with regard to a reference material (i.e. Al_2O_3). For this purpose a known amount of sample and the reference material are taken into crucibles of suitable materials. Both are simultaneously heated and cooled in programmed manner with desired rates. The outputs of two independent thermocouples, attached to these crucibles are compared and processed to get DTA plot. DTA plot indicates thermo-physical changes taking place in the samples, such as phase transformation, softening, melting, and solidification as function of temperature. For such studies about 50- 100 mg of samples are needed.

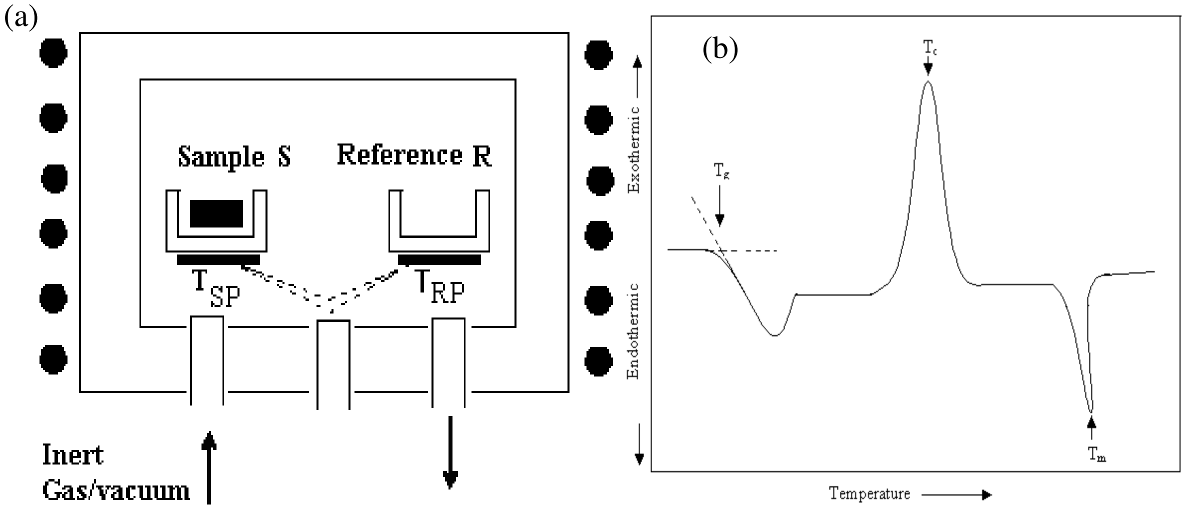

Fig. 2.3. (a) Schematic illustration of a DTA cell (b) A typical DTA curve of a glass.

A typical DTA trace of a glass is shown in ***Fig. 2.3b***. As a glass is heated at a constant heating rate in a DTA, the heat flow exhibits an endothermic base line shift at the glass transition temperature (T_g), followed by an exothermic crystallization peak at T_c. Further heating results in melting of the sample at T_m, which is an endothermic transformation. Generally, it has been observed that glasses, which are unstable, show one or more exothermic peaks corresponding to devitrification of various phases. Such glasses may sometimes show multiple melting endotherms as well. T_g and T_c values correspond to the onset of the glass transition and the devitrification behaviour in the glass respectively (Fig. 2.3b).

In present investigation, DTA measurement was carried out on TG-DTA system model 92.18 of M/s Setaram, France. About 20-25 mg of powder sample was taken in a 100-µl Pt crucible. The chamber was initially pumped to 10^{-3} Torr and then flushed by Ar gas, for about 15 min, before starting the experiment. Sample was heated up to different temperatures depending on the type of system under investigation. The measurements were done at the heating rate of 10K/min in O_2 atmosphere using empty crucible (Pt) as reference.

2.3.2.3. Hot Stage Microscopy (HSM)

The sintering behaviour of the BASP glasses was studied by means of a hot stage microscope (HSM, Hesse, Germany, ***Fig. 2.4a***). For these measurements, the sample powders were pelletized and placed on an Alumina support. This was then placed within a furnace and heated at 10 °C.min^{-1}. The shape of the sample was monitored using a camera. The projected area of the sample viewed in side elevation was then used to characterize the sintering, deformation, sphere and flow temperatures of the glasses (***Fig. 2.4b***).

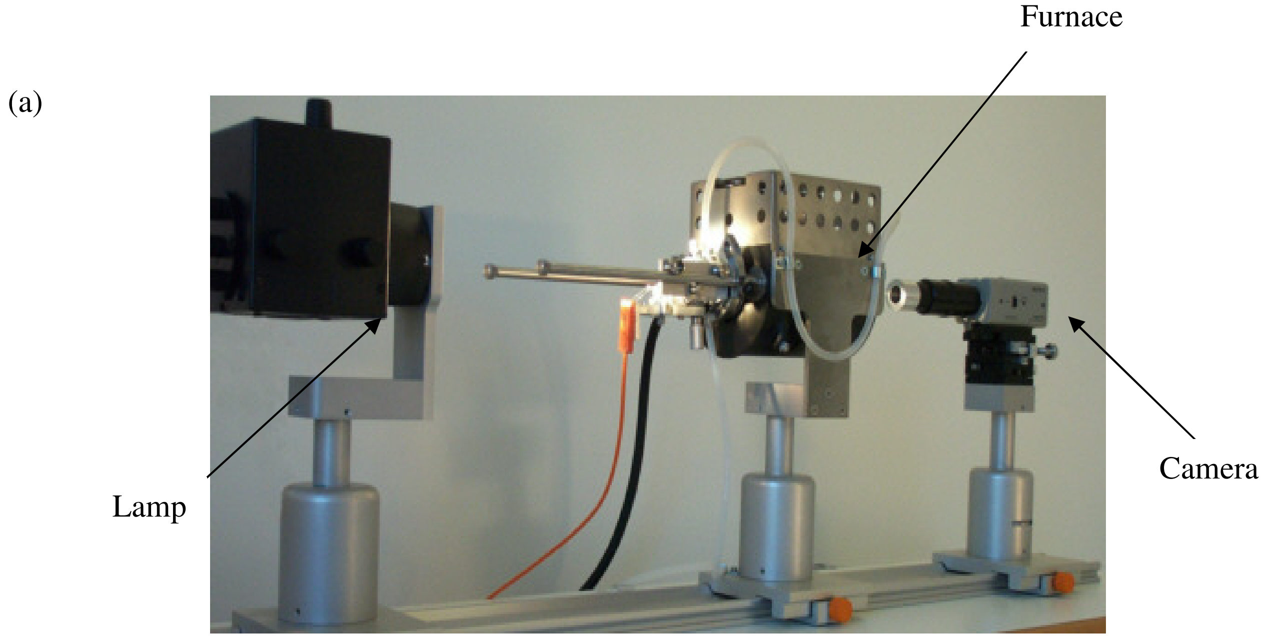

(b)

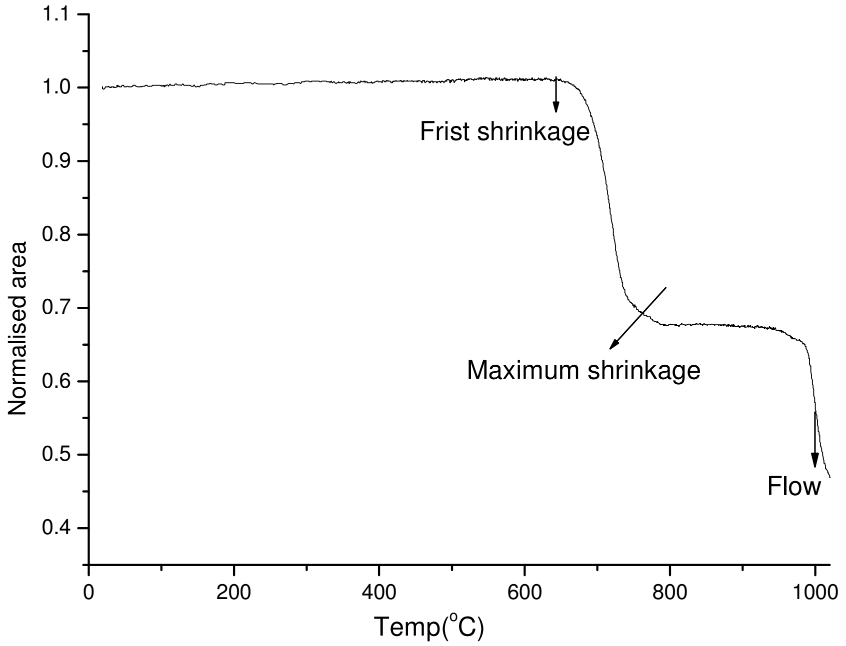

Fig. 2.4 *(a) Schematic illustration of a HSM instrument (b) A typical HSM curve of a glass sample.*

2.3.3. Structural characterisation

2.3.3.1. Powder X-ray diffraction

X-ray diffraction is one of the techniques, most widely used to confirm the glass formation. For glasses, the diffraction pattern consists of a broad peak. This is because glasses do not have long range periodicity, and there is considerable distribution in the bond angles and bond lengths between the constituent atoms present in the glass. Unlike this, the crystalline materials are characterized by sharp peaks in their diffraction patterns due to the presence of long range periodicity. Schematic diagram of an X-ray diffractometer is shown in ***Fig.2.5***. The basic principle of the XRD is the Bragg's diffraction of X-rays, in which following condition is satisfied.

$$2d \sin \theta = n \lambda, \qquad \textbf{(2.5)}$$

where d is the interplanar distance, θ the angle of incidence and λ the wavelength of x-ray used.

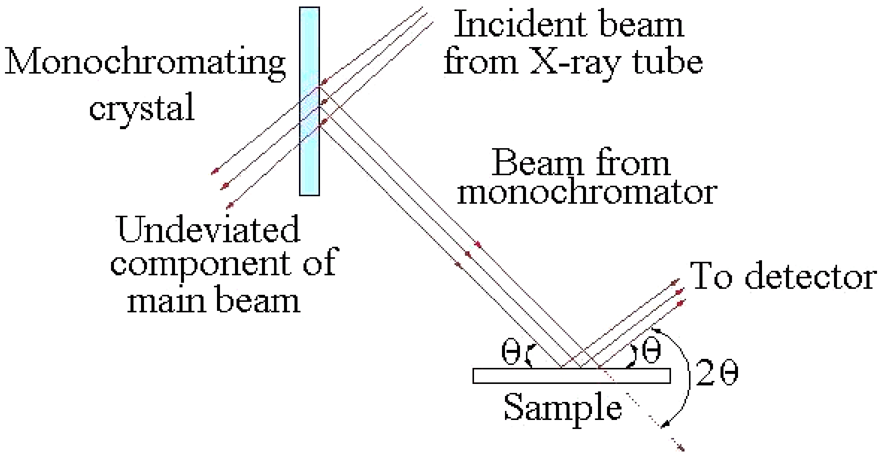

Fig. 2.5. Ray diagram for X-ray diffractometer.

In the present investigation, for XRD measurement, powdered sample was taken in a tube or on a slide, mounted on a rotating spindle and exposed to x-rays from a Cu target. The diffracted x-rays were collected by a GM counter/scintillation detector, which was rotated at a speed say 1°/min. The detector output was plotted as a function of 2θ using a microprocessor controlled system. The peak positions giving the inter-planar spacing and the relative intensities of the peaks were measured. The crystalline phases present in the samples were identified using MATCH® software.

2.3.3.2. Infrared transmission (FTIR)

IR transmission of glass can be measured using FTIR technique. It is based on Michelson interferometer, which is an optical device consisting of a fixed mirror, movable mirror and a beam splitter. The interferometer shifts the phase of one of the beams with respect to another by moving one of the mirrors and keeping the other mirror at a fixed position. When the two beams overlap, depending on whether they are in phase or out of phase, constructive or destructive interference takes place. If the light source is monochromatic, the intensity of the interference pattern will rise and fall periodically and the detector will measure a sinusoidal signal as a function of the optical path difference. When the light source contains many frequencies, like the radiation emitted from a globar IR source, the intensity ‘I’ measured as a function of optical path difference ‘x’ is known as the interferogram. Fourier transformation of the interferogram results in the frequency spectrum, I(ν). The optical path difference ‘x’ can be accurately obtained from the interference patterns generated from the interferometer using a laser source whose frequency is accurately known [83].

In the present study all infrared experiments were carried out using a Bomem MB102 FTIR machine with a resolution of 4 cm^{-1} having a range of 400-4000 cm^{-1}. IR radiation was generated from a Globar source (bonded silicon carbide rod). The instrument used CsI single crystal, as the beam splitter and deuterated triglycine sulphate (DTGS) as the detector. A He-Ne laser having a wavelength of 632.8 nm, with a max power of 25 μW was used for the calibration purpose. Sample to KBr ratio was taken as 0.5/99.5 %. Prior to IR measurements, the samples were ground thoroughly by mixing with dry KBr powder made in the form of a thin pellet and introduced into the sample chamber for recording IR spectra.

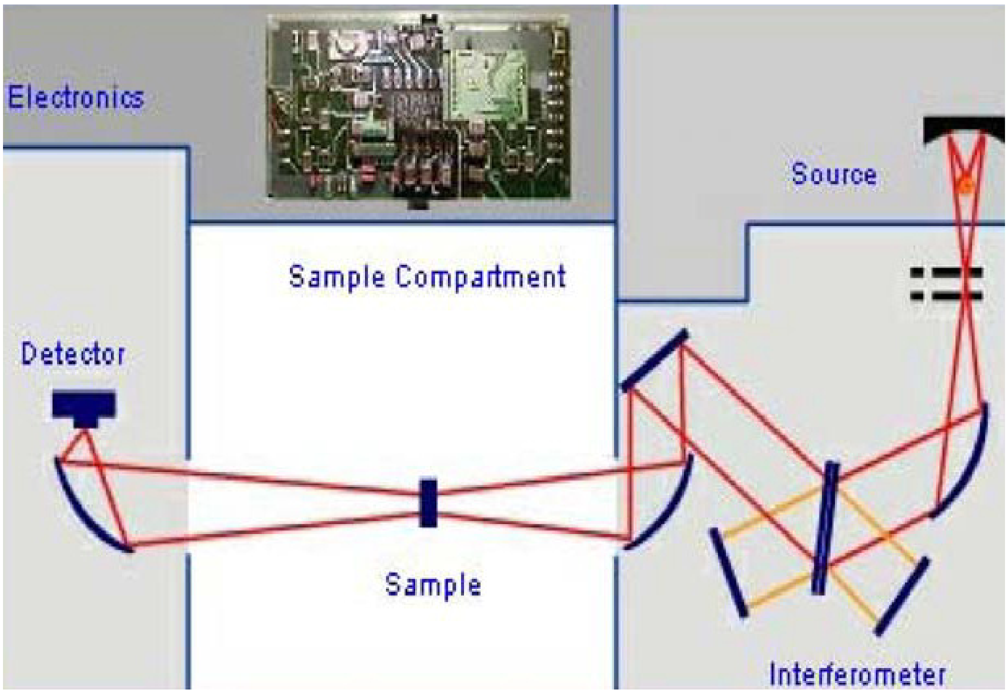

***Fig. 2.6**. Ray diagram of recording FTIR spectra along with electronic circuit.*

2.3.3.3 NMR Spectroscopy

Solid-state NMR is powerful tool for conceptual description of structure and disorder in glasses [85]. In contrast to solution NMR where sharp lines are obtained, solid-state NMR spectra are characterized by presence of very broad NMR line shapes. This is due to the presence of effects of anisotropic and orientation dependent interactions in the spectrum. These are averaged out in liquids due to rapid random tumbling. However, during recent years, several specialized techniques have been developed for averaging these interactions to zero, or reduce them to their isotropic values allowing the registration of high-resolution NMR spectra of solids.

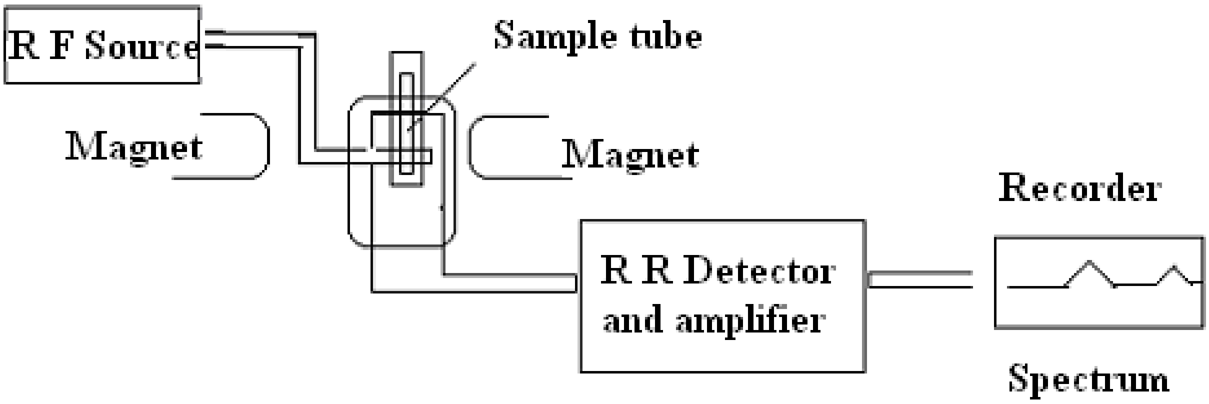

Fig. 2.7 Schematic diagram of an NMR spectrometer.

NMR lines shapes contain valuable structure and dynamic information. Technique has been developed where by choosing appropriate experimental protocols, one can access the anisotropic part of NMR interaction while maintaining high resolution. Broadening of the NMR lines in solid samples occurs mainly because of (i) anisotropic effect, (ii) dipolar interaction and (iii) quadrupolar effect, for the nuclei with spin>1/2. The anisotropic and dipolar interaction can be overcome by MAS NMR technique; where as the quadrupolar effect is partially overcome using CQ MAS NMR.

Magic angle spinning (MAS) NMR

This most popular experimental method for getting high-resolution NMR patterns from solids, is called MAS NMR technique [86, 87]. Hamiltonian for different anisotropic interactions in samples have $3\cos^2\theta-1$ term, when $\theta = 54.7^o$, the term $3\cos^2\theta-1$ becomes zero. This term arises as a quadrupolar term in the series expansion of the magnetic diplole moment experienced as a result of other nearby dipoles.

The technique involves rotating the powder samples at high speeds at the angle of 54.7^o called magic angle with respect to the applied magnetic field direction. Thus the anisotropic interactions get averaged out in time during fast spinning. Rapidly spinning the sample at the magic angle w.r.t. B_o, (5 to 35 kHz) nullifies the effect from the $3\cos^2\theta-1$ containing term, thus, improving the resolution of NMR spectra.

2.3.4. Surface studies

The surface properties of biomaterials have been shown to influence the interactions at the tissue–implant interface, thus controlling their response when implanted inside the human body. Hence it is necessary to investigate the surface modification of samples when immersed in body fluid. The following section provides some basic information of surface techniques used for in-vitro studies.

2.3.4.1. XPS

XPS technique provides excellent information about the elements and their oxidation states. XPS studies were carried out on a custom-built XPS machine. The sample was excited by Mg-K_α radiations ($h\upsilon$=1254.6 eV), photoelectron spectra were analyzed using a VG make CLAIM 2 analyzer system in the energy range of 0-1000 eV. The samples were mounted on a specimen holder using silver paste. The conducting path was provided from bottom to the top surface of the sample by silver paste, to avoid the surface charging effect. The sample chamber was then evacuated to a vacuum better than 1×10^{-9} Torr.

2.3.4.2. SIMS

TOF-Static-SIMS studies were carried out on a custom-built TOF SIMS machine (KORE Technology, UK). The instrument has an operating pressure of < 1×10^{-9} mbar. Samples were bombarded with a pulsed liquid metal ion source ($^{69}Ga^{+}$), at an energy of 20 keV. The gun was operated with a 20 ns pulse width, 0.9 pA pulsed ion current for a dosage lower than 5×10^{11} ions cm^{-2}, well below the threshold level of 1×10^{13} ions cm^{-2} for static SIMS. Secondary ions were extracted with a wide angle secondary ion extraction column, mass analyzed with a two-stage Reflectron time-of flight analyzer (RTOF) and detected and counted by a microchannel plate (MCPs) and a time-todigital converter (TDC). Measurements were performed with a typical acquisition time of 100 s, at a TDC time resolution of 500 ps. Charge neutralization was achieved with an electron flood gun. Secondary ion spectra were acquired from an area of 50 µm × 50 µm. The maximum mass resolution, R = m/Dm, was > 10,000, where m is the target ion mass and Dm is the resolved mass difference at the peak half-width. All ion images were acquired over 5 µm × 5 µm, with 128 × 128 pixels (1 pulse per pixel), using at least at three different positions per sample. Chemical imaging is done by rastering the primary beam on the sample surface and selecting regions of interest (ROI) in the mass spectrum. Thus, by putting suitable time-windows, the dispersion of individual elemental/chemical information on the sample surface is obtained.

2.3.4.3. Scanning electron microscopy (SEM)

It is near surface technique useful for studying the surface morphology and microstructure of the samples. SEM uses electrons instead of light to form an image. Interaction of the electrons of moderate energy (20-25 keV) with the matter gives rise to a number of signals from the sample which can be used to know the microstructure of sample (***Fig. 2.8a***). A beam of electrons is produced at the top of the microscope by heating of a metallic filament. The electron beam follows a vertical path through the column of the microscope. It makes its way through electromagnetic lenses which focus and direct the beam down towards the sample. Once it hits the sample, other electrons (backscattered or secondary) are ejected from the sample (***Fig. 2.8a***).

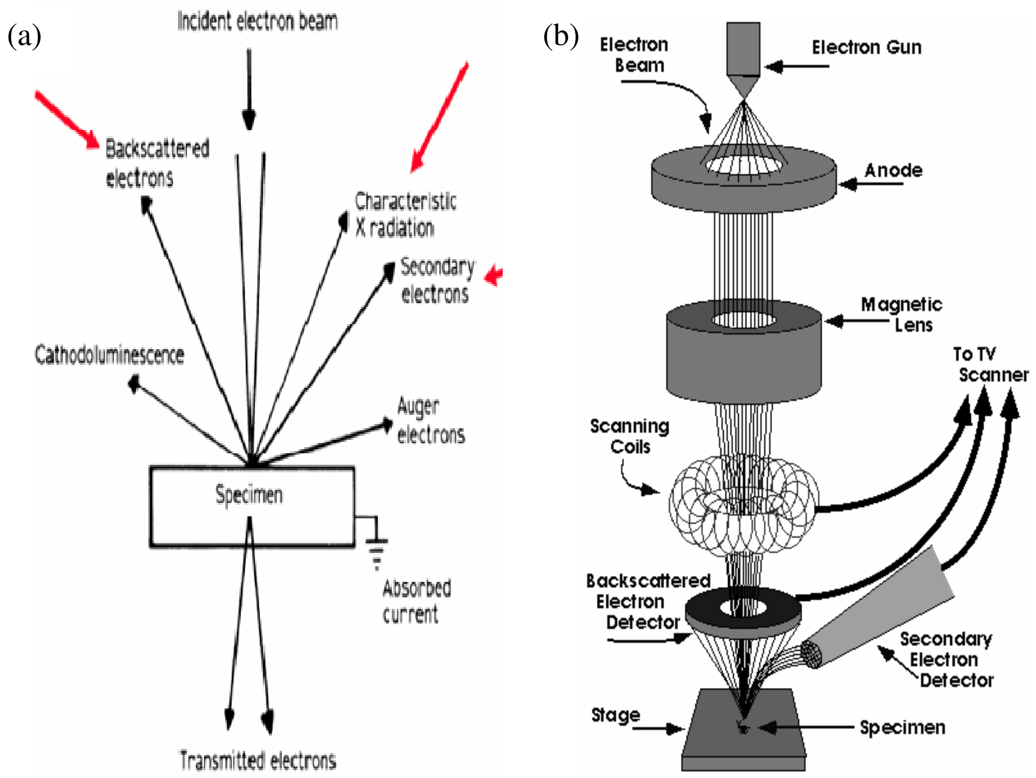

Fig.2.8 *(a) Interaction of electrons with the matter (b) Schematic of SEM.*

Detectors collect the secondary or backscattered electrons, and convert them to a signal that is sent to a viewing screen similar to the one in an ordinary television, producing an image. The secondary electrons constituting the signaling emission mode are normally preferred as they give rise to a large signal and enable viewing areas of the sample that are not in direct line of vision of the collector. SEM is particularly useful in studying the microstructure of the materials. In our studies, the morphological analyses were carried out by means of SEM (Model: Tescan Vega MV 2300T/40) technique. This technique is also useful to study the interface of the glass-to-metal seals.

2.3.5. Magnetic characterization

2.3.5.1. SQUID (Superconducting Quantum Interference Device) measurement

The magnetic response versus applied magnetic field H was measured at room temperature, with $|H| \leq 5$ kOe using SQUID magnetometer (Quantum Design – MPMS5). These data have been analyzed to obtain the saturation magnetization ($M_{s)}$, remnant magnetization ($M_{r)}$, and coercive field (H_c) for each sample. The samples were also subjected to zero field cooled (ZFC) and field cooled (FC) measurements. For zero field cooled measurement, the sample was cooled initially to low temperature in the absence of magnetic field. At low temperature, the field was applied and measurement was performed upto room temperature. In case of FC measurements, the sample was cooled in the presence of magnetic field from room temperature to low temperature and data was taken.

2.3.5.2. Mössbauer

The basic elements of a Mössbauer spectrometer are a source, sample, detector, and a drive to move the source or absorber. Most commonly, this is done by moving the source toward and away from the sample, while varying velocity linearly with time. For example, for ^{57}Fe, moving the source at a velocity of 1 mm/sec toward the sample increases the energy of the emitted photons by about ten natural line-widths. For simplicity, "mm/sec" is the conventional "energy" unit in Mössbauer spectroscopy. It is also possible to leave the source stationary and oscillate the sample, as is done with synchrotron Mössbauer. The location of the detector relative to the source and the sample defines the geometry of the experiment; most commonly, either transmission or backscatter modes as shown in ***Fig. 2.9***. The decay of ^{57}Co to ^{57}Fe, emission of γ-ray and all probable interactions with the absorber are shown in ***Fig. 2.10***.

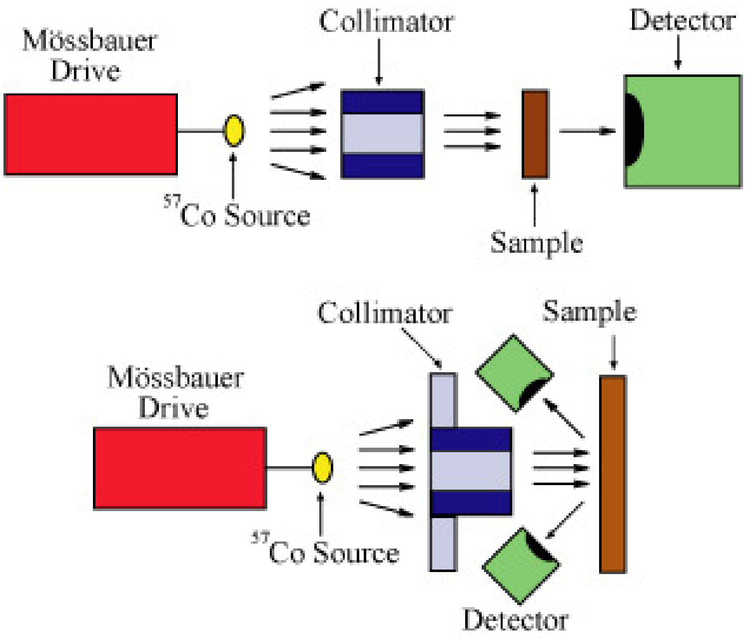

Fig. 2.9. *Geometry of the experimental set up with transmission and backscatter modes.*

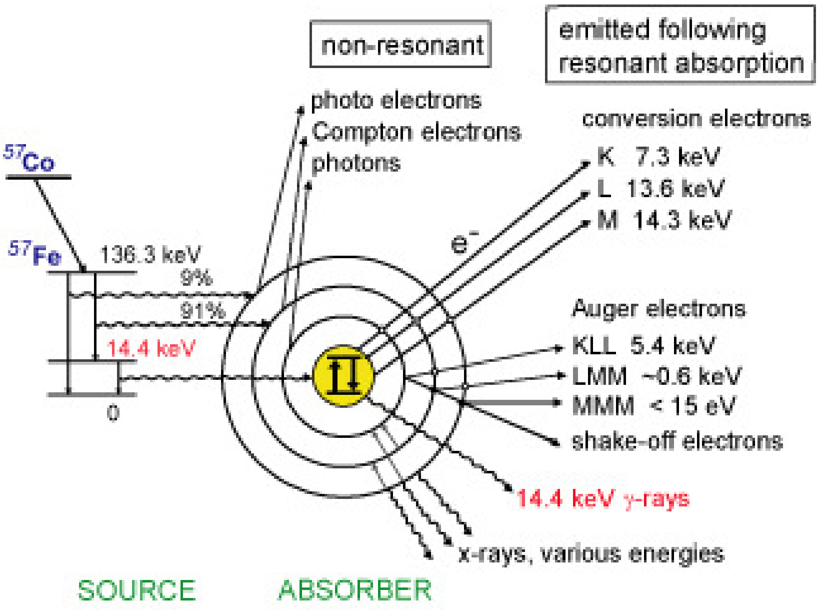

Fig. 2.10. *The decay of ^{57}Co to ^{57}Fe, emission of γ-ray and all probable interactions with the absorber.*

For the present study Mössbauer spectra were obtained using a spectrometer (Nucleonix Systems Pvt. Ltd., Hyderabad, India) operated in constant acceleration (triangular wave) mode in transmission geometry. The source employed was ^{57}Co in Rh matrix of strength 50 mCi. The calibration of the velocity scale was done using α-iron metal foil. The outer line width of calibration spectra was 0.29 mm/s. Mössbauer spectra were fitted by a least square fit programme assuming Lorentzian line shapes.

2.3.6. Seal fabrication

Silicate glasses containing low phosphate content are studied for sealing applications. The major requirements of sealing material for SOFC application is good gas tightness at the high operating temperature (600-800°C), thus, glass-to-metal seals are prepared and sealant materials are tested for adherence and stability at high temperature.

The process involves three stages;

2.3.6.1. Glass preparation

The glasses were powdered and sieved to obtain the average particles size less than 63μm. The slurry was made in water or in acetone for applying on the metal surface.

2.3.6.2. Cleaning of metal

Metal parts were cleaned with organic solvent and soap solution to remove grease. The cleaned metal parts were washed under running tap water and later dried.

2.3.6.3. Fabrication of glass-to-metal (GM) seal

GM Seal were fabricated in a resistance-heating furnace having PID temperature controller. Seals were made at around 950-1000°C. The temperature was held for 30-45 minutes and then slowly cooled to room temperature. The seal thus fabricated are tested using pressure and vacuum testing.

2.3.7. Testing of seals

GM seals fabricated were tested either for their pressure endurance or vacuum leak rates.

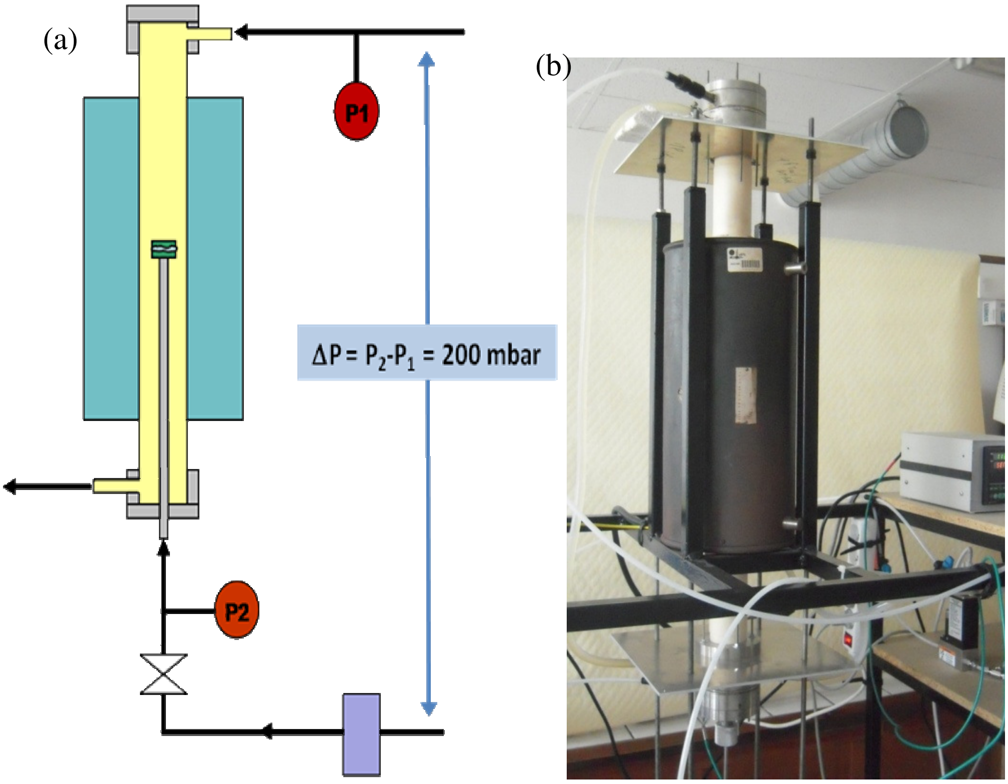

Fig. 2.11. *Testing of seals under pressure; (a) Block diagram, and (b) Photograph; of experimental set up.*

2.3.7.1. Pressure testing

The GM seals were tested on a pressure test set up as shown schematically in ***Fig.2.11.*** The seal was securely mounted on a platform. The GM seal was pressurized with argon gas of 200 mbar pressure. The pressure was monitored by pressure gauges. If the seal was leaky, the pressure immediately drops to zero level.

2.3.7.2. Vacuum testing

Fig.2.12 shows schematic of a conventional type MS leak detector. The GM seal was connected to a vacuum system using a suitable jig. The vacuum system has a diffusion pump backed by the rotary pump.

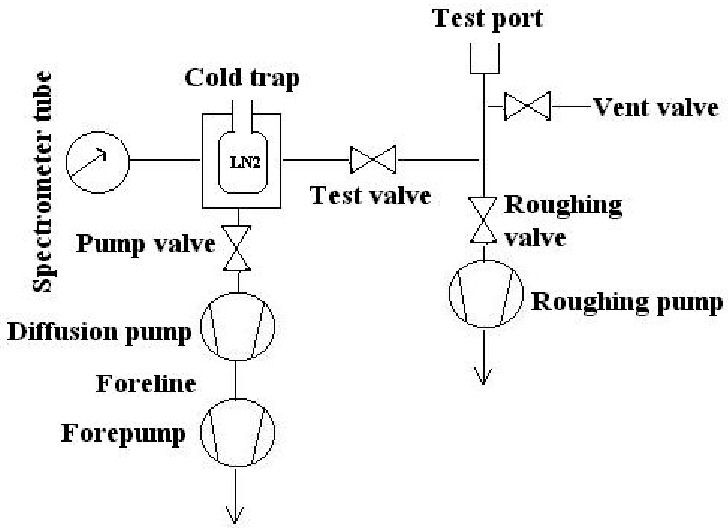

Fig.2.12. *Conventional type of the helium leak detection apparatus.*

The system is initially evacuated using rotary vacuum pump to about 10^{-3} mba. It is further evacuated to 10^{-6} mbar using oil diffusion pump and liquid N_2 trap to condense the oil and water vapors. Thus, the GM seal is tested upto 10^{-6} torr. The Helium leak rate is measured by passing Helium gas through the system and the rate at which Helium leak out is analyzed in the mass spectrometer.

Chapter 3

Structural, microstructural and in-vitro studies of calcium silico-phosphate glass/ glass-ceramics containing iron oxide

---

In this chapter, preparation and results on structural, micro-structural and magnetic properties of glass/glass-ceramics with nominal composition $34SiO_2$*-*$(45-x)CaO$*-*$16P_2O_5$*-*$4.5\ MgO$*-*$0.5CaF_2$ *–*xFe_2O_3 *(where x = 5, 10, 15, 20 wt %) are discussed.*

3.1 Introduction

3.2 Experimental

3.3 Results and discussion

3.4 Conclusion

3.1. Introduction

Calcium-silico-phosphate glasses have potential as implant materials for human body because of their bioactivity and biocompatibility. Hench et al [88] have reported the first bioactive glass having composition (wt %) 45% SiO_2, 24.5% Na_2O, 24.5% CaO and 6% P_2O_5 commonly known as 45S5. Since then many glasses with modified 45S5 or different compositions have been developed to improve the bioactive response of the materials [89, 90].

Biocompatibility and bioactivity properties of the material are surface phenomena [42, 91]. The formation of Si–OH functional groups takes place at the surface when the material interacts with body fluid [42]. These Si–OH groups take part in the subsequent reactions and lead to the formation of bioactive layer. Thus, optimum response of the materials can be influenced by the surface properties of the materials, which are closely related with the structural properties of the materials.

Structural and surface properties of glass/glass-ceramics can be modified by varying the composition of alkaline earths like CaO, MgO and ZnO in glass matrix [43, 92-94]. The glasses with improved surface activity are obtained when calcium oxide is partially replaced by magnesium oxide [43]. Addition of alumina tends to decrease the bioactivity of these glasses [95]. Improvement in the bioactive response of glasses has been observed with addition of small amount of P_2O_5 [96].

Preparation of glass–ceramics in SiO_2–CaO–Fe_2O_3, SiO_2–CaO–Fe_2O_3–B_2O_3–P_2O_5, SiO_2–Al_2O_3–Fe_2O_3–P_2O_5–Li_2O and CaO-SiO_2–P_2O_5-Na_2O-Fe_2O_3 bioglasses, have been reported [97-99]. These glasses and glass–ceramics show an important application in cancer treatment by elimination of cancerous cells in bones; by means of hyperthermia [100]. The magnetic properties arise from magnetite [Fe_3O_4] that is produced from the Fe_2O_3. When this material is placed in the region of the tumor and is subjected to an alternating magnetic field, heat is generated by hysteretic losses [101-103]. The tumor is effectively heated and the temperature locally rises to 42–45 °C. As a result, the cancerous cells perish while the healthy ones survive [104-106].

Magnetic properties of these materials depend on the quantity and the environment of Fe ions, therefore the knowledge of oxidation states of iron ions is important for better understanding of the magnetic properties of glass and glass-ceramic. Further, desired magnetic response can be obtained by controlling the content of iron oxide (magnetic phase) in the glass structure. Higher amounts of Fe_2O_3 would result in an improved magnetic properties but the bioactive response is limited by the glass forming capability of the system. In this chapter, preparation and results on structural, micro-structural and magnetic properties of glass/glass-ceramics with nominal composition $34SiO_2$-(45-x)CaO-$16P_2O_5$-4.5 MgO-0.5CaF_2 –xFe_2O_3 (where x = 5, 10, 15, 20 wt %) are discussed. This system is of particular interest due to its both magnetic and bioactive properties. The effect of Fe_2O_3 on magnetic and bioactivity related properties in SBF and bovine serum albumin (BSA) was studied. The surface modifications of these samples as a function of exposure time in SBF and BSA were investigated by XPS and SEM/EDX. The dissolution behaviour in the solution was explained on the basis of the surface reactions.

3.2. Experimental

Base glasses of nominal compositions as given ***Table 3.1*** were prepared by melt quench technique. About 100 g batches were prepared by mixing reagent grade SiO_2, $CaCO_3$, NH_4 H_2PO_4, $MgCO_3$, Fe_2O_3, and CaF_2. The charge was calcined at maximum of 900°C for 12 h, holding at intermediate temperature for 6-8 h, decided by the decomposition temperatures of various precursors. To ensure complete decomposition of carbonates into oxides, the batch was weighed before and after calcinations of the precursors. The calcined charge was melted under air ambient at 1500°C in a Pt-Rh crucible in a raising lowering hearth electric furnace

(Model OKAY R-70 M/s Bysakh and Co. Kolkatta). The melt was held for 2 h at this temperature for homogenization and then poured into a graphite mould followed by annealing at 600°C. Glassy nature was confirmed by XRD. The base glass was powdered in a ball mill and pelletized using a hydraulic press. They were converted into glass-ceramics (hereafter called FBC) through controlled heat treatment using DTA data. Glass-ceramics FBC5, FBC6, FBC7 and FBC8 with iron concentration 5, 10, 15 and 20 wt% respectively, were heat treated at 1000ºC for six hours.

Table 3.1. *Nominal composition of starting charge investigated (wt. %).*

Sample	SiO2	P_2O_5	CaO	MgO	Fe_2O_3	CaF_2
FB5	34	16	40	4.5	5	0.5
FB6	34	16	35	4.5	10	0.5
FB7	34	16	30	4.5	15	0.5
FB8	34	16	25	4.5	20	0.5

Archimedes principle was employed to measure the density of all glasses using water as immersion fluid as described in chapter 2. Glass samples were made flat by polishing and used for thermo-mechanical analysis (TMA). TMA was employed to measure the thermal expansion coefficient (TEC), glass transition temperature (T_g). The experiments were carried out in a precisely controlled furnace under flowing Ar ambient. Sample expansion was measured using a hemispherical silica probe with the sample under compressive load of 50g.

DTA measurements on glass powders were performed on a Setaram Labsys (TG/DTA) apparatus that was calibrated using the melting points of high purity indium and zinc as mentioned in chapter 2. The non-isothermal experiments were performed by heating approx. 40 mg of the sample in Alumina crucibles under protective ambient, using empty

Alumina crucible as a reference. A heating rate of 10° K/min was employed in the range 25-1100°C.

The Fourier transform infra-red (FTIR) spectra of the sample were recorded by using using a Bomem D8 Fourier transform spectrometer. For FTIR measurements glass powders were mounted in KBr pellet. FTIR spectra were recorded in the 400-2000 cm^{-1} range. The emergence of different crystalline phase as a result of heat treatment was studied using X-Ray diffraction (XRD). XRD of the powder sample was carried out on Philips PW 1710 X-ray diffractometer.

The magnetic response versus applied magnetic field H was measured at room temperature, with $|H| \leq 5$ kOe using a Superconducting Quantum Interference Device (SQUID) magnetometer. These data have been analyzed to obtain the saturation magnetization ($M_{s)}$, remnant magnetization ($M_{r)}$, and coercive field (H_c) for each material. Mössbauer spectra have been obtained using a spectrometer operated in constant acceleration mode. The source employed is ^{57}Co in Rh matrix of strength 50mCi. The Mössbauer spectra are fitted with appropriate paramagnetic doublets and magnetic sextets using least square fit program. The ratio of Fe^{2+} and Fe^{3+} ions has been determined from the relative areas obtained by computer fitting of experimental spectra.

For in-vitro studies, the pellets were immersed in simulated body fluids (SBF) solution for 1-4 weeks, incubated at 37.4ºC. After the exposure to SBF, samples were removed and their surfaces were analyzed using SEM/EDX. BSA solutions were prepared in buffer (tris-buffer) at pH of 7. All solutions were prepared in high purity water. The glass-ceramics pellets were immersed and incubated at 37.4°C in solution for different time periods. The samples were removed and their surfaces were analyzed using XPS, SEM and TOF-SIMS.

3.3. Results & discussion

3.3.1. Density

Densities of the as prepared glasses increase marginally with an increase in Fe_2O_3 content. Densities varied in the range of 2.96 to 3.06 g/cc (***Fig. 3.1***). In glasses, Fe_2O_3 was added at the expense of CaO, which has a relatively higher density. Thus, marginal increase in the densities of glasses was observed.

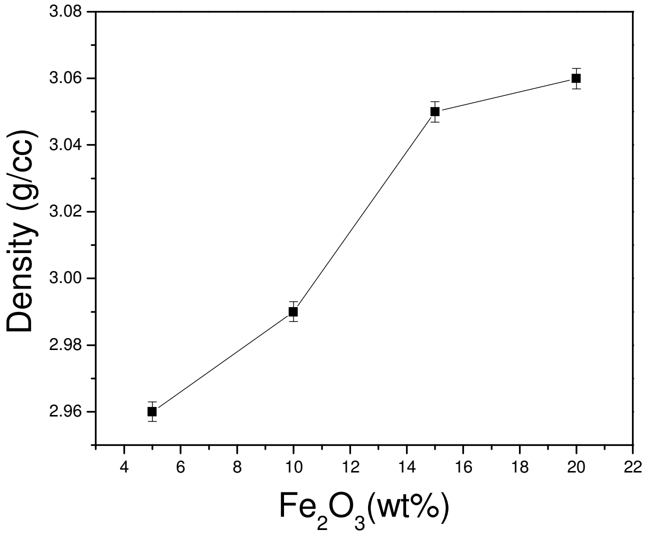

Fig. 3.1. *Densities of glass samples having different content of* Fe_2O_3.

3.3.2. Thermal characterization

Fig. 3.2 *shows the* variation in T_{soft} and TEC of glass samples having different content of Fe_2O_3. TEC values of the glass samples increased from 9.6×10^{-6} °C^{-1} to 12×10^{-6} °C^{-1} as iron oxide content was increased upto 15 wt % and then decreased to 8.78×10^{-6} °C^{-1} with an increase of iron oxide content to 20 wt %. It was observed that the glass transition temperature decreased with increasing Fe_2O_3 content upto 15 wt % and then increased with increase in Fe_2O_3 content. T_g found to be decreased from 715°C to 665°C as Fe_2O_3 was increased from 5 to 15 wt %. Tg was minimum for a glass with 15 wt % of Fe_2O_3 and showed a slight increase with increase in the Fe_2O_3 content to 20 wt.%.

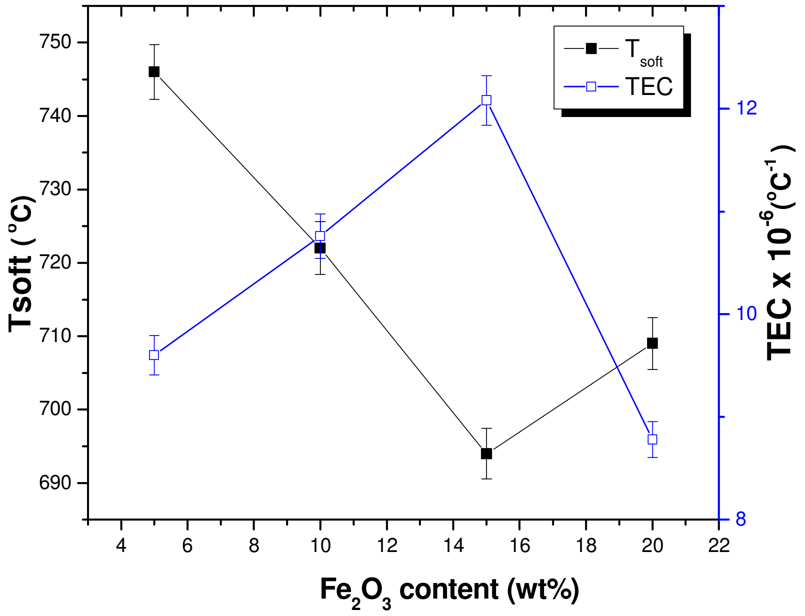

Fig. 3.2. *Variation in T_{soft} and TEC of glass samples having different content of Fe_2O_3.*

An increase in modifier content is expected to decrease the connectivity of the network, creating more non-bridging oxygens (NBOs). Consequently the network becomes weaker and thus requires lesser energy to break. Thus when iron oxide is added to glass network, it acts as a modifier at least up to this composition (~15 wt.%). The decrease in T_g and T_{soft} reflects weak bonding in the glass network. However, when Fe_2O_3 was added beyond 15 wt. %, there was marginal increase in T_g and decrease in TEC. This indicates the formation of relatively stronger glass network and therefore suggested that the addition of Fe_2O_3 stabilized the glass network at higher concentration i.e. beyond ~15wt. %.

DTA plots are shown in ***Fig. 3.3.*** Sample with 5 wt. % Fe_2O_3 showed two closely spaced crystallization peaks around 858°C and 875°C. The peak temperature of crystallization (T_p) for glass samples decreased with the addition of Fe_2O_3. The peaks were relatively broader for sample having 5 wt % iron oxide and became sharper with addition of iron oxide content. In addition, we observed that the crystallization peaks tended to come closer as the iron oxide content was increased to 15 wt. %. The sample having 20 wt. % iron oxide showed one prominent crystallization peak around 728°C having small shoulder around

768°C. This is thought to be due to modification in local structure in glass, thereby enhancing nucleation and crystallization.

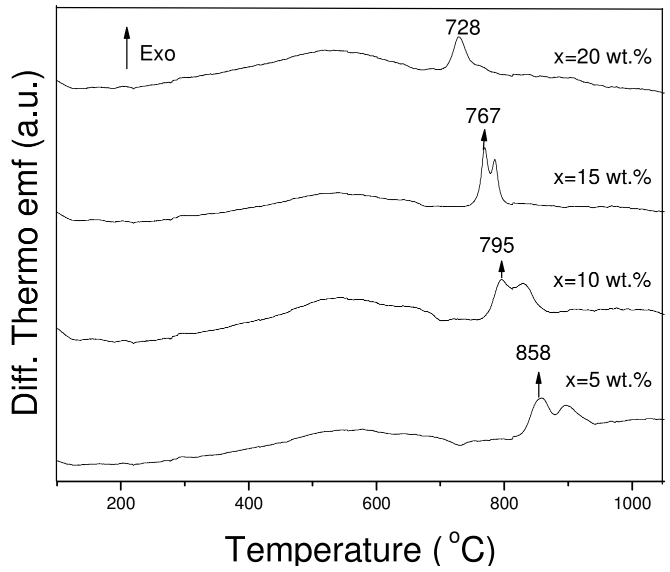

Fig. 3.3. *DTA of glass samples having different content of* $Fe_2O_3(x)$.

3.3.3. Structural characterization

3.3.3.1 FTIR measurements

IR spectroscopic studies carried out on glass samples revealed useful information regarding the modification in various structural units. ***Fig. 3.4*** shows the IR spectra of glass samples having different iron content. The spectra of glass having 5 wt.% iron oxide showed the broad absorption band around 1050 cm^{-1}. This band was associated with two shoulders around 800 cm^{-1} and 1000 cm^{-1}. When 10 wt % iron oxide was added, the shoulder at lower wave number diminished and finally disappeared in the glass sample having 20 wt.% iron oxide. In addition, the band around 460 cm^{-1} having shoulder at 550 cm^{-1} started appearing. When the iron oxide content increased to 15- 20 wt. % the broad bands around 450 cm^{-1} and 550 cm^{-1} became pronounced.

FTIR spectra of all the samples, in general exhibited broad absorption bands in the region of 300–1500 cm^{-1}, which implies the disorder in the glasses. The broad bands in the 800–1300 cm^{-1} are assigned to the stretching vibrations of the SiO_4 tetrahedron with a different number of bridging oxygen atoms, while the bands in the 300–600 cm^{-1} regions are due to bending vibrations of Si–O–Si and Si–O–Ca linkages [108-110]. A slight shift towards higher wave numbers was registered in the 800–1300 cm^{-1} band with the addition of 20 wt. % Fe_2O_3. This suggests that iron oxide polymerizes the silicate glass network at higher content. The absorption bands in the 540–650 cm^{-1} as evident in ***Fig. 3.4***, became stronger with an increase in Fe_2O_3 are related to the stretching vibrations of the Fe-O bonds [111].

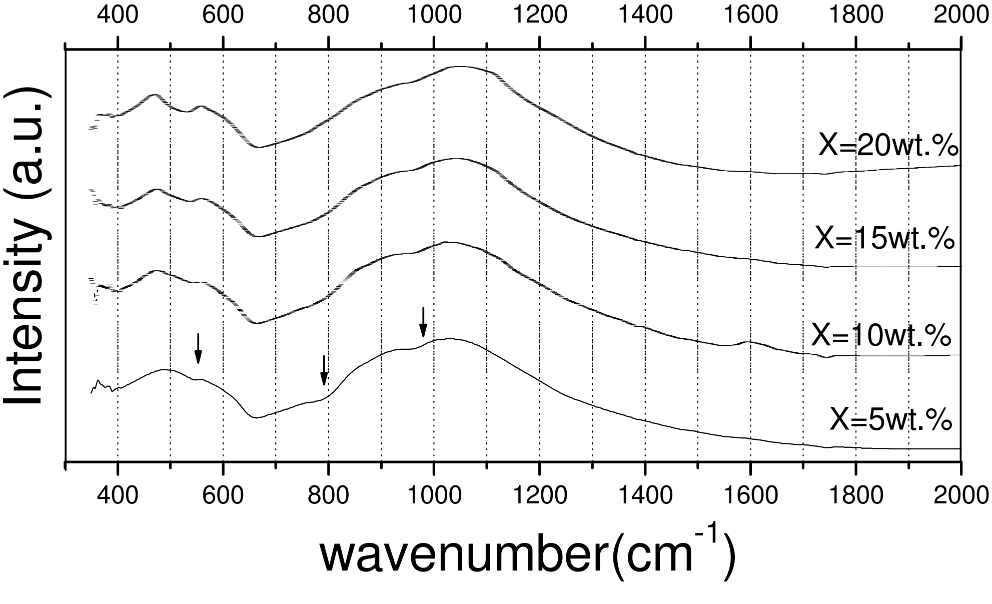

Fig. 3.4. *IR spectra of glass samples having different content of* $Fe_2O_3(x)$.

3.3.3.2 ESCA

X-ray photoelectron scans were recorded in the binding energy (BE) region 0 to 1000 eV. The peaks for the constituent elements were identified and marked on the spectra. XPS spectra of glass samples are shown in ***Fig. 3.5***. The peak at the binding energy around 284.6 eV was assigned to the C1s core level and used as a reference for assigning the other peaks.

The peak at around 346 eV assigned to Ca2p, decreased in intensity as the Fe_2O_3 content was increased. The O1s photoelectron spectra for different glass samples are shown in ***Fig. 3.6.*** The peak shape was changed with an increase in Fe_2O_3 content and the maximum peak width (FWHM) was observed for 10 wt. % Fe_2O_3 (FB6).

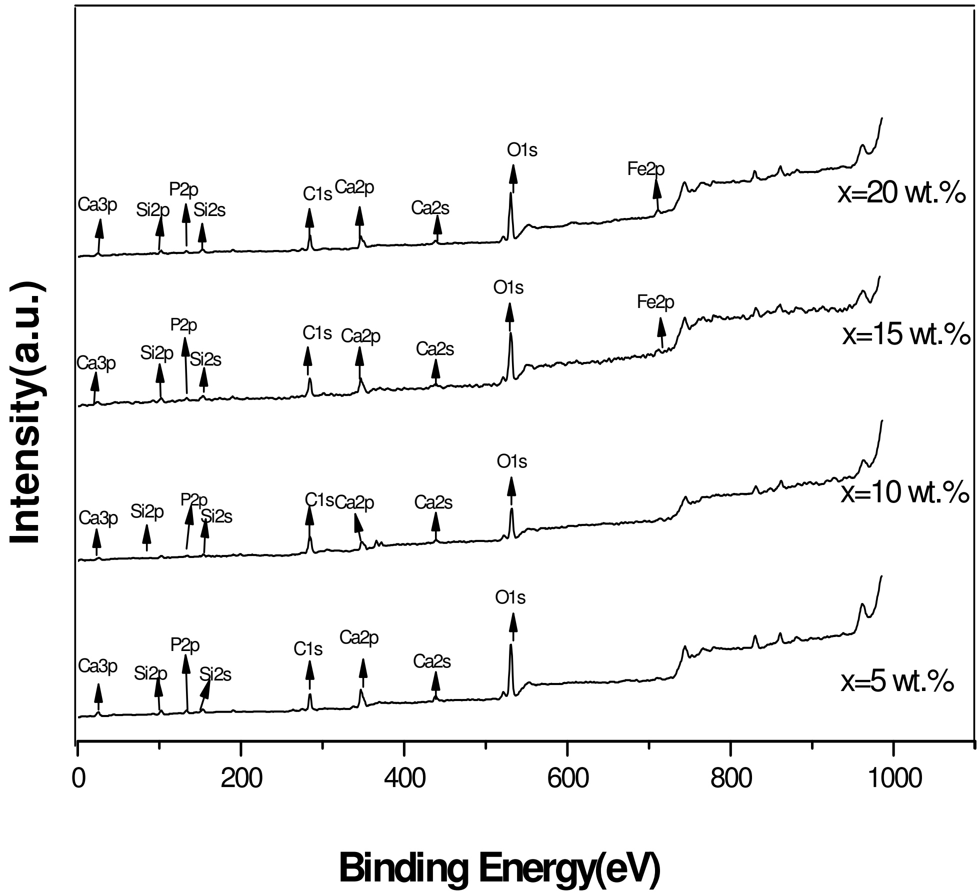

Fig. 3.5*. XPS spectra of glass samples having different content of* $Fe_2O_3(x)$.

XPS technique can be used to resolve the contributions to the O1s core level spectrum from the bridging and non-bridging oxygen atoms [112-113]. The curve fitting of O1s photoelectron plot for the samples having different amount of iron oxide is shown in ***Fig. 3.6***. The low binding energy peak at ~ 530 eV corresponds to the contribution from the non-bridging oxygen atoms, while the peak at ~ 531 eV is attributed to the bridging oxygen. The areas of the two peaks (non–bridging and bridging) were calculated to find out the fraction of non-bridging oxygen (***Table 3.2***). The fraction of non bridging oxygens first increased (upto 15 wt. % of iron oxide) and then decreased at the higher iron oxide content (20 wt.%).

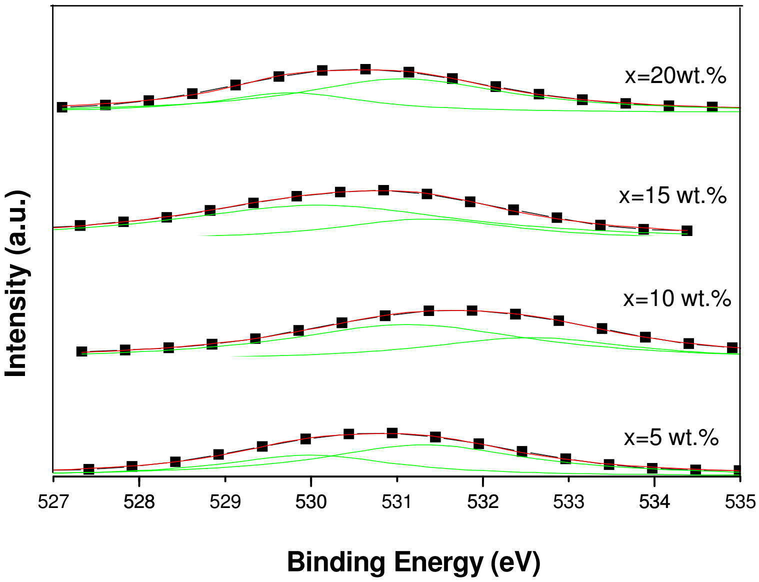

Fig. 3.6. *XPS for Oxygen of glass samples with peak fitting.*

When Fe_2O_3 is added in the silica network, the electronic density of the bonding states of the silicon and oxygen atoms are modified. The difference between bridging and non-bridging oxygen atoms is reflected in the XPS chemical shift of the O1s peak (***Fig. 3.6***). This shift in core level transitions in an XPS spectrum is sensitive to oxidation states. If an element exists in more than one oxidation state, XPS spectrum of that element has more than one peak, each corresponding to a different oxidation state [114].

Table 3.2: *Ratio of structure units calculated from XPS data.*

Sample	Fraction of non bridging oxygen groups (NBO/BO)
FB5	0.56
FB6	0.64
FB7	0.72
FB8	0.30

The shift in the peak position is generally toward the higher binding energy as the oxidation state of the element increases. It was observed that the addition of iron oxide causes the fraction of non- bridging oxygens to increase with increase in iron oxide content to 15 wt% (***Table 3.2***). Further increase in iron oxide to 20 wt.% leads to decrease in the fraction of non-bridging oxygens, indicating stabilization of glass network.

3.3.3.3 XRD study

XRD patterns of the glass samples after heat treatment at 1000°C for 6h are depicted in ***Fig. 3.7***. The sample FBC5 showed the formation of apatite ($Ca_5(PO_4)_3(OH)$), wollastonite ($CaSiO_3$), magnetite and hematite phases. However, with an increase of iron oxide content to 10-20 wt %, relative intensity of peak corresponding to apatite (around 31°) decreased, while the intensity of wollastonite phase increased.

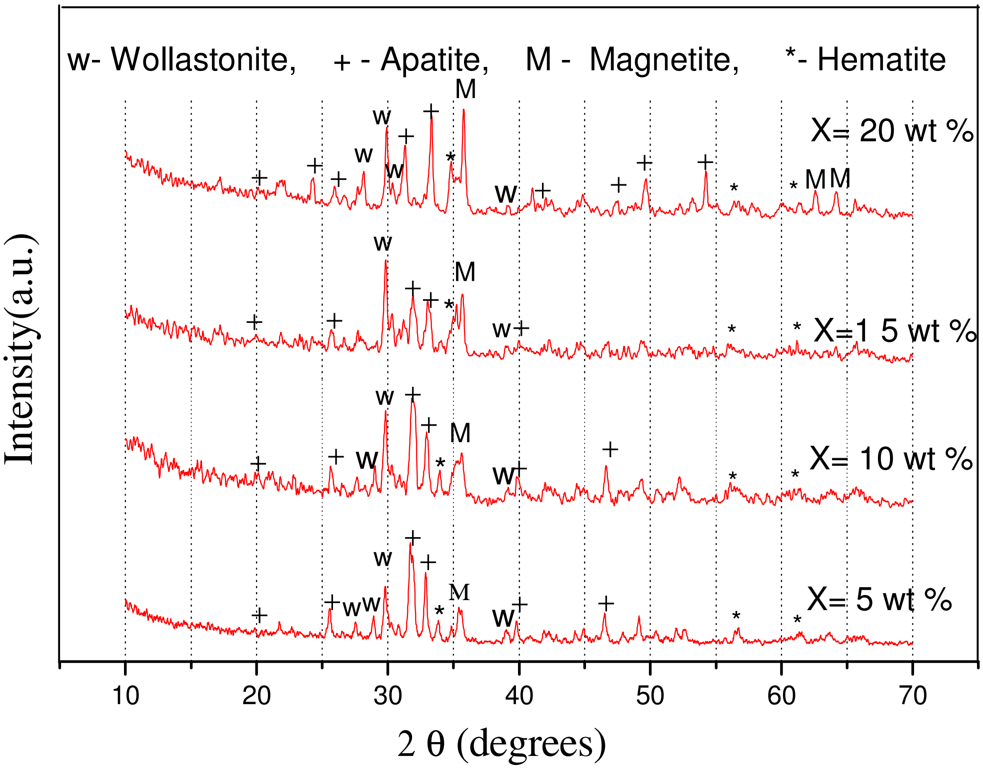

Fig. 3.7. *XRD of glass samples after heat treatment at 1000℃ for 6h.*

The formation of $CaSiO_3$ phase was expected as the CaO has the tendency to react with SiO_2 to produce this phase. Magnetite (Fe_3O_4) phase is responsible for the magnetic properties in the glass-ceramic samples.

This is formed in the glass matrix by the reaction given by

$$6Fe_2O_3 \rightarrow 4Fe_3O_4 + O_2 \qquad \textbf{(3.2)}$$

The conversion of hematite into magnetite depends on heat treatment of the base glass. It was observed that the intensity of peaks corresponding to magnetite phase has increased with an increase in Fe_2O_3 content.

3.3.4 Magnetic characterization

3.3.4.1 SQUID

M-H plots of the different glass-ceramic samples are shown in ***Fig. 3.8***. Magnetic parameters estimated from the M-H plot are given in ***Table 3.3***. Saturation magnetization increased with increase in Fe_2O_3 concentration from 10 to 20 wt.%. The quantity of magnetic phase present in the glass-ceramic samples was determined from the ratio of saturation magnetization of sample with that of magnetite (Ms =92 emu/g) [115].

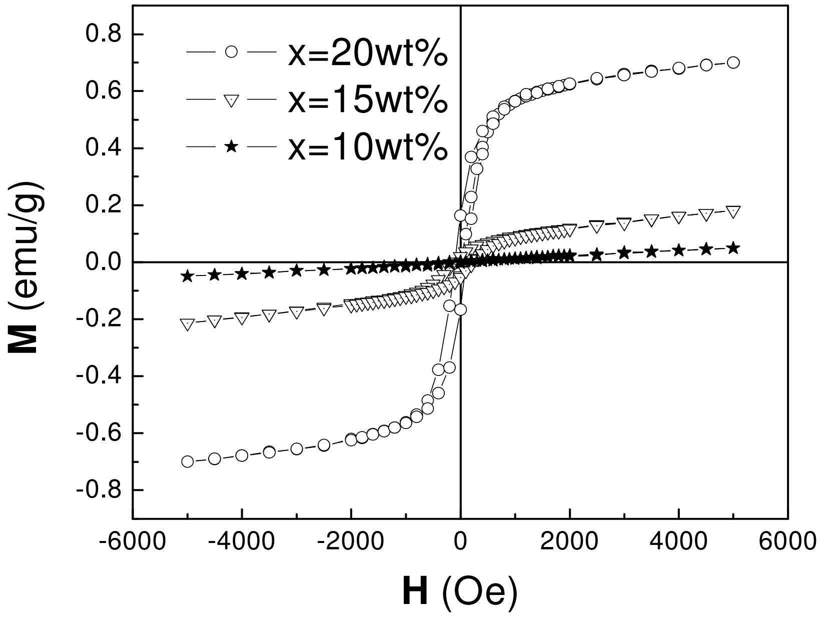

***Fig. 3.8**. M-H plots of the different glass-ceramic samples.*

Magnetic properties of glass-ceramics are attributed to the development of magnetite phase in the samples. The volume fraction of the magnetite phase was found to increase with an increase in Fe_2O_3 concentration, which resulted in an increased of saturation magnetization.

Table 3.3. *Magnetic parameters estimated from M-H plots*

Magnetic parameter	FBC6	FBC7	FBC8
M_s (emu/g)	0.0304	0.129	0.64
M_r (emu/g)	0.0037	0.020	0.164
H_c (Oe)	211	167	103
Magnetic Phase (wt %)	0.032	0.14	0.69
Hysteresis area (erg/g)	121.8	513	2795

3.3.4.2. ^{57}Fe Mössbauer spectroscopy

The Mössbauer spectra for different glass samples are shown in ***Fig. 3.9***. It was found that these spectra were composed of two paramagnetic doublets. Related Mössbauer parameters like isomer shift (IS), quadrupole splitting (QS) are given in ***Table 3.4***. Typical values of Fe^{3+} tetrahedrally (Th) coordinated to oxygen in silicate glass are in the range of 0.20–0.32 mm s^{-1} while for octahedrally (Oh) coordinated these values are in the range of 0.35–0.55 mm s^{-1}. For Fe^{2+} these values are in the range of 0.90–0.95 mm s^{-1}(tetrahedral) and 1.05–1.10 mm s^{-1} (octahedral) [116]. IS values indicate that in glass structure, Fe^{3+} and Fe^{2+} were in octahedral and tetrahedral coordination, respectively.

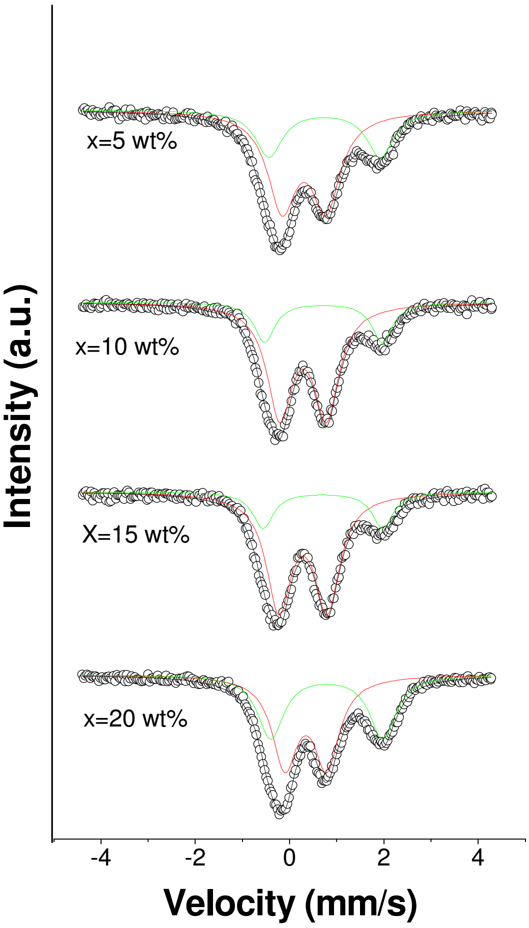

Fig. 3.9. *Mössbauer spectra for different glass samples.*

The presence of some iron ions in the Fe^{2+} state attributed to the reduction of Fe_2O_3 by the presence of MgO, CaO in the melt [117]. It was seen that in the glass containing 5 wt.% Fe_2O_3, nearly 68% of the total iron entered as Fe^{3+} ions in octahedral coordination i.e. entered in the glass as a modifier. The rest of iron ions entered in the glass as network former. The iron ions in the octahedral coordination increased to 78% of total iron ions, as Fe_2O_3 content was increased to 15 wt.%. When content of Fe_2O_3 was raised to 20 wt.%, the decrease in the Fe^{3+} (Oh) ions was observed, suggesting that the addition of Fe_2O_3 (x>15 wt.%) resulted in the formation of more of Fe^{2+} ions and stabilized the glass network.

***Table 3.4:** Various parameters obtained from Mössbauer spectra of glass samples.*

Sample	(Paramagnetic) Fe^{3+}				(Paramagnetic) Fe^{2+}				
	QS	IS	RI	Γ	QS	IS	RI	Γ	Fe^{2+}/Fe^{3+}
FB5	0.94	0.2916	68.16	0.7436	2.36	0.7274	31.84	0.6983	0.47
FB6	0.99	0.2724	77.30	0.6543	2.492	0.7015	22.69	0.5296	0.29
FB7	1.03	0.2717	78.89	0.6491	2.532	0.6888	21.11	0.5416	0.26
FB8	0.89	0.3440	57.09	0.6505	2.370	0.7864	42.90	0.6787	0.73

IS: Isomer shift (mm/s), QS: Quadrupole Splitting (mm/s), RI: relative intensity,
H_{int}: Internal Field (kG), Γ: Line width (mm/s), Com: component

It can also be seen in ***Table 3.4*** that the isomer shift value for Fe^{2+} ions of different components decreased with the increase in the Fe_2O_3 content upto 15 wt.%, then increased with increase in Fe_2O_3 content to 20 wt.%. This result can be attributed to the replacement of the iron (Fe_2O_3 with x=15 wt.%) in the network as former thus causing a decrease in the s electron density at the iron nuclei and hence an increase in the IS values. The increase of QS up to 15 wt.% Fe_2O_3 attributed to an increase in the asymmetry around the iron ions. Further, QS decreased with increase in Fe_2O_3 content to 20 wt.% as iron entered in network as former.

The Mössbauer spectra for different glass-ceramics samples are shown in ***Fig. 3.10*** and related Mössbauer parameters are given in ***Table 3.5***. On heat treatment of samples (FBC) magnetic and paramagnetic components were observed. The glass-ceramics samples with 5 and 10 wt.% Fe_2O_3 showed paramagnetic doublet arising from Fe^{3+} and Fe^{2+} ions. When Fe_2O_3 was increased to 15 wt.%, two magnetic (Fe^{3+} in octahedral coordination) and two paramagnetic components (Fe^{3+} in tetrahedral coordination) were observed. Further increasing of Fe_2O_3 to 20 wt.%, similar spectra (two magnetic and two paramagnetic contributions) were observed. In addition, the contribution of magnetic component increased to 48% in FBC8 from 35% in FBC7.

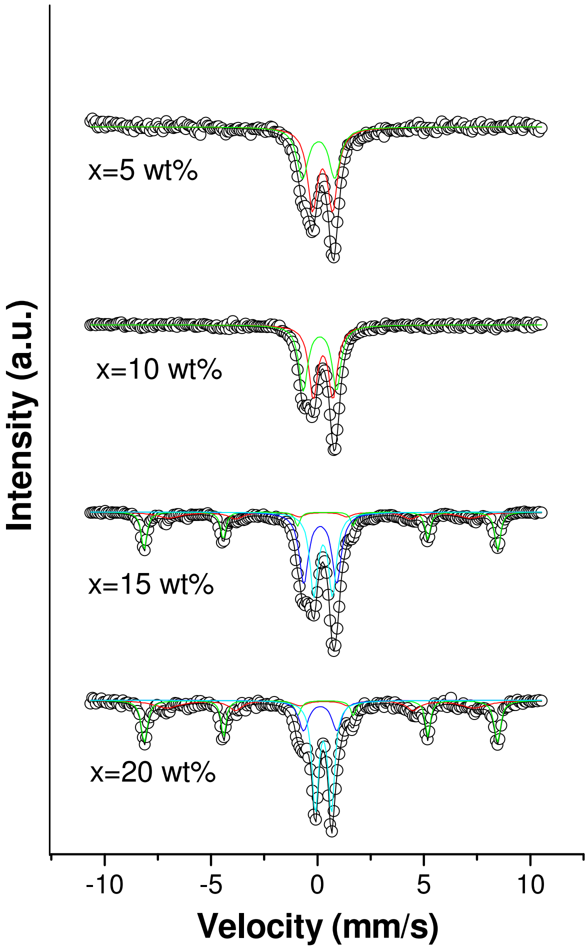

Fig. 3.10. *Mössbauer spectra for different glass-ceramics samples.*

Isomer shift values of these glasses suggest that Fe^{3+} ions were in octahedral coordination in magnetic component and in tetrahedral coordination in paramagnetic component. The spectra of FBC7 and FBC8 glass-ceramics had shown the two paramagnetic doublets and two sextets. The two sextets were associated to the nanostructure hematite and magnetite (FeO, Fe_2O_3) [118, 119] suggesting the presence of two kinds of Fe^{3+} ions in the glass-ceramics samples. This correlates well with the starting composition and XRD analysis of the sample, which had shown the presence of such a phase.

__Table 3.5:__ Various parameters obtained from Mössbauer spectra of glass-ceramics samples.

Sample	Com	Magnetic				Paramagnetic			
		H_{int}	QS	IS	RI	QS	IS	RI	Γ
FBC5	Com1					0.9480	0.2412	58.60	0.5688
	Com2					1.5147	0.0545	41.39	0.6305
FBC6	Com1					0.9281	0.2633	51.74	0.4915
	Com2					1.5592	0.1143	48.25	0.4966
FBC7	Com1	440.37	0.07	0.2636	14.92	1.5413	0.1316	32.33	0.5230
	Com2	515.90	0.10	0.3727	21.03	0.8813	0.268	31.70	0.4470
FBC8	Com1	448.07	0.09	0.3248	20.44	1.5570	0.1307	14.94	0.5493
	Com2	515.12	0.11	0.3844	28.28	0.7660	0.2761	36.32	0.3683

3.3.5. In-vitro study

3.3.5.1. In SBF

Chemical analyses of SBF solutions after immersion of glass-ceramics for 1- 2 weeks are given in ***Table 3.6***. It was observed that after 1 week of immersion, the concentrations of Si, Ca and P were increased slightly when compared to as prepared SBF concentration. Amount of Si leaching out from the surface increased marginally when the Fe_2O_3 concentration was increased from 10 to 20 wt.%.

__Table 3.6:__ Concentration (ppm) of different constituents of SBF solution

Sample		Si	Ca	P
FBC6	One week	14	1.5	83
	Two weeks	53	26	19
FBC7	One weeks	14	1.1	77
	Two week	17	13	10
FBC8	One weeks	18	0.8	79
	Two weeks	27	15	21
SBF		12	0.9	77

The pH of the SBF solutions was also monitored during the experiment. ***Fig. 3.11*** shows the change in pH during the course of experiment. The pH was found to increase from

7.4 to 8.2. Initially, pH was increased sharply from 7.4 to 8.1 (up to 1 week) and then it increased gradually from 8 to 8.3 for 1–4 weeks.

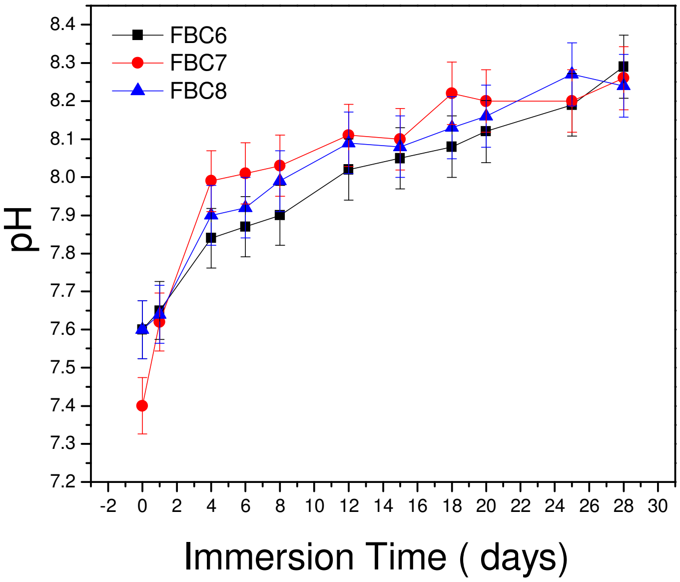

Fig. 3.11. *pH of SBF solutions at different time periods during immersion of samples.*

3.3.5.1. XPS analysis

XPS analysis was used to study the surface modifications of samples in SBF. XPS scans of as prepared FBC6, FBC7 and FBC8 glass-ceramic were compared with XPS spectra of these samples immersed in SBF for 1 week (***Fig. 3.12(a–c)***). We observed that the intensities of peaks corresponding to Si and P varied with the increase in the immersion time of samples. The XPS spectra also showed the appearance of the N1s core level signal which was absorbed from the solution. XPS scans of FBC7 samples immersed in SBF for 2 weeks and 4 weeks are compared in ***Fig. 3.12d***, which showed the depletion of Si with an increase in immersion time. There was also an increase in intensity of peaks corresponding to P. The sample surface got depleted of Si and Ca during its interaction with SBF, which was evident from these spectra. ***Fig. 3.12e*** shows the surface composition for glass-ceramics samples after different immersion times in SBF. With exposure to SBF solution (1-2 weeks) percentages of Si remained very low while that of P increased implying the growth of Ca–P rich phase.

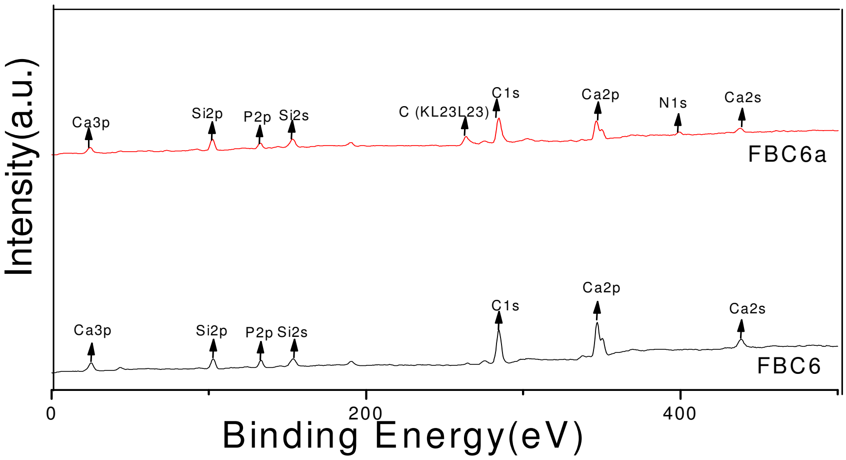

Fig. 3.12a. *XPS of FBC6 before and after immersion (FBC6a) in SBF for 1 week.*

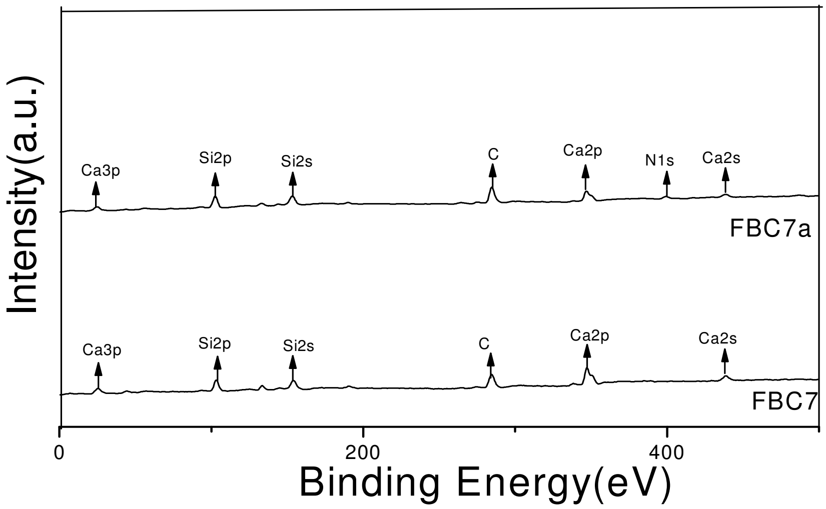

Fig. 3.12b*. XPS of FBC7 before and after immersion (FBC7a) in SBF for 1 week.*

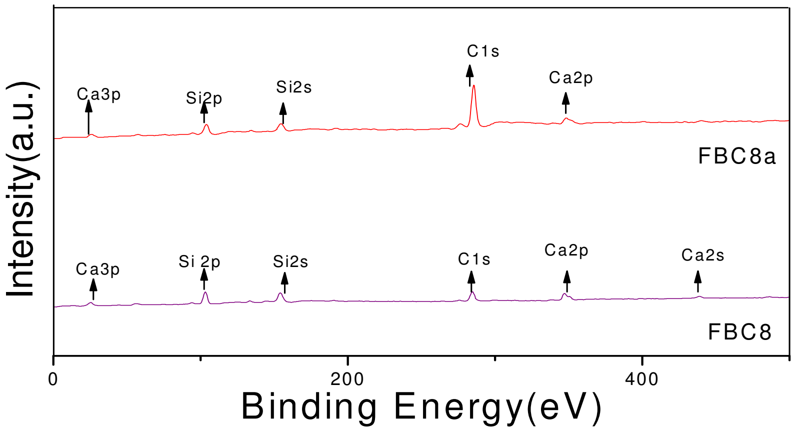

***Fig. 3.12c**. XPS of FBC8 before and after immersion (FBC8a) in SBF for 1 week.*

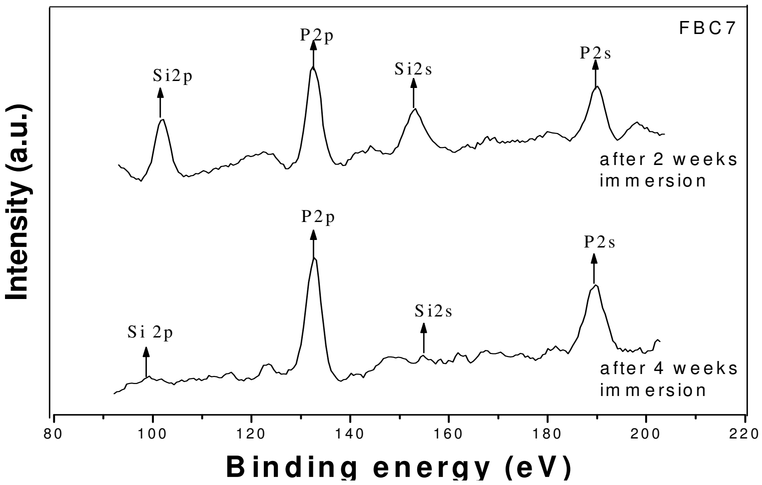

week.

***Fig. 3.12d**. XPS of FBC7 after immersion in SBF for 2-4 weeks.*

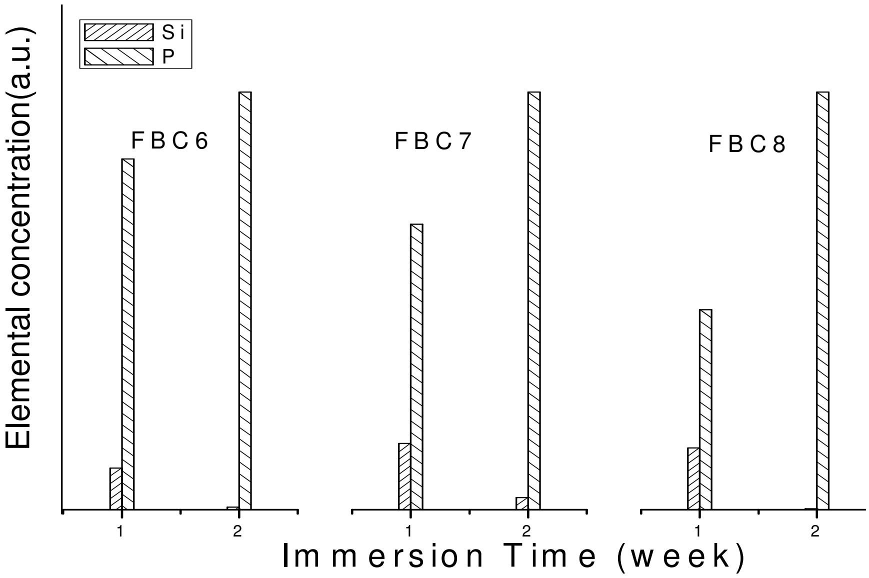

***Fig. 3.12e.** Surface composition (Si & P) for glass-ceramics samples after different time of immersion in SBF.*

3.3.5.1.2 SEM analysis

The SEM images of the glass-ceramic samples before immersion in SBF are shown in ***Fig. 3.13(a-c)***. The specimen with 10 wt % iron oxide reveals a granular microstructure (***Fig. 3.13a***). The grain size of particles measured was around 40 nm. Microstructure exhibited the formation of needle like feature along with coarse precipitates when Fe_2O_3 content was increased to 15 wt % (Fig. 3.13b). The length of needle varied from 250 nm to 1000 nm with width around 50 nm. The homogeneity of the microstructure was seen at the higher iron concentration (***Fig. 3.13c***).

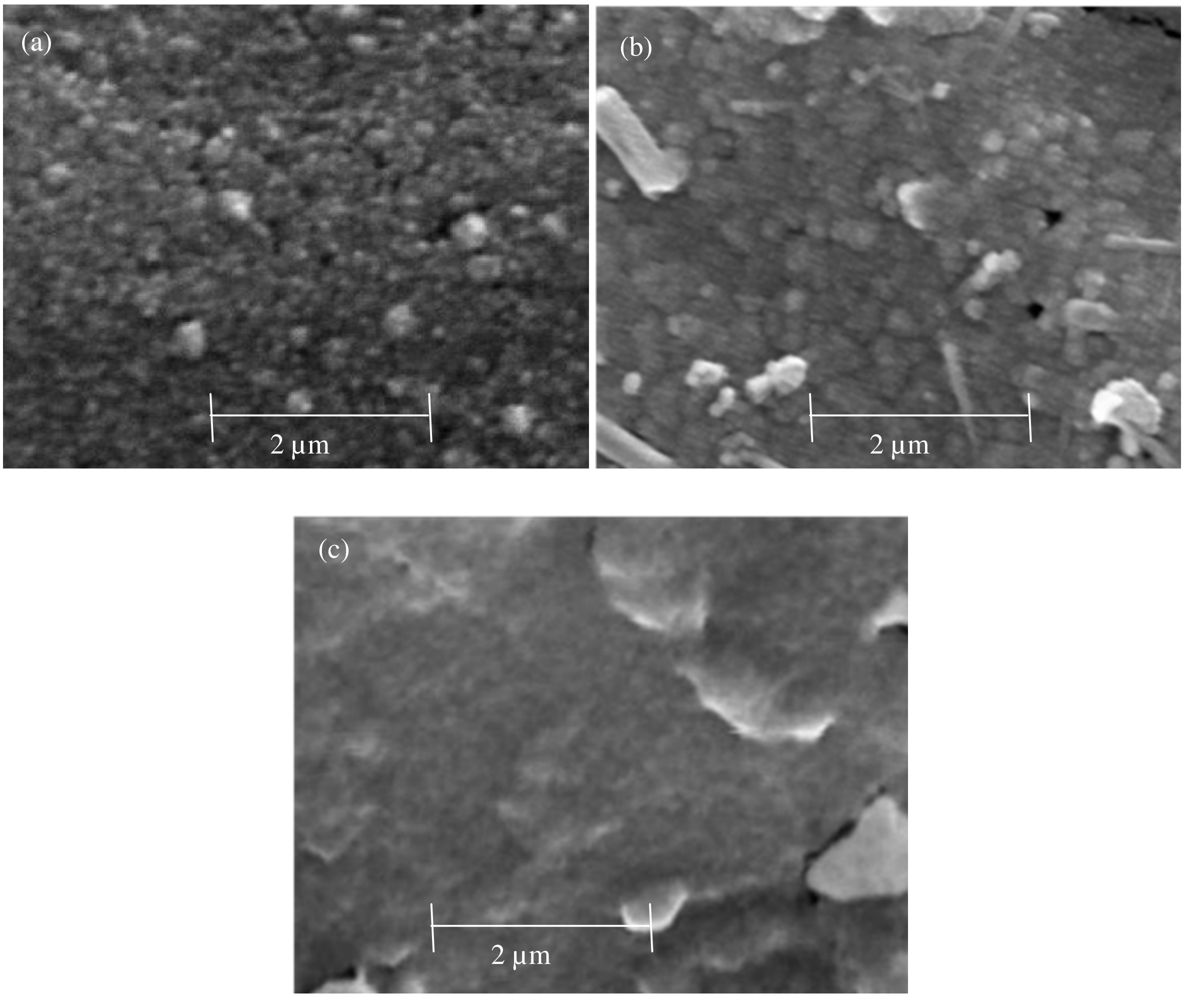

Fig. 3.13*. SEM images of the glass-ceramic samples before immersion in SBF; (a) FBC6, (b) FBC7, (c) FBC8.*

Fig. 3.14(a–b) illustrates the evolution of microstructure of the FBC7 (15 wt.% iron oxide) sample after different immersion time in SBF. Surface morphology exhibited the growth of particles of different sizes ranging from 0.05 to 5 μm, with some localized coagulation of the particles. The particle size increased as the immersion time was increased from 2 to 4 weeks. Surface morphologies for the FBC6 and FBC8 samples immersed in SBF for 4 weeks are shown in Fig***. 3.15(a–b)***. These surfaces also exhibited the fine spread of particles but the size of particles was smaller as compared with FBC7 sample. Typical sizes observed were in the range of 50–100 nm, and less area was covered by the additional layer in FBC6 and FBC8 samples. There were some voids/cracks visible on the surface as seen in SEM image. These voids were possibly formed in the initial stage of reaction in SBF with the surface. EDX analysis showed the presence of Ca and P as the major constituent elements at the surface (***Fig.3.16***).

The formation of a CaO-P_2O_5 rich layer on the surface of bioactive glasses upon interaction with simulated body fluids has been reported by many authors [120-122]. The formation of Ca-P bioactive layer involves several steps and governed by the nucleation and growth of particles at the surface [123]. In SBF, Si–O–NBO bonds are involved in the ionic exchange with H^+ or H_3O^+ from the aqueous solution leading to the formation of silanols (Si–OH) at the interface, which provides the nucleation sites for the growth of apatite. Thus the interactions in SBF solution depend on the structure of residual glass. Subsequently, the formation and condensation of silanol groups take place. This is followed by adsorption of calcium and phosphate ions to the surfaces, which nucleate and grow calcium phosphate rich layer.

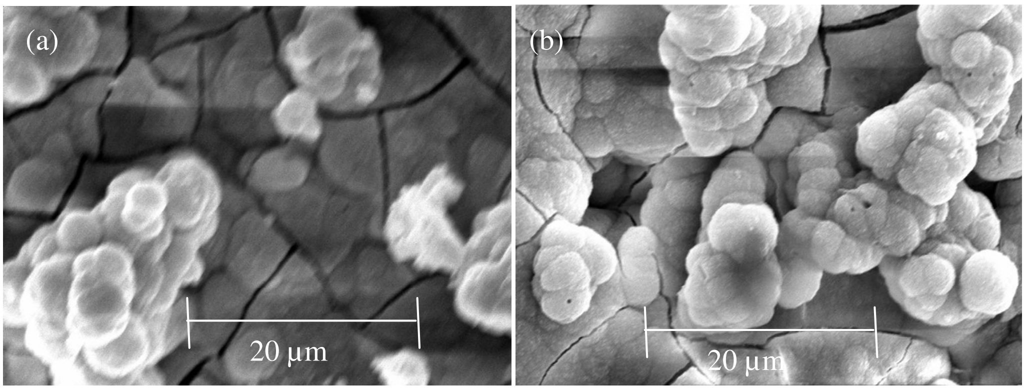

***Fig. 3.14**. Microstructure of the FBC 7 after (a) 1 week, (b) 4 weeks immersion in SBF.*

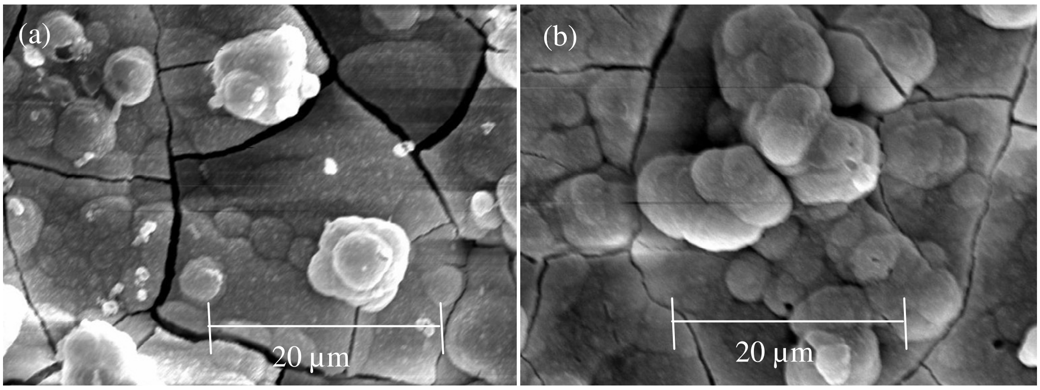

***Fig. 3.15**. Microstructure of FBC samples after 4 weeks immersion in SBF (a) FBC6, (b) FBC8.*

In the present studies, the amount of silica was kept constant and the role of increasing Fe_2O_3 on surface chemistry was elucidated through in-vitro experiment. The pH of SBF solutions initially increased rather fast and then gradually reached to 8.2 (***Fig. 3.11***). The fast change in pH for sample FBC7, implies the prompt surface interaction with body fluid. The change in pH indicates the dissolution of ions from the surface into the solution (ion-exchange). This slow change in the pH is due to the fact that these interactions in body fluid are time dependant and kinetic in nature. This interaction is controlled by the diffusion [124–126]. This loss of Si from the surface to the solution results in Si–OH bond at the surface. Thus interactions on the sample surface, resulted in marginal increase in Si, Ca and P concentrations in the solutions (***Table 3.6***). The sharp decrease in P concentrations in the solution was observed due to migration of Ca^{2+} and PO_4^{3-} from the solution to the surface forming a $CaO–P_2O_5$ rich layer. This inference is also supported by the fact that there was an increase in the basic nature of the solutions and attributed to the increase in absorption of phosphate from the solution to the surface (***Table 3.6***).

XPS study of glass-ceramics showed a marked increase in P content and a net decrease in Si on the sample surface. This can be interpreted as the formation of a calcium phosphate layer on the sample surface, caused by the adsorption of phosphate ions from the SBF solution.

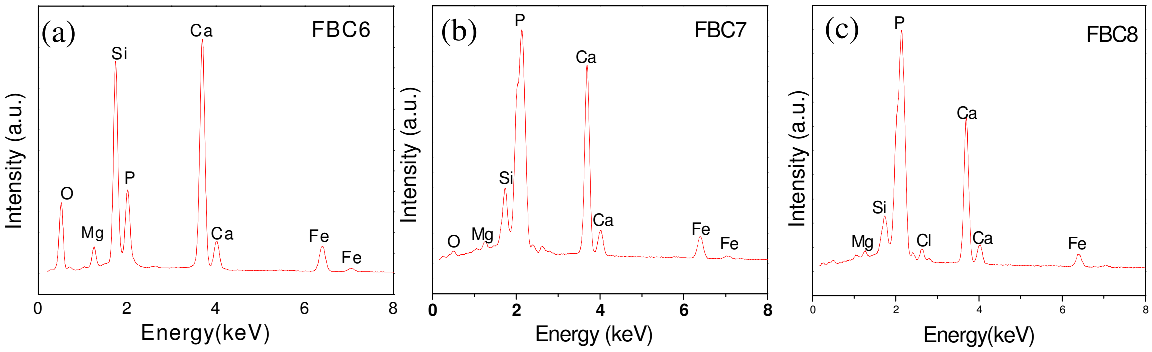

Fig. 3.16*. EDX of glass-ceramics samples (a) FBC6, (b) FBC7 and (c) FBC8 after 4 weeks immersion in SBF.*

As mentioned before in-vitro response of glass-ceramics in SBF depends on the surface conditions. In addition, the emergence of different crystalline phases also plays an important role in deciding the in-vitro response of glass-ceramics. The glass-ceramics are a kind of polycrystalline materials prepared by the controlled crystallization of glass. These can have 10-60% residual glass depending upon the composition and the heat treatment of the base glass.

Li et al. [127] reported that the crystalline phases have much lower dissolution rates, thus the glassy phase in glass-ceramics controls the in-vitro response of these materials. The increase in the iron oxide resulted in better crystallized samples as evident in XRD. This will affect the interfacial reactions with body fluids. Evolution of the crystalline phases in the glass matrix tends to decrease the apatite formation on the surface. However, the fraction of non-bridging oxygen of residual glass increased with an increase in the iron oxide content to 15 wt % (***Table 3.2***). Thus, surface dissolution increased and the better surface response was observed when iron oxide content increased to 15 wt%. Further increase of iron oxide to 20 wt % helped in polymerizing the glass network. Consequently, surface coverage by bioactive layer decreased.

3.3.5.2. In vitro studies in BSA

SEM micrographs of the glass-ceramics samples, after immersion in BSA for 7 days are shown in ***Fig. 3.17(a-c)***. After immersion of sample FBC6, surface morphology was found similar to that of sample before immersion in BSA. However, the surface was covered with polymeric layer (BSA) as the iron oxide content was increased to 15 wt.%. Some inter-connecting pores of 100 -500 nm were observed, implying that the surface was not uniformly covered with polymer (***Fig 3.17b***). Formation of such kind of layer was also observed for sample containing 20 wt% of iron oxide (***Fig 3.17c***).

SIMS spectra of glass-ceramics samples after immersion in BSA for 7 days are shown in ***Fig. 3.18a***. The FBC6 surface showed Ca (m/z = 40) and Fe (m/z = 56) as major peaks while some peaks corresponding to C and Si were also visible. In addition, peaks corresponding to polymeric chains were observed, when iron oxide content was increased to 15 wt% . The peak around (m/z = 69) was assigned to Ga ions, which were used (ion source) for bombardment the samples. Secondary positive ions peaks corresponding to CH_3, CHN, CO, $CONH_2$,C_2H_5 NH_2, CN_3H_3, C_2H_6NO, $C_2H_2CONH_2$, $C_3H_4CONH_2$, related to adsorbed BSA, were evident at m/z = 15, 27, 28, 44, 45, 57, 60, 70 and 84 respectively. Similar features were observed on sample surface when iron oxide content was further increased to

20 wt%. These fragments (CH_2–CH_2–NH_2 and others) related to the adsorption of BSA were not observed on the FBC6 surface.

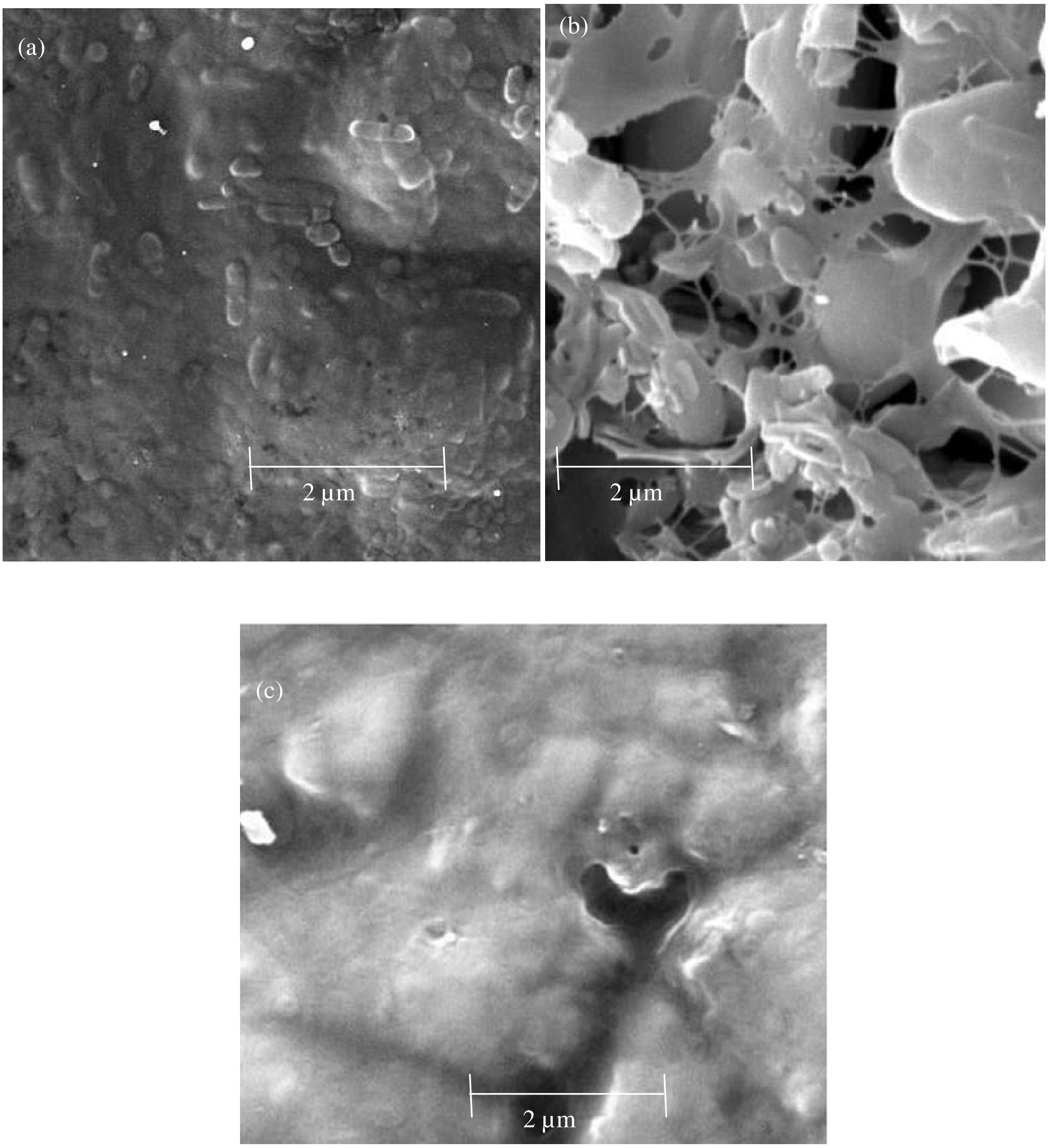

***Fig. 3.17**. SEM of glass-ceramics samples (a) FBC6, (b) FBC7 and (c) FBC8 after 7 days immersion in BSA.*

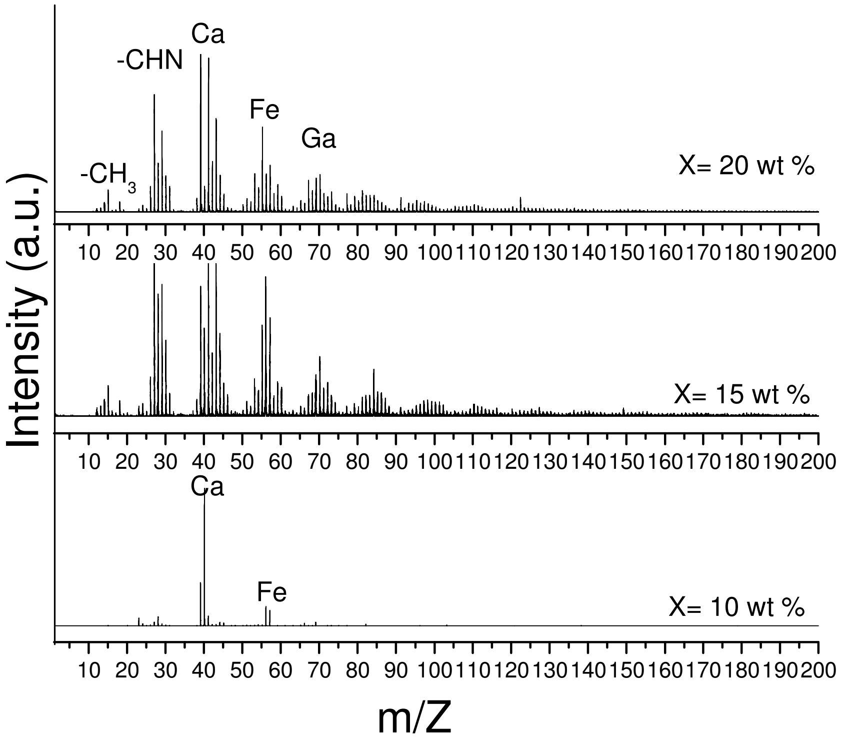

__Fig. 3.18a__. SIMS of glass-ceramics samples after 7 days immersion in BSA

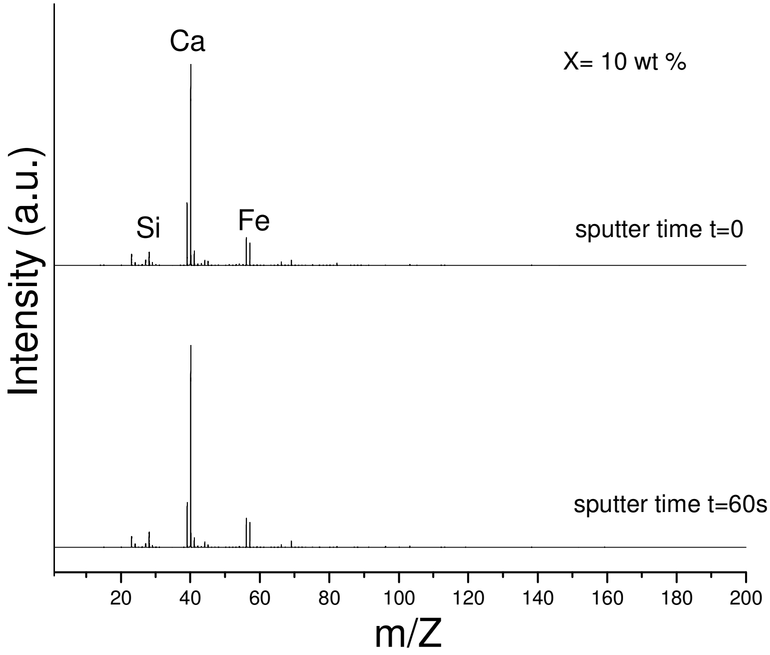

__Fig. 3.18b__. SIMS spectra of glass-ceramic FBC6 after sputtering of surface layer.

The samples after immersion in BSA were sputtered in order to remove the upper layer. The SIMS spectra of the samples were recorded after sputtering. There was no marked difference observed after sputtering for the sample containing 10 wt% of iron oxide (***Fig 3.18b***). However, a significant difference between spectra before and after sputtering was observed for others samples (***Fig 3.18c & d***). Sputtering leads to removal of surface layer by breaking the interfacial bonds and exposing the substrate to the primary ions. Thus as sputtering time is increased more of surface layer will remove. Therefore, when the sputtering time was increased the peaks corresponding to polymeric chain were removed and the peaks corresponding to Ca (*m/z* = 40) and Fe (*m/z* = 56) were observed as major peaks. A comparison between the sputtered and non-sputtered surfaces indicated that the surface was covered with polymeric layer for samples containing 15-20 wt% iron oxide.

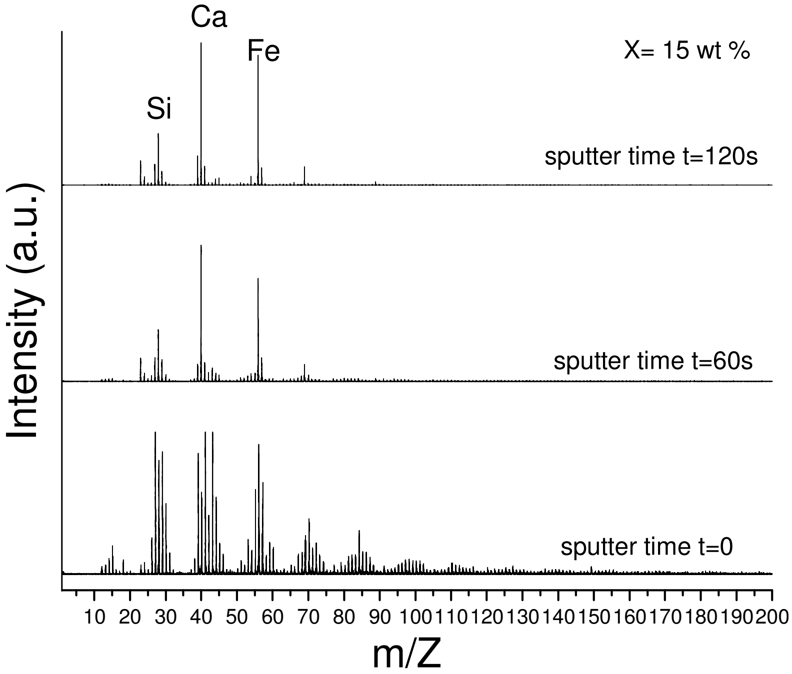

Fig. 3.18c. *SIMS spectra of glass-ceramic FBC7 after sputtering of surface layer.*

BSA is an amphiphilic protein due to the presence of $-NH_2$ and -COOH group in its molecular structure. It shows a different net charge at different pH media. The isoelectric point of bovine serum albumin is pI=4.7. It indicates that BSA has a positive charge below pI 4.7 and negative charge above pI 4.7. The magnetic particles have been reported to have isoelectric point in between 6-8 [128]. However, the isoelectric point of silica is around 2 [129]. Thus, isoelectric point of the magnetic particles in glass-ceramic (phospho silicate) corresponds to that of silica, implying that at pH 7.0 the surface will be negatively charged. Therefore, the adsorption of BSA by hydrophobic interaction will be minimal.

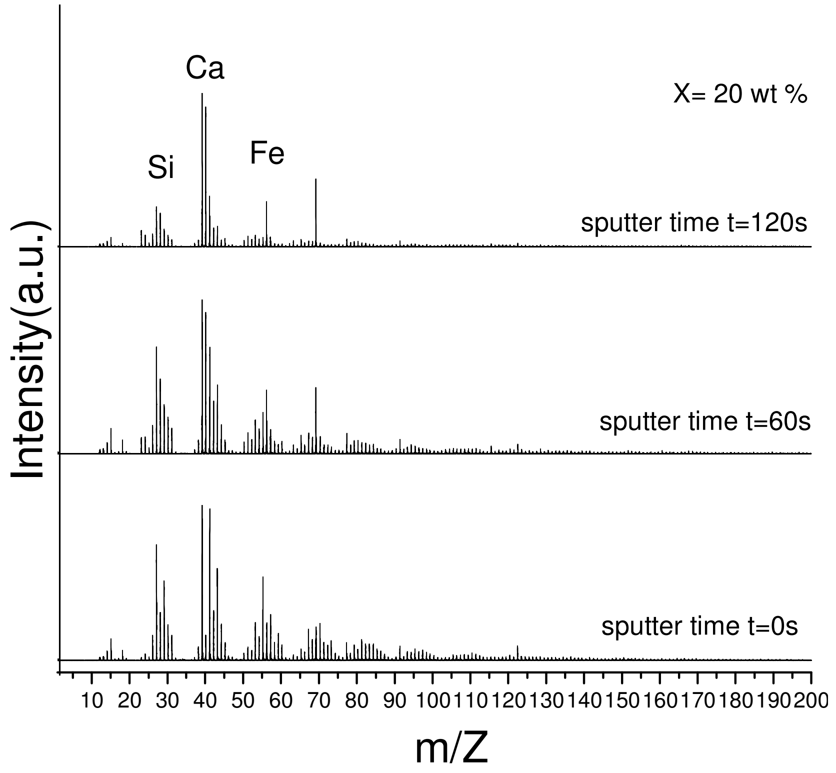

***Fig. 3.18d**. SIMS spectra of FBC8 glass-ceramic after sputtering of surface layer.*

A possible explanation for adsorption may be related to the physical absorption of BSA. During interaction of samples with BSA solution, formation of –OH groups takes place at the surface. Since BSA has high affinity for silanol group and formed H-bond with the –OH groups present at the surface [130]. Thus the interactions of BSA solution with surface depend on structure and bonding of residual glass.

Introduction of Fe_2O_3 induces several structural modifications in the glasses. It was seen that the glass transition temperature decreased as the iron content was increased to 20 wt%. The glass-transition temperature is closely related with the strength of glass network. An increase in modifier content is expected to decrease the connectivity of the network. Consequently the network becomes less rigid and requires less energy to break. Thus, when iron oxide was added to glass network, it resulted in an increase in non-bridging oxygen. This resulted in increased surface dissolution and forming a large numbers of –OH groups (-Si–OH) on surfaces. Since the BSA binds to these groups, the adsorption of protein was increased.

3.4. Conclusion

The studies of thermo-physical and structural properties of glasses with the chemical composition $34SiO_2$-(45-x)CaO-$16P_2O_5$-4.5MgO-$0.5CaF_2$–xFe_2O_3 (x = 5 - 20 wt %) showed an increase in disorder in the glass structure with the addition of iron oxide content upto 15 wt%. Further increase in Fe_2O_3 promoted polymerization of the glass network, thereby increasing T_g and TEC. The glasses upon heat treatment showed the formation of magnetite, apatite and wollastonite phases. There was an increase in the formation of magnetite phase with an increase in iron oxide content. In glass-ceramics, Fe^{3+} ions are found in octahedral coordinations and Fe^{2+} in tetrahedral coordinations. The samples with iron oxide concentration above 10 wt % were ferrimagnetic. The bioactivity of glass-ceramics was found to depend on the composition. The interaction with SBF solution yielded the calcium phosphate layer formation on the surface of glass-ceramics samples. The surfaces of these materials were modified differently with increase in the amount Fe_2O_3 in the glass matrix. The glass-ceramics showed the better surface response in SBF and in BSA when iron oxide content was increased from 10 to 20 wt%.

Chapter 4

Structural, microstructural and in-vitro studies of calcium silico-phosphate glass/ glass-ceramics containing iron oxide and zinc oxide

---

In previous chapter we observed that the bioactive response of glass-ceramics depends on the iron oxide content. In continuation of the work, the glasses containing zinc and iron oxide were prepared. The effect of ZnO addition on structural, micro-structural and magnetic properties of glass/glass-ceramics with nominal composition $25SiO_2$-$50CaO$-$15P_2O_5$-$(10-x)Fe_2O_3$-$xZnO$ *(where* $x = 0\text{-}7$*) mol % are discussed in this chapter.*

4.1. Introduction

Bioactive glass and glass-ceramics have been used clinically in dental, craniomaxillofacial and spinal applications [36-38]. Some of the bioactive glass compositions have also been studied as possible vehicles for the delivery of ions like zinc [33-35]. Zinc is an essential mineral required to synthesis about 300 enzymes in human body. These enzymes control the vital functions such as cell reproduction, immunity, protein synthesis, wound repair, vision, free radical protection and immunity inside the body. The addition of zinc to iron containing glass may lead to formation of zinc ferrites which enhances the magnetic properties, thus, a number of glass systems containing iron and zinc have also been studied and developed [131, 132].

ZnO containing bioglass/glass-ceramics have shown a stimulatory effect on bone formations [47]. Balamurugan et al. [133] studied the apatite-forming ability of SiO_2–CaO–P_2O_5–ZnO system and reported that incorporation of Zn into a bioglass does not diminish apatite-forming ability of the material. Sing et al [134] observed an increase in the apatite forming ability of ZnO containing glass-ceramic samples with the evolution of zinc ferrites in the glass-ceramics. ZnO is amphoteric oxide and hence it tends to modify the local structure of the glass. This will affect the interaction of the magnetic particles, having a significant impact on the structural and magnetic properties of the ferrimagnetic glass-ceramics.

Therefore, in order to study the effect of ZnO addition on structural, microstructural and bioactive response of the glasses, glasses with composition $25SiO_2$-50CaO-$15P_2O_5$-(10-x)Fe_2O_3-xZnO (where x = 0-7) mol % were prepared. In the present chapter, we report a systematic study on phase formation, microstructure and surface modification of these glass/ glass-ceramics using XRD, XPS, FTIR and SEM. The bulk magnetic properties, like magnetization versus temperature and room temperature hysteresis were measured using SQUID magnetometer. These measurements revealed the effect of ZnO concentration on magnetic and structural ordering in these samples. The strength of dipolar interactions found to decrease with increase in ZnO content. In-vitro studies in SBF have shown the formation of Ca-P rich layer on the glass-ceramics when immersed in SBF, implying the bioactive nature of the samples. In-vitro studies in BSA have shown that the adhesion of BSA decreases with an increase in ZnO content.

4.2. Experimental

Base glasses of compositions as given in ***Table 4.1*** were prepared by melt quench technique. About 100 g batches were prepared by mixing reagent grade SiO_2, $CaCO_3$, Fe_2O_3, NH_4H_2PO4 and ZnO. The charge was calcined at maximum 900°C for 12 h, holding at intermediate temperatures for 6-8 h, decided by the decomposition temperatures of various precursors. Melting was carried out in a Pt-Rh crucible at 1450-1500°C in a lowering and raising hearth furnace. The melt was held for 30 minutes at this temperature for homogenization and was then poured in water. Glassy nature was confirmed by XRD. The base glass was powdered in a planetary ball mill and then pelletized. They were converted into glass-ceramics (hereafter called MGC) through controlled heat treatment at 800°C for 6h based on DTA data. The glass-ceramics samples are named as MGC0, MGC2, MGC5 and MGC7 with ZnO concentration 0, 2, 5 and 7 mol %, respectively.

Table 4.1. *Base glass compositions (nominal) in mol %.*

Sample	SiO2	P_2O_5	CaO	Fe_2O_3	ZnO
MG0	25	15	50	10	0
MG2	25	15	50	8	2
MG5	25	15	50	5	5
MG7	25	15	50	3	7

Phase emergence in glass-ceramics was investigated using XRD on the powder samples as mentioned in chapter 2. The microstructure of glass-ceramic is characterized by scanning electron microscopy. Prior to mounting sample in analysis chamber of microscope thin Au conducting coating was deposited on the sample surface.

For XPS measurements samples, sample was excited by Mg-K_α radiations ($h\upsilon$=1254.6 eV), photoelectron spectra were analyzed using a VG make CLAIM 2 analyzer system in the energy range of 0-1000 eV.

The magnetic response versus applied magnetic field H was measured at room temperature, with $|H| \leq 5$ kOe using SQUID magnetometer. The samples were also subjected to zero field cooled (ZFC) and field cooled (FC) measurements. These data were analyzed to obtain the blocking temperatures, saturation magnetization ($M_{s)}$, remnant magnetization ($M_{r)}$, and coercive field (H_c) for each sample.

Mössbauer spectra were obtained using a spectrometer operated in constant acceleration mode using ^{57}Co source in Rh matrix. Mössbauer spectra were fitted with appropriate paramagnetic doublets and magnetic sextets using least square fit program.

In-vitro response was studied in simulated body fluid (SBF). SBF was prepared according to the procedure proposed by Kokubo and Takadama [135]. For studying surface modifications, the pellets of around 10 mm in diameter (approx. 500 mg) were immersed in 50 ml of SBF for 1-4 weeks, incubated at 37.4ºC. These were removed periodically and surfaces were analyzed using XPS technique. Changes in concentrations of Ca, Zn and Fe in SBF solutions as a result of surface dissolution were measured using atomic absorption spectrophotometer (Model Chemito AA 203). Structural changes on the surface of the samples treated in SBF were analyzed using Fourier transform infrared reflection spectroscopy (Model Bruker Vertex 80 V Fourier transform infrared (FTIR) spectrometer) and scanning electron microscopy (SEM) techniques.

To determine protein adsorption, the glass-ceramic samples of approx 11 mm diameter and 600mg were immersed in 1 mg/ml BSA solution. Structural changes on the surfaces of samples after immersion in BSA solutions were analyzed using diffuse reflection Fourier transform infrared reflection spectroscopy (Model Bruker Vertex 80V Fourier transform infrared (FTIR) spectrometer). The samples were removed and their surfaces were also analyzed using SEM (Model: Tescan Vega MV 2300T/40) and TOF-SIMS.

4.3. Results and discussion

The bubble free transparent glass samples with brownish tinge were obtained. XRD analysis of prepared glasses has shown the absence of any long range order.

4.3.1.1. Thermal characterization

DTA plots are shown in **Fig. 4.1**. Peak crystallization temperatures were determined from these plots. Sample without ZnO showed two peaks; one broad peak observed around 648°C while other peak was found around 742°C. With the addition of ZnO, only one prominent peak of crystallization (T_p) was observed around 715°C. This temperature (T_p) further increased to 732°C when ZnO content was increased to 7 mol%.

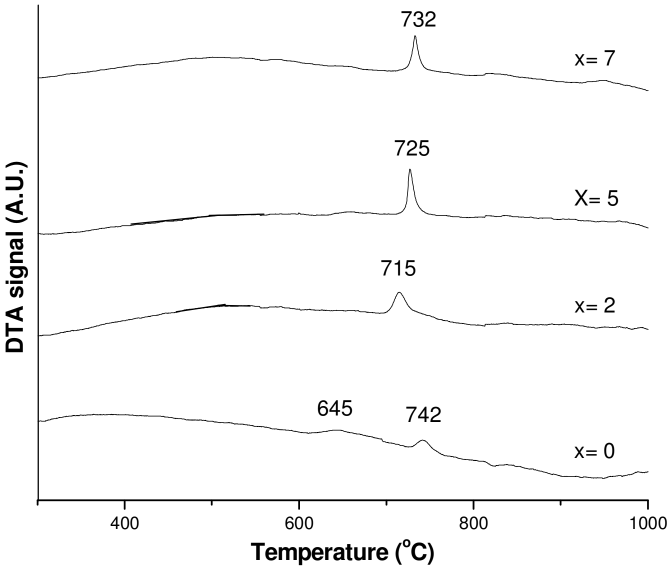

Fig.4.1. *DTA of glass samples having different content of ZnO (mol%)*

4.3.2. Structural studies

4.3.2.1. XRD study

The XRD patterns of glass-ceramics prepared by controlled heat treatment at 800°C are depicted in ***Fig. 4.2***. Calcium phosphate, hematite and magnetite were formed as major crystalline phases. CaO has more affinity towards phosphate leading to the formation of $Ca_3(PO_4)_2$ like phase.

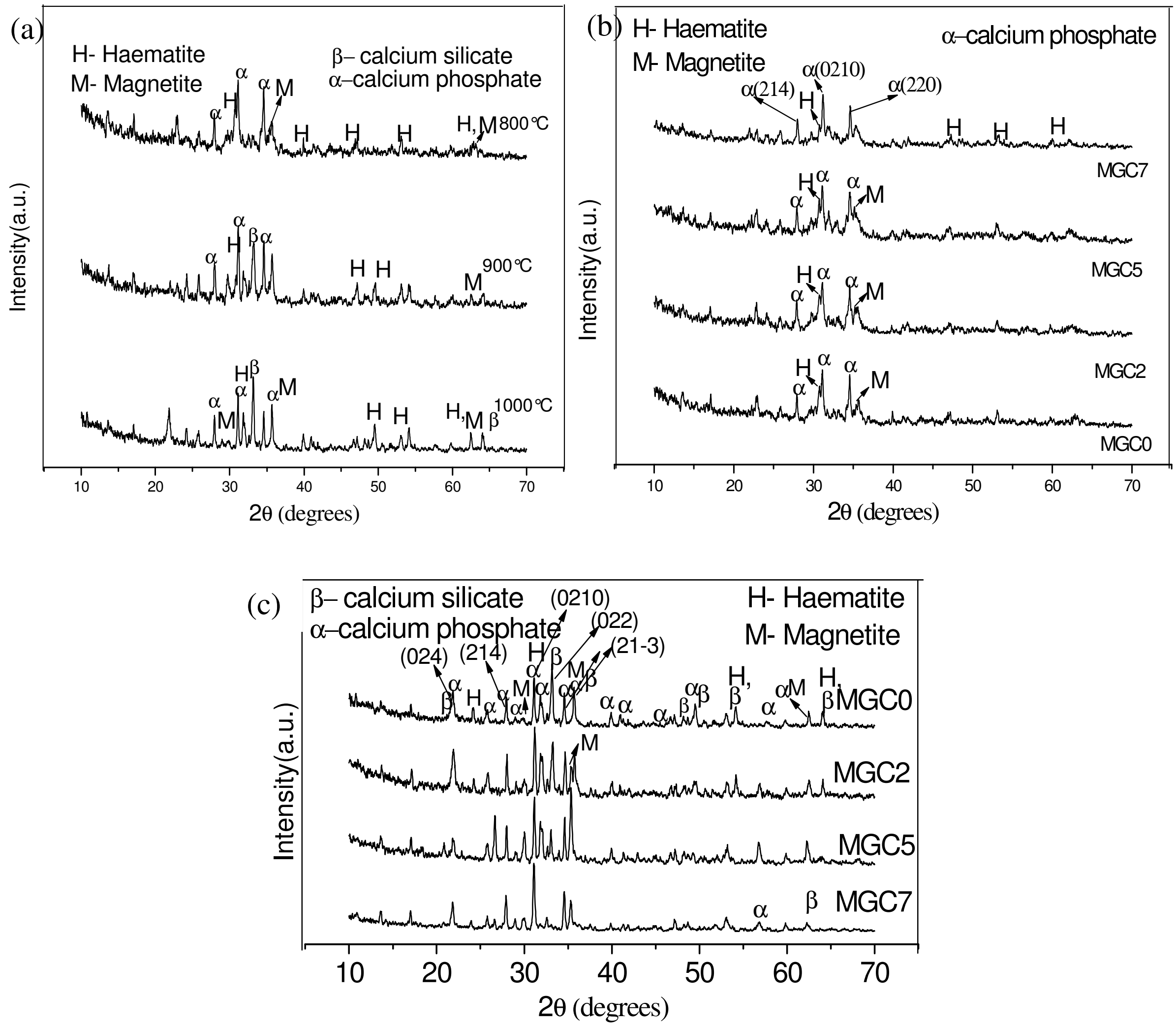

Fig. 4.2. *XRD patterns of (a) MGC0 glass-ceramics prepared at different temperatures; (b) MGC0, MGC2, MGC5 and MGC7 glass-ceramics prepared at 800ºC; and (c) MGC0, MGC2, MGC5 and MGC7 glass-ceramics prepared at 1000°C.*

Magnetite was formed in the glass matrix by the reaction

$$6Fe_2O_3 \rightarrow 4Fe_3O_4 + O_2 \qquad \textbf{(4.1)}$$

The extent of conversion of hematite into Fe_3O_4 depends on the reducing environment produced by the relative presence of ZnO and CaO in the melt [117]. These oxides have the high affinity for oxygen and thus reduction of the Fe_2O_3 will depend on their amount in the batch. With addition of ZnO the zinc ferrite can also be formed by the following reaction

$$ZnO+7Fe_2O_3 \rightarrow 4Fe_3O_4 + ZnFe_2O_4+O_2 \qquad \textbf{(4.2)}$$

However, formation of zinc ferrite phase could not be detected in XRD.

4.3.2.2. ESCA study

X-ray photoelectron scans for as prepared glass samples in the binding energy (BE) region 0 to 1000 eV, are shown in ***Fig. 4.3a***. The core level peaks for the constituent elements were identified and marked on the spectra. As mentioned earlier the peak at 284.6 eV assigned to C1s used as a reference. The peaks at 346 eV was assigned to Ca2p, around 531eV to O1s and around 710 eV to Fe2p photoelectrons.

In order to bring clarity about the O1s photoelectron spectra, the magnified view of the peak (XPS) is re-plotted and shown in ***Fig. 4.3b***. The peak shape changed with increasing ZnO content and the maximum peak width (FWHM) of 1.7 eV was observed for sample MG0. The O1s peak was fitted with two Gaussian peaks and shown in ***Fig 4.3b***. Since Fe_2O_3 is replaced by ZnO in the silica network, the electronic density of the bonding states of the silicon and oxygen atoms are modified. As a result, the fractions of bridging and non bridging oxygen are also changed.

The fraction of non bridging oxygen units was calculated from the core level XPS spectra of O1s peak. The difference between bridging and non-bridging oxygen atoms was reflected in the XPS chemical shift of O1s peak (***Fig. 4.3b***). The low binding energy peak at ~ 529eV was due to the contribution from the non-bridging oxygen atoms, while the peak at

~ 531 eV was attributed to presence of the bridging oxygen. The areas of the two peaks (non–bridging and bridging) were calculated to find out the fraction of non-bridging oxygen. The fraction of non-bridging oxygens was decreased as the zinc oxide content was increased to 7 mol % (***Table 4.2***). This is correlated to the fact that the zinc oxide stabilizes the glass network and results in the formation of rigid network.

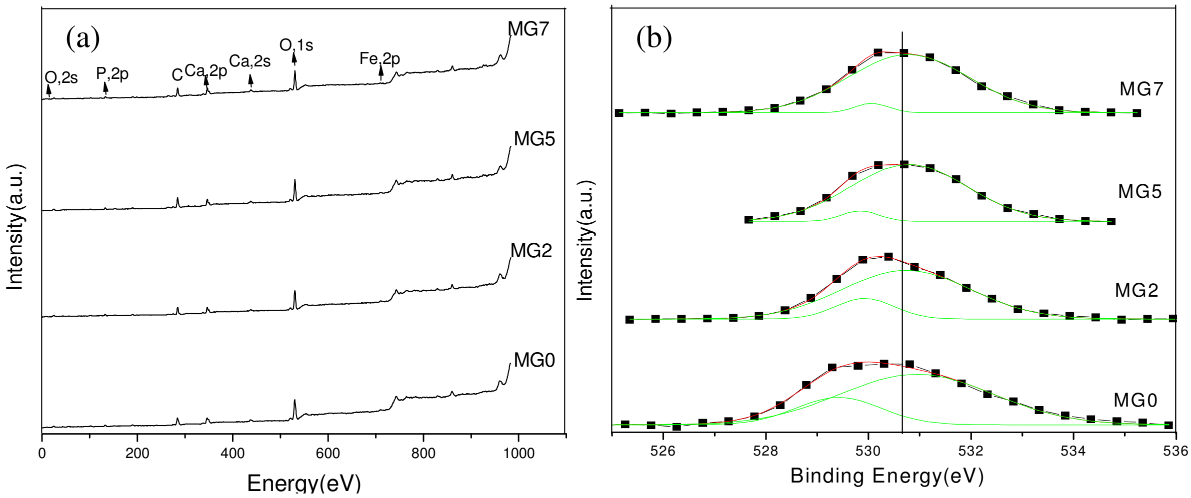

Fig. 4.3. *(a)XPS spectra of MG0, MG2, MG5 and MG7 glass samples; (b) Deconvolution of oxygen core level spectra of glass samples (Fig. 4.3a).*

Table 4.2. *Ratio of non-bridging and bridging structure units for different glass samples obtained from XPS data.*

Sample	Ratio of non bridging to bridging oxygen groups
MG0	0.301
MG2	0.193
MG5	0.057
MG7	0.045

XPS spectra of different glass-ceramic samples are shown in ***Fig. 4.4a***. Peaks become sharp as compared to that of glasses. ***Fig. 4.4b*** shows the P2p core level spectra as a function of composition. The P2p peak was observed at binding energy 133 eV. These peaks were broad in nature, implying that the phosphorus could be present as a mixture of phosphate and pyrophosphate (Q^1).

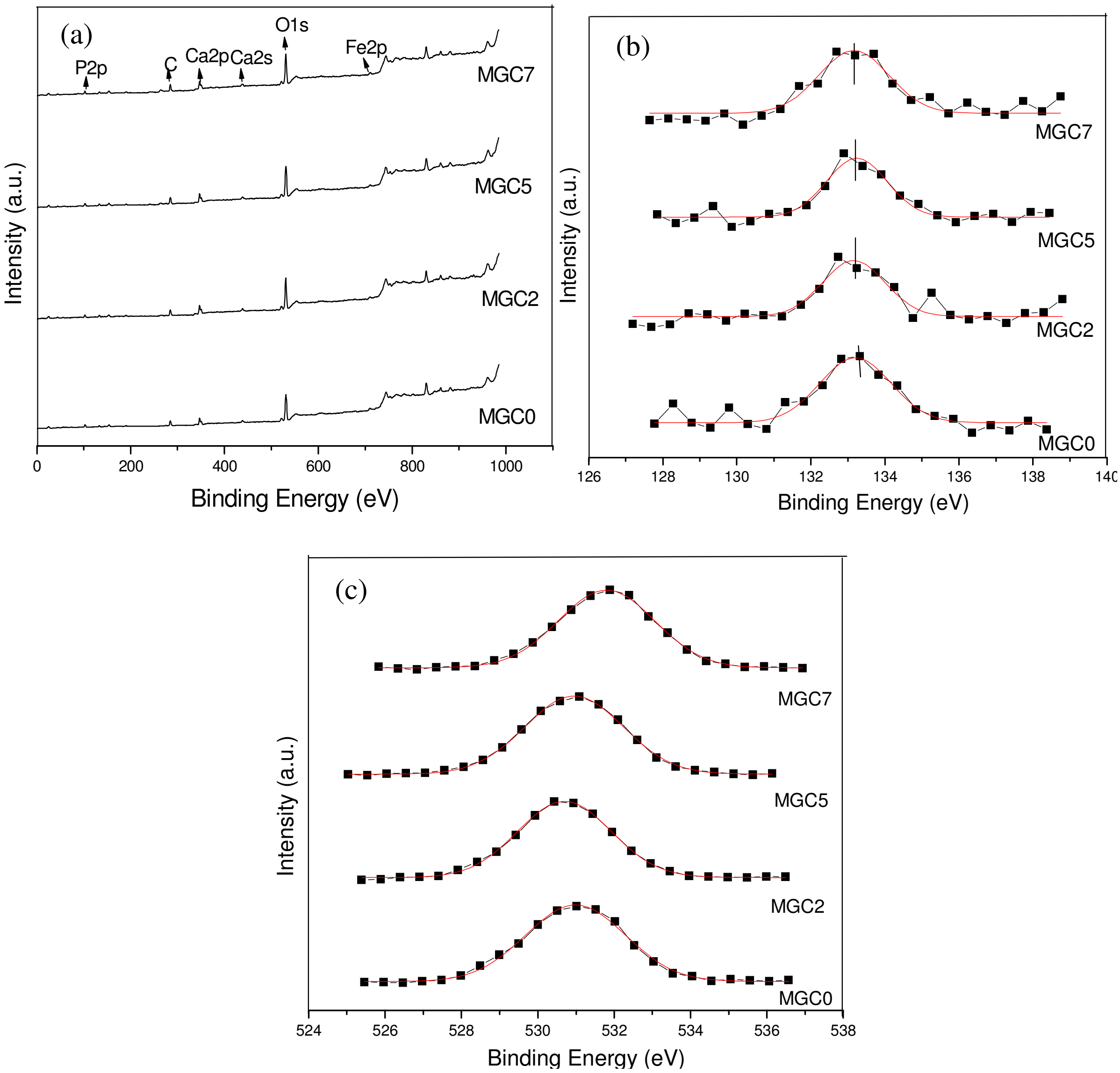

Fig. 4.4. *(a) XPS spectra of MGC0, MGC2, MGC5 and MGC7 glass-ceramics prepared at 1000℃ samples; Magnified view for core level spectra of glass-ceramics samples for (b) P2p, (c) O1s.*

Fig. 4.4c shows the O1s core level peak of heat treated (1000°C) samples as a function of composition. The peak shifted to the higher energy side with an increase in ZnO content (x> 5 mol %). The binding energy for the oxygen in phosphate is in the range of 530-532.8 eV. The shift of O1s core level peak with increase in ZnO content (x> 5 mol %) to the higher energy side is possibly due to increase in the formation of phosphate.

4.3.3. Microstructure studies

Figs. 4.5(a-d) show the scanning electron micrographs of glass samples heat treated at 800°C. The microstructure exhibited the granular morphology; grains having size of about 50 nm. The microstructure became more homogeneous and granular with the addition of ZnO content. This is possibly due to reduction of crystallite size (due to formation of more nucleating centers) helping in their uniform distribution.

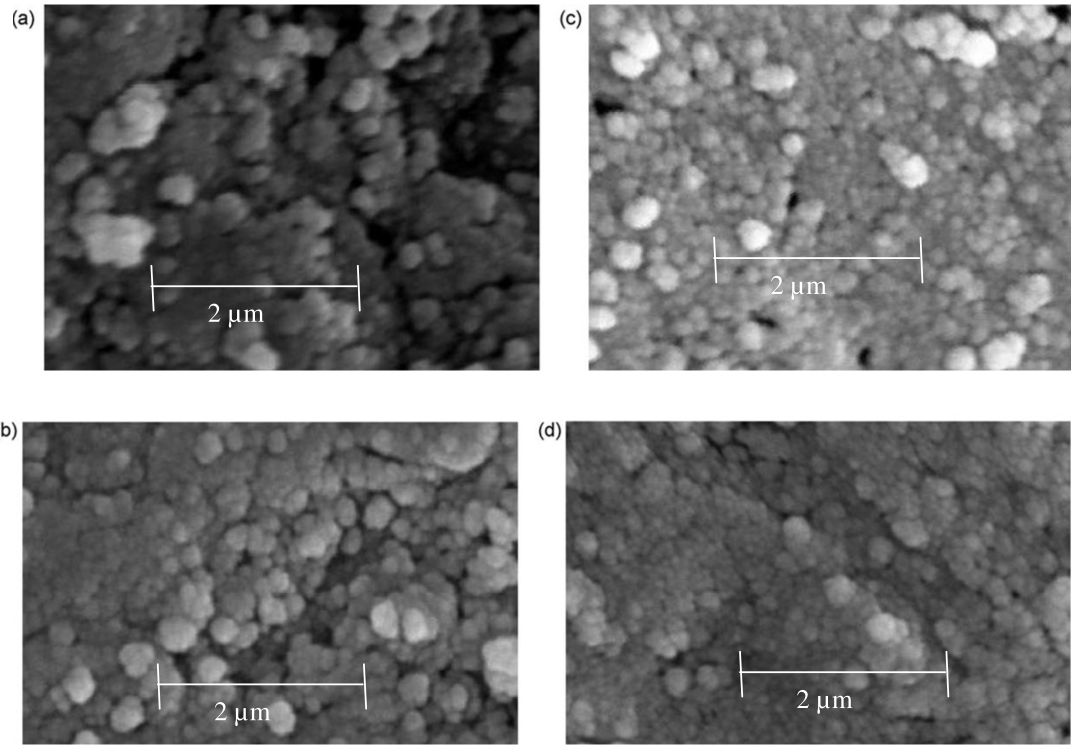

Fig. 4.5. *SEM micrographs of different glass–ceramics samples prepared at 800ºC, (a) MGC0; (b) MGC2; (c) MGC5 and (d) MGC7.*

The microstructures of glass samples after heat treatment at 1000°C are shown in ***Fig. 4.6(a-d)***. Glass-ceramics sample without ZnO content showed the evolution of small size particles. The microstructure was seen to have densely packed crystallites when compared to that of glass samples heat treated at 800°C. Overall microstructures were seen to be composed of elongated grains and increase in particle size. The densification occurred at higher temperature (1000°C) because there was an increase in the atomic and molecular mobility at higher temperature and consequently enhanced diffusion, resulting in densely packed structure.

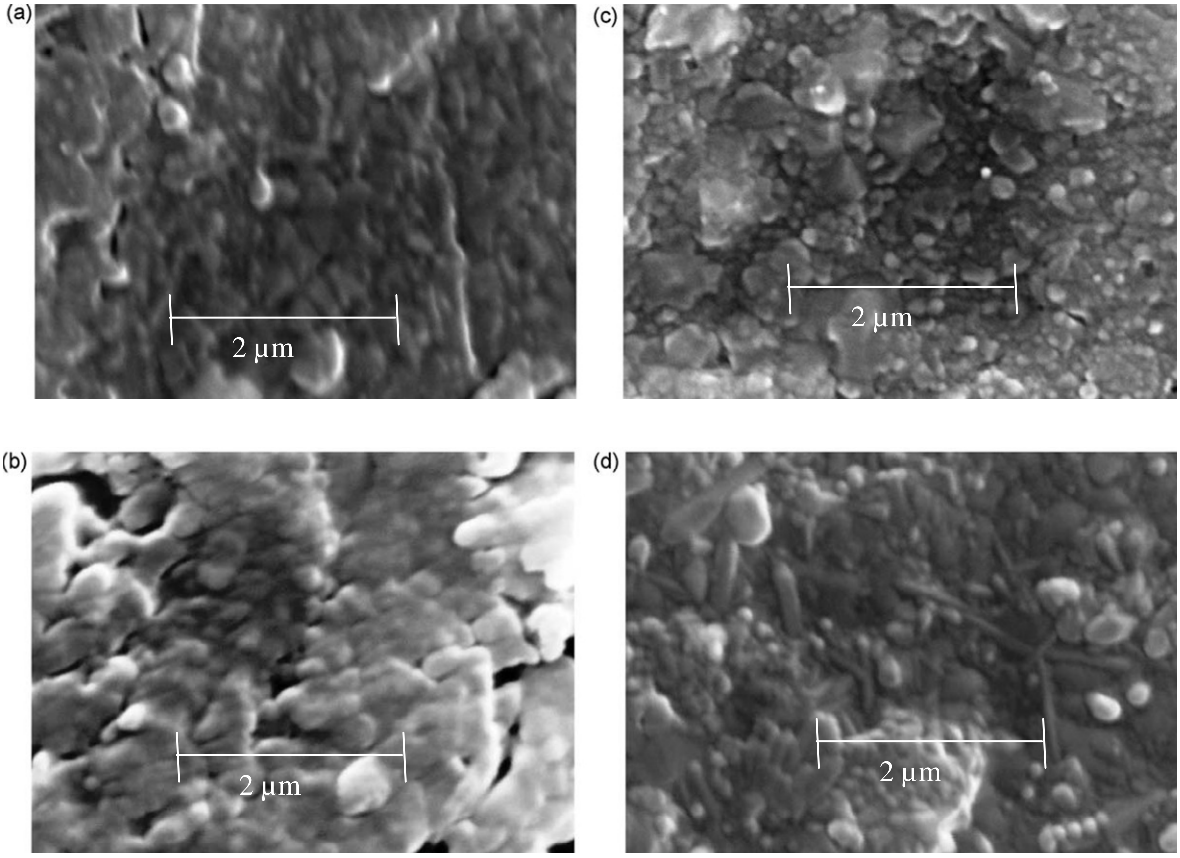

Fig. 4.6. *SEM micrographs of different glass–ceramics samples prepared at 1000ºC, (a) MGC0; (b) MGC2; (c) MGC5 and (d) MGC7.*

In specimen with 5 mol % zinc oxide this feature changed into a microstructure with smaller particles (***Fig. 4.5c***). The formation of thin rod like structure with coarser particles was observed at high zinc oxide concentration (x = 7 mol %). The average size of spherical particles was 50 nm and that of thin rods was of the order of 30-60 nm in width and 1000 nm length. The crystallite size was determined from XRD data (using Debye –Scherer formula), and the measured values were roughly in agreements with the measured values from SEM micrographs.

Fig. 4.7 shows the variation in crystallite size with ZnO content of glass-ceramics samples heat treated at different temperature. The crystallites sizes were sub 50 nm in glass-ceramics samples heat treated at 800°C and were above 50 nm in the glass-ceramics samples heat treated at 1000°C.

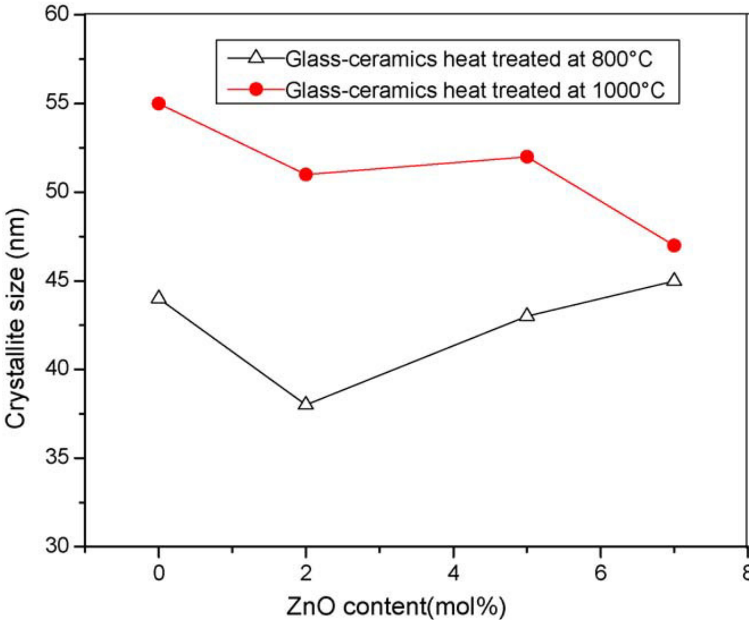

Fig. 4.7. *Variation of crystallites size with ZnO content as calculated from the XRD data using Debye–Scherer formula.*

4.3.4. Magnetic studies

Fig. 4.8a shows the temperature dependence of the magnetization (M) for glass samples in both zero field cooling and field cooling regimes in the applied magnetic field of 100 Oe. ZFC/FC curves have the tendency to superpose as the temperature increases. ZFC and FC magnetizations were represented by open and solid circles, respectively. The ZFC curves for glass samples MG0 and MG2 exhibited a broad peak at around 111K and 74 K (blocking temperature T_B) and the ZFC–FC curves were separated up to 300 K. For glass samples MG5, ZFC and FC curves were overlapped and T_B was not determined.

The blocking temperature is a measure of the thermal energy required to overcome the anisotropy energy barrier and defined as the average temperature at which the nanoparticles do not relax during the time of measurement; they are blocked [136]. With the application of magnetic field particles tend to align in the direction of the field. In ZFC measurement, net magnetization increases with increase in temperature, as more particles are able to overcome the anisotropy energy barrier and orient themselves in the field direction. The temperature at which the relaxation time of most of the particles is equal to experimental resolution time, ZFC curve comes to a maximum. This temperature is called blocking temperature. It depends on size and shape of the particles. The blocking temperature is evaluated by

$$T_B = \frac{E_0}{k_B \ln(t / t_0)} \qquad \textbf{(4.3)}$$

Where E_0 is the barrier, k_B is Boltzmann constant, t is the experimental resolution time, and t_0 is of the order from 10^{-9} to 10^{-11} s. Eq. (4.3) indicates that T_B is proportional to the potential barrier E_0. The latter is proportional to volume of the particles and anisotropic energy barrier.

At temperature higher than T_B, magnetization decreases. The divergence between the FC and ZFC curve is a characteristic feature of superparamagnetism and results from the anisotropy energy barrier of the nanoparticles. In the ZFC process, the nanoparticles need to overcome the anisotropy energy barrier, as the magnetic moments of the nanoparticles are oriented along their easy axes. The anisotropy energy barrier does not have an effect on the FC curve as the nanoparticles are aligned with the field during the cooling process.

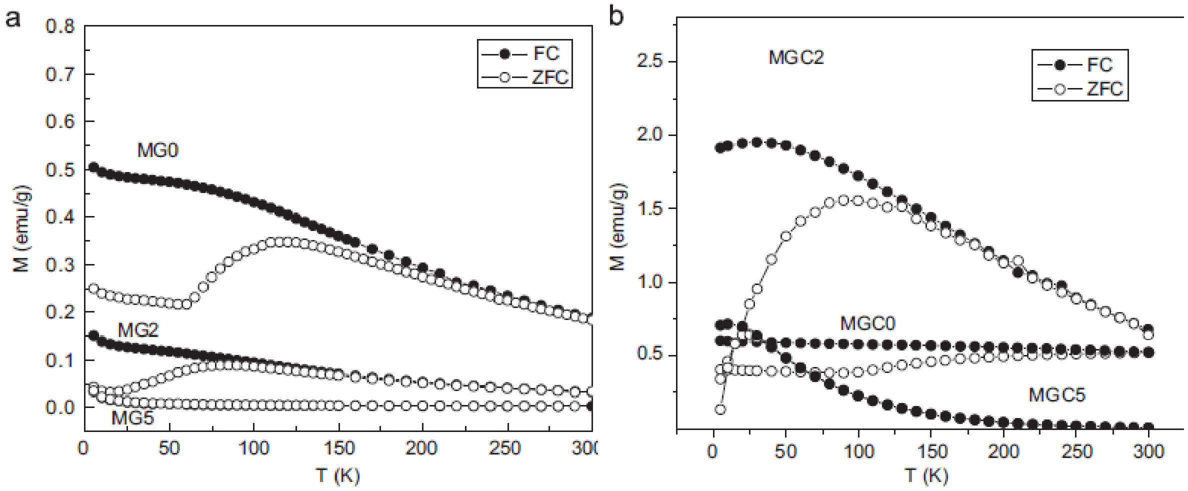

***Fig. 4.8**. Magnetization vs temperature (ZFC and FC) plots of glass samples (a) as prepared and (b) heat treated at 800 ℃ for six hours.*

The blocking temperature is dependent on the volume of the particles as the energy barrier (Eq. (4.3) is proportional to volume of the magnetic particles. An important feature of magnetic particles is that the resultant magnetic moments of individual particles can cause interparticle magnetic interaction. These interactions affect the magnetic properties of the materials and arise from the dipole-dipole interactions or exchange interactions [137]. The energy associated with dipole-dipole interactions is given by

$$\mathrm{E_d} = \frac{\mu_0 m^2}{4\pi \mathrm{l}^3} \qquad \textbf{(4.4)}$$

Where μ_0 is the permeability, m is the magnetic moment and l is the particle-particle separation. This dipole-dipole energy term will modify the energy barrier $E_{0.}$ Thus the blocking temperature is determined by the volume of the particles and the inter-particle interactions.

It was observed that the FC curve tends to flatten below $\mathrm{T_B}$. This is understood as the magnetization is blocked below $\mathrm{T_B}$. It also suggests the existence of strong interactions among the particles. The interaction may be of dipole-dipole interaction among the particles.

This kind of behaviour (flattening of FC curve below T_B) has been shown by nanoparticle systems with random anisotropy and strong dipole-dipole interactions [138,139].

The magnetization M as a function of temperature for glass-ceramics samples for FC and ZFC conditions are shown in ***Fig 4.8b***. The ZFC curves for samples MGC0, MGC2 and MGC5 exhibited broad peaks at around 175 K, 80 K and 40 K (T_B). ZFC/FC curves stayed separated up to 300 K in MGC0 while for MGC2 upto 250 K. Glass-ceramics showed higher magnetization compared to glass samples mainly due to creation of magnetic nanoparticles. These particles were nucleate out in the silica network as a result of heat treatment and correspond to net increase in magnetic properties of the glass-ceramics.

Monte Carlo (MC) simulations of zero field/field cooling magnetizations on nanoparticles with random anisotropy show that the T_B increases with increasing strength of dipolar interaction [140]. It is also known that the ZFC/FC curves of samples crucially depend on the volume and spatial arrangement of the magnetic particles. It was observed that the T_B tended to shift at lower temperature with addition of ZnO content, indicating the decreasing strength of dipolar interactions. This is explained in terms of reduction in the magnetic ions concentrations as the ZnO content was increased at the expense of Fe_2O_3.

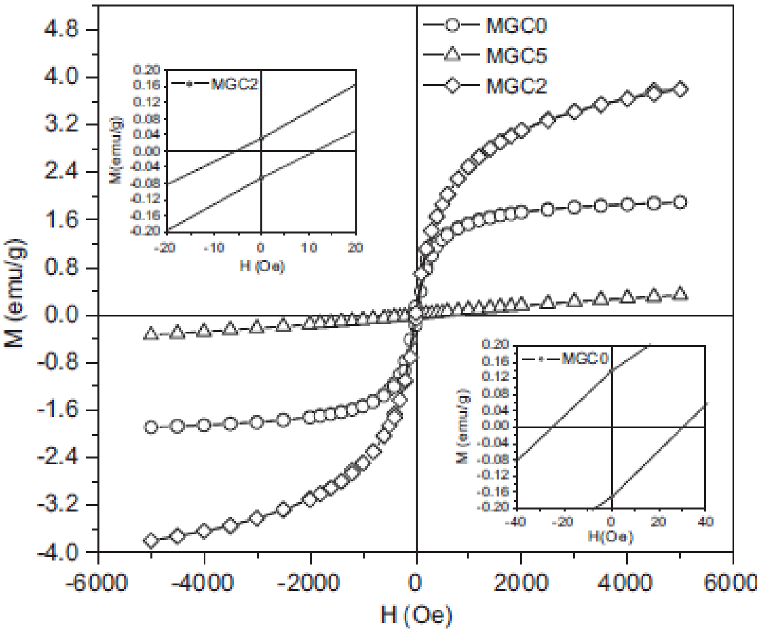

***Fig. 4.9**. M-H plots of the glass-ceramics samples having different ZnO concentration. The insets show low field magnetization behaviours of the samples (MGC0 and MGC2).*

The magnetization as a function of field at room temperature for glass-ceramics is shown in ***Fig. 4.9***. Glass-ceramic without ZnO content showed magnetization of 1.7 emu/g at 5000 Oe. The sample showed the typical hysteresis loop with coercive field of 28 Oe. The value of coercive field decreased to 8 Oe with addition of 2 mol% ZnO while the saturation magnetisation was increased significantly. The low value of coercive field implies that particles were in the superparamagnetic regime.

With further increase of ZnO to 5 mol%, concentration of magnetic particles was reduced as the content of Fe_2O_3 decreased. Consequently, there was an increase in the spatial arrangements of magnetic nanoparticles. It is known that the interaction between magnetic nanoparticles in insulating matrix (glass) has a significant impact on the magnetic properties, in particular on the superparamagnetic relaxation of the particles, which depends on the interaction strength [141,142]. In case of ferro/ferri-magnetic systems, long-range dipole-dipole interactions have significant effects, even if the magnetic particles are embedded in a non-magnetic matrix like glass.

However, since the dipolar energy contribution is related with the spatial arrangements of the particles [143,144], and in the case of hematite nanoparticles the dipole-dipole interaction is generally weak whereas the exchange interactions between nanoparticles have a significant impact on the magnetic properties [145]. The sample with higher zinc (5 mol% ZnO) content has the low concentration of magnetic particles with large spatial distribution and thus showed the paramagnetic behaviour.

^{57}***Fe Mössbauer spectroscopy***

The Mössbauer spectra for different glass samples (MG) are shown in ***Fig. 4.10a***. It was found that these spectra were composed of two paramagnetic doublets. Related

Mössbauer parameters like isomer shift (IS), and quadrupole shift (QS) were determined from these spectra of glass samples and given in ***Table 4.3***. Typical values of IS for Fe^{3+} tetrahedrally coordinated to oxygen in silicate glass are in the range of 0.20-0.32 mm s^{-1} while for octahedrally coordinated these values are in the range of 0.35-0.55 mm s^{-1}. For Fe^{2+}, IS values are in the range of 0.90-0.95 mm s^{-1} (tetrahedral) and 1.05-1.10 mm s^{-1} (octahedral) [116]. The isomer shift (IS) of Fe^{3+} and Fe^{2+} indicate that in glass structure Fe^{3+} and Fe^{2+} were present in tetrahedral coordination (Th). The presence of some iron ions in the Fe^{2+} state attributed to the reduction of Fe_2O_3 by the presence of ZnO and CaO in the melt [117]. From ***Table 4.3***, it can be seen that in the glass containing 2 mol % ZnO nearly 58 % of the total iron entered as Fe^{3+} ions in tetrahedral sites. Fe^{3+} ions in tetrahedral state ware increased to nearly 62 % of the total iron with increase of ZnO content to 5 mol %.

Table 4.3. *Various parameters obtained from Mössbauer spectra of glass samples.*

Sample	Component 1 (Fe^{3+} (Paramagnetic))				Component 2 (Fe^{2+} (Paramagnetic))				Fe^{2+} /Fe^{3+}
	QS	IS	RI	Γ	QS	IS	RI	Γ	
MG0	1.02	0.27	58.8	0.69	1.77	0.97	41.2	0.81	0.70
MG2	1.08	0.25	57.7	0.68	1.92	0.98	42.2	0.74	0.73
MG5	1.14	0.24	61.5	0.65	2.03	0.97	38.4	0.65	0.63

IS: Isomer shift (mm/s), QS:Quadrupole Splitting (mm/s), RI: relative intensity,
Γ: Line width (mm/s)

The ratio of Fe^{2+} and Fe^{3+} ions was determined from the relative areas obtained by computer fitting of experimental spectra. It was seen that with increase of ZnO content to 5 mol%, Fe^{2+} / Fe^{3+} ions ratio was in the range of 0.71-0.66. IS value of Fe^{3+} (Th) decreased with addition of ZnO. The increase of QS was attributed to an increase in the asymmetry around the iron ions.

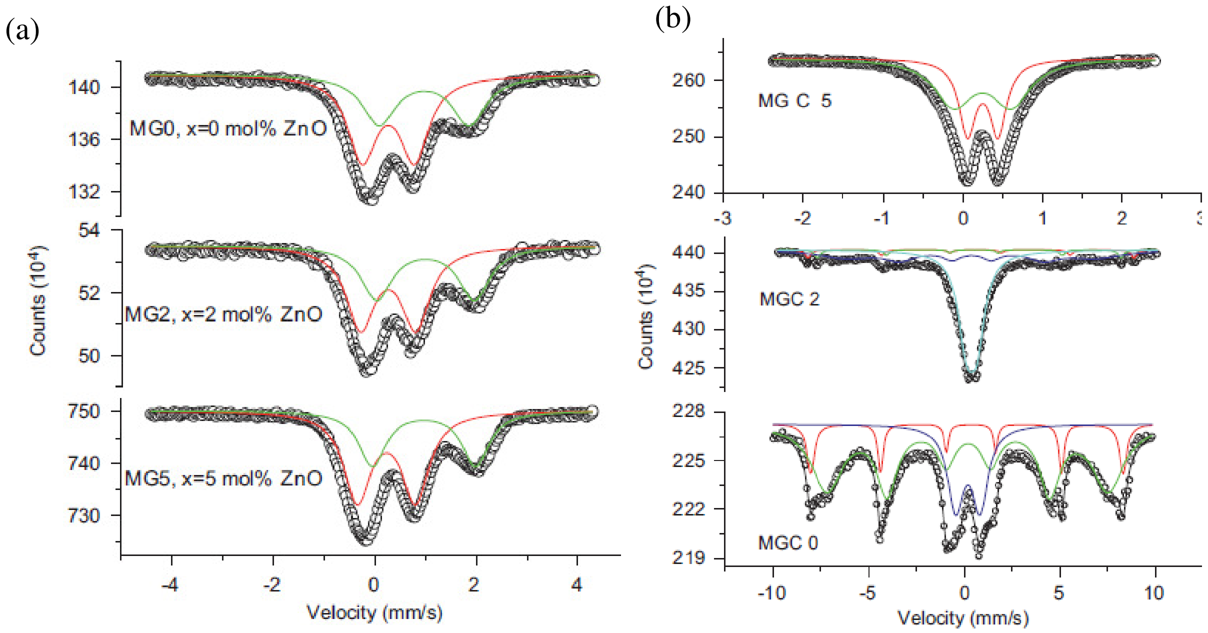

Fig. 4.10. *Mössbauer spectra recorded at room temperature for (a) glass; (b) glass-ceramics.*

The Mössbauer spectra for different glass-ceramics samples are shown in **Fig. 4.10b** and related Mössbauer parameters are given in ***Table 4.4***. On heat treatment the sample (MGC) showed magnetic and paramagnetic components due to Fe^{3+} and Fe^{2+} ions depending upon the compositions. Sample (MGC0) without ZnO showed two magnetic components (Fe^{3+} in octahedral coordination) with the magnetic hyperfine fields H_{hf}=507 and 456 kOe and one paramagnetic component (Fe^{3+} in tetrahedral coordination). Analysis of Mössbauer spectra indicated that Fe nanoparticles were in ordered magnetic states as two sextets were observed. The presence of doublet was either due to distribution in particle size or presence of isolated Fe (+3 octahedral) ion-clusters showing complete magnetic relaxation. The sextet with an isomer shift of 0.52 mm/s, quadrupole splitting of 0.10 mm/s, and hyperfine field of 507 kOe was attributed to the presence of Fe_2O_3 phase (hematite) [118]. Other sextet was due to spinel phase in magnetic ordered state. The values of isomer shift 0.35-0.55 mm s^{-1} are consistent with iron ions in trivalent state (octahedral) and the hyperfine fields having values between 484 –453 kOe are typical for spinel ferrite. The low value of quadrupole splitting of 0.020 mm/s was attributed to cubic symmetry around iron ions.

Table 4.4. *Various parameters obtained from Mössbauer spectra of glass-ceramics samples.*

Sample	Com	Magnetic				Paramagnetic			
		H_{int}(kG)	QS	IS	RI	QS	IS	RI	Γ
MGC0	Com1	507.65	0.107	0.526	12.13	1.2790	0.3615	21.02	0.9935
	Com2	456.73	0.020	0.386	66.85				
MGC2	Com1	515.6	0.026	0.686	3.73	0.558	0.396	56.45	1.008
	Com2	509.8	0.127	0.535	3.97				
	Com3	407.7	0.025	0.396	36.22				
MGC5	Com1					0.3834	0.4627	42.09	0.2562
	Com2					0.7232	0.4575	57.90	0.5771

H_{int}: Internal Field (kG), Com: component

When 2 mol % ZnO was added, spectrum showed sextets as well as doublets. The spectrum was fitted with three magnetic components having magnetic hyperfine fields H_{hf}=515, 509, 407 kOe. The sextet with H_{hf}=515 attributed to the nanostructured hematite phase. The formation of Fe_3O_4 and $ZnFe_2O_4$ was observed on heat treatment of the glass sample. This sample exhibited somewhat large magnetization when compared with the sample without ZnO (***Fig. 4.9***). The large magnetization was due to substitution of some of Fe ions at A site by Zn resulting in increased net magnetization. Further it may be possible that Fe^{3+} occupy the tetrahedral (A) as well as octahedral (B) sites, resulting in strong super exchange interactions between the Fe^{3+} ions occupying A and B site. The other two sextets with hyperfine fields of 509 and 407 kOe attributed to magnetite and zinc ferrite, respectively. The very small values of QS for the sextets indicate cubic symmetry around the iron sites. The spectrum also showed a doublet indicating the presence of complete superparamagnetic relaxations, i.e., some particles have size lower than the critical size of the present mixed spinel ferrite nanoparticle. The glass-ceramics sample with 5 mol % ZnO showed paramagnetic doublet arising from Fe^{3+} and Fe^{2+} ions. The doublet was assigned to hematite (Fe_2O_3) [118]; this correlates well with the starting composition and XRD analysis of the sample showing the presence of such a phase. The other doublet was attributed to small sizes particles (ferrites, Zn-ferrites) in the specimen giving rise to a superparamagnetic relaxation.

4.3.5. In vitro studies

4.3.5.1. In SBF

Fig. 4.11 shows the infrared spectra of the MGC0 sample after immersion in simulated body fluid for 0, 1 and 4 weeks. The spectrum before the immersion revealed bands around 1200, 985, 784, 648 cm^{-1} which correspond to P–O stretching, Si–O stretching, Si–O–Si stretching and Fe–O stretching frequencies, respectively [121].

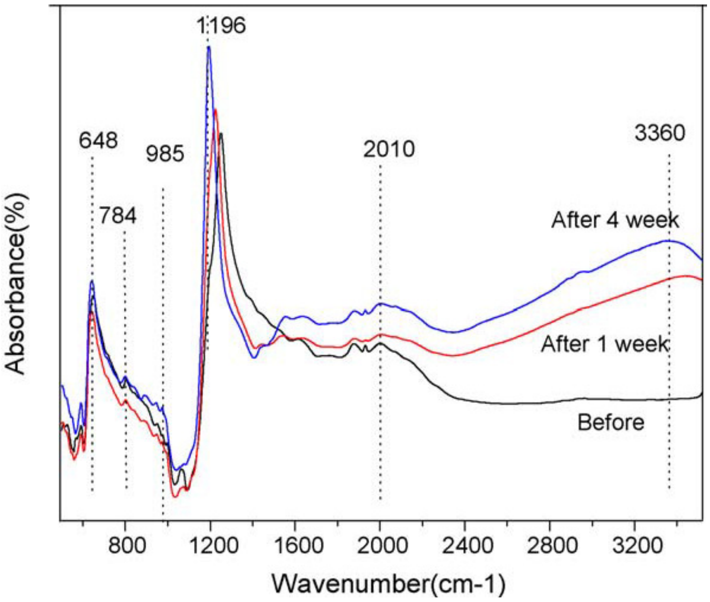

***Fig. 4.11**. FTIR spectra of glass–ceramics (ZFC0) samples after different time of immersion in SBF.*

After 1 week of immersion in SBF, new band around 3360 cm^{-1} appeared. This band is associated with non-hydrogen bonded hydroxyl group of apatite. This implies the formation of hydroxyapatite upon immersion in SBF. The intensity of this band increased with increase in immersion time in SBF. This is related with the increase in surface coverage with apatite. In addition, the band around 980 cm^{-1}, related to calcium phosphate (hydroxyapatite) surface layer was observed. The band at 1300-1600 cm^{-1} was assigned to C–O vibration mode of CO_3^{2-}. These bands signify the incorporation of carbonate anions from the SBF in the apatite crystal lattice.

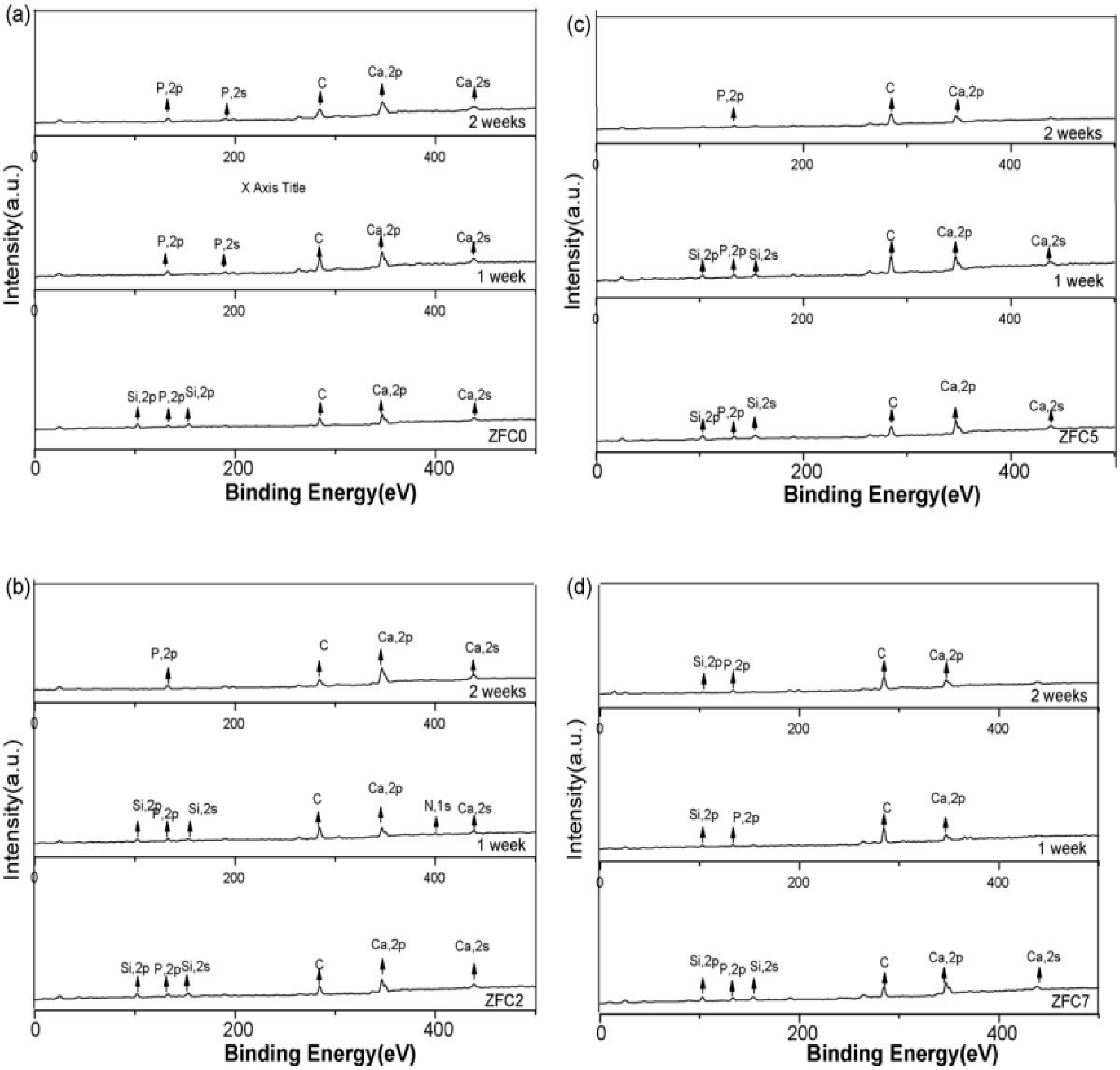

Fig. 4.12. *XPS spectra of different glass–ceramic (1000°C) before and after immersion in SBF; (a) ZFC0, (b) ZFC2, (c) ZFC5, and (d) ZFC7.*

The interactions of SBF solutions with bioglass/glass-ceramics as suggested by Hench [39] start with ion exchange process resulting in the increase in pH of solution. This causes the surface dissolution. The sample surface of MGC0 (***Fig. 4.12a***) got depleted of Si and Ca during its interaction with SBF (after 1 week). This was evident from the decrease in the intensity of peaks corresponding to Ca and the absence of peak corresponding to Si2p in the XPS spectra (after 1 week). Si concentration in the SBF solution increased as the immersion time of sample in SBF was increased (***Fig. 4.13***). This increase of Si in SBF solution was resulted from the surface dissolution.

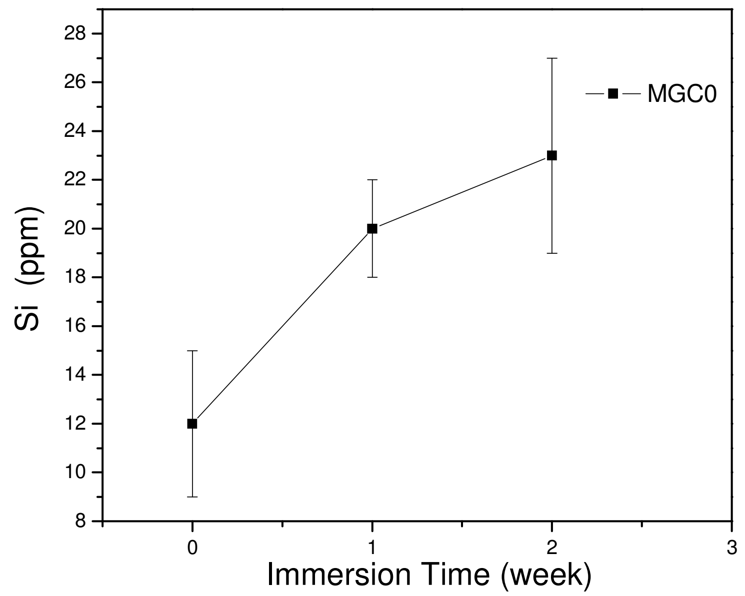

Fig. 4.13. *Si concentration in the SBF solution after different time of immersion of MGC0 samples.*

Chemical analyses of SBF solutions after immersion period for 1–2 weeks are given in ***Table 4.5***. After 1 week immersion, the concentration of Ca slightly increased from that of as prepared SBF concentration while the Fe and Zn were not detected in the SBF solution. This implies the dissolution of Ca from the surface. On exposure of these samples to SBF solution for 2 weeks, intensity of XPS peaks corresponding to Ca and P increased when compared with that of spectra of sample after 1 week immersion (***Fig. 4.12a–d***). This indicates the formation of the some Ca–P-rich layer at the surface. This kind of behaviour was observed for all the samples. However, the presence of Si2p signal (with some attenuation in intensity) in the wide scan spectra for MGC7, provides the evidence of partially coverage of surface after 2 weeks of exposure (***Fig. 4.12d***).

Table 4.5. *Concentration (ppm) of different constituents (Ca, Zn and Fe) of SBF solutions after immersing glass–ceramic samples for different durations.*

Sample		Concentration (ppm)		
		Ca	Fe	Zn
MGC0	One week	25±2	Nil	Nil
	Two weeks	23±3	Nil	Nil
MGC2	One week	21±2	Nil	Nil
	Two weeks	24±2	Nil	Nil
MGC 5	One week	19±3	Nil	Nil
	Two weeks	18±2	Nil	Nil
MGC7	One week	21±3	Nil	Nil
	Two weeks	22.±3	Nil	Nil
SBF		21±2	Nil	Nil

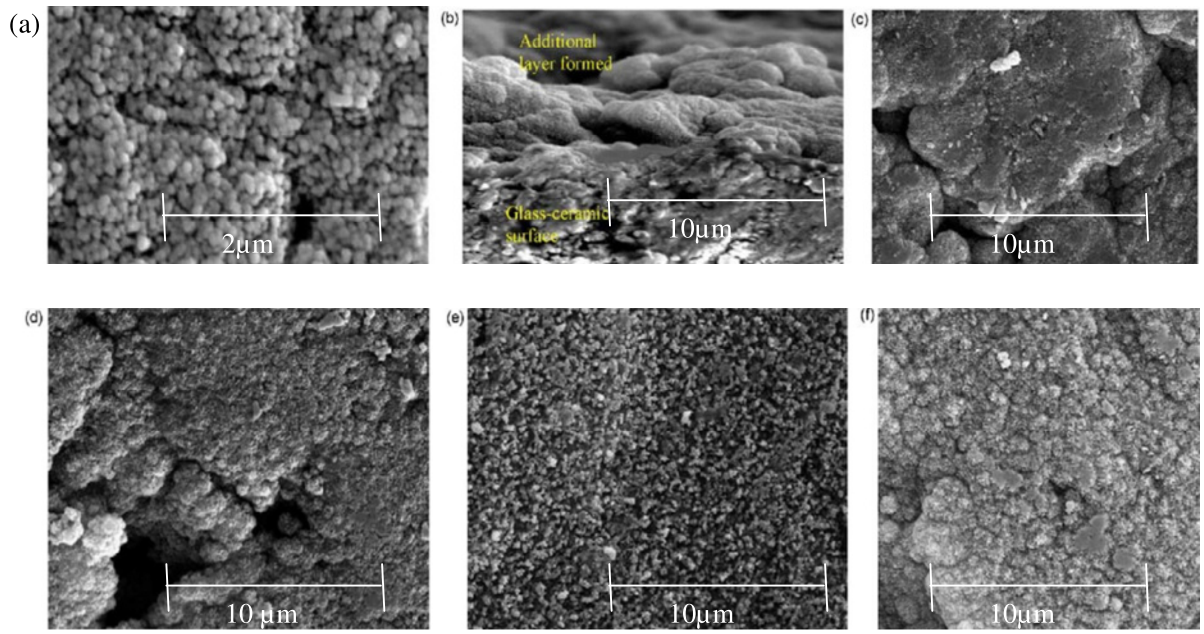

Fig. 4.14. *SEM micrographs of MGC0 sample after immersion in SBF for 1week (a) surface morphology; (b) the cross-section of the surface; and, surface morphology of different glass–ceramics (1000 8C) sample after 4 weeks immersion in SBF (c) MGC0; (d) MGC2; (e) MGC5 and (f) MGC7.*

Fig. 4.14(a–f) illustrates the evolution of microstructure of the samples heat treated at 1000° C, upon immersion in SBF for different durations. ***Figs. 4.14(a, b)*** show the surface morphology and cross-section of the surface of the MGC0 sample immersed in SBF for 1 week. ***Figs. 4.14(c–f)*** show the surface morphology of MGC0, MGC2, MGC5, and MGC7 after immersion in SBF for 4 weeks. It was seen that the growth of apatite-like layer started growing on the sample surface after 1week immersion in SBF. Surface morphology and cross-section of the surface of MGC0 sample exhibited the growth of the apatite layer. The surface morphology also showed the presence of some voids on the surface. The surface morphologies of the other samples also exhibited the growth of the particles of different sizes with some localized coagulation of the particles. With increase in immersion time to 4 weeks there was increase in growth of the particles, along with the presence of some voids. These voids could be the gaps between the agglomerates as the particles have grown with increase in immersion time.

The formation of $CaO–P_2O_5$ rich layer on the surface of bioactive glasses upon interaction with simulated body fluid has been reported by many authors [123,146]. The formation of such layer on the MGC samples surfaces was observed, however, the area of surface covered with Ca–P layer was increased with the addition of ZnO content up to 5 mol% as seen from SEM (***Fig. 4.14***). Further increase of ZnO content resulted in the decrease in growth of the layer.

The formation of Ca–P bioactive layer involves several steps and governs by the nucleation and growth of particles at the surface [7, 39]. The formation of hydroxyapatite is commenced when surface dissolution takes place. Chemical analysis of the SBF solution has shown the surface dissolution has taken place. It involved the dissolution of residual glass and crystallites in glass matrix. Hence, the interactions of SBF solution with surface will depend on both the structure of residual glass and the emergence of different crystallite phases.

It was seen by XRD that the composition of phases evolved in the microstructure was changed with addition of ZnO. Three major phases calcium phosphate, calcium silicate and hematite were formed in glasses when heat treatment at 1000ºC. The peaks intensities corresponding to calcium phosphate, calcium silicate was increased as the ZnO content in the glass was increased. $Ca_3(PO_4)_2$ and calcium silicate (rankinite) phases are reported to be bioactive [147]. Thus the area of the Ca–P layer formed at the surface increased with an increase in ZnO content upto 5 mol% as the content of bioactive phases was increased.

Though the contents of bioactive phases was increased with increase in ZnO content to 7 mol%, but the growth of additional layer formed on the surface was reduced. With the increase in ZnO content, the fraction of non-bridging oxygen was decreased (***Table 4.2***). This decreased the surface dissolution during the interactions of the body fluids with the sample. Hence, the subsequent surface reactions, which involve nucleation and growth of the apatite particles, were affected. Thus reduction in growth of Ca–P rich layer was observed. A comparison of the results suggests that, for the glass–ceramic samples containing ZnO up to 5 mol%, the formation of the Ca–P-rich layer occurred rapidly as compared to sample without ZnO. Further increase in the ZnO content to 7 mol% the surface dissolution decreases as the fraction of non-bridging oxygen has decreased with a consequent decrease in the ability of forming bioactive layer.

4.3.5.2. In-vitro analysis in BSA

SEM micrographs of the glass-ceramic samples, after immersion in BSA are shown in ***Fig. 4.15(a-d)***. After 3 days immersion of sample MGC0, SEM micrograph showed the surface coverage with small size particles (***Fig. 4.15a***). These particles were grown in size when sample was immersed for 7 days. After 7 days immersion, with addition of 2 mol% ZnO, surface morphology exhibited the surface coverage with smaller particle sizes (***Fig. 4.15c***). However, when ZnO content was increased to 5 mol%, surface morphology with little adsorption of BSA was observed.

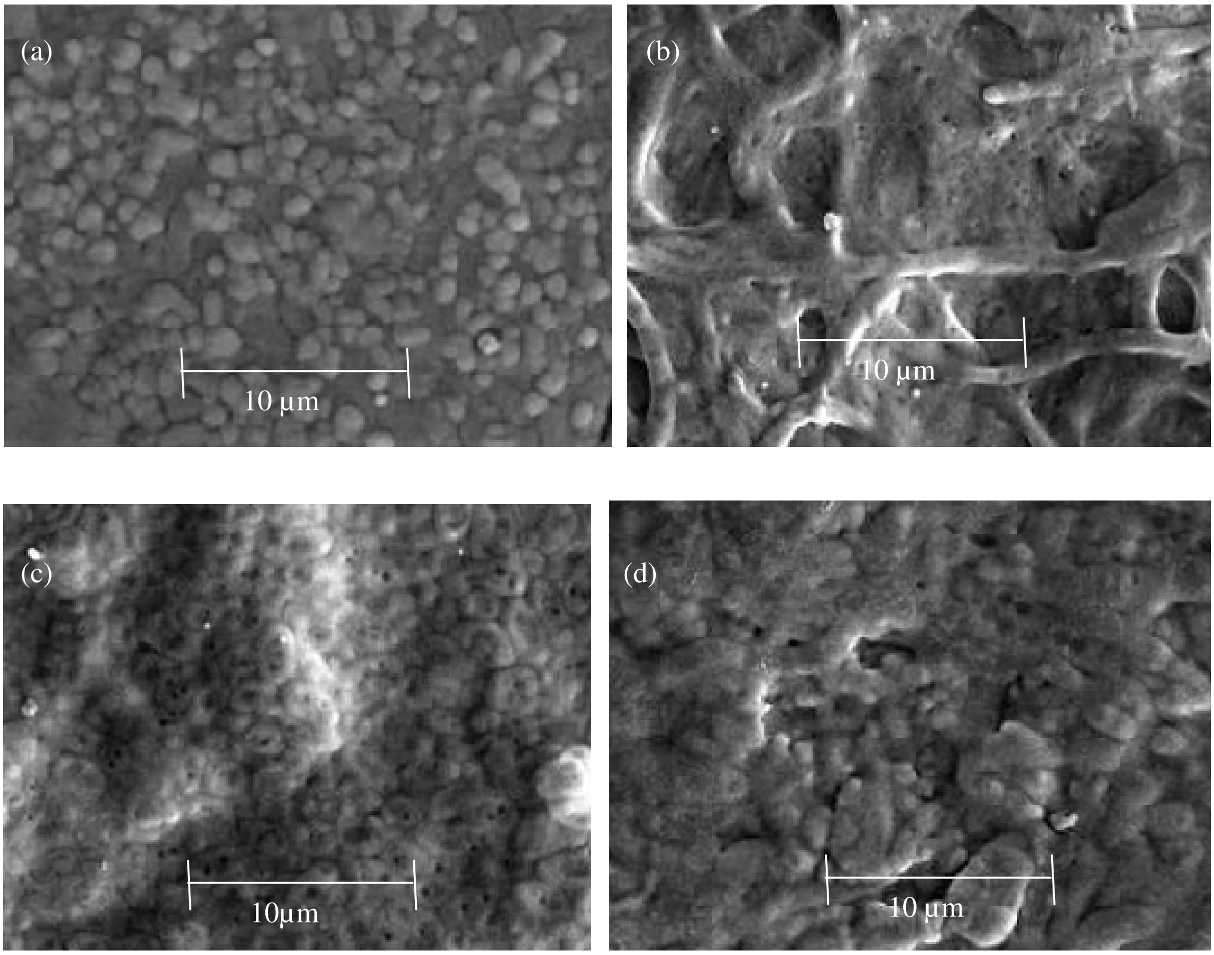

Fig. 4.15. *SEM photographs of MGC0 glass-ceramics after (a) 3 days immersion in BSA, and surface morphology of different glass-ceramics samples after 7 days immersion in BSA (b) MGC0; (c) MGC2 and (d) MGC5.*

SIMS spectra of glass-ceramic samples after immersion in BSA for 7 days are shown in ***Fig. 4.16a***. SIMS spectra of sample MGC0 showed Ca (m/z = 40) as major peaks while peaks corresponding to C, Si and Fe were also visible. The peak around (m/z = 69) was assigned to Ga ions which were used (ion source) for bombardment of the samples. In addition of these peaks, peaks corresponding to polymeric chains were observed. Secondary positive ions peaks corresponding to CH_3, CHN, CO, $CONH_2$, $C_2H_5NH_2$, CN_3H_3, C_2H_6NO, $C_2H_2CONH_2$, $C_3H_4CONH_2$, related to adsorbed BSA, were observed at m/z = 15, 27, 28, 44, 45, 57, 60, 70 and 84 respectively. Similar features were observed on sample containing 2 mol% zinc oxide (***Fig. 4.16b***). Since the surface analysis of sample containing 5 mol % ZnO did not show good adhesion of polymers, this sample was not considered for SIMS analysis.

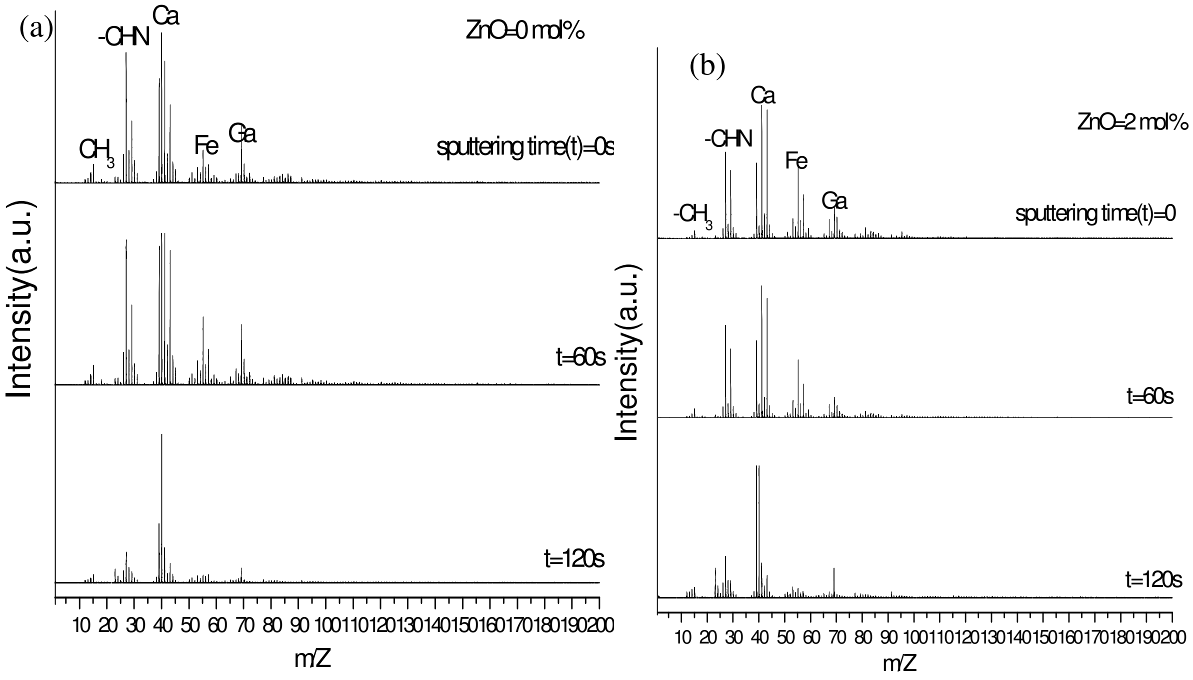

Fig 4.16. *SIMS spectra of different glass-ceramics after immersion in BSA for 7 days; (a) MGC0 and (b) MGC2.*

The SIMS spectra of the samples were recorded after sputtering the surface layer formed during immersion in BSA. When the sputtering time was increased to 120s the peaks corresponding to polymeric chain were removed and the peaks corresponding to Ca (*m/z* = 40) and Fe (*m/z* = 56) were observed as major peaks. A comparison between the sputtered and non-sputtered surfaces indicates the presence of BSA layer on the surfaces of samples MGC0 and MGC2 .

Fig. 4.17a shows the infrared spectra of the MGC0 sample after immersion in BSA solution for 0, 3, 5 and 7 days. After 3 days of immersion in BSA, new band around 3320 cm^{-1} was appeared. This band was associated with O–H stretching and adsorbed water at the surfaces. The band at 1685 cm^{-1} was also observed after immersion, which arose from the O–

H bending. In addition, bands around 2975 cm^{-1}, 2000 cm^{-1}, 1886 cm^{-1}, 1550 cm^{-1} were also appeared. After 7 days of immersion in BSA, these bands become stronger. The bands around 2800 cm^{-1} and 2900 cm^{-1} were assigned to $–CH_3$ and $–CH_2$ stretching vibration modes. The vibration bands around 1550 cm^{-1}, 1475 cm^{-1} and 1310 cm^{-1} were assigned to NH-C=O modes. These bands were associated with C=O stretching, C-H bending, N-H bending and N-H stretching, respectively [148-150]. This implies the adsorption of polymer on the surface upon immersion in BSA.

FTIR spectra of glass-ceramic samples having 2 mol% ZnO before and after BSA adsorption is shown in ***Fig. 4.17b***. The difference between FTIR spectra before and after 5 days immersion in BSA was not significant as a few additional bands were observed. However, after 7 days immersion in BSA, absorption bands at around 1320 cm^{-1} 1400 cm^{-1}, 1560 cm^{-1}, 1475 cm^{-1} were observed. The amide band near 1560 cm^{-1} was due to the C=O stretching mode, and the band near 1320 cm^{-1} was attributed to the bending and the stretching mode of N–H and C–N vibrations. FTIR spectra of glass-ceramic samples having 5 mol% ZnO before and after BSA adsorption is shown in ***Fig. 4.17c***. The additional bands around 2920 cm^{-1} and 2970 cm^{-1} were observed, which were assigned to $–CH_3$ and $–CH_2$ stretching vibration modes. The band observed at 3320 cm^{-1} was associated with O–H stretching and adsorbed water at the surface.

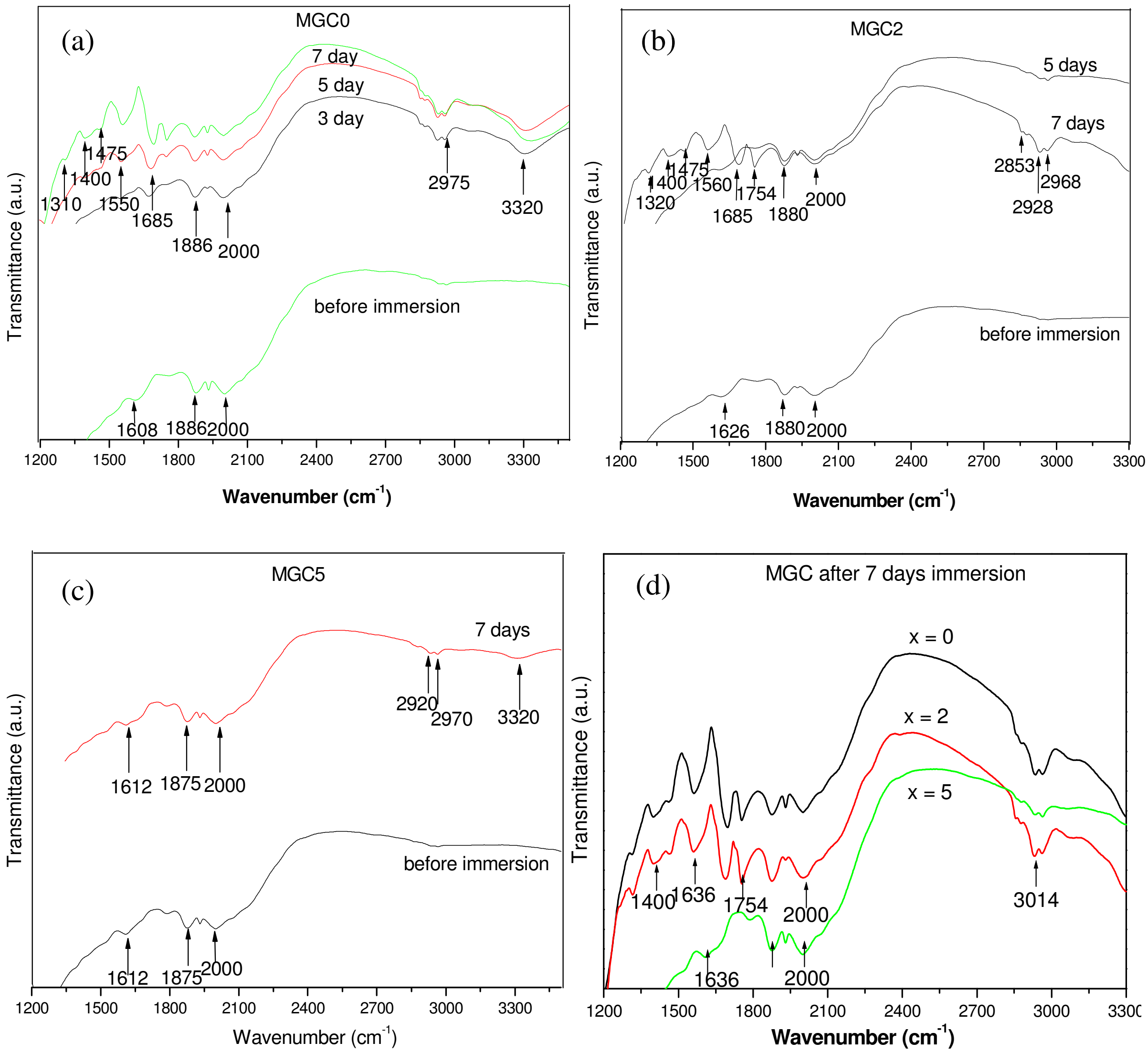

Fig. 4.17. *FTIR spectra of different glass-ceramics before and after immersion in BSA for different time period MGC0; (b) MGC2; (c) MGC5 and (d) MGC0-5 after 7 days immersion in BSA.*

On comparison the FTIR spectra of samples MGC0-5 after 7 days immersion in BSA solution, absorption bands corresponding to N–H and C–N vibrations were observed for MGC0 and 2 (***Fig.4.17d***). This indicates the adhesion of polymer on these surfaces. However, the weak vibration bands corresponding to C-H were observed for the samples containing 5 mol% ZnO, which implies the poor adhesion of polymer. The adhesion of BSA on the samples surfaces was also seen in the SEM micrographs (***Fig. 4.15***) as reported earlier. Thus, the surface analysis of the MGC samples after immersion in BSA revealed the adhesion of polymer on the surface, however poor absorption of BSA was observed for sample having 5 mol% of ZnO.

BSA is a long protein and have -NH_2 and -COOH group in its molecular structure. The isoelectric point of bovine serum albumin is pI=4.7, which indicates that BSA has a positive charge below pI 4.7 and negative charge above pI 4.7. The silca coated magnetic particles have reported to have isoelectric point in between 2-3 [128,151]. This implies that at pH 7.0 the surface will be negatively charged. Therefore, the adsorption of BSA by hydrophobic interaction will be minimal.

Glass-ceramics are polycrystalline materials and prepared by controlled crystallization of parent glasses. Thus glass-ceramics can have a residual glass, which may influence the surface response. Upon immersion in BSA, Si–OH functional groups are formed on the material surface, which make a bond between material and proteins. The formation of Si–OH functional groups in vitro and in vivo analyses of bioglass and glass-ceramics are reported by many authors [39, 152].

The adhesion of polymer starts with the initiation of –N-H and C=O group on the surface. These groups can make the hydrogen bonds with Si–OH groups present at the surface. It was observed that the formation of Si–OH groups initiated after 3 days immersion in BSA. The bands at 3360 and 1680 cm^{-1} suggested the formation of –OH bonds at the surfaces (Fig 4.16). As the immersion time in BSA increased NH and C=O groups of BSA made bond with these group and the band at 1400 cm^{-1} and 1310 appeared.

Crystalline phases have much lower dissolution rates than the glasses. The glass phase in glass-ceramics controls the surface chemistry, which in turn decides the in-vitro response of glass/glass-ceramics [127, 153]. It was found that ZnO stabilized the glass structure as the fraction of non bridging oxygen was decreased (***Table 4.2***). Consequently the network became rigid and it took long time for formation of –OH groups. Formation of these groups took place on MGC0 after 3 days of immersion, while it took 5 days for MGC2 and 7 days for MGC5 to have a significant hydroxylation. Thus, when ZnO content was increased surface dissolution decreased; forming a less numbers of –OH groups on surfaces. Since the BSA bind to these groups, the adsorption of protein decreased.

4.4. Conclusion

Structural and microstructural properties of glass/glass-ceramics with chemical composition $25SiO_2–50CaO-15P_2O_5-(10-x)Fe_2O_3-xZnO$ (x =0, 2, 5, 7 mol %) were studied. The fraction of non-bridging oxygen decreased as the ZnO content was increased. On heat-treatment at 1000°C calcium phosphate and calcium silicate were developed as major crystalline phases with nano-size crystallites. The glass-ceramics showed ferrimagnetic behaviour. Mössbauer spectroscopy determined that both Fe^{3+} and Fe^{2+} ions were present in tetrahedral coordination in glass samples. The magnetic nano-particles were found in ordered magnetic states with cubic symmetry around Fe sites. Blocking temperature of investigated samples decreased with the addition of ZnO implying the decrease in strength of dipolar interaction. These were observed to develop Ca-P rich layer at the surface when immersed in SBF, thereby indicating the bioactive nature of the material. According to the surface analysis, glass-ceramics containing upto 5 mol % ZnO have shown better bioactive response than the sample having no ZnO. Higher ZnO content (7 mol %) decreases the surface activity due to reduction in non-bridging oxygens. Adhesion of BSA was seen on the glass-ceramics; however, the polymeric adhesion was decreased with addition of ZnO. These materials thus exhibited the property, which can be exploited to bind specific proteins on the surface for magnetic drug targeting or polymer detection and separation.

Chapter 5

Studies of calcium silico-phosphate glass-ceramics containing iron oxide, zinc oxide and Ag

---

The glass and glass-ceramics can be used as possible vehicles for the delivery of ions like Ag and zinc. Glasses containing silver, zinc and iron were prepared and magnetic, structural and antibacterial properties of these materials are discussed in this chapter.

5.1 Introduction

5.2 Experimental

5.3 Results and Discussion

5.4 Conclusion

5.1 Introduction

Magnetic materials are gaining increased importance owing to a variety of applications in health care for cell separation, magnetic resonance imaging contrast agents, drug delivery, and magnetic hyperthermia treatment of cancer [154, 155]. In the recent past, a large number of magnetic materials including magnetic glass-ceramics possessing a variety of functional attributes have been developed [156-158].

Silver is currently used to control bacterial growth in a variety of applications, including dental work, catheters, and burn wounds. Ag ions are toxic to microorganisms, showing strong biocidal effects in as many as 12 species of bacteria including Escherichia.coli (E.coli) [159-161]. Glass/glass-ceramics can be potential carriers of antibacterial ions like silver because these materials can accommodate these ions in their structure. The rate of release of Ag ions can be controlled by modifying the structure of the materials or using some external stimuli like magnetic or electric field.

However, addition of metallic ions like Ag modifies the local structure of the glass. These can induce nucleation in the glass matrix and affect the local arrangement of particles. In addition, the magnetic properties depend on the microstructural parameters such as crystallite size, phase distribution and volume fraction of the magnetic phase [115]. Iron ions (Fe^{2+} and Fe^{3+}) can exist in tetrahedral or octahedral coordination. Mössbauer spectroscopy provides information on the coordination of the iron ions, which will be useful in understanding their magnetic properties [161, 162].

Preparation of iron doped glass-ceramics in SiO_2-CaO-B_2O_3-P_2O_5 has been reported [97, 99]. Besides, there are some reports of antibacterial property due to the incorporation of different metal ions such as Ag^{+}, Cu^{+2}, Zn^{+2} [163, 164]. The glass-ceramics containing both Fe and Ag are of interest as addition of Ag modifies the arrangement of magnetic particles and may lead to improvement in magnetic properties. Further the presence of Ag will induce the antibacterial properties.

Therefore, glass/glass-ceramics with $25SiO_2$-(50-x)CaO-$15P_2O_5$-$8Fe_2O_3$-2ZnO-xAg (where x = 0, 2 and 4 mol %) have been prepared. Structural and magnetic properties of glass/glass-ceramic containing iron, zinc oxide and Ag are discussed in this chapter. Isomer shift values obtained by Mössbauer spectroscopy suggest that Fe^{3+} ions were in octahedral co-ordinations. Magnetization improved with an increase in Ag content up to 4 mol% and has been attributed to increase in magnetic ordering. Antibacterial response of Ag containing glass-ceramics samples was studied against E. coli and found to depend on Ag ions concentration in the glass matrix. The glass-ceramic containing 4% Ag showed complete inhibition of bacterial growth at a concentration of 10% (w/v). However, the glass-ceramic containing 2% Ag showed the similar effect at 20% (w/v).

5.2 Experimental

The nominal compositions of base glasses given in ***Table 5.1*** were prepared by melt quenching technique. About 100 g batches were prepared by mixing appropriate amounts of reagent grade SiO_2, $CaCO_3$, NH_4 H_2PO_4, ZnO, $AgNO_3$ and Fe_2O_3. The charge was calcined at 900°C for periods up to 12 h after holding at different intermediate temperatures for 6-8 h as dictated by the decomposition temperatures of various precursors. The calcined charge was melted under ambient air at 1500 °C in a covered Pt-Rh crucible in a raising-lowering hearth electric furnace. The melt was held for 30 minutes at this temperature for homogenization and then poured into water. The frit was powdered in a ball mill. Hereafter, glass-ceramics samples would be referred to as MAGx while annealed samples as MAGCx, where x refers to the Ag mole%. On heat treatment of MAG0, MAG2 and MAG4 samples at 800 °C for 6 h, we got MAGC0, MAGC2 and MAGC4 having 0, 2 and 4 mol% of Ag respectively.

Table 5.1. *Base compositions (nominal) in mol %.*

Sample	SiO2	P_2O_5	CaO	Fe_2O_3	ZnO	Ag
MAG0	25	15	50	8	2	0
MAG2	25	15	48	8	2	2
MAG4	25	15	46	8	2	4

Structural phase emergence in the powdered samples was investigated using XRD and the crystalline phases present in the samples were identified. The microstructure of the MAGC samples was characterized by SEM. Prior to mounting the samples in analysis chamber of SEM, a thin Au conducting coating was deposited on their surfaces to prevent charging effect.

The magnetization (M) versus applied magnetic field (H) plots were obtained at room temperature using vibrating sample magnetometer (VSM, Lakeshore 7410) equipped with a high temperature oven. VSM was calibrated using a standard reference (high purity nickel sphere) supplied with the instrument. These data have been analyzed to obtain the saturation magnetization (M_s), remanence magnetization (M_r), and coercive field (H_c) for each sample. Mössbauer spectra were obtained using a Mössbauer spectrometer operated in constant acceleration mode. The source employed was ^{57}Co in Rh matrix of strength 50 mCi. The calibration of the velocity scale was done using iron metal foil. Mössbauer spectra were fitted with appropriate doublets and sextets using a least squares fitting program. The ratio of Fe^{2+} and Fe^{3+} ions was determined from the relative areas obtained by least squares fitting of experimental spectra.

Elemental release of Si, P, Ag and Fe in DI water as a result of dissolution of glass-ceramics samples was measured using atomic absorption spectrophotometer (Model Chemito AA 203). For antibacterial studies, a single colony of *E.coli* (MG1655) was grown overnight in 10 ml of Luria-Bertani broth in a rotary shaker (Orbitek, Scigenics Biotech Pvt. Ltd., India) (125 rpm) at 37°C. Next day the culture was subcultured in 50 ml LB (1:25 dilution) containing different concentrations (0.1 to 20% w/v) of Ag magnetic glass-ceramics and grown at 37°C in shaking condition (125 rpm). The cell culture was later centrifuged at 8000g for 10 min in a centrifuge (Tigra, model: CMF 15 KR, Poland). The cell pellet was washed twice using LB broth and re-suspended in LB. Proper dilutions were spread plated in LB agar plates for enumerating viable cells. The plates were incubated at 37°C for 24 h in an incubator (Sanyo, model: MIR-262, Japan) and later colony forming units were counted.

5.3. Results and discussion

5.3.1. Structural studies

The XRD patterns of glass-ceramics are depicted in ***Fig. 5.1(a-c)***. XRD patterns of samples MAG0, MAG2 and MAG4 showed peaks corresponding to β-Fe_2O_3, hematite and magnetite phases. Some peaks corresponding to $Ca_3(PO_4)_2$ and calcium silicate phases were also observed. CaO reacts with P_2O_5 leading to the formation of $Ca_3(PO_4)_2$ crystallites in the glassy matrix [18,19].

$$3CaO+P_2O_5 \rightarrow Ca_3(PO_4)_2 \qquad \textbf{(5.1)}$$

Magnetite has formed in the glass matrix by the reaction

$$6Fe_2O_3 \rightarrow 4Fe_3O_4 + O_2 \qquad \textbf{(5.2)}$$

The conversion of hematite (Fe_2O_3) into Fe_3O_4 depends on the reducing environment in the melt. Zinc ferrite can also be formed by the following reaction

$$ZnO+7Fe_2O_3 \rightarrow 4Fe_3O_4 + ZnFe_2O_4+O_2 \qquad \textbf{(5.3)}$$

However, detection of low quantity phase (zinc ferrite) was not possible in XRD. A slight shift in the XRD peak around (31.5°) was observed with addition of Ag, which might be due to incorporation of some zinc in iron oxide (***Fig. 5.1c***).

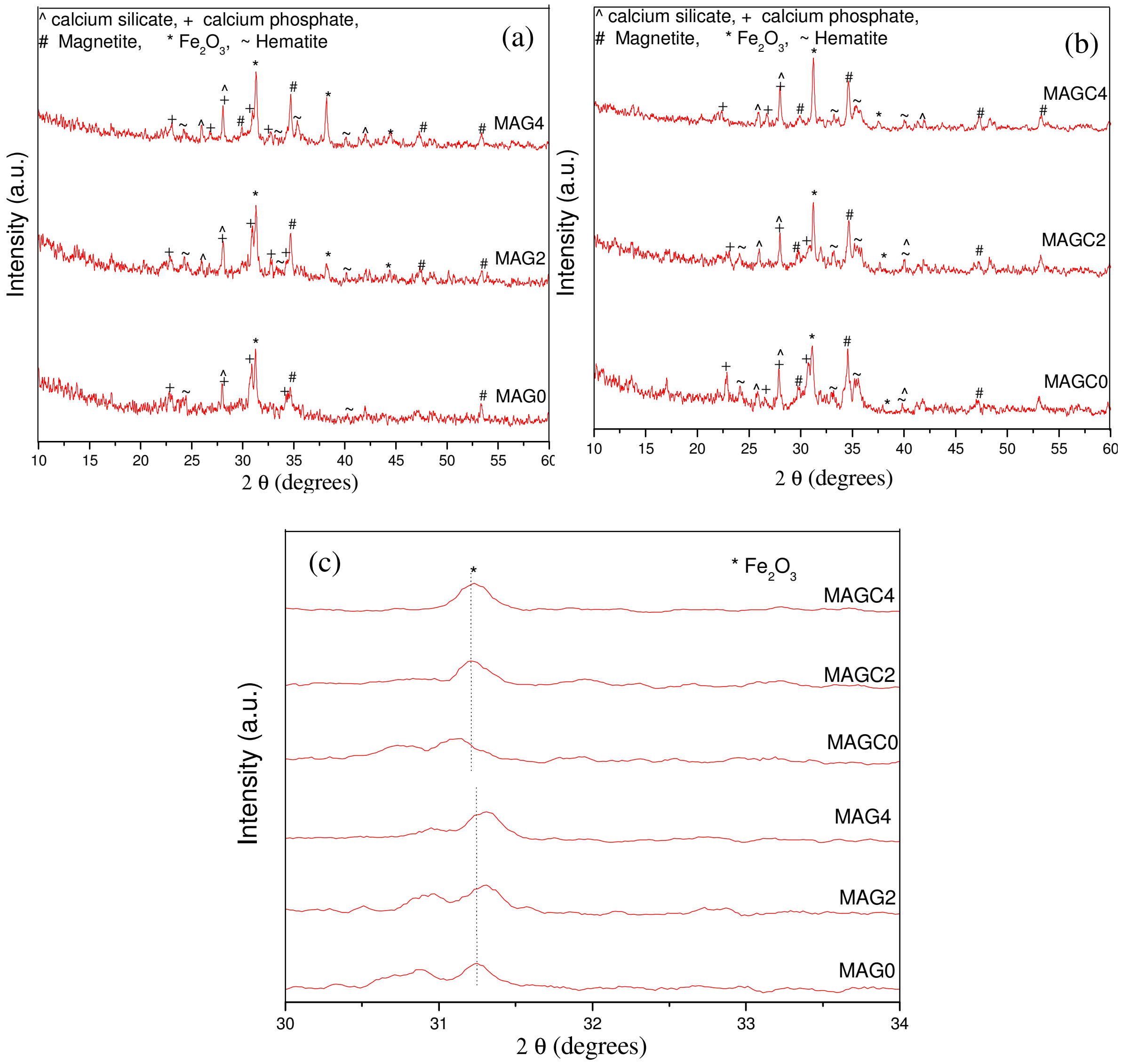

Fig. 5.1. *XRD patterns of glass-ceramics having different Ag ion concentration (a) MAG, (b) MAGC, (c) showing slight shift in XRD peak around (31.5°).*

Structural rearrangement or ordering process takes place as a consequence of decrease in free energy of the system when the melt is cooled below its liquid temperature. This involves the nucleation and crystallization processes. Addition of Ag induces nucleation and promotes crystallization. We have observed that with addition of Ag peaks have become relatively sharp implies improved crystallization (***Fig 5.1a***). The average crystallite sizes (d) were estimated using the Scherrer's formula [165],

$$d = \frac{0.89\lambda}{\beta \cos\theta} \qquad \textbf{(5.4)}$$

where β, θ, λ are the measured full width at half maximum intensity, Bragg angle and wave length (0.15418 nm) of the X-ray, respectively. The average crystallites size was calculated using Fe_2O_3 peak (116) and Eq. (5.4). The average crystallite sizes were estimated to be between 30-35 nm.

5.3.2. Microstructural studies

Microstructures of annealed samples exhibited the granular morphology (***Fig.5.2***). SEM images showed the formation of crystallites of nanometer sizes dimensions.

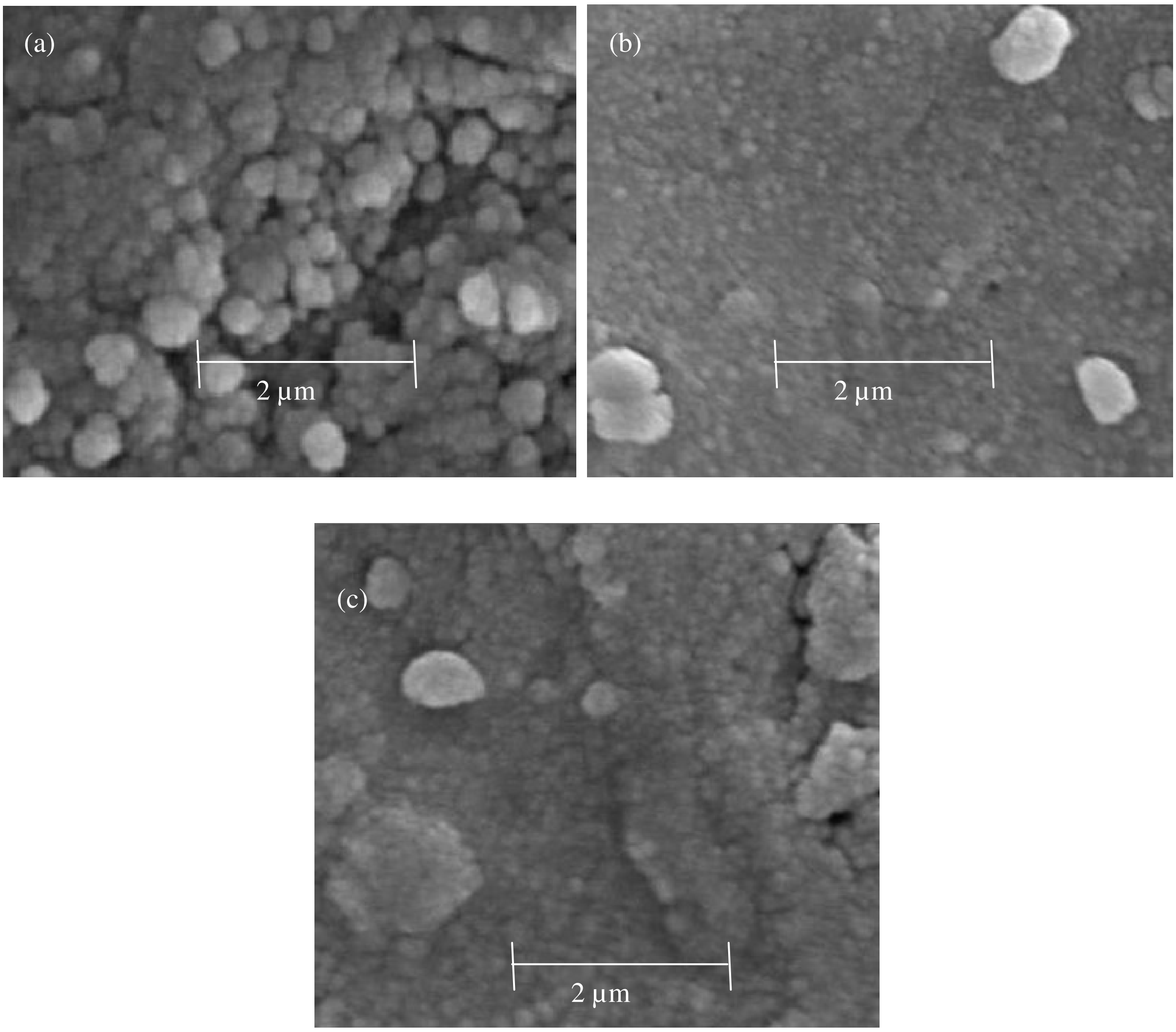

Fig. 5.2. *SEM photographs of glass-ceramics (a) MAGC0, (b) MAGC2 and (c) MAGC4.*

5.3.3. Magnetic studies

The magnetization curves of glass-ceramics samples measured at room temperature are shown in ***Fig. 5.3*** and magnetic parameters estimated from the plots are given in ***Table 5.2***.

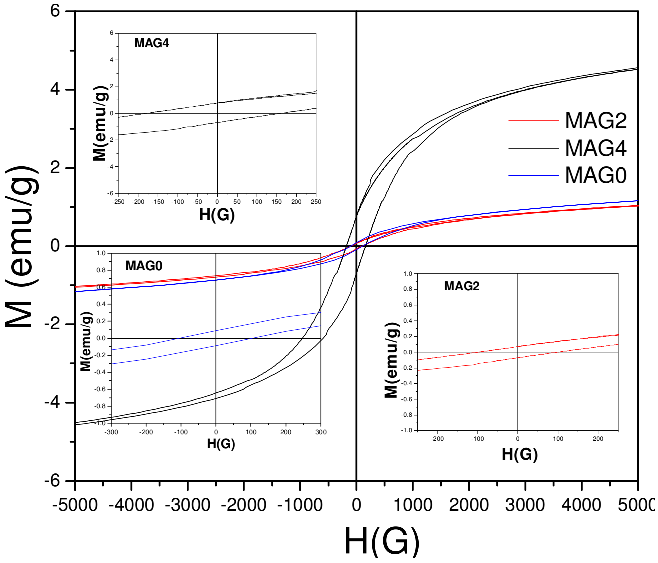

Fig. 5.3. *M-H plots of glass-ceramics samples having different Ag concentration. The insets show low field magnetization behaviours of the samples (MAG0, MAG2 and MAG4).*

The magnetization of these samples did not saturate up to an applied magnetic field of 5000 kA/m. It can be inferred from the nature of the curves that the samples exhibited a combination of paramagnetic and ferrimagnetic behaviour. The value of saturation magnetization obtained in all samples was found to be higher than that of commercial hematite (0.6 emu/g) [166]. The sample containing MAG0 showed the saturation magnetization of 0.75 emu/g and coercive field of 102 Oe. With addition of 2 mol% Ag, sample MAG2 showed similar hysteresis loop with a coercive field of 100 Oe. However, the value of coercive field increased to 166 Oe with an increase of Ag content to 4 mol%. In addition, the saturation magnetization also increased from 0.78 emu/g to 4.34 emu/g. The paramagnetic contribution reduced with an increase in Ag content.

Table 5.2. *Magnetic parameters estimated from M-H plots of glass-ceramics samples.*

Glass-ceramics	Coercive field (Oe)	Remanence magnetization (emu/g)	Saturation magnetization (emu/g)
MAG0	102	0.08	0.75
MAG2	100	0.09	0.78
MAG4	166	0.95	4.34
MAGC0	8	0.06	3.30
MAGC2	14	1.28	3.10
MAGC4	35	1.20	4.40

The coercivity is an extrinsic property of a material and depends on the shapes, sizes and pinning of crystallites [167, 168]. However, glass-ceramics are polycrystalline materials, polycrystalline nature of aggregated nanoparticles can result in an enhancement in coercivity values [169]. The formation of different crystalline phases in glass matrix is governed by nucleation and crystallization processes, which are influenced by nucleating agents. Thus increase in Ag content had resulted in the formation of more nuclei in the glass matrix and thereby forming more aggregates of magnetic particles [170]. This results in an increase in coercive field due to the directional aggregation of magnetic particles.

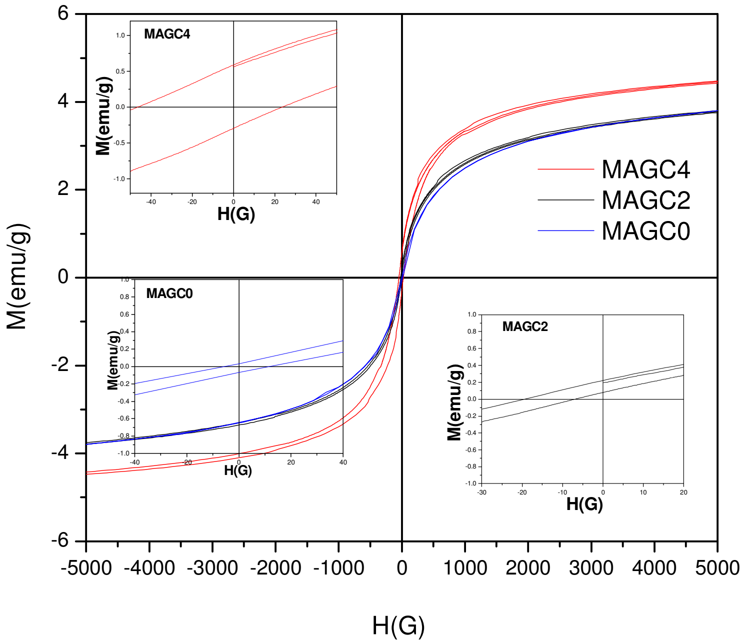

Fig. 5.4. *M-H plots of the heat treated glass-ceramics samples having different Ag concentration. The insets show low field magnetization behaviours of the samples (MAGC0, MAGC2 and MAGC4).*

Variation of magnetization as a function of field at room temperature for heat treated samples is shown in ***Fig. 5.4***. On heat treatment, saturation magnetization was increased. The increase in saturation magnetization was due to the completion of the magnetic structure, as atoms have sufficient energy to form magnetically order state. The hysteresis curves of samples MAGC0 and MAGC2 are shown as insets in ***Fig. 5.4***, were shifted with respect to zero applied field position. Such a phenomenon is known as exchange bias and observed in materials in which both ferromagnetic and antiferromagnetic components are present [171]. Hematite and magnetite were formed as major crystalline phases. Hematite behaves as a weak ferromagnet above Morin's transition and as a perfect antiferomagnet below this transition while magnetite is ferrimagnetic at room temperature [156]. Further, increase of Ag to 4 mol% showed an increase in the saturation magnetization (4.4 emu/g) which was slightly higher than that of MAGC2. This is related to an increase in nucleation of magnetic particles when Ag content was increased to 4 mol%.

Mössbauer spectroscopy

Mössbauer spectra for as prepared and heat treated are shown in ***Figs. 5.5 & 5.6***, respectively. These spectra were composed of sextets and doublets. Related Mössbauer parameters like isomer shift (IS) and quadrupole shift (QS) determined from these spectra are listed in ***Table 5.3***. Typical values of IS for Fe^{3+} tetrahedrally coordinated to oxygen in silicate glass are in the range of 0.20–0.32 mm s^{-1}, while for octahedrally coordinated Fe^{3+}, these values are in the range of 0.35–0.55 mm s^{-1}. For Fe^{2+}, IS values are in the range of 0.90–0.95 mm s^{-1}(tetrahedral) and 1.05–1.10 mm s^{-1}(octahedral) [162].

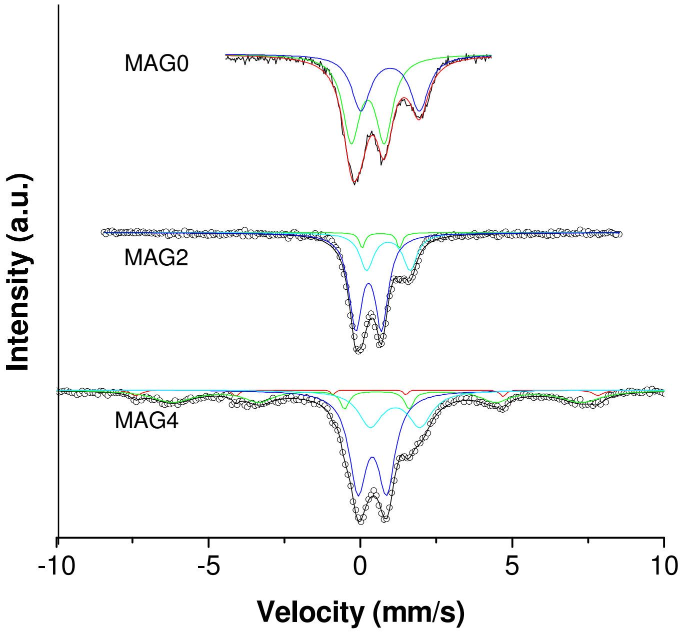

Fig. 5.5. *Room temperature Mössbauer spectra of as prepared samples.*

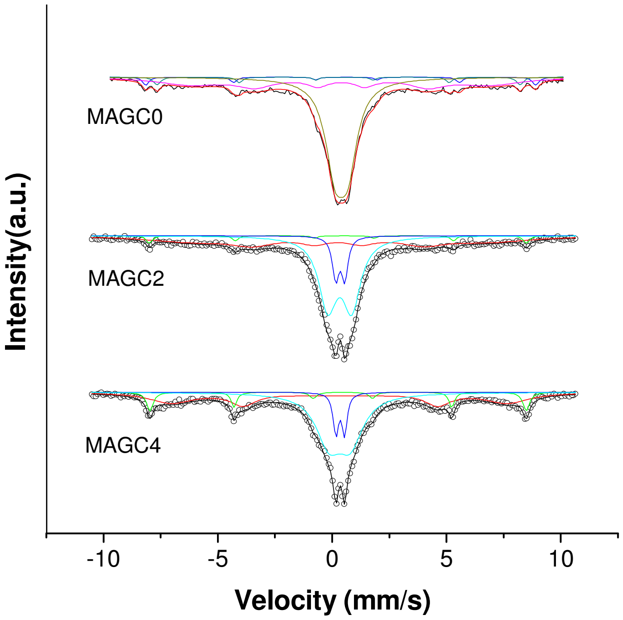

Fig. 5.6. *Room temperature Mössbauer spectra of heat treated (MAGC0, MAGC2 and MAGC4) samples.*

Table 5.3*. Various parameters obtained from room temperature Mössbauer spectra of glass-ceramic samples.*

Sample	Com	Magnetic (sextet)				Paramagnetic (doublet)			
		H_{int}(kG)	QS	IS	RI(%)	QS	IS	RI(%)	Γ
MAG0	Com1					1.08	0.25	57.7	0.68
	Com2					1.92	0.98	42.2	0.74
MAG2	Com1					1.54	0.85	4.76	0.274
	Com2					1.78	1.55	28.36	0.695
	Com3					1.06	0.34	66.88	0.662
MAG4	Com1	472	0.004	0.30	3.26	0.94	0.39	46.26	0.695
	Com2	418	0.006	0.55	27.17	1.63	1.15	29.30	0.948
MAGC0	Com1	515	0.026	0.69	3.73	0.55	0.39	56.45	1.008
	Com2	509	0.127	0.54	3.97				
	Com3	407	0.025	0.40	36.22				
MAGC2	Com1	511	0.140	0.53	3.46	1.04	0.33	46.88	0.948
	Com2	400	0.005	0.39	39.40	0.39	0.35	10.25	0.338
MAGC4	Com1	511	0.101	0.47	9.47	0.88	0.32	47.67	1.399
	Com2	457	0.016	0.38	35.38	0.37	0.35	7.46	0.260

IS: Isomer shift (mm/s), QS: Quadrupole Splitting (mm/s), RI: relative intensity, Γ: Line width (mm/s), H_{int}: Internal Field (kG), Com: component

The magnetization (M) is related with the ordering of magnetic ions, which have the tendency to align in the easy magnetization direction. However, when the size of these particles is smaller than the critical grain size (*grain behaves as a single domain)*, there are many single magnetic domains even though there is no external magnetic field. So M will be jumping from an easy-magnetization direction to another one. The spin-flip process [172] of the magnetic moment in superparamagnetic nanoparticles is described by a flip frequency f

$$f = f_0 \exp(KV/k_BT) \qquad \textbf{(5.5)}$$

Where f_0 is frequency factor, K is the effective anisotropic barrier per unit volume, V is particle volume and k_B is Boltzmann constant. The arising of doublet lines in Mössbauer spectrum is attributed to small particles sizes which behave in a superparamagnetic manner. Observation of superparamagnetic doublet in Mössbauer spectra of magnetic nanoparticle has been reported by many authors [173, 174]. Such behaviour was observed in all samples.

Though the coercivity values of samples MAG0 and MAG2 were non-zero, the Mössbauer spectra of these could not be fitted with sextet. However, the spectra of these samples could be fitted well with doublets. Superparamagnetic relaxation gives rise to line broadening and a pronounced central peak in Mössbauer spectra [175]. We observed the Mössbauer lines in the spectra have a large line-width implying that magnetic structure is relaxed. Broad Mössbauer spectra in nanoparticle samples were reported by several authors [176, 177]. In polycrystalline materials, the particles are randomly agglomerated and have a large number of grain boundaries and some cases may affect bond angles and bond lengths, which may give rise among others, in broadening of the Mössbauer lines [178].

Sample containing 4 mol% Ag showed two magnetic components (Fe^{3+} in octahedral coordination) with the magnetic hyperfine fields H_{hf} = 472 kOe and 418 kOe and two doublet components (Fe^{3+} in tetrahedral coordination). The sextets can be attributed to spinel phase in the magnetically ordered state. Though the spinel component in spectra were not further resolvable, estimated values of IS and hyperfine fields appear to be that for octahedrally coordinated Fe^{3+}. The low value of quadrupole splitting of 0.004 mm/s was attributed to cubic symmetry around iron ions. The doublet with IS = 0.39 and QS = 0.94 was assigned to Fe^{3+} in octahedral coordination. This doublet was due to the presence of isolated ion-clusters showing complete magnetic relaxation. The other doublet with IS = 1.15 and QS = 1.63 was assigned to Fe^{3+} in octahedral coordination. The QS of the doublet was larger than that of the sextet. It was because, the particle sizes represented by the doublet are small and their magnetic structure is not complete. These signify more crystal defects and lattice distortions, which result in reducing the symmetry around the Fe ions.

The magnetic sextets along with doublets were observed for MAGC samples (***Fig. 5.6***). Spectra of MAGC0 sample was fitted with three magnetic components having magnetic hyperfine fields H_{hf} = 515, 509, 407 kOe. The sextet with H_{hf} = 515 kOe was attributed to the hematite phase [118, 119]. The other two sextets with hyperfine fields of 509 and 407 kOe were attributed to magnetite and zinc ferrite, respectively. The spectrum was also fitted with a doublet indicating the presence of complete superparamagnetic relaxation, i.e., some particles have sizes lower than the critical size of the present mixed spinel ferrite nanoparticle.

The spectra of MAGC2 sample was fitted with two magnetic sextets and two doublets. The sextet with an isomer shift of 0.53 mm/s, quadrupole splitting of 0.14 mm/s, and hyperfine field of 511 kOe was identified to the presence of Fe_2O_3 phase (hematite) while the other sextet with an isomer shift of 0.39 mm/s, quadrupole splitting of 0.005 mm/s, and hyperfine field of 400 kOe was attributed to formation of spinel structure. The doublets with IS = 0.33, 0.35 and QS = 1.04, 0.39, respectively were assigned to Fe^{3+} in octahedral coordination.

Sample having 4 mol% Ag also showed two sextets and two doublets. The relative intensity of magnetic sextets was increased to 45% from 30% in the case of MGC4 sample. This signifies an increased ordering of the magnetic particles as a result of heat treatment. The sextet with an isomer shift of 0.47 mm/s, quadrupole splitting of 0.101 mm/s, and hyperfine field of 511 kOe can be attributed to the presence of Fe_2O_3 phase (hematite). Another sextet with an isomer shift of 0.38 mm/s, quadrupole splitting of 0.016 mm/s, and hyperfine field of 457 kOe was observed. We had observed a slight increase in the magnetization value in this sample as compared to MAGC2. This was attributed to an increase in magnetic sextet components which increased from 43% (MAGC2) to 45% (MAGC4). The doublets with IS = 0.35, QS = 0.37, and IS = 0.32, QS = 0.88 were assigned to Fe^{3+} ions in octahedral coordination. These two doublets were due to the existence of small clusters whose magnetization appears completely relaxed.

5.3.4. Release of Ag ions and Antibacterial assays

Elemental release from different glass-ceramics samples after one day immersion in DI water is given in ***Table 5.4***. It was observed that silica, PO_4^{-3}, Fe and Ag leach out from the surface. After immersion of the sample MAGC4, the concentrations of Fe and Ag were increased when compared to that of MAGC2. The increase in Ag release was expected as the total amount of Ag content in glass matrix was increased.

Table 5.4. *Elemental release from different glass-ceramics (MAGC) samples after one day immersion in DI water.*

sample	Si (µg/ml)	P (µg/ml)	Fe (µg/ml)	Ag (µg/l)
MAGC2	13±0.03	12.±0.06	7±0.01	25±0.41
MAGC4	9±0.02	10±0.05	12±0.02	37±2.63

The antibacterial activity of Ag containing glass-ceramics evaluated using *Escherichia coli* MG1655, Gram negative coliform bacteria is shown in ***Table 5.5***. There are various mechanisms by which Ag ions manifest the antibacterial activity. The released Ag ions from the ceramic may attach to the negatively charged bacterial cell wall and rupture it, leading to cell death [179]. It has also been hypothesized that oxygen associates with silver and reacts with the sulfhydryl (-S-H) groups on cell wall to form R-S-S-R bonds, subsequently blocking respiration and causing cell death [180].

Table 5.5*. Antibacterial tests of glass-ceramics (MAG) samples against E.coli.*

Concentration (%w/v) of glass in LB broth	Colony forming unit (cfu/ml) in presence of MAG2	Colony forming unit (cfu/ml) in presence of MAG4
1	7.4×10^8	3.7×10^8
5	2.1×10^6	1.6×10^5
10	4.5×10^3	Nil
15	2.3×10^2	Nil
20	Nil	Nil

The glass-ceramic containing 4% Ag showed complete inhibition of bacterial growth at a concentration of 10% (w/v). However, the glass-ceramic containing 2% Ag showed the similar effect at 20% (w/v). A similar observation has been noted by sondi et al [181], who observed a growth delay of *E.coli* in liquid media at a concentration that resulted in complete inhibition of bacterial growth on agar plate.

5.4. Conclusion

Magnetic glass-ceramics were obtained from the base compositions of $25SiO_2$-$(50-x)CaO$-$15P_2O_5$-$8Fe_2O_3$-$2ZnO$-xAg (where x = 0, 2 and 4 mol %). The glass-ceramics exhibited both magnetic and antibacterial properties. Hematite and magnetite were formed as major crystalline phases. Magnetic properties of the samples improved on heat treatment of the samples. There was an increase in saturation magnetization with increase in amount of

Ag. This trend was attributed to the completion of magnetic ordering. Mössbauer spectroscopy showed the relaxation of magnetic particles, indicating the size of magnetic clusters was small. The antibacterial response was found dependant on Ag ions concentration in the glass matrix. The glass-ceramics samples showed significant antibacterial activity and thus may be used as bactericidal material.

Chapter 6

Studies on barium alumino strontium silicate (BASP) glass/glass-ceramics containing P_2O_5

P_2O_5 is a common nucleating agent in glass-ceramics. To avoid the negative effect of P_2O_5 on sealing properties, we combined it with barium oxide in the glass formulation. The effect of $Ba_3(PO_4)_2$ incorporation on thermo-physical, structural and sealing characteristics of a glass of composition (mol%) $30SiO_2$-20SrO-30BaO-$10B_2O_3$-$5La_2O_3$-$5Al_2O_3$ is discussed in this chapter.

6.1 Introduction

Solid oxide fuel cells (SOFCs) convert chemical energy into electrical energy, which present higher efficiency and lower environmental impact as compared to conventional power generation systems [49, 50]. The SOFCs operate at the temperature in the range 600–900°C for thousands of hours. In planar design of SOFC, it requires a hermetic seal for channeling of fuel and oxygen. In addition, sealing material has to meet several rigorous requirements, including chemical, electrical compatibility and stability with the cell components [75].

Glass and glass-ceramics have been explored as promising materials for sealing application in SOFC [59]. In order to develop suitable sealant materials for high temperature applications, several glass and glass-ceramics mainly based on silicates and borates have been studied [186-187]. Haanappel *et al.* [188] studied the behaviour of BaO-CaO-Al_2O_3-B_2O_3-SiO_2 glass seals in presence of oxidizing and reducing atmospheres and reported excess corrosion of interconnect. Lara et al [60, 65, 66] studied the RO-Al_2O_3-BaO-SiO_2 (R = Ca, Mg, Zn) glass system and reported their glass forming ability, sintering, thermal and electrical properties. A major challenge for this kind of sealants is to avoid the formation of undesirable crystalline phases during working of the cell, for instance celsian ($BaAl_2Si_2O_8$) and its polymorph hexacelsian crystalline phases having low thermal expansion coefficients (TEC) induce stress in glass and failure of seals may take place [182]. The significant amount of BaO in glasses leads to degradation of seals due to formation of $BaCrO_4$[183-184]. Thus, in order to avoid this, SrO based glasses have been studied.

Tiwari *et al.* [189] reported bonding of SrO and ZnO based silicate glasses with Crofer-22 APU. Ojha *et al.* [190] studied the SrO and La_2O_3 based Al_2O_3-B_2O_3-SiO_2 glasses and reported that SrO modified the network and resulted in change in thermo-physical properties. Thermal expansion coefficients of glasses are reported around 9×10^{-6} $^{o}C^{-1}$. Wang *et al.* [191] prepared La_2O_3-Al_2O_3-B_2O_3-SiO_2 glasses free of alkaline earth metals and reported a decrease in softening temperature of glasses with an addition of La_2O_3. However, there is still a need to reduce the softening temperature (T_s), so that seals can be prepared at temperatures lower than 1000°C. It is also desired to match the TEC with the metallic interconnects ($12\times10^{-6}\,^{\circ}C^{-1}$) of SOFCs.

In the present study, SrO-BaO based aluminosilicate glasses with various compositions were prepared by melt quench technique. The system is of particular interest as replacing BaO with SrO mitigates the formation of $BaCrO_4$. It was also expected that this induce the formation of $SrAl_2Si_2O_8$, which has higher TEC than $BaAl_2Si_2O_8$. Further, originality of our approach lies in the combined addition of BaO and P_2O_5 to tailor the sealing and thermo physical properties of the sealants. Phosphate based glass exhibit insufficient durability for sealing but addition of silica can increase the stability of phosphate in the glass [192]. Moreover, P_2O_5 can be useful as nucleating agent to avoid undesirable reaction at the metal glass interface [193]. Finally, addition of P_2O_5 in alumino-silicate glasses scavenges the modifier cations and thus, increases the network polymerization and sealing temperature, which is detrimental for the sealing application [194].

Thus, a series of glasses have been formulated by addition of $Ba_3(PO_4)_2$ to a base glass composition. According to previous studies [195], it is expected that with this combined addition, the network polymerization will not get affected but we will get a decrease in glass transition and softening temperatures. Thermo-physical properties of the glasses (Tg, Ts and TEC) with increasing quantity of $Ba_3(PO_4)_2$ have been studied. The glasses were characterized for structural features with XRD and solid-state NMR. Seals of the glasses with Crofer-22 APU metallic alloy were made, and the microstructure at the interface and chemical stability of seals at high temperature were investigated.

6.2 Experimental

Nominal compositions (mol%) of glass samples are given in ***Table 6.1***. These were prepared by using melt-quench technique. $Al(OH)_3$, $BaCO_3$, H_3BO_3, La_2O_3, $NH_4H_2PO_4$, SiO_2 and $SrCO_3$ of 99.9% purity were mixed, ground and calcined at a maximum temperature of 900°C in a Pt-10% Rh crucible. It is to be noted that the $Ba_3(PO_4)_2$ was obtained in the glass composition from the decomposition of $BaCO_3$ and $NH_4H_2PO_4$. The calcined charge was then melted at 1450-1550°C and held at this temperature for 1h for homogenization. The melt was then poured on a stainless steel plate. The glass samples were annealed at around 650°C for 4h. Weight losses were carefully checked during glass preparation, hence actual composition is considered to be similar to nominal composition.

***Table 6.1**. Nominal compositions (mol%) of glass samples.*

Sample	SiO_2	BaO	SrO	B_2O_3	La_2O_3	Al_2O_3	P_2O_5
BASP0	30	30	20	10	5	5	0
BASP1	28.8	31.7	19.2	9.6	4.8	4.8	0.9
BASP2	27.7	33.3	18.5	9.2	4.6	4.6	1.8

Differential thermal analysis (DTA) was carried out from room temperature to 950°C using a TG/DTA instrument. DTA measurements were carried out on powdered samples with particle size less than 63µm. Thermal expansion was measured from room temperature to 900°C using TMA instrument. The sintering behavior of the BASP glasses was studied by means of a hot stage microscope (HSM, Hesse, Germany).

The crystalline phases in glass-ceramics samples were identified using powder X-ray diffractometer (Bruker) with CuK_α as X-ray source. XRD data were collected on powder samples with particle size less than 63µm. These measurements were done in the range (2θ angle) 10–80° with a step of $0.02^\circ\ s^{-1}$ and dwell time of 0.2 s.

^{11}B, ^{27}Al, ^{29}Si and ^{31}P MAS-NMR spectra were recorded at 18.8, 18.8, 9.4 and 9.4 T respectively, on Bruker AVANCE spectrometers, with 4 mm probes at 12.5 kHz spinning speed, except for ^{29}Si for which a 7 mm probe at 5 kHz was used. The Larmor frequencies were 128.4, 104.2, 79.4 and 162.3 MHz for ^{11}B, ^{27}Al, ^{29}Si and ^{31}P, respectively. For ^{11}B, the pulse duration was 2 µs ($\pi/6$), and the recycle delay was 10 s. For ^{27}Al, the pulse duration was 1.5µs ($\pi/8$), and the recycle delay was 2s. For ^{29}Si, the pulse duration was 1.6 µs ($\pi/5$), and the recycle delay was 180 s. For ^{31}P, the pulse duration was 1.6 µs ($\pi/6$), and the recycle delay was 120s. All relaxation delays were chosen long enough to enable relaxation at the field strength that was used. ^{11}B chemical shifts are given relative to BPO_4 at 3.6 ppm, ^{27}Al chemical shifts are relative to $AlCl_3$ at 0 ppm, ^{29}Si chemical shifts are relative to tetramethylsilane (TMS) at 0 ppm, and ^{31}P are relative to 85% H_3PO_4 at 0 ppm.

For studying the adhesion/bonding, sealing with Crofer 22 alloy was carried out at a maximum temperature of 1000°C employing the sandwich geometry. Microstructure near the interface was investigated using Cameca SX 100 electron probe microanalyser (EPMA) and wavelength dispersive analysis of X-Rays (WDAX) was carried out for determining element diffusion across the interface.

6.3. Results and discussion

The compositions reported in ***Table 6.1*** yielded bubble-free glasses, named BASP in the following text. XRD analyses of these glasses have shown absence of any long range order.

6.3.1. Thermal Analysis

6.3.1.1. TMA/DTA

The thermo-physical properties of the BASP glasses are listed in ***Table 6.2***. The glass transition temperature decreased from 650-584°C when P_2O_5 was increased from 0 to 1.8

mol% and BaO from 30 to 33.3 mol%. The TEC values of the glass samples were found to increase from 11.4 to 13×10^{-6}°C^{-1}.

Table 6.2. *Thermo-physical properties of the BASP glasses.*

Sample	TEC ($\pm 0.2\text{x}10^{-6}$ K^{-1})			Tg (± 2°C)	Flow Temperature (± 3°C)
	As prepared	after 6h at 800°C	after 100h at 800°C		
BASP0	11.4	12.2	12.4	650	1145
BASP1	12	12	12.5	592	1107
BASP2	13	13	12.1	584	1108

DTA plots of glass samples are shown in ***Fig. 6.1***. The sample BASP0 shows an onset for crystallization (T_{cry}) at 756°C. With addition of $Ba_3(PO_4)_2$, T_{cry} was not changed much but onset of crystallization was detected at slightly higher temperature (764°C) for BASP1.

Thermo-physical properties of glasses and glass-ceramics are strongly dependent upon the composition [7]. According to continuous random network theory, SiO_2 is a network forming oxide and BaO is a network modifying oxide [3]. The addition of barium phosphate leads to decrease in overall silica content, which is expected to decrease the rigidity of the network. Thus, TEC values of BASP glasses increased with the addition of barium phosphate, concomitantly T_g values decreased.

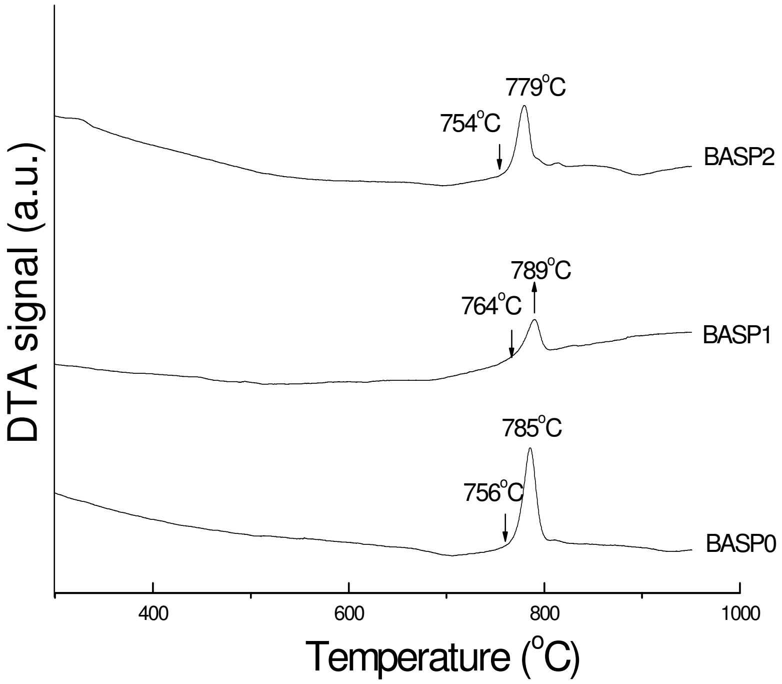

Fig. 6.1. *DTA plots of BASP glass samples.*

6.3.1.2. Hot Stage Microscopy

The normalized areas of BASP samples as recorded with HSM are plotted as a function of temperature in ***Fig. 6.2***. The incorporation of $Ba_3(PO_4)_2$ did not modify the sintering temperature, which remained at 710°C. However, the maximum shrinkage temperature (T_{shri}) and flow temperature decreased with addition of $Ba_3(PO_4)_2$. The shape of the normalized area versus temperature curves indicates that BASP0 and BASP1 glasses soften over a wide temperature range indicating glassy behavior. BASP2 glass exhibited a wide plateau before flow, which is a characteristic of materials exhibiting devitrification upon heating [196]. This indicates the occurrence of significant crystallization in BASP2 glass.

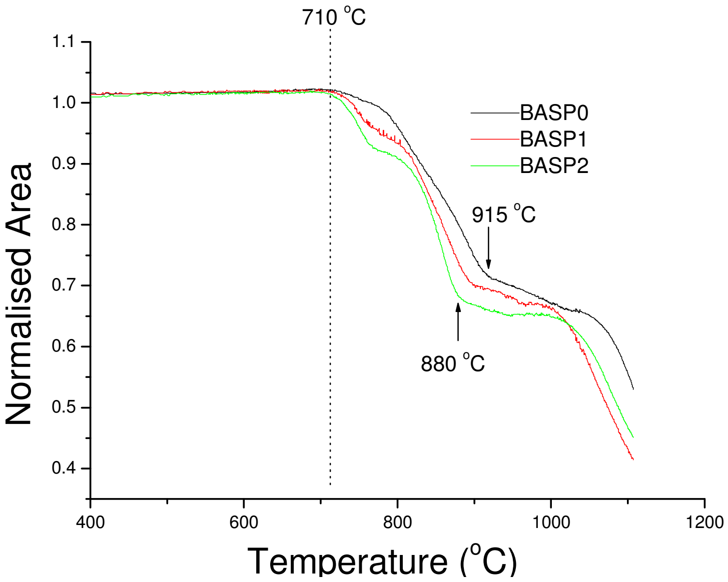

Fig. 6.2. HSM plots of BASP glass samples.

6.3.2 Structural studies

6.3.2.1 X-ray diffraction (XRD)

XRD patterns of the glass samples after heat treatment at 800°C for 6h are depicted in ***Fig.6.3a***. The glass BASP0 showed the formation of Ba_2SiO_4, Sr_2SiO_4 and $BaAl_2Si_2O_8$ as major phases. However, with addition of 1 mol% $Ba_3(PO_4)_2$, relative intensity of peak corresponding to $BaAl_2Si_2O_8$ (around 23°) decreased. It implies the tendency of formation of such a phase reduces, when $Ba_3(PO_4)_2$ was added to base composition (BASP0). Overall, the peaks have become sharp, which implies better crystallized samples. Evolution of crystalline phases in BASP0 glass after different heat treatment time is shown in ***Fig. 6.3b***. XRD peaks were sharp when sample were heat treated for 500 h. Intensities of peaks corresponding to formation of $BaAl_2Si_2O_8$ decreased (for instance at 22.5°) while peak at 27° for Sr_2SiO_4 increased. It implies that the tendency to form Sr_2SiO_4 is more prevalent than formation $BaAl_2Si_2O_8$ when glass was heat treated at 800°C for long time (500 h). XRD plots for the other glass samples (BASP1&2) after heat treatment at 800°C for 100 to 500 h are shown in ***Fig. 6.3c***. There was no evolution of additional phase when heat treatment time was increased from 100 h to 500 h.

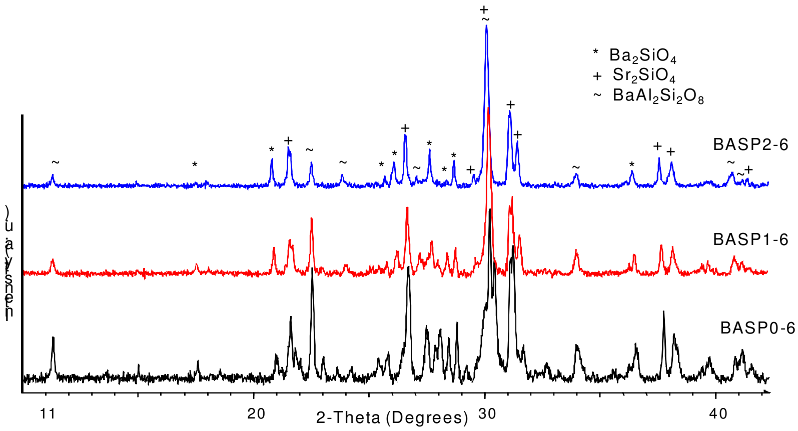

Fig. 6.3.a XRD patterns of the glass samples after heat treatment at 800℃ for 6h.

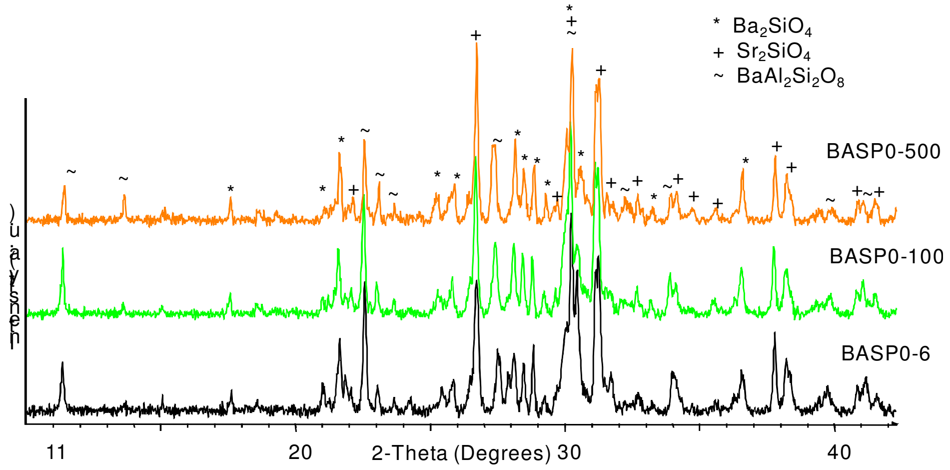

Fig. 6.3.b XRD patterns of the BASP0 after different time of heat treatment at 800℃.

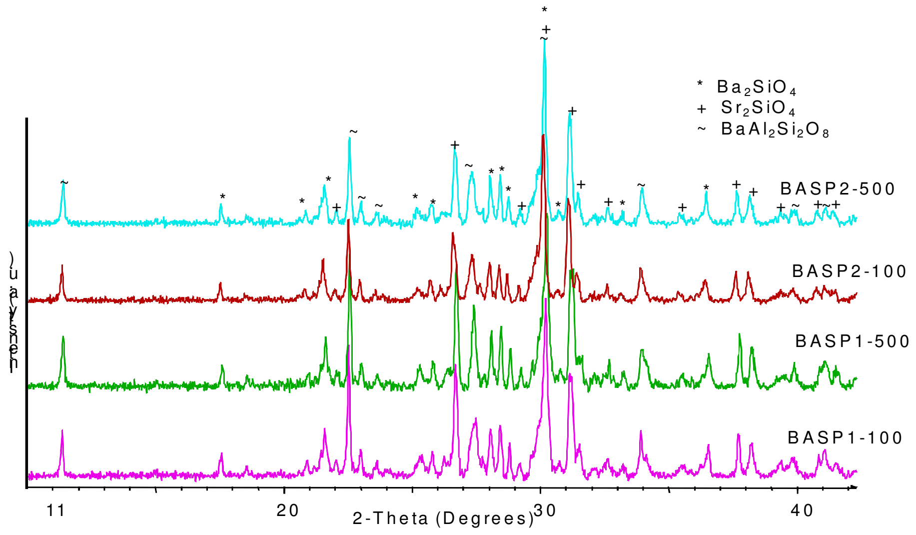

Fig. 6.3.c XRD patterns of the glass samples after heat treatment at 800℃.

6.3.2.2 MAS-NMR

6.3.2.2.1. ^{29}Si MAS-NMR

Fig. 6.4 shows the ^{29}Si MAS-NMR spectra of the as prepared BASP glasses and after 100 h heat treatment at 800°C. The spectra of the as prepared glasses showed a broad feature in -70 to -90 ppm range with a Gaussian line shape, characteristic of bond angle and length distributions inherent to the amorphous state. Its chemical shift was centered on -80 ppm, which indicates that Q^2 SiO_4 units dominate in the glass network [197]. This result is in accordance with the glass composition, which contains a large quantity of network modifying oxides. Some Q^3 SiO_4 units bonded to Al or B may be present, since chemical shift of such units shift towards less negative values [198,199].

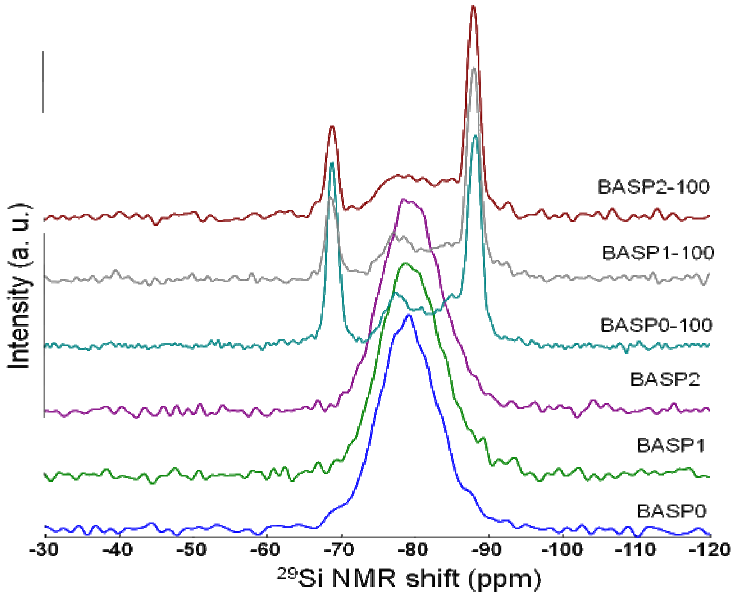

***Fig. 6.4**. ^{29}Si MAS-NMR spectra of the as-prepared BASP glasses and after 100 h heat treatment at 800°C.*

After 100 h of heat treatment at 800°C, large modifications were observed on the ^{29}Si MAS-NMR spectra (**Fig. 6.4**). Two narrow resonances with large intensity were presented at -68 and -89 ppm, which indicate the presence of crystalline phases. According to literature data, these were assigned to Ba_2SiO_4, with chemical shift reported at -70 ppm, and to $BaAl_2Si_2O_8$, with chemical shift reported at -88 ppm [200, 201]. The resonance at -68 ppm was assigned to Sr_2SiO_4 or a mixed $(Ba,Sr)SiO_4$, owing to the close values of Ba^{2+} and Sr^{2+} field strengths [202]. The weak resonance at -85 ppm assigned to $(Ba,Sr)Al_2Si_2O_8$ mixed celsian phase.

It is known that modifier cations are required for charge compensation for PO_4^{3-} anions, when P_2O_5 is added to glass. But no evolution in ^{29}Si spectra of the as prepared glasses was observed for the 3 different compositions (***Fig. 6.4***). This was expected, since we formulated the glasses by the simultaneous addition of BaO and P_2O_5 in proportion 3/1, to obtain an equivalent amount of $Ba_3(PO_4)_2$. It has indeed been shown that, when $Ba_3(PO_4)_2$ is added to silicate glasses in small amount, P_2O_5 does not participate to the silicate glass network and remains as isolated orthophosphate species [203].

6.3.2.2.2 ^{11}B MAS-NMR

^{11}B NMR spectra of the parent and heat treated BASP glasses are shown in ***Fig. 6.5***. The spectra were found similar for all the compositions. The resonance observed at 16 ppm can be assigned to BO_3 and a very weak one at 1 ppm assigned to BO_4 units [204]. Despite the use of a high-field spectrometer that enables a high resolution for quadrupolar nuclei like ^{11}B (nuclear spin I=3/2), the spectra were broad and featureless, meaning that all ^{11}B nuclei are present in a very similar environment. The formation of less rigid planar BO_3, units as observed in ^{11}B NMR contributes to keep moderate values of flow temperature and T_g for BASP glasses.

After heat treatment for 100 h (***Fig. 6.5***), ^{11}B NMR spectra of glass-ceramics remained quite similar to those of the parent glasses. Nevertheless, the main resonance showed the presence of two singularities around 18 and 17 ppm. These suggest that some boron nuclei were involved in regular crystalline environments [205]. Celsian is indeed known to incorporate many different elements in its structure to form solid solution [201, 206]. Concerning boron, we have already reported that NMR gave evidence for the formation of a mixed Al, B phase [207].

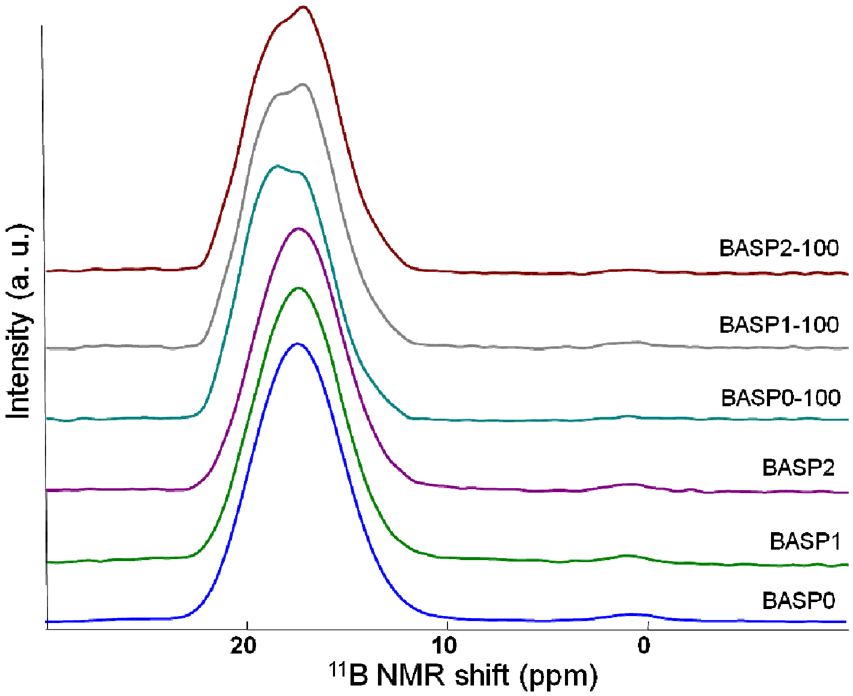

Fig. 6.5. *^{11}B MAS-NMR spectra of the as-prepared BASP glasses and after 100 h heat treatment at 800°C.*

6.3.2.2.3. ^{27}Al MAS-NMR

^{27}Al NMR spectra for BASP glasses and glass-ceramics are reported in ***Fig. 6.6***. The spectra of glasses consist of a broad resonance centered at ~65 ppm, which is characteristic of aluminum in tetrahedral coordination [208]. Owing to the large quantity of charge compensating cations available in the glasses, tetrahedral coordination was expected. A much narrower resonance was observed for the glass-ceramics, thus revealing that Al was fully involved in the crystalline phases. The spectra consist of a resonance centered at ~55 ppm, which is characteristic of AlO_4 tetrahedral units in celsian $(Ba,Sr)Al_2Si_2O_8$ crystals [200, 209].

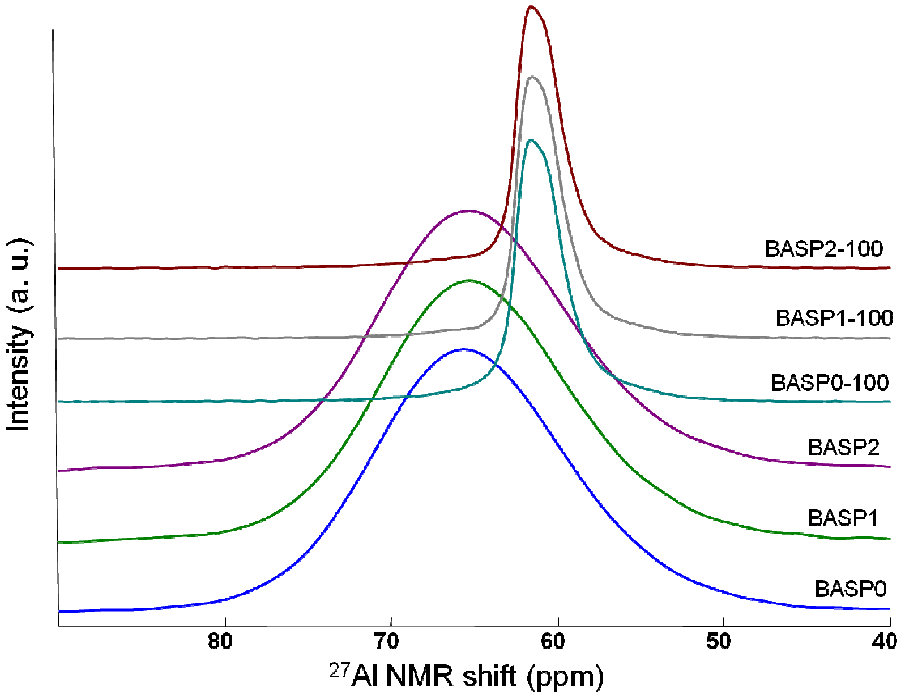

Fig. 6.6. *^{27}Al MAS-NMR spectra of the as-prepared BASP glasses and after 100 h heat treatment at 800°C.*

6.3.2.2.4. *^{31}P MAS-NMR*

^{31}P NMR spectra of the glasses and glass-ceramics are shown in ***Fig. 6.7***. A main broad resonance was observed at ~8 ppm, and assigned to Q^0 (orthophosphate units) [210]. This chemical shift is close to that of Q^0 units in $Ba_3(PO_4)_2$ crystal (9 ppm) [211], but different from that of $Sr_3(PO_4)_2$ crystal (3 ppm) [212]. Hence the orthophosphate anions were mainly charge balanced by Ba^{2+} but some Sr^{2+} could not be excluded. The resonance became somewhat sharper in glass-ceramic samples. Nevertheless, the Ba and Sr atomic distribution in Q^0 orthophosphate site may be at the origin of broad line shape, thus we can expect the presence of phosphate crystal in the glass-ceramics samples. Since the P_2O_5 quantity was small in these glasses, the presence of these phosphate crystals could not be confirmed by XRD analyses.

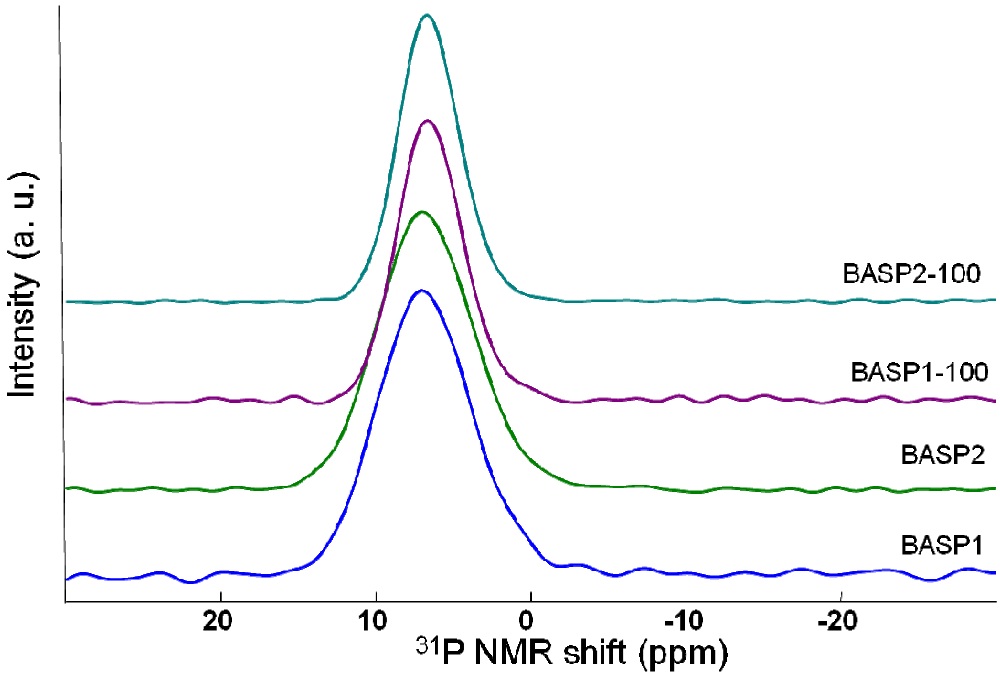

Fig. 6.7. *^{31}P MAS-NMR spectra of the as-prepared BASP glasses and after 100 h heat treatment at 800°C.*

6.3.3. Microstructure and chemical stability

Figs. 6.8(a-c) show the microstructures at interfaces of BASP glasses with Crofer-22 APU. All the sealing glasses bonded well to the metallic part as no bubbles and cracks were observed at the interface. A limited interdiffusion of Cr, Sr and Ba across the boundary was observed, which is required for good adhesion between metal and glass (***Fig. 6.8d***).

Figs.6.9 (a-f) show the EPMA images recorded at the interface of metal/glass joints after heat treatment at 800°C for 100 h and 500 h. The microstructure of BASP0 was composed of coarse crystals as seen from EPMA images, while BASP1 and BASP2 show more homogeneous microstructure with smaller crystals. There were no major changes observed in microstructure after heat treatment at 800°C for 500 h. As seen from the images, all the seals were found with good interfaces. EPMA images of seals confirmed limited enrichment of Cr at the interface (***Fig. 6.10 (a-f)***) even after heat treatment at 800°C for 500 h. ***Fig. 6.10g*** shows the comparison of Cr diffusion at interface of BASP1 glass with Crofer22 APU alloy after different time of heat treatment at 800°C. In BASP1 glass, Cr diffusion of around 3 μm observed for as prepared seal and it increased marginally to 5 μm after 500 h of heat treatment at 800°C.

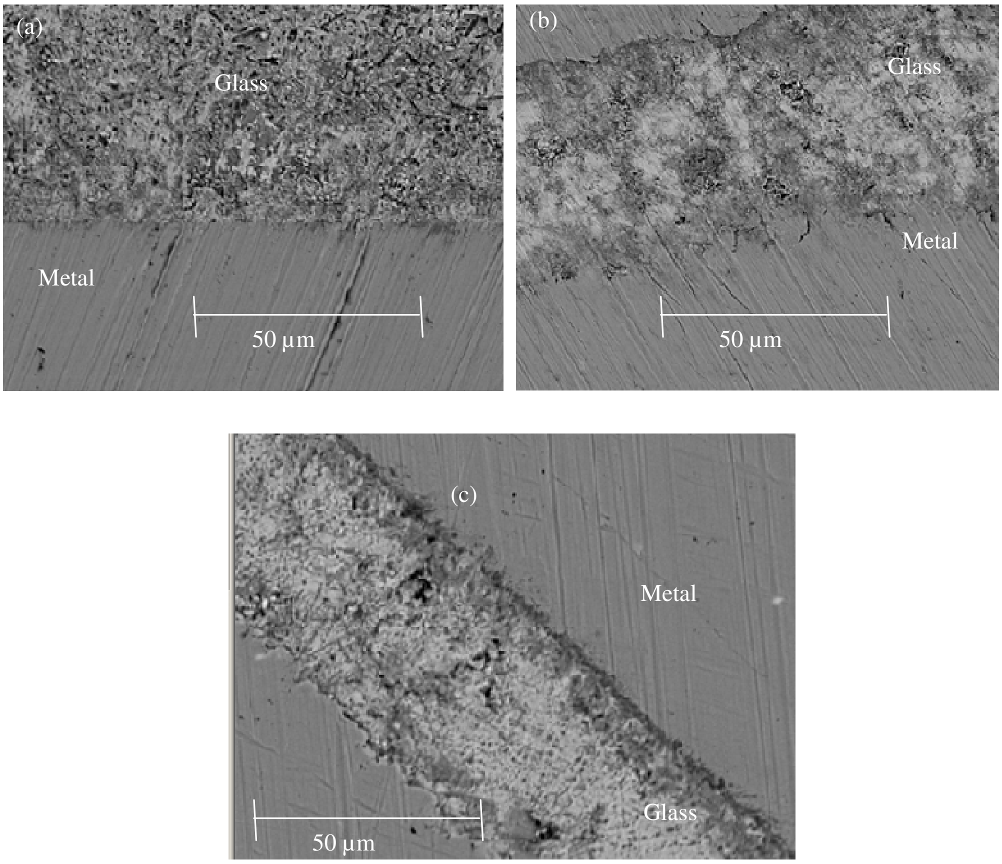

Fig. 6.8. *Microstructures at interfaces of BASP glasses with Crofer-22 APU*

(a) BASP0, (b) BASP1, (c) BASP2.

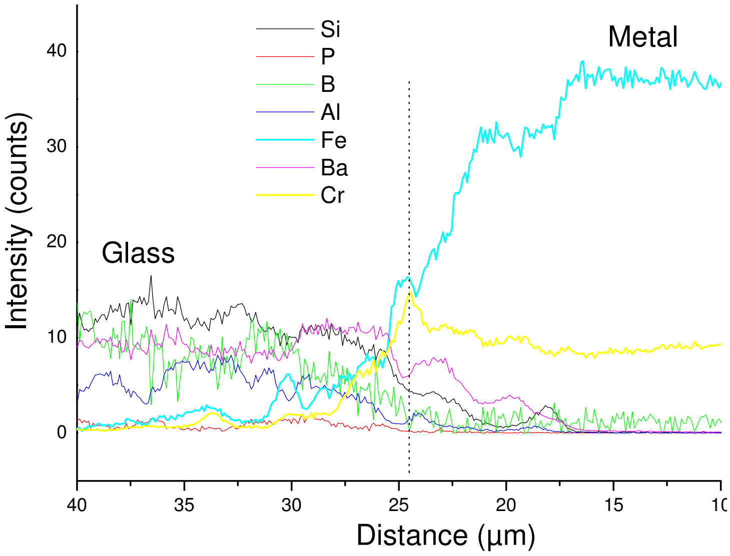

Fig. 6.8.d *EPMA line scan of BASP1 glass.*

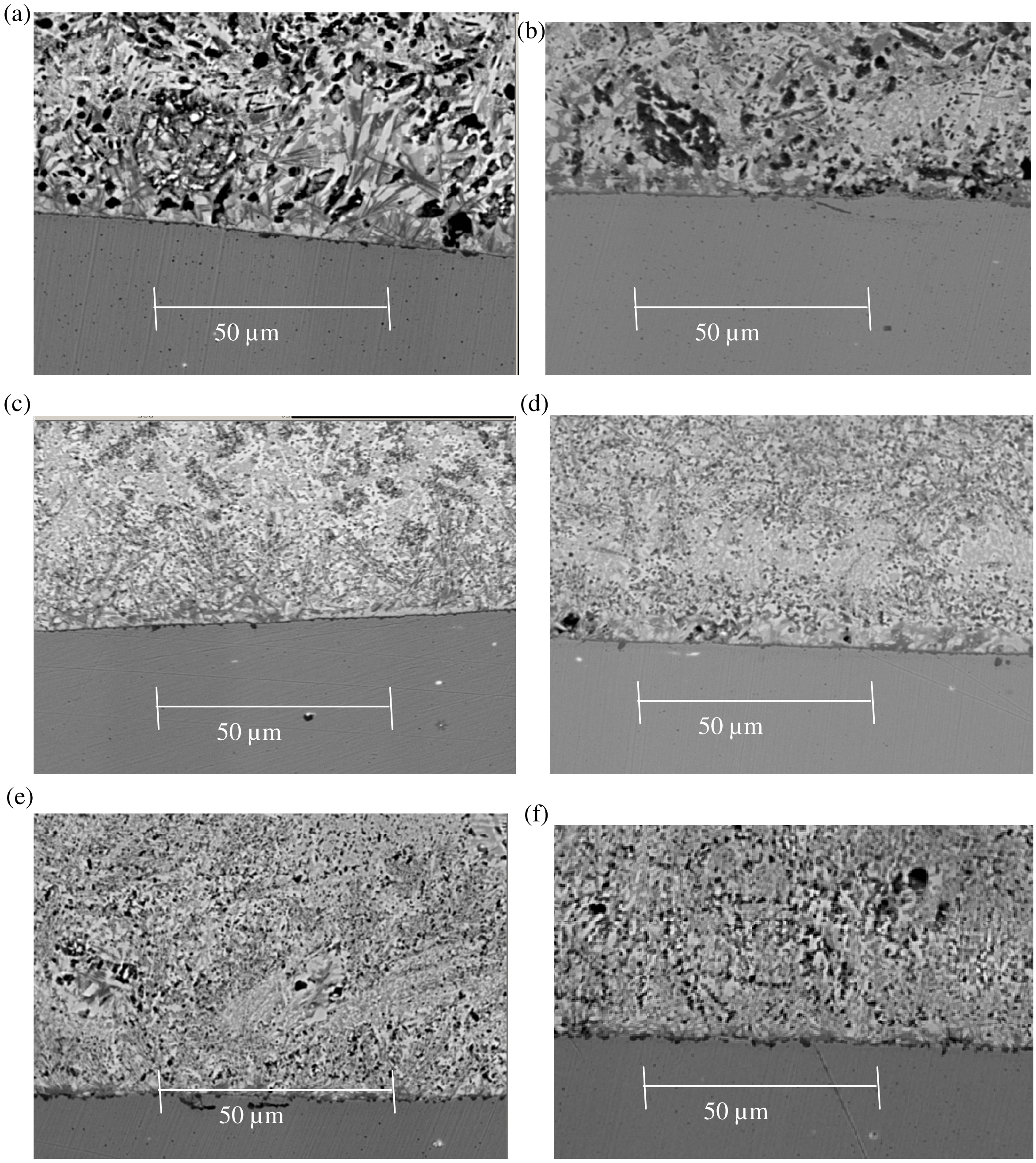

Fig.6.9. *Microstructure near the interface between glass and Crofer-22 APU after heat treatment at 800°C: (a) BASP0 (for 100h); (b) BASP0 (for 500h);(c) BASP1 (for 100h); (d) BASP1 (for 500h); (e)BASP2 (for 100h); (f) BASP2 (for 500h).*

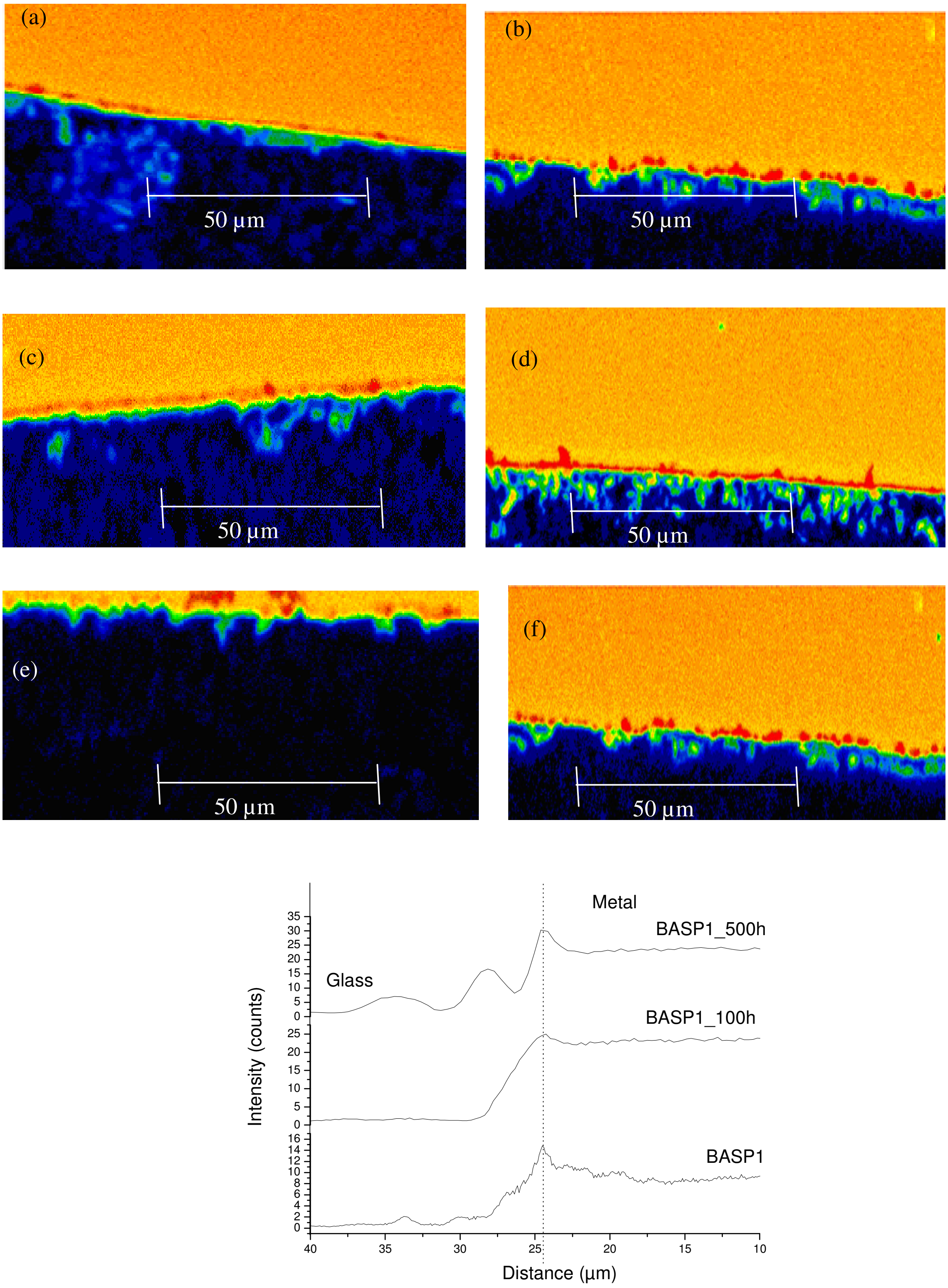

Fig. 6.10. *Cr mapping at the BASP glass Crofer-22 APU interface after heat treatment at 800^{o}C: (a) BASP0 (for 100h); (b) BASP0 (for 500h); (c)BASP1 (for 100h); (d) BASP1 (for 500h); (e) BASP2 (for 100h); (f) BASP2 (for 500h); (g) Cr diffusion at BASP1 glass - Crofer-22 APU interface after different time of heat treatment at 800°C.*

The decrease in flow and sealing temperatures with addition of $Ba_3(PO_4)_2$ in BASP glasses helps in forming good bonds with Crofer-22 APU at temperature lower than 1000°C, however we have carried out all the sealing experiment at 1000°C for comparing the results for BASP glasses. For effective sealing, it is required that the glass should attain maximum shrinkage before crystallization. All the BASP glasses have shown attainment of maximum shrinkage before crystallization enabling the good sealing with Crofer.

Results of MAS-NMR spectra of the glass-ceramics were found in accordance with the phase emergence observed by XRD. Since the incorporation of $Ba_3(PO_4)_2$ did not affect the network the major phases formed were not much changed. However, there was an increased crystallisation and phase stabilisation. We observed the formation of Ba_2SiO_4, Sr_2SiO_4 and $BaAl_2Si_2O_8$ phases. As crystallization of B is evident on B MAS-NMR spectra, we suggest the formation of $(Ba,Sr)(Al,B)_2Si_2O_8$ like phase.

In glass-ceramics, thermo-physical properties depend on the crystalline phase evolved during crystallization. BASP glass-ceramics have shown high TEC ($12\times10^{-6}\ {}^{o}C^{-1}$) despite the crystallization of hexacelsian like phase, which has lower than desired TEC ($8\times10^{-6}\ {}^{o}C^{-1}$) [75]. This suggests the formation of $(Ba,Sr)Al_2Si_2O_8$; since $SrAl_2Si_2O_8$ has a higher TEC ($11\times10^{-6}\ {}^{o}C^{-1}$). B incorporation in such a phase may further lead to increase in TEC.

All the seals with Crofer-22 APU have shown good adhesion. The seals were found intact after heat treatment at 800°C up to 500h. It has been reported that the BaO containing glasses interact chemically with chromia-forming alloys forming $BaCrO_4$, which leads to the separation of GCs from the alloy matrix due to thermal expansion mismatch [183]. We did not observe major enhancement in Cr-diffusion after 500h at 800°C and no adverse reactions at interface were observed even after 500h of heat treatment. Therefore, we conclude that incorporation of $Ba_3(PO_4)_2$ improves the sealing characteristics of BASP glasses/glass–ceramics.

6.4. Conclusion

Barium alumino-silicate glasses were studied for structural, thermo-physical properties and sealing properties. The glasses did not show major structural changes with addition of BaO and P_2O_5 in the form of $Ba_3(PO_4)_2$. Moreover, this leads to decrease in softening temperatures, thus enabling the seal fabrication (with Crofer-22 APU) below 1000°C. The glass transition temperature decreases from 650°C to 584°C when $Ba_3(PO_4)_2$ is increased from 0 to 2 mol%. Thermal expansion coefficient of the glass samples are found around 11.4 to 12.0×10^{-6}°C^{-1}, which is close to that of Crofer-22APU. ^{29}Si MAS-NMR measurements indicate that glass network is composed of mainly Q^2 units, while ^{31}P forms Q^0 units The glasses showed the development of Ba_2SiO_4, $BaAl_2Si_2O_8$, and Sr_2SiO_4 crystalline phases upon heat treatment at 800°C, which were not found to be detrimental for high temperature sealing applications. Interfaces of seals revealed good bonding with Crofer-22 APU, which did not deteriorate even after heat treatment at 800°C for 500 h.

Chapter 7

Studies on barium alumino strontium silicate (BASP) glass/glass-ceramics containing V_2O_5 and P_2O_5

In the previous chapter we had seen the influence of P_2O_5 on thermo-physical and structural properties of different glasses. To avoid the negative effects of P_2O_5, it was added in the form of $Ba_3(PO_4)_2$. The positive effects of P_2O_5 as a nucleating agent can be further corroborated in presence of some other oxide such as V_2O_5. In this chapter, effects of combined addition of V_2O_5 and P_2O_5 on thermal, microstructure and sealing behaviour of glasses are reported.

7.1 Introduction
7.2 Experimental
7.3 Results and discussion
7.4 Conclusion

7.1. Introduction

The glass/glass-ceramics have been studied as potential materials for sealing application in solid oxide fuel cells (SOFCs) [65-66, 186-188]. As mentioned in previous chapter, sealants must show good matching of thermal expansion coefficient (TEC) with other SOFC components, low reactivity with other fuel cell components and long term stability at elevated temperature in either oxidizing or wet reducing atmosphere [75].

The crystallization in glasses used as sealants in SOFC cannot be avoided due to high operating temperature. The thermo-physical properties of glass-ceramics depend on the formation of different crystalline phases; therefore, it is necessary to avoid the formation of undesirable phases. It is also required that the crystalline phases remain stable for longer period of time. Crystal growth in the glasses is influenced by the presence of nucleating agents. Cr_2O_3 and NiO are used to control the formation of desired phase in the glass sealant. However, addition of these has lead to increase in the glass transition temperatures, which is not desirable for sealants for SOFC [75]. P_2O_5 is a common nucleating agent used for controlling microstructure and phase stabilisation. But its addition to glass leads to an increase in sealing temperature [194]. To avoid the negative effects of P_2O_5, it had been added in the form of $Ba_3(PO_4)_2$ [213].

The addition of V_2O_5 as an intermediate oxide leads to decrease in the glass transition temperature. Further its addition is likely to reduce the glass surface tension, which may result in good sealing behaviour [214]. The effect of more than one nucleating agent has been studied by Alizadeh et al in SiO_2-MgO-CaO glass system and reported that V_2O_5+MoO_3 can be used as effective nucleating agents [215]. Marghussian et al reported the effectiveness of V_2O_5 in the presence of a small amount of BaO as a nucleating agent in magnesium aluminum silicate glass [216]. Thus it is interesting to investigate the effect of combined addition of V_2O_5 and P_2O_5 on thermal, microstructure and sealing behavior of glasses.

A series of glasses have been prepared with nominal composition $27SiO_2$-23SrO-32BaO-$4Al_2O_3$-$10B_2O_3$-(4-x) P_2O_5-xV_2O_5 where x=0-4 mol%. Crystallization kinetics and thermo-physical properties of the glasses (Tg, Ts and TEC) were studied. The glasses were characterized for structural features with XRD and solid-state NMR. Seals of the glasses with Crofer-22 APU metallic alloy were made, and the microstructure at the interface and chemical stability of seals at high temperature were investigated.

7.2. Experimental

Nominal compositions (mol%) of glass samples are given in ***Table 7.1***. These were prepared by using melt-quench technique. $Al(OH)_3$, $BaCO_3$, H_3BO_3, $NH_4H_2PO_4$, SiO_2, $SrCO_3$ and V_2O_5 of 99.9% purity were mixed, ground and calcined at a maximum temperature of 900°C in a Pt-10% Rh crucible. The calcined charge was then melted at 1450-1550°C and held at this temperature for 1h for homogenization. The melt was then poured on a stainless steel plate. The glass samples were annealed at around 650°C for 4h. Weight losses were carefully checked during glass preparation, hence actual composition is considered to be similar to nominal composition.

Table 7.1. *Nominal compositions (mol%) of glass samples*

Sample	SiO_2	BaO	SrO	B_2O_3	Al_2O_3	V_2O_5	P_2O_5
BASPV0	27	32	23	10	4	0	4
BASPV2	27	32	23	10	4	2	2
BASPV4	27	32	23	10	4	4	0

Thermal expansion was measured from room temperature to 900°C using TMA instrument. DTA measurements were carried out room temperature to 900°C on powdered samples with particle size less than 63µm. The sintering behaviour of the glasses was studied by means of a hot stage microscope (HSM, Hesse, Germany). The crystalline phases in glass-ceramics samples were identified using powder X-ray diffractometer (Bruker) with CuK_{α} as X-ray source.

^{11}B, ^{27}Al, ^{29}Si and ^{31}P MAS-NMR spectra were recorded at 18.8, 18.8, 9.4 and 9.4 T respectively with 4 mm probes at 12.5 kHz spinning speed, except for ^{29}Si for which a 7 mm probe at 5 kHz was used. The Larmor frequencies were 128.4, 104.2, 79.4 and 162.3 MHz for ^{11}B, ^{27}Al, ^{29}Si and ^{31}P, respectively. For ^{11}B, the pulse duration was 2 μs (π/6), and the recycle delay was 10 s. For ^{27}Al, the pulse duration was 1.5 μs (π/8), and the recycle delay was 2 s. For ^{29}Si, the pulse duration was 1.6 μs (π/5), and the recycle delay was 180 s. For ^{31}P, the pulse duration was 1.6 μs (π/6), and the recycle delay was 120 s. All relaxation delays were chosen long enough to enable relaxation at the field strength that was used. The ^{11}B chemical shifts are given relative to BPO_4 at 3.6 ppm, ^{27}Al chemical shifts are relative to $AlCl_3$ at 0 ppm, ^{29}Si chemical shifts are relative to tetramethylsilane (TMS) at 0 ppm, and ^{31}P are relative to 85% H_3PO_4 at 0 ppm.

For studying the adhesion/bonding, sealing with Crofer 22 alloy and Haynes metal was carried out at a maximum temperature of 1000°C employing the sandwich geometry. Microstructure near the interface was investigated using Cameca SX 100 electron probe microanalyser and wavelength dispersive analysis of X-Rays (WDAX) was carried out for determining element diffusion across the interface.

7.3. Results and discussion

The compositions investigated in ***Table 7.1*** yielded bubble-free and transparent glasses. The glasses turned yellow when V_2O_5 content was increased. XRD analysis of prepared glasses has shown the absence of any long range order. The base glasses were powdered and mean particle size of the glass powder used in subsequent investigations was less than 63 μm.

7.3.1. DTA/TMA

The thermo-physical properties of the glasses are listed in ***Table 7.2***. The glass transition temperature decreased from 610°C to 586°C when V_2O_5 was increased to 4 mol%. The TEC values of the glass samples were found around 12×10^{-6} °K^{-1}.

Table 7.2*.Thermo-physical properties of the glasses*

Sample	TEC (± $0.2x10^{-6}$ K^{-1})			Tg (± 2°C)	Tsoft (± 2°C)	Flow Temperature (± 3°C)
	As prepared	after 6h at 800°C	after 100h at 800°C			
BASPV0	12.2	12.2	12.4	610	654	1145
BASPV2	11.9	12.7	12.5	597	641	1107
BASPV4	12	12.6	12.1	586	638	1108

In glass and glass-ceramics, the thermo-physical properties depend on the composition and the formation of different crystalline phases within the glass matrix [3, 7]. TEC values of glasses were increased with the addition of V_2O_5. It has been reported that the P_2O_5 scavenges the modifier, hence the matrix viscosity increases. This results in an increase in thermo-physical properties [194,195]. In the glasses, P_2O_5 content was decreased while the V_2O_5 content increased. Thus, the more of the modifiers cations were available in glass. Increase of modifier oxide content is expected to decrease the connectivity of the network. Thus T_g values decreased. The thermo-physical properties are also dependent upon the various crystalline phase evolved during crystallization in glass samples. We observed that the TEC values do not change as the glass samples are heat treated at 800°C for upto 100 h. It implies the formation of the stable crystalline phases.

DTA plots of glass samples are shown in ***Fig. 7.1***. The sample BASPV0 showed an onset for crystallization (T_{cry}) at 720°C and two exotherms at 737°C and 805°C correspond to peak crystallization temperatures. The crystallization temperature (1st peak) was increased to 775°C with the addition of 2 mol % V_2O_5. However, the peak corresponding to crystallization (1st peak) temperature was observed at 755°C for sample BASPV4.

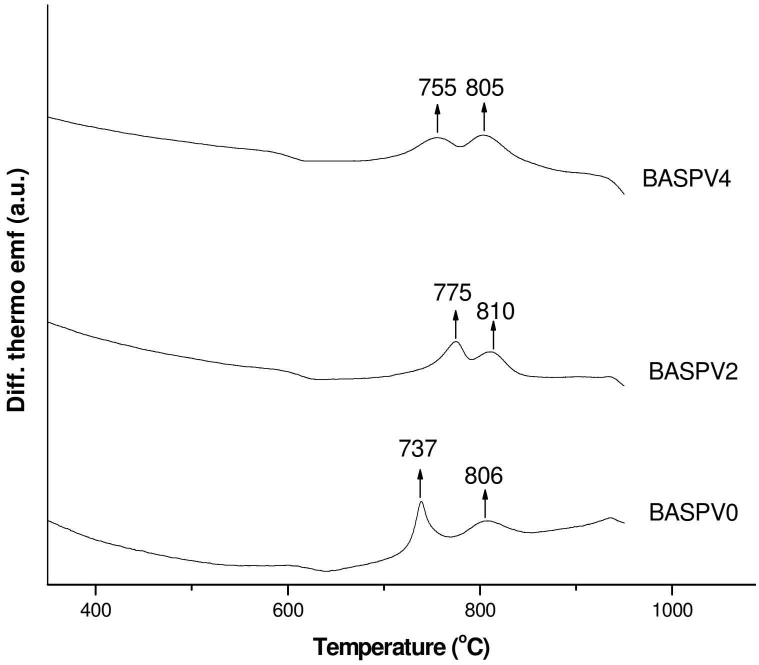

Fig. 7.1. *DTA plots of glass samples.*

The crystallization kinetics of the glasses was studied using Avrami, Kissinger and Augis-Bennett [217, 218] equations.

$$k = \nu \exp\left(\frac{-E}{RT}\right) \quad \textbf{(7.1)}$$

$$\ln\left(\frac{T_p^{\ 2}}{\alpha}\right) = \frac{E}{RT_p} + \ln\frac{E}{R} - \ln\nu \quad \textbf{(7.2)}$$

$$n = \frac{2.5}{\Delta T} \times \frac{RT_p^{\ 2}}{E} \quad \textbf{(7.3)}$$

Where *E* is the effective overall activation energy for the crystal transformation process, *υ* an effective frequency factor, which is a measure of the probability that a molecule having energy *E* participates in the transformation, *R* the gas constant, and *T*p the crystallization peak temperature. The crystallization peak maximum in the DTA scans corresponds to the temperature at which the rate of transformation of the viscous liquid into crystals becomes maximum.

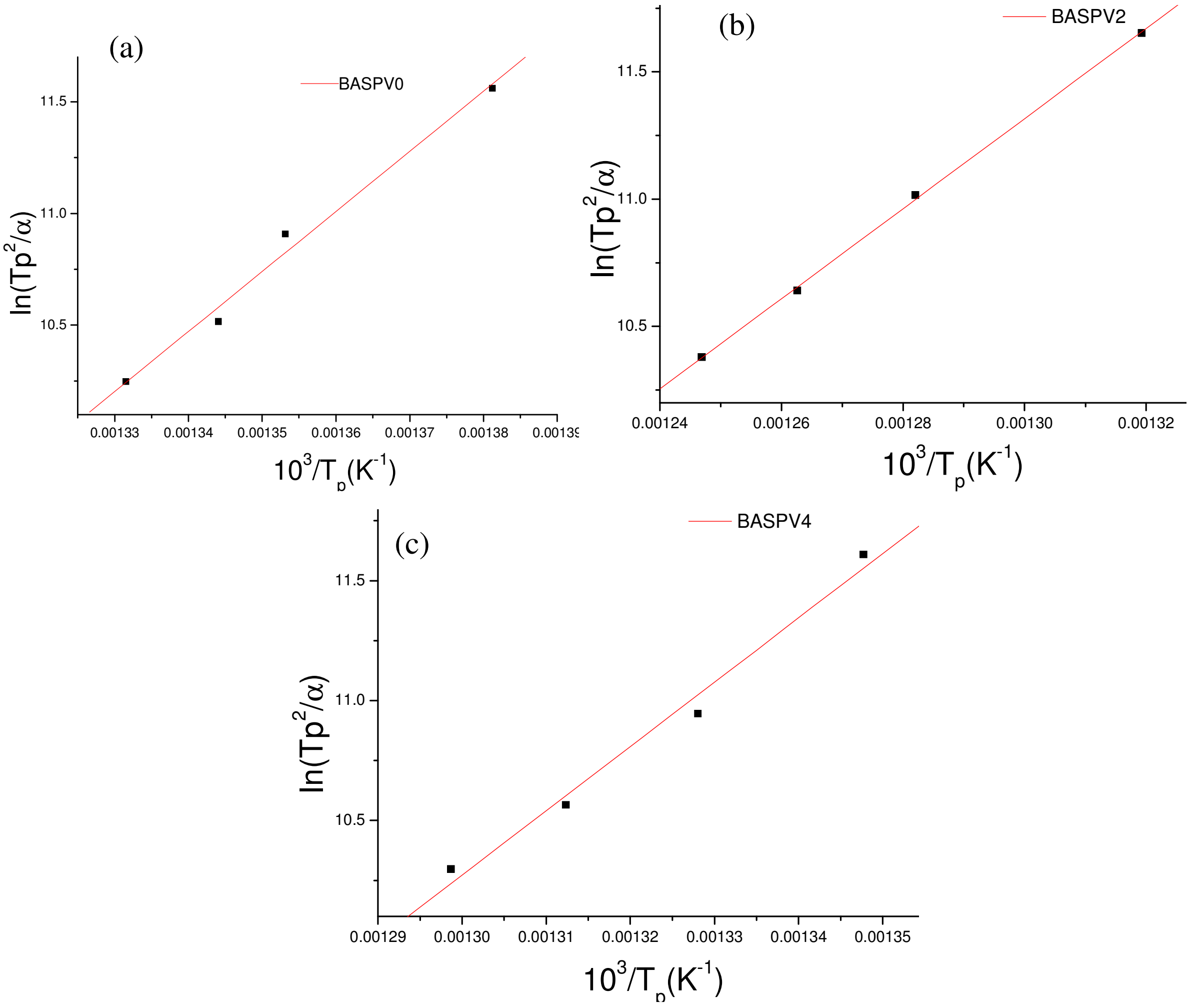

Fig. 7.2. *The plot of ln(T_p^2/α) versus 1/T_p for glasses, (a)BASPV0, (b)BASPV2 and (c) BASPV4.*

According to equation (7.2) a plot of ln(T_p^2/α) versus 1/T_p should be linear and slope of the straight line gives the activation energy for the crystallization. The plot of ln(T_p^2/α) versus 1/T_p is shown in ***Fig. 7.2a-c***. BASPV0 glass showed the activation energy of 224 kJ/mol. Activation energy for crystallization was decreased to 154 kJ/mol when vanadium oxide content was increased to 2 mol%. However, for sample BASPV4, this value increased to 225 kJ/mol.

7.3.2. Hot Stage Microscopy

The normalized areas of the glass samples as recorded with HSM are plotted as a function of temperature in ***Fig. 7.3***. The sintering temperature for all the glass samples was observed at 643°C, however the maximum shrinkage temperature (T_{shri}) decreasd from 764°C to 738°C when V_2O_5 content was increased from 0 to 4 mol%.

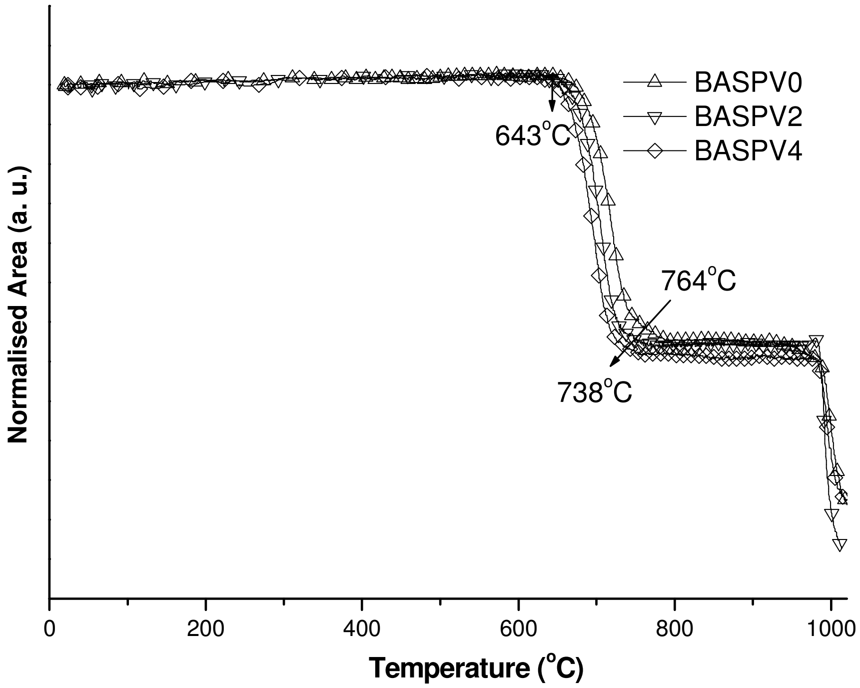

Fig. 7.3. *HSM plots of glass samples*

.

7.3.3. Structural studies

7.3.3.1. XRD

The appearance of different crystalline phases was observed for glass samples after heat treatment. XRD patterns of different glass samples after controlled heat treatment at 800°C for 100 h are depicted in ***Fig. 7.4***. The glass after heat treatment for 100 h showed the formation of $BaSiO_3$, $SrSiO_3$, $BaAl_2Si_2O_8$, $SrAl_2Si_2O_8$ and Sr_2SiO_4.

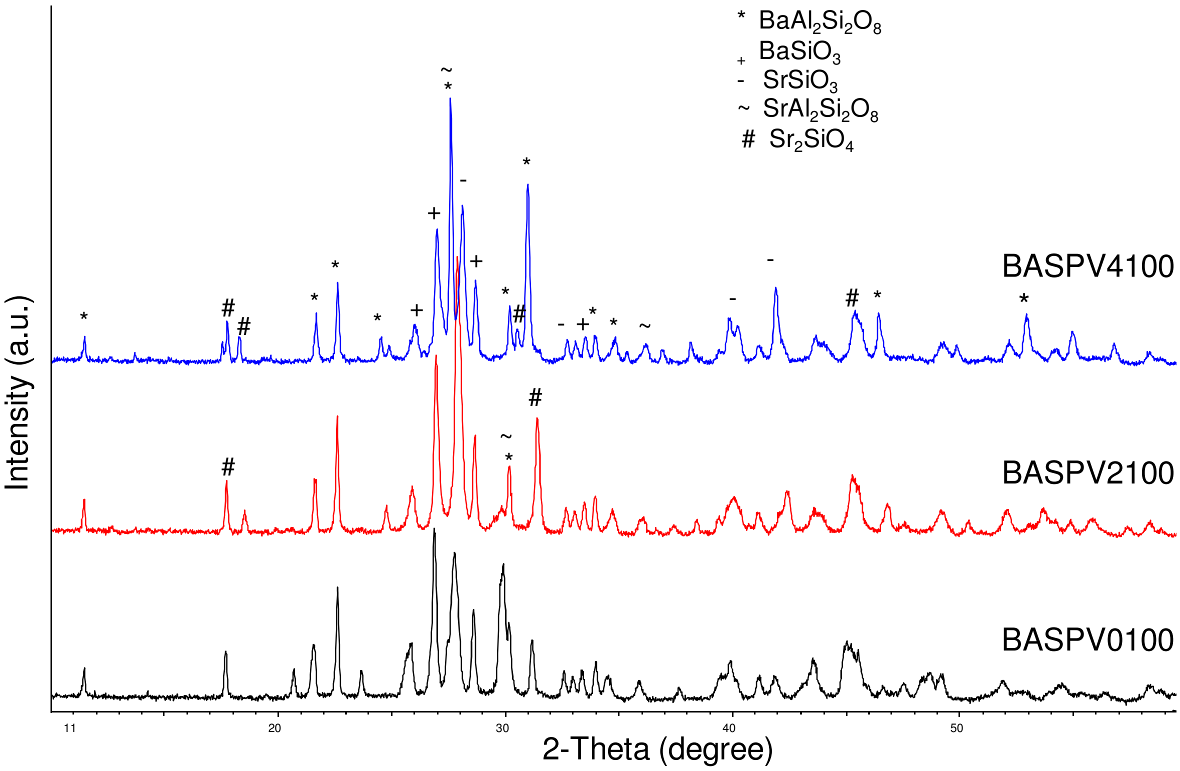

Fig. 7.4. *XRD plots of glass samples after heat treatment at 800°C for 100 h.*

7.3.3.2. MAS-NMR

7.3.3.2.1. ^{29}Si MAS-NMR

^{29}Si NMR spectra of the glasses are shown in ***Fig. 7.5***. NMR spectra exhibited broad absorption bands for all glass samples, which imply general disorder in structure of samples. Appearance of broad feature in the -70 to -90 ppm range revealed Q^2 contribution of Si in the glasses. In silicate glasses, substitution of Si by Al in Q_4 structural units results in a change in ^{29}Si chemical shift towards less negative values, which is also affected by the next-nearest-neighbour A1[197, 200]. Schmticker et al reported a negative shift with increasing $A1_2O_3$ content in aluminosilicate glasses [201]. This was interpreted in terms of a lower degree of network polymerisation as the concentration of network modifiers increased. Thus, the broad resonances observed in glass samples was attributed to the Q^3 and Q^2 structural units as reported in other aluminosilicate glasses [197-202].

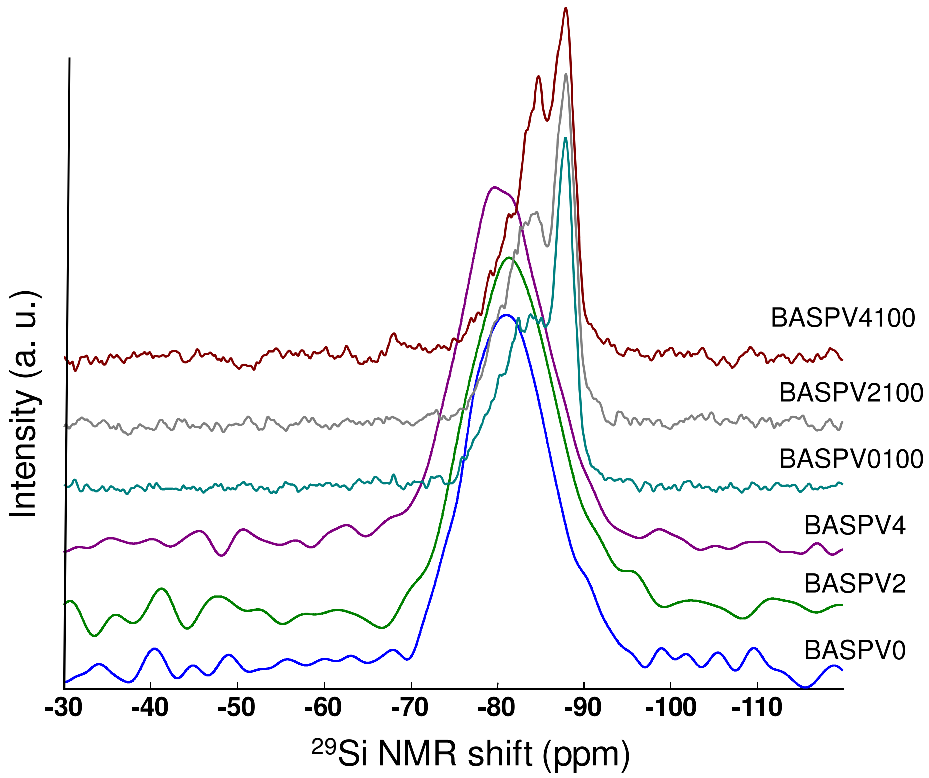

Fig. 7.5. ^{29}*Si MAS NMR spectra of different glass and glass-ceramics samples.*

However, NMR spectra of glass-ceramics samples showed sharp peaks as compared to that of the glass samples. The broad feature -70 to -90 ppm range as observed in glass samples demerged to give two resonances. The narrow resonance at -85 ppm is a characteristic of barium or strontium silicate. The other resonance at -88 ppm corresponds to the crystallization of Al and B containing alumino silicate phase $(Ba,Sr)Al_2Si_2O_8$.

7.3.3.2.2. ^{11}B MAS-NMR

^{11}B NMR spectra of the parent glasses are shown in ***Fig. 7.6***. The spectra consist of two resonances centered on 16 ppm and 1 ppm. The resonances can be assigned to BO_3 and BO_4 units respectively [204]. ^{11}B NMR spectra of glass-ceramics showed a presence of only one resonance peaks around at 16 ppm. These peaks became narrow indicating the formation of regular crystalline environments [201].

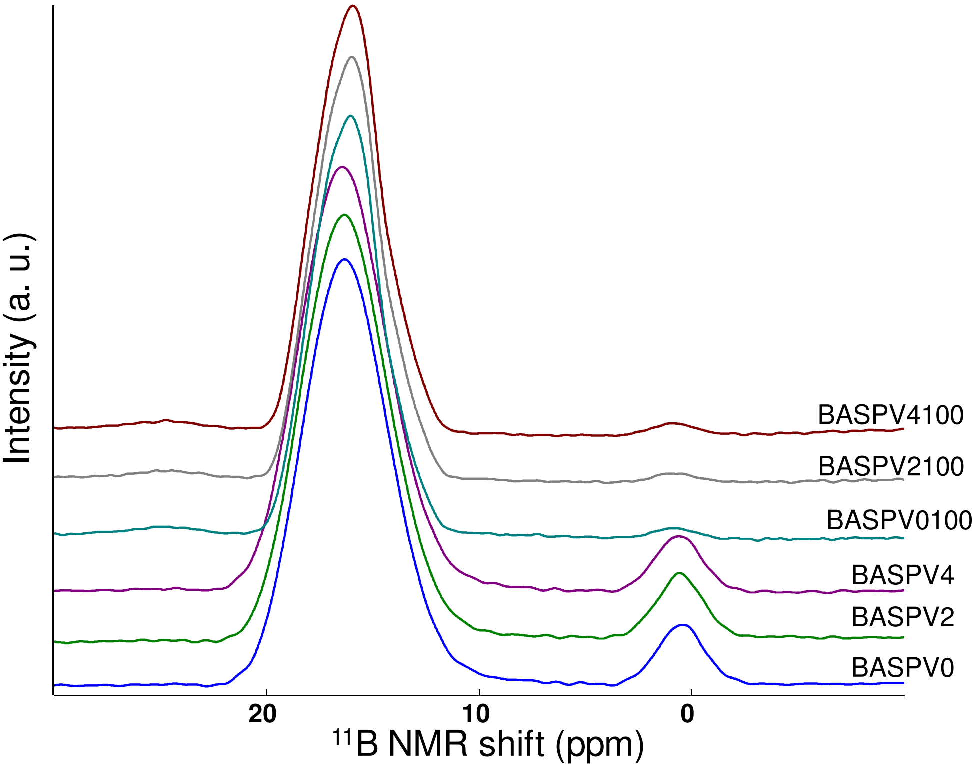

Fig. 7.6. *^{11}B MAS NMR spectra of different glass and glass-ceramics samples.*

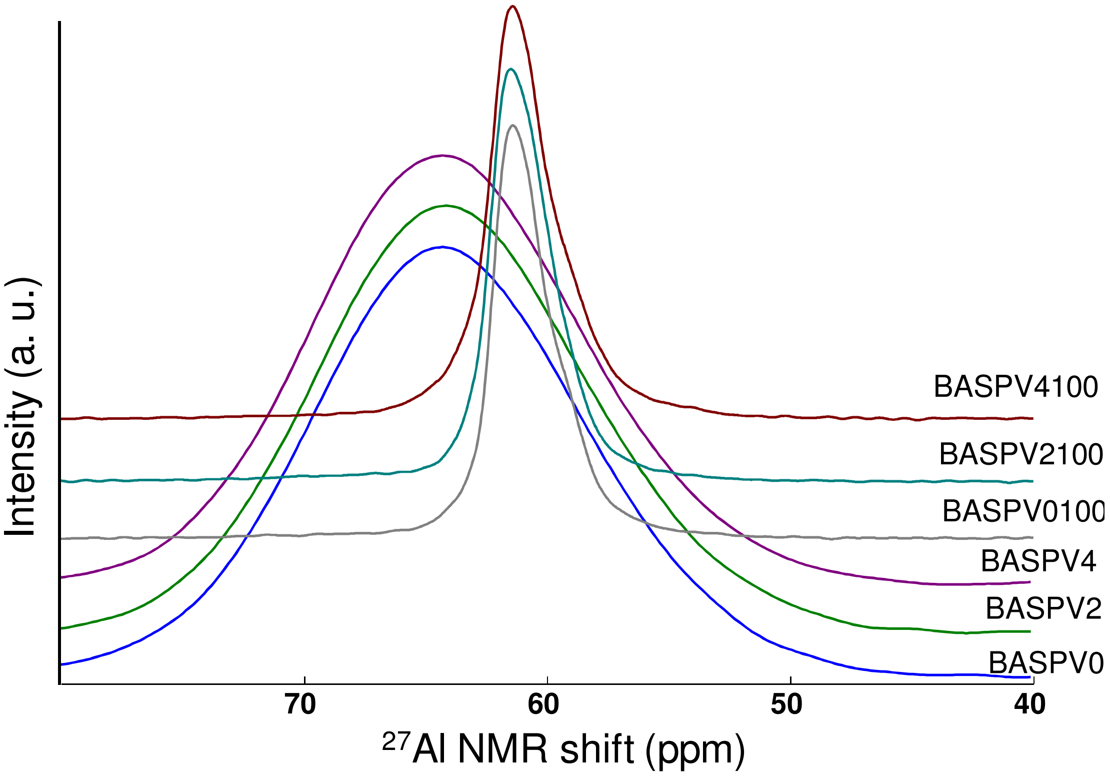

Fig. 7.7. *^{27}Al MAS NMR spectra of different glass and glass-ceramics samples.*

7.3.3.2.3. ^{27}Al MAS-NMR

^{27}Al NMR spectra for glasses and glass-ceramics are reported in ***Fig. 7.7***. A broad resonance centered at 65 ppm was observed, which is a characteristic of tetrahedral AlO_4 structural units [201, 208]. ^{27}Al NMR spectra of the glass-ceramics show a shift in resonance. In addition, the peaks have become sharp, indicating Al^{3+} ions were involved in the formation of crystalline phases. ^{29}Si chemical shifts of the compounds with Q_4(2A1) was reported earlier around - 85 to -90 ppm [200, 209], indicating the formation of (Ba,Sr,B)$Al_2Si_2O_8$ like phase.

7.3.3.2.4 . ^{31}P MAS-NMR

^{31}P NMR spectra of the glasses and glass-ceramics are shown in ***Fig. 7.8***. A main broad resonance was observed at ~ 3 ppm and assigned to Q^0 (orthophosphate units) [210].

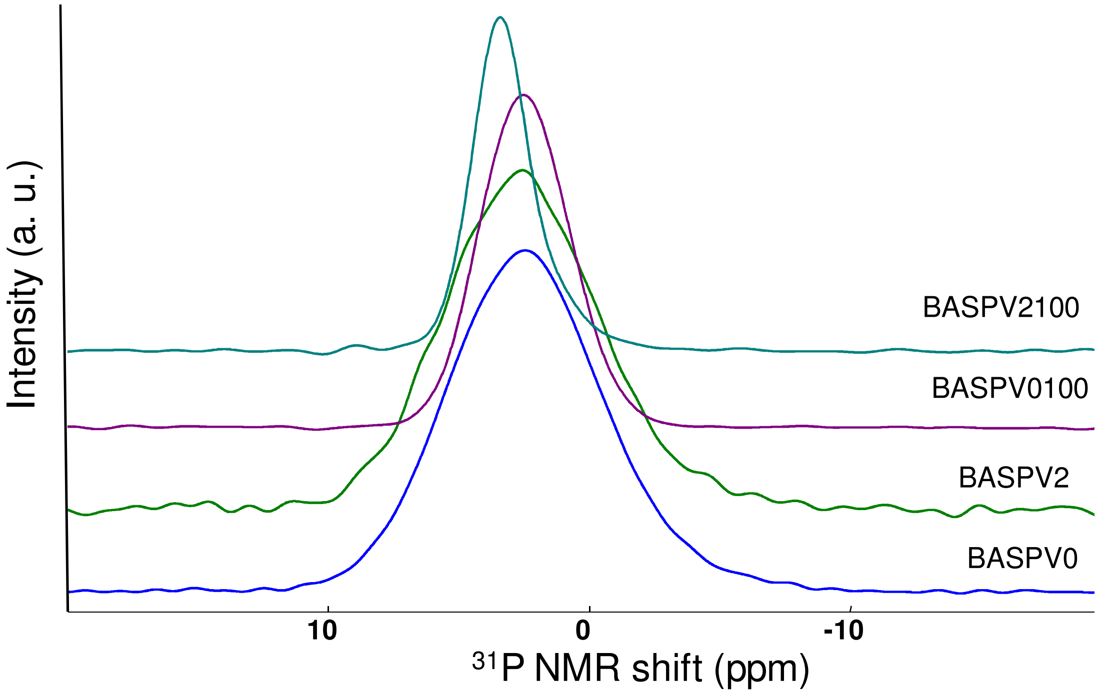

Fig. 7.8. *^{31}P MAS NMR spectra of different glass and glass-ceramics samples.*

Presence of a narrower peak in glass-ceramics around ~3 ppm implies the crystallization of $Ba_3(PO4)_2$ or $Sr_3(PO4)_2$ in glass-ceramics [211]. In addition, a reduction in the width of the resonances compared to glass samples was observed. This implies regular crystalline environment around P atoms.

7.3.3.2.5. ^{51}V MAS-NMR

^{51}V NMR spectra of the glasses and glass-ceramics are shown in ***Fig. 7.9***. A main broad resonance was observed at ~ 590 ppm and assigned to $Ba_2V_2O_7$ [200]. In glass-ceramics, presence of resonance peaks around ~ 605, 610 ppm implies the crystallization of $Ba_3(VO_4)_2$ or $Sr_3(VO_4)_2$ [200]. In addition, a reduction in the width of the resonances was observed due to crystalline environment around V atoms.

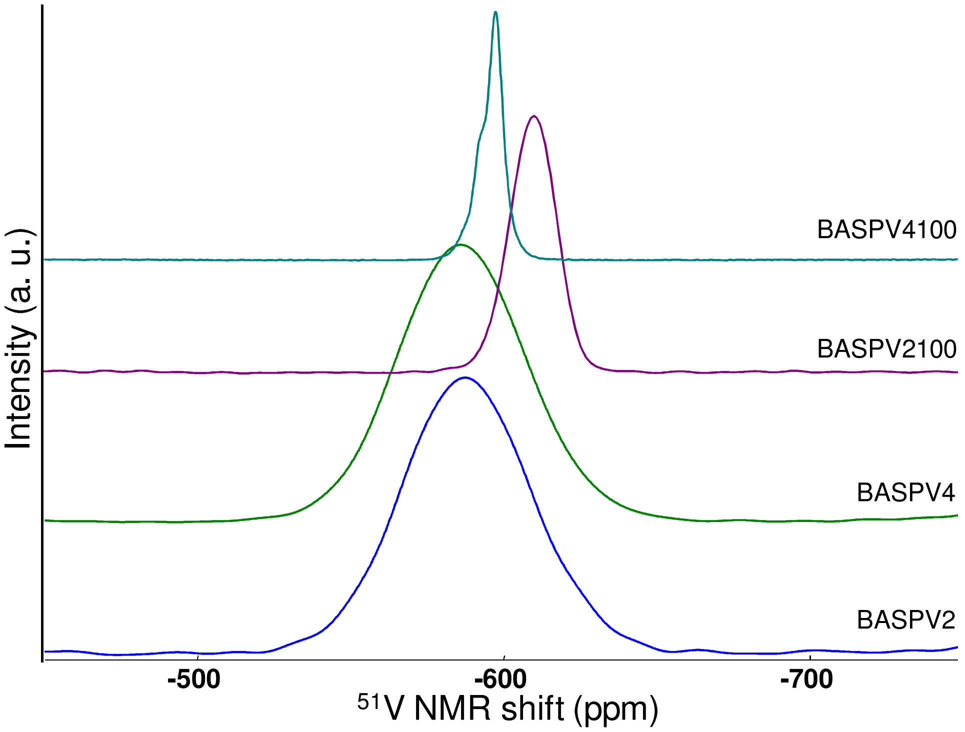

Fig. 7.9. *^{51}V MAS NMR spectra of different glass and glass-ceramics samples.*

7.3.4. Microstructure and chemical stability of seal

Figs. 7.10 (a-c) show the microstructures at interfaces of glasses with Crofer-22 interconnect. All the sealing glasses bonded well to the metallic part, as the sharp interfaces were observed. The microstructure of BASPV0 was composed of a few crystals. However, microstructures become more homogeneous with addition of V_2O_5. Microstructure of

BASPV2 was composed of bigger crystals, while BASPV4 showed microstructure with smaller crystals.

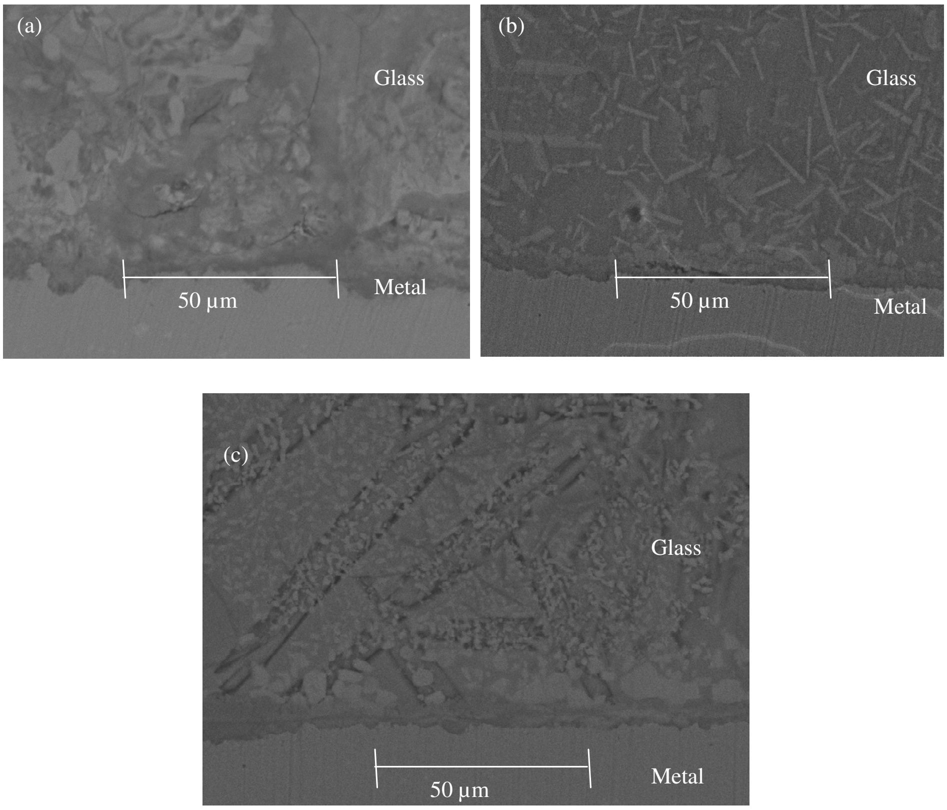

Fig. 7.10. *Microstructures at interfaces of glasses with Crofer-22 interconnect, (a) BASPV0, (b) BASPV2 and (c) BASPV4.*

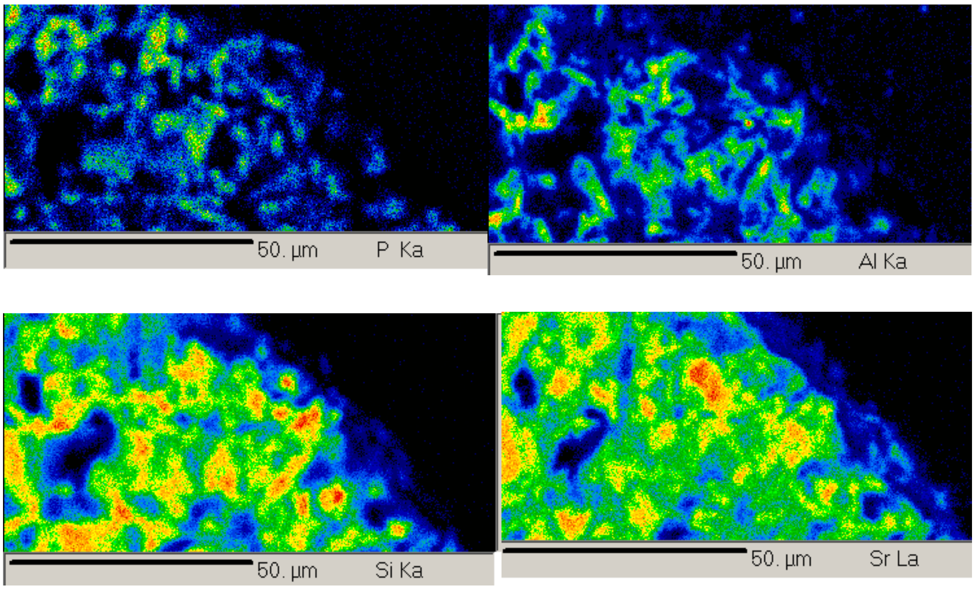

Fig. 7.11a. *Element mapping of the different elements near the interface of BASPV0 glass-metal interface.*

Element mapping of the different elements near the interface are shown in ***Fig. 7.11***. It revealed the presence of Ba and Sr uniformly in glass at the interface. From the mapping we concluded that these are some regions near the interface which have relatively higher Ba, Si and Al concentrations. In addition to this, elemental mapping of BASPV2 glass-metal interface also showed the involvement of the P and V. Fig 7.11b showed concurrent precipitation of P and V with Ba and Si. The enrichment of Cr at the interface of Crofer 22 alloy was observed, however, the diffusion of Cr in the glass was minimal (***Fig 7.12***).

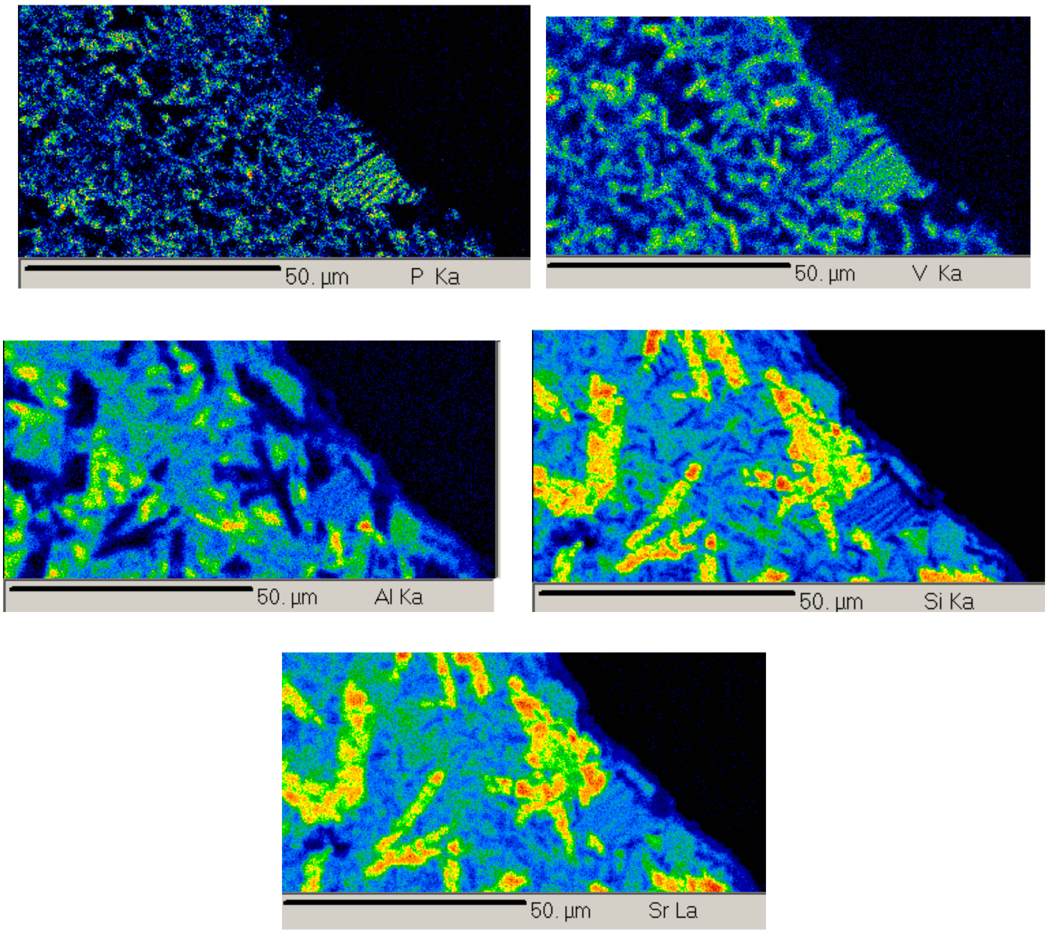

Fig. 7.11b. *Element mapping of the different elements near the interface of BASPV2 glass-metal interface.*

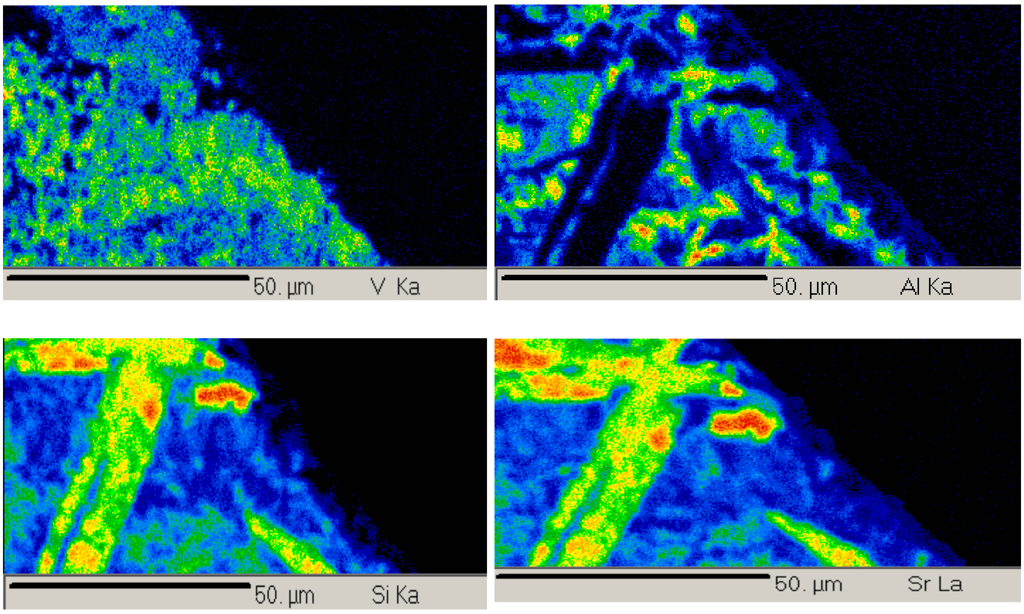

Fig. 7.11c. *Element mapping of the different elements near the interface of BASPV4 glass-metal interface.*

Vanadium may exist in the glass structure in V^{+3} or V^{+5} oxidation states, depending upon the composition and melting condition [219]. As a network former, the additional positive charge on V^{5+} as compared with neighbouring Si^{4+} ions may induce instability in the glass structure. In addition, V^{+5} ions having high ionic field strength value ($z/a^2 = 1.40$) exhibit a marked tendency for separation and promotes the occurrence of nuclei in the glass.

We had observed the formation of vanadium in V^{+5} oxidation states. V_2O_5 addition lowers the surface tension, i.e. smaller energy barrier for nucleation process, thus, facilitates the formation of nuclei. Therefore when V_2O_5 was added to glass, it resulted in the formation of $Ba_2V_2O_7$ nuclei. It is also reported that the effectiveness of V_2O_5 as a nucleating agent can be increased when used with some other nucleating agent [215, 216]. We had also seen activation energy for crystallisation was decreased for BASPV2 glass when both V_2O_5 and P_2O_5 were used in glass formulation, which can be attributed to synergic effect of V_2O_5 and P_2O_5 as nucleating agents.

EPMA images for Cr diffusion at the interface of metal-glass joints, after different time of heat treatment at 800°C are shown in ***Fig. 7.12***. The seals with Crofer showed good adhesion after long term heat treatment (1500 h) at 800°C. BaO containing glasses reported to interact with chromia-forming alloys forming BaCrO4 at the interface, which leads to the separation of GCs from the alloy matrix due to thermal expansion mismatch [183]. In the present investigation, though the Cr diffusion was observed across the interface but we did not observe separation of sealant from the metal even after 1500 h of heat treatment. However, Cr accumulation at the interfaces increases when seals interfaces were investigated after 1500 h.

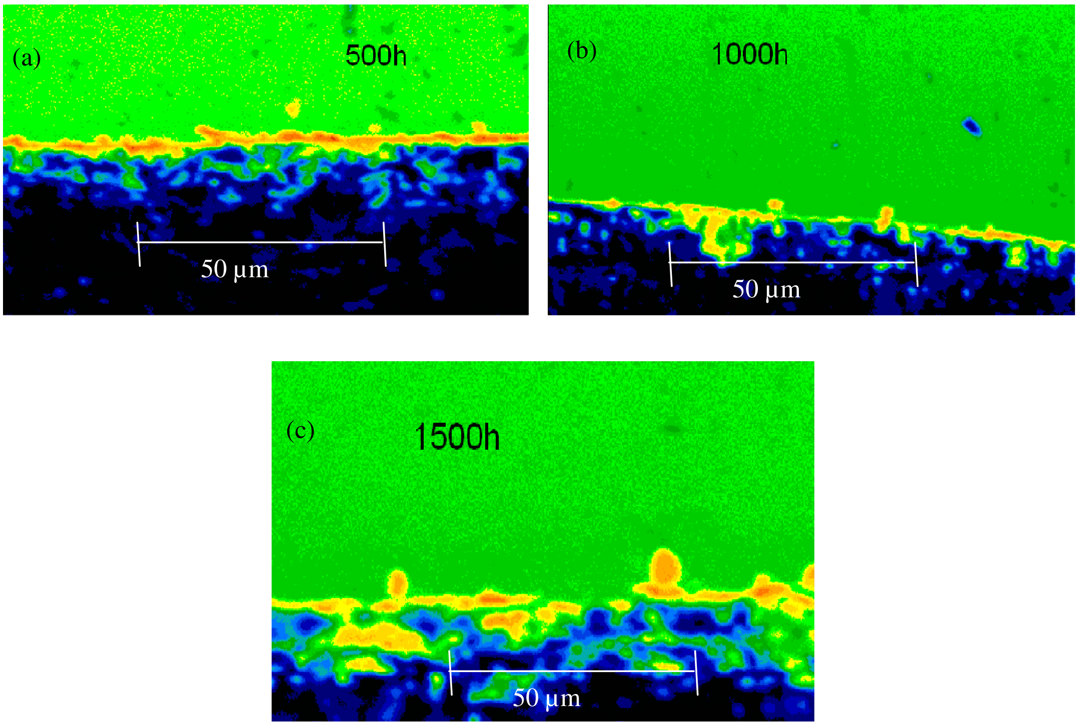

Fig. 7.12. *EPMA images of the interface of metal/glass joints, after different time of heat treatment at 800^{o}C.*

The seals were also made with innovative seal design using Haynes metal. The groove of about 3mmW and 0.5mm deep was made in Haynes metal and used for sealing (***Fig.7.13***). Seals were tested for hermeticity at high operating temperatures (800ºC) using pressure difference technique as described in chapter 2.

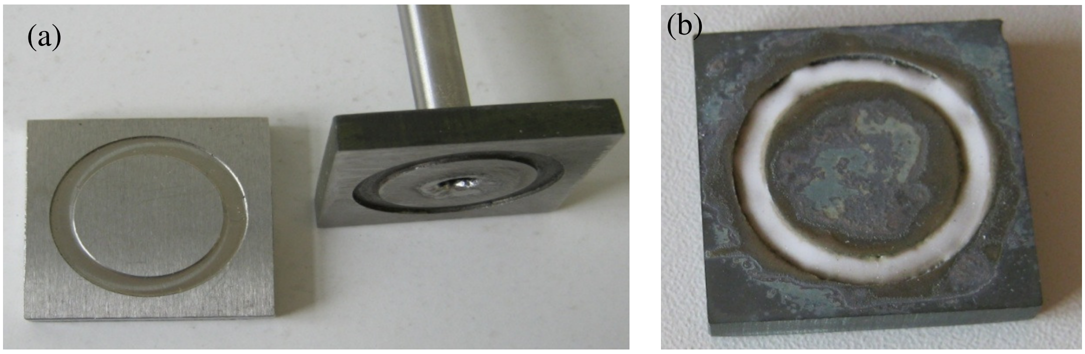

Fig. 7.13. *(a) Images of metal with special geometry used for sealing experiments and (b) Filling of groove with glass powder.*

The seals were pressurized with argon gas with a pressure of 200 mbar. The pressure was monitored by pressure gauges. The seals were found pressure tight. The seals were also subjected to different heating and cooling cycles and found hermetic after 15 heating and cooling cycles.

7.4 Conclusion

Barium alumino silicate glasses were studied for structural, thermo-physical and sealing properties. The glasses did not show major structural changes with addition of V_2O_5. However, softening temperatures of glasses were decreased with the increase of V_2O_5. Thermal expansion coefficient of the glass samples were found in the range of 12-13 $\times10^{-6}$ °K^{-1} which is close to that of Crofer-22. Development of $BaSiO_3$, $SrSiO_3$, $BaAl_2Si_2O_8$, $SrAl_2Si_2O_8$ and Sr_2SiO_4 crystalline phases upon heat treatment were observed. Seals with crofer-22 plates were made around 975°C and interface of seals revealed the inter-diffusion of ions at the interface. These seals had shown good bonding even after heat treatment at 800°C for 1500h. The seals were also made with Haynes metal with a groove of at the surface and tested for hermeticity at high operating temperatures (800ºC) using pressure difference technique. They were found hermetic after different thermal cycling, implying the good sealing capability of the material.

Chapter 8

Summary and future scope

The chapter summarizes the work carried out in the thesis and discusses the scope for further extension of the work reported here.

8.1. Summary

In the thesis, the preparation, thermo-physical, structural and microstructural properties of two different glass systems having different amount of P_2O_5 are studied. In addition, to demonstrate the applicability of these materials, specific properties related to bio and bonding behaviour are also investigated. The calcium phospho-silicate glass/glass-ceramics with different additives like iron oxide, ZnO and Ag are investigated as prospective bio-materials. Silicate glasses containing SrO and BaO with different modifiers are studied for bonding/sealing applications.

In conclusion, we have investigated a few alkaline earth based silicate glass/glass-ceramics having different amount of P_2O_5. The glass/glass-ceramics with nominal compositions $34SiO_2$-(45-x)CaO-$16P_2O_5$-4.5 MgO-$0.5CaF_2$ –xFe_2O_3 (x = 5, 10, 15, 20 wt %), $25SiO_2$-50CaO-$15P_2O_5$-(10-x)Fe_2O_3-xZnO (x = 0-5 mol %) and $25SiO_2$-(50-x)CaO-$15P_2O_5$-$8Fe_2O_3$-2ZnO-xAg (x = 0, 2 and 4 mol %) were studied. It was found that the addition of iron oxide and zinc oxide modifies the structural, microstructural properties. Iron oxide behaves as network modifier at low concentration and stabilizes the glass network at higher content. ZnO stabilizes the glass network when its content increases. Crystallization of glasses produced nanometer size crystallites of calcium phosphate, hematite and magnetite, which were evenly dispersed in the glassy silica matrix. In-vitro studies have shown the formation of bioactive layer after different time of immersion in SBF. The adhesion of polymer has been seen on the glass-ceramics when immersed in BSA, implying good biocompatibility. However, polymeric adhesion decreases with addition of ZnO. Antibacterial response of Ag containing glasses against with *Escherichia coli (E. coli)* was studied. The glass samples with 4 mol % Ag have shown effective antibacterial activity against *E. coli*. Magnetization also increased with increase in amount of Ag. This trend is attributed to the completion of magnetic ordering

In a novel idea, sealing glasses have been formulated by the combined addition of P_2O_5 and BaO [$Ba_3(PO_4)_2$] to a base glass composition (mol%) $30SiO_2$-20SrO-30BaO-$10B_2O_3$-$5La_2O_3$-$5Al_2O_3$, to avoid the negative effect of P_2O_5 on sealing properties of glass. The positive effect of $Ba_3(PO_4)_2$ incorporation on thermo-physical properties has been demonstrated by the decrease in softening temperature, enabling the seal fabrication (with Crofer-22APU) below 1000°C. Moreover, crystalline phases and TEC were found to be stable and compatible for sealing applications. The effects of P_2O_5 as a nucleating agent can be further corroborated in the presence of some other oxide such as V_2O_5. The effect of combined addition of P_2O_5 and V_2O_5 on glasses with nominal composition (mol%) $27SiO_2$-23SrO-32BaO-$4Al_2O_3$-$10B_2O_3$-(4-x) P_2O_5-xV_2O_5 was studied. The V_2O_5 and P_2O_5 were involved in the crystallization process. $BaSi_2O_5$, $BaAl_2Si_2O_8$, $Ba_{0.9}Sr_{0.1}Al_2Si_2O_8$ and Sr_2SiO_4 are observed as major crystalline phases. The addition of V_2O_5 has been found beneficial in glass formulation as the sealing temperature was reduced. The seals fabricated have shown good thermal and chemical stability when treated at long time at 800°C.

8.2. Future scope

In the thesis, an effort has been made to study the structural, thermo-physical, bio-related and sealing properties of glasses having different amount of P_2O_5. The results are co-related with structural changes resulted by incorporation of different additives. However, there is a need to investigate the structure of glasses with a variety of other structure sensitive techniques like high resolution EXAFS, as well as small angle X-ray and neutron scattering. MAS-NMR experiments like spin echo double resonance (SEDOR) and rotational echo double resonance (REDOR) are being proposed to investigate the structure and environment around next nearest neighbour of Si atom. In case of bio-glass/glass-ceramics, in-vitro experiments need to be further extended to cell culture. The work may be further pursued for in-vivo studies, to gauge the tissue response and material performance in a physiological environment. Sealant materials may be further tested in oxidizing and reducing environment. Insulating properties of glasses and glass-ceramics may be evaluated by measuring the electrical conductivity at elevated temperature. Further scope also exists in terms of interactions studies of sealant with other fuel cell components such as the anode, cathode and the interconnect material, especially over long term use. The glass sealant can be further tested after different thermal cycles. The work may further be pursued to prevent the damages that occur during thermal cycling by introducing the particles with self-healing characters like vanadium boride in a glass matrix.

References

[1] G. W. Morey, “The properties of glass”, Reinhold, New York, 1954.

[2] G. P. Kothiyal, Arvind Ananthanarayanan, G. K. Dey, Glass and Glass-ceramics, Functional Materials, 2012,323-386.

[3] J. E. Shelby, Introduction to Glass Science and Technology, Royal Society of Chemistry, Cambridge, 1997.

[4] L. Holland, The properties of glass surface, Wiley, New York, 1964.

[5] W. Lutze, R.C.Ewing, “Radioactive waste Forms for the Future”, North Holland, Amsterdam, (1988) 31.

[6] P. W. Macmillan, Glass–Ceramics, Academic Press, New York, 1977.

[7] W. D. Kingery, H. K. Bowen, D. R. Uhlmann, Introduction to Ceramics, Wiley, New York, 1976.

[8] S. D. Stookey, Glastech. Ber. Fifth International Congress on Glass,Verlag der Deutchen Glastechnischen Gesellshaft, Frankfurt am Main, (1959)1.

[9] K. Coroneos, “The complete guide to Corning ware and Vision Cookware”. Schiffer books for collectors, 2000.

[10] S. D Stookey, G. H. Beall, “Explorations in Glass: An Autobiography”, Wiley Blackwell, (2001).

[11] R. R. Tumala, J. Am. Ceram. Soc. 74 (2005) 895.

[12] K. L. Ngai, J. Non-Cryst. Solids 353 (2007) 709.

[13] W. H. Zachariasen, J. Am. Chem. Soc., 54 (1932) 3841.

[14] B. E. Warren, J. Am. Ceram. Soc. 24 (1941) 256.

[15] K. H. Sun, J. Am. Ceram. Soc. 30 (1948) 277.

[16] J. E. Stanworth, Phys. Chem. Glasses 20 (1979) 116.

[17] P. Boolchand, Series on Directions in Condensed Matter Physics-Vol 17, Insulating and Semiconducting glasses, World Scientific, Singapore, 2000.

[18] E. M. Levin, H. F. McMurdie, J. Am. Ceram. Soc. (1975) 513.

[19] R. Dupree, N. Ford, D. Holland, Phys. Chem. Glasses 28 (1987) 78.

[20] W. Poch, Glastech. Ber. 37 (1964) 533.

[21] M. Imaoka, Advances in Glass Technology, Plenum Press, New York, 1962.

[22] L. D. Pye, V. D. Frechette, C. G. Bergeron, N. J .Kreidl, Borate Glasses, Plenum Press, New York, (1978).

[23] M. E. Milberg, J. G. O. Kefe, R. A. Verhelst and H. O. Hopper, Phys. Chem. Glasses 13 (1972) 79.

[24] T. Abe, J. Am. Ceram. Soc. 35 (1952) 284.

[25] P. J. Vergano, D. R. Ulhmann, Phys. Chem. Glasses 11 (1970) 39.

[26] E. S. Shepherd, G. A. Rankin, F. E. Wright, J. Am. Sci. 28 (1909) 293.

[27] J. E. Stanworth, J. Soc. Glass Technol. 38 (1954) 425.

[28] E. P. Denton and H. Rawson, J. Soc. Glass Tech. 40 (1956) 252.

[29] Y. Dimitriev, I. Ivanova, E. Gatev, J. Non-Cryst. Solids 45 (1981) 297.

[30] A. Ghosh, B. K. Chaudhuri, J. Mater. Sci. 22 (1987) 2369.

[31] G. P. Kothiyal, Rakesh Kumar, Madhumita Goswami, D. Bhattacharya and M. Roy, J. Non-Cryst. Solids 353 (2007) 1337.

[32] E. B. Shand, Glass Engineering Handbook, second Edition, Mc-Graw Hill Book Company, INC, New York, 1958.

[33] W. Xia, J. Chang, J. Controlled Release 110 (2006) 522.

[34] A. Hoppe, N. S. Güldal, A. R. Boccaccini, Biomater. 32 (2011) 2757.

[35] J. Jones, L. Ehrenfried, P. Saravanapavan, L. Hench, J. Mater. Sci. Mater. Med. 17 (2006) 989.

[36] L. L. Hench, J. Mater. Sci. Mater. Med. 17 (2006) 967.

[37] Materials for Medical Engineering, Euromat Series, Wiley Interscience, 2000.

[38] P. Dost, S. Ellermann, N. N. Missfeldt, P. J. Leyden, K. Jahnke, J. Oto-Rhyno-Laryngology, Head and Neck Surgery 64(2002) 429.

[39] L. L. Hench, J. Am. Ceram. Soc. 74 (1991) 1487.

[40] J. Massera, S. Fagerlund, L. Hupa, M. Hupa, J. Am. Ceram. Soc. 95 (2012) 607.

[41] G. Goller, H. Demirkaran, F. N. Otkar, E. Demirkesen, Ceram. Int. *29* (2003)721.

[42] L. L. Hench and S. Best Biomaterials Science, An introduction to materials in medicine, 2nd Ed. Ratner, B., Hoffman, A.S., Schoen, F. J., Lemons, J. E., pp 154, Elsevier, 2004.

[43] T. Kokubo, M. Shigematsu, Y. Nagashima, M. Tashiro, T. Nakamura, T. Yamamuro, S. Higashi, Bull Inst Chem Res Kyoto Univ; 60 (1982) 260.

[44] J. M. Oliveira, R. N. Correia, M. H. Fernandes, Biomaterials 23 (2002) 371.

[45] Y. Ebisawa, T. Kokubo, K. Ohura, T. Yamamuro, J. Mater. Sci.: Mater. Med. 4 (1993) 225.

[46] A. Ito, H. Kawamura, M. Otsuka, M. Ikeuchi, H. Ohgushi, K. Ishikawa, Mater. Sci. Eng. C 22 (2002) 21.

[47] M. Yamaguchi, A. Igarashi, S. Ychiyama, J. Health Sci. 50 (2004) 75.

[48] S. B. Sohn, S. Y.Choi, G. H. Kim, H. S. Song, G. D. Kim, J. Non-Cryst. Solids 297 (2002) 103.

[49] M. J. Pascual, A. Guillet, A. Durán, J. Power Sources 169 (2007) 40.

[50] B. C. H. Steele, A. Heinzel, Nature 414 (2001) 345.

[51] S. P. S. Badwal, Solid State Ionics 143 (2001) 39.

[52] Y. S. Touloukian, Thermophysical Properties of High Temperature Solid Materials, Oxides and Their Solutions and Mixtures, The MacMillan Co., New York, NY, vol. 4, 1967.

[53] K. S. Weil, J. E. Deibler, J. S. Hardy, D. S. Kim, G. G. Xia, L. A. Chick, C. A. Coyle, J. Mater. Eng. Perf. 13 (2003) 316.

[54] N. H. Menzler, M. Bram, H. P. Buchkremer, D. Stoever, J. Eur. Ceram. Soc. 23 (2002) 445.

[55] N. P. Bansal, M. J. Hyatt, C.H. Drummond, Ceram. Eng. Sci. Proc. 12 (1991) 1222.

[56] I. W. Donald, J. Mater. Sci. 28 (1993) 2841.

[57] K. A. Nielsen, M. Solvang, F. W. Poulsen, P. H. Larsen, Ceram. Eng. Sci. Proc. 25 (2004) 309.

[58] A. Bieberle, L. J. Gauckler, NATO ASI Series Ser. E: Appl. Sci. 368 (2000) 389.

[59] K. L. Ley, M. Krumpelt, R. Kumar, J. H. Meiser, I. D. Bloom, J. Mater. Res. 11 (1996) 1489.

[60] C. Lara, M. J. Pascual, A. Duran, J. Non-Cryst. Solids 348 (2004) 149.

[61] N. Lahl, K. Singh, L. Singheiser, K. Hilpert, D. Bahadur, J. Mater. Sci. 35 (12) (2000) 3089.

[62] N. Lahl, D. Bahadur, K. Singh, L. Singheiser, K. Hilpert, J. Electrochem. Soc. 149 (5) (2002) A607.

[63] S. Ohara, K. Mukai, T. Fukui, Y. Sakaki, M. Hattori, Y. Esaki, J. Ceram. Soc. Japan 109 (2001) 186.

[64] Y. Sakaki, M. Hattori, Y. Esaki, Y. Ohara, T. Fukui, K. Kodera, Y. Kubo, Proc. Electrochem. Soc. (SOFC V) 97(1997) 652.

[65] C. Lara, M. J. Pascual, M. O. Prado, A. Dur´an, Solid State Ionics 170 (2004) 201.

[66] C. Lara, M. J. Pascual, A. Dur´an, J. Non-Cryst. Solids 348 (2004) 149.

[67] D. Bahadur, N. Lahl, K. Singh, L. Singheiser, K. Hilpert, J. Electrochem. Soc. 151(4) (2004) A558.

[68] S. B. Sohn, S.Y. Choi, G. H. Kim, H.S. Song, G. D. Kim, J. Non-Cryst. Solids 297 (2002) 103.

[69] K. L. Ley, M. Krumpelt, R. Kumar, J. H. Meiser, I. D. Bloom, J. Mater. Res. 11 (1996) 1489.

[70] S. B. Sohn, S. Y. Choi, G. H. Kim, H. S. Song, G. D. Kim, J. Am. Ceram. Soc. 87 (2004) 254.

[71] T. Schwickert, U. Reisgen, P. Geasee, R. Conradt, J. Adv. Mater. 35 (2003) 44.

[72] L. Esposito, A. Bellosi, Ceram. Eng. Sci. Proc. 23 (2002) 793.

[73] T. L. Wen, D. Wang, M. Chen, H. Tu, Z. Lu, Z.R. Zhang, H. Nie, Solid State Ionics 148 (2002) 513.

[74] R. E. Loehman, H. P. Dumm, H. Hofer, Ceram. Eng. Sci. Proc. 23 (2002) 699.

[75] J. W. Fergus, J. Power Sources 147 (2005) 46.

[76] P. H. Larsen, P. F. James, J. Mater. Sci. 33 (1998) 2499.

[77] P. H. Larsen, F. W. Poulsen, R. W. Berg, J. Non-Cryst. Solids.244 (1999) 16.

[78] R. K. Brow, D. R. Tallant, J. Non-Cryst. Solids, 222(1997)396.

[79] C. A. Lewinsohn, S. Elangovan, S M. Quist, Ceram. Eng. Sci. Proc. 25(2004) 315.

[80] C. A. Lewinsohn, S. Elangovan, Ceram. Eng. Sci. Proc. 24 (2003) 317.

[81] B. Vaidhyanathan, S. Murugavel, S. Asokan, K. J. Rao, J. Phys. Chem. B 101 (1997) 9717.

[82] D. S. Rao, P. P. Karat, Phys. Chem. Glasses 35 (1994) 124.

[83] C. N. Banwell, E. M. McCash, Fundamentals of Molecular Spectroscopy, 4th Edition, Tata McGraw-Hill publishers Ltd., New Delhi, 2000.

[84] G. Gouadec, P. Colomban, Prog. Cryst. Growth Charact. Mater. 53 (2007) 1.

[85] H. Eckert, Structural Characterization of Non crystalline solids and Glasses using Solid State NMR, progress in Nuclear Magnetic Resonance Spectroscopy, Eds: J. W. Emsley, J. Freeney, Pergamon press ltd., New York, (1992)159.

[86] E. R Andrew, A. Bradbury, R. G. Eades, Nature 183 (1959)1802.

[87] I. J. Lowe, Phys. Rev. Lett. 2 (1959) 285.

[88] L. L. Hench, R. J. Splinter, W. C. Allen, T. K. Greenlee, J. Biomed Mater. Res. Symp. 36 (1971)117.

[89] G. Heness and B. Ben-Nissan, Materials Forum 27 (2004) 104.

[90] S. M. Best, A. E. Porter, E. S. Thian, J. Huang, J. Eur. Ceram. Soc. 28 (2008) 1319.

[91] Materials for Medical Engineering, Euromat Series, Wiley Interscience, 2000.

[92] M. N. Rahaman, D. E. Day, B. S. Bal, Q. Fu, S. B. Jung, L. F. Bonewald, Acta Biomater.7 (2011) 2355.

[93] R. K. Singh, A. Srinivasan, App. Surf. Sci. 256 (2010) 1725.

[94] K. Sharma, A. Dixit, S. Bhattacharya, Jagannath, G. P. Kothiyal, App. Surf. Sci. 256 (2010) 3107.

[95] L. L. Hench, J. Am. Ceram. Soc. 81 (1998) 1705.

[96] E. A. Abou Neel, D. M. Pickup, S. P. Valappil, R. J. Newport, J. C. Knowles, J. Mater. Chem. 19 (2009) 690.

[97] Y. K. Lee, S. Y. Choi, J. Am. Ceram. Soc. 79 (1996) 992.

[98] K. Singh, D. Bahadur, J. Mater. Sci.: Mater. Med. 10 (1999) 481.

[99] R. K. Singh, G. P. Kothiyal, A. Srinivasan, J. Mag. Magn. Mater. 320 (2008) 1352.

[100] R. K. Singh, A. Srinivasan, G. P. Kothiyal, J. Mater. Sci.: Materials for Medicine 20 (2009) S147**.**

[101] P. Wust, B. Hildebrandt, G. Sreenivases, B. Rau, J. Gellermann, H. Reiss, R. Felix, P. M. Schlag, The Lancet Oncology 3 (2002) 487.

[102] T. Kokubo, Y. Ebisawa, Y. Sugimoto, M. Kiyama, K. Ohura, T. Yamamuro, M. Hiraoka, M. Abe, Bioceramics 5 (1992) 213.

[103] K. Ohura, M. Ikenaga, T. Nakamura, T. Yamamuro, Y. Ebisawa, T. Kokubo, Y. Kotoura, M. Oka, Bioceram. 3 (1992) 225.

[104] Y. Ebisawa, T. Kokubo, K. Ohura, T. Yamamuro, J. Mater Sci: Mater. Med. 4 (1993) 225.

[105] M. Ikenaga, K. Ohura, T. Yamamuro, Y. Kotoura, M. Oka, T.Kokubo, J. Orthop. Res. 11(1993) 849.

[106] K. Takegami, T. Sano, H. Wakabayashi, J. Sodona, T. Yamazaki, S. Morita, T. Shibuya, A. Uchida, J. Biomed. Mater. Res. 43 (1998) 210.

[107] Y. Ebisawa, F. Miyaji, T. Kokubo, K. Ohura, T. Nakamura, Biomater. 18 (1997)1277.

[108] S. L. Lin, C. S. Hwang, J. Non-Cryst. Solids 202 (1996) 61.

[109] J. T. Kohli, R. A. Condratr, J. E. Shelby, Phys. Chem. Glasses 34 (1993) 81.

[110] M. Handke, M. Sitarz, M. Rokita, E. Galuskin, J. Mol. Struct. 651 (2003) 39.

[111] T. Nishida, M. Suzuki, S. Kubuki, M. Katada, Y. Maeda, J. Non-Cryst. Solids 194 (1996) 23.

[112] B. P. McGrail, J. P. Icenhower, D. K. Shuh, P. Liu, J. G. Darab, D. R. Baer, S. Thevuthasen, V. Shutthananandan, M. H. Engelhard, C. H. Booth, P. Nachimuthu, J. Non-Cryst. Solids. 296 (2001) 10.

[113] Y. Miura, H. Kusano, T. Nanba, S. Matsumoto, J. Non-Cryst. Solids. 290 (2001) 1.

[114] J. Serra, P. Gonzalez , S. Liste , C. Serra , S. Chiussi , B. Leon , M. P. Amora, H.O. Ylanenc, M. Hupa, J. Non-Cryst. Solids 332 (2003) 20.

[115] D. Cullity, Introduction to Magnetic Materials, Addison-Wesley, Reading, 1972.

[116] D. M. Darby, Am. Minerals. 70 (1985) 304.

[117] X. Fang, C. S. Ray, A. M. Milanokovic, D. E. Day. J. Non-Cryst. Solids 283 (2001) 162.

[118] C. Ederer, N. A. Spaldin, Nature Mat. 3 (2004) 849.

[119] J. D. Sitter, C. Dauwe, E. D. Grave, A. Govaert, Solid State Commun. 18 (1976) 645.

[120] T. Kokubo, J. Non-Cryst. Solids 120 (1990) 138.

[121] C.Y. Kim, A. E. Clark, L.L. Hench, J. Non-Cryst. Solids 113 (1989) 195.

[122] S. B. Cho, K. Nakanishi, T. Kokubo, N. Soga, C. Ohtsuki, T. Nakamura, Biomed. Mater. Res. 33 (1996) 145.

[123] M. R. Filgueiras, G. La Torre, L. L. Hench, J. Biomed. Mater. Res. 27 (1993) 445.

[124] L. L. Hench, D. E. Clark, J. Non-Cryst. Solids 28 (1978) 83.

[125] R. W. Douglas, T. M. El-Shamy, J. Am. Ceram. Soc. 50 (1967) 1.

[126] C. M. Jantzen, Mat. Res. Soc. 125 (1988) 143.

[127] P. Li, C. Ohtsuki, T. Kokubo, K. Nakanishi, N. Soga, T. Nakamura, T. Yamamuro, J. Mater. Sci. Mater. Med. 4 (1993) 127.

[128] S. Kitaka, J. Collid. Interf. Sci. 48 (1974) 327.

[129] A. A. Jara, S. Goldberg, M. L. Mora, J. Collid. Interf. Sci. 292 (2005) 160.

[130] W. Xue, A. Bandyopadhyay, S. Bose, Acta Biomater. 5 (2009) 1686.

[131] K. Sharma, Sher Singh, C. L. Prajapat, S. Bhattacharya, Jagannath, M. R. Singh, S. M. Yusuf, G. P. Kothiyal, J. Magn. Magn. Mater. 321 (2009) 3821.

[132] R. K. Singh, A. Srinivasan, App. Surf. Sci., 256 (2010) 1725.

[133] A. Balamurugan, G. Balossier, S. Kannan, J. Michel, A. H. S. Rebrlo, J. M. F. Ferreira, Acta. Biomater. 3 (2007) 255.

[134] R. K. Singh, A. Srinivasan, Mater. Sci. Eng. C 30 (2010) 1100.

[135] T. Kokubo, H. Takadama, Biomater. 27 (2006) 2907.

[136] D. L. Leslie-Pelecky, R. D. Ricke, Chem. Mater. 8 (1996) 1770.

[137] M. E. Hilo, K. O. Grady, R. W. Chantrell, J. Magn. Magn. Mater. 114 (1992) 295.

[138] X. Jiao, D. Chen, Y. Hu, Mater. Res. Bull. 37 (2002) 1583.

[139] C. Cannas, G. Concas, D. Gatteeschi, A. Falqui, A. Musinu, G. Piccaluga, C. Sangregorio, G. Spano, J. Phys. Chem. 3 (2001) 832.

[140] Z. Mao, D. Chen , Z. He, J. Magn. Magn. Mater. 320 (2008) 2335.

[141] M. F. Hansen, C. Bender Koch, S. Mørup, Phys. Rev. B 62 (2000) 1124.

[142] F. Bødker, M.F. Hansen, C. Bender Koch, S. Mørup, J. Magn. Magn. Mater. 221 (2000) 32.

[143] M. Porto, Eur. Phys. 45 (2005) 369.

[144] D. Kechrakos, K. N. Trohidou, Phys. Rev. B 58 (1997).

[145] L. Suber, P. Imperatori, G. Ausanio, F. Fabbri, H. Hofmeister, J. Phys. Chem. B 109 (2005) 7103.

[146] G. Lusvardi, D. Zaffe , L. Menabue , C. Bertoldi , G. Malavasi , U. Consolo, Acta Biomater. 5 (2009) 419.

[147] T. Kitsugi, T. Yamamuro, T. Nakamura, M. Oka, Biomater. 16 (1995) 1101.

[148] M. Hartmann, Chem. Mater. 17 (2005) 4577.

[149] S. K. Parida, S. Dash, S. Patel, B. K. Mishra, Adv. Colloid. Inter. Sci. 121 (2006) 77.

[150] N. B. Colthup, L. H. Daly, S. E. Wiberley, Introduction to Infrared and Raman Spectroscopy, Academic Press, London, 1990.

[151] K. Sharma, S. Bhattacharya, C. Murali, G. P. Kothiyal, App. Surf. Sci. 258 (2012) 2356.

[152] W. C. Xue, X. Y. Liu, X. B. Zheng, C. X. Ding, Biomater. 26 (2005) 3455.

[153] K. Sharma, M. N Deo, G. P Kothiyal, J. Non-Cryst. Solids 358 (2012) 1886.

[154] J. Kora, R. Manjusha, J. Arunachalam, Mate. Sci. and Eng. C 29 (2009) 2104.

[155] S. Purushotham, R.V. Ramanujan, Acta Biomater. 6 (2010) 502.

[156] A. K. Gupta, M. Gupta, Biomater. 26(2005) 3995.

[157] K. Sharma, A. Dixit, Sher Singh, C. L. Prajapat, S. Bhattacharya, Jagannath, M. R. Singh, S. M. Yusuf, P. K. Sharma, A. K. Tyagi, G. P. Kothiyal, Mate. Sci. and Eng. C 29 (2009) 2226.

[158] A. Dupraz, T. P. Nguyen, M. Richard, Biomater. 20 (1999) 663.

[159] H. L. Su , C. C. Chou , D. J. Hung, S. H. Lin, I. C. Pao, J. H. Lin, F. L. Huang, R. X. Dong, J. J. Lin, Biomater. 30 (2009) 5979.

[160] K. M. Hindi, A. J. Ditto , M. J Panzer, D. A. Medvetz, C. E. Hovis, J. K. Hilliard, J. B. Taylor, Y. H. Yun, C. L. Cannon, W. L. Youngs, Biomater. 30 (2009) 3771.

[161] W. Ghandour, J. H. Hubbard, J. Deistung, M. N. Hughes, R. K. Poole, Appl. Microbiol. Biotechnol. 28 (1998) 559.

[162] J. A. Johnson, C. E. Johnson, J. Phys: Condens Matter 17(2005) 381.

[163] E. A. Neel, I. Ahmed, J. Pratten, S. N. Nazhat, J. C. Knoles, Biomater. 26 (2005) 2247.

[164] J. Husheng, H. Wensheng, W. Liqiao, X. Bingshe, L. Xuguang, Dental Mater. 2 4 (2008) 244.

[165] B. D. Cullity, Elements of X-ray Diffraction, Addison-Wesley, Reading, 1978.

[166] Z. X. Tang, S. Nafis, M. C. Sorensen, J. Magn. Magn. Mater. 31(1983) 896.

[167] S. Mitra, S. Das, K. Mandal, S. Chaudhuri, Nanotechnology 18 (2007) 1.

[168] H. L. Sun, H. T. Shi, F. Zhao, L. M. Qi, S. Gao, Chem. Commun. 34 (2005) 4339.

[169] K. K. Sahu, C. Rath, N. C. Mishra, S. Anand, R. P. Das, J. Colloid Interf. Sci. 185 (1997) 402.

[170] S. A. M. A. Hameed, A. M. El Kaady, J. Adv. Res.doi 10.1016 j. jare2011.07.001.

[171] J. Noguésa, J. Sorta, V. Langlaisb, V. Skumryeva, S. Suriñachb, J. S. Muñozb, M. D. Barób, Phys. Reports 422 (2005) 65.

[172] M. F. Hansen, S. Morup, J. Magn. Magn. Mater. 203 (1999) 214.

[173] S. Kamali, T. Ericsson, R.Wappling, The Solid Films 515 (2006) 721.

[174] J. Wanga, H. Y. Wua, C. Q. Yanga, Y. L. Lina, Mate. Charact. 59 (2008) 1716.

[175] H. N. Ok, M. S. Han, J. Appl. Phys. 44 (1973) 1931.

[176] J. G. dos, S. Duque, M. A. Macedo, N. O. Moreno, J. L. Lopez, H. D. Phanes, J. Magn. Magn. Mater. 226 (2001) 1424.

[177] S. Music, I. Czako-Nagy, I. Salaj-Obelic, N. Ljubesic, Mater. Lett. 32 (1997) 301.

[178] C. Fransden, S. Morup, Phys. Rev. Lett. 94 (2005) 027202.

[179] R. L. Davies, S. F. Etris, Catal. Today (1997) 36.

[180] V. S. Kumar, B. M. Nagaraja,V. Shashikala, A. H. Padamshri, S. S. Madhavendra, B. D. Raju, K. S. Rama Rao, J. Mol. Cata. A: Chem. 223 (2004) 313.

[181] I. Sondi, B. S. Sondi, J. Colloid. Interf. Sci. 275 (2004) 177.

[182] M. Brochu, B. D. Gauntt, R. Shah, G. Miyake, R. E. Loehman, J. Eur. Ceram. Soc. 26 (2006) 3307.

[183] P. Batfalsky, A. A. C. Haanappel, J. Malzbender, N. H. Menzler, V. Shemel, I. C. Vinke, J. Power Sources 155 (2006) 128.

[184] Z. Yang, G. Xia, K. D Meinhardt, K. S. Weil, J. W. Stevenson, J. Mater. Eng. Perform. 13 (2004) 327.

[185] M. K. Mahapatra, K. Lu, Mater. Sci. Eng. R. 67 (2010) 65.

[186] Z. Yang, K. D. Meinhard, J. W. Stevenson, J. Electrochem. Soc. 150 (2003) A1095.

[187] S. Ghosh, A. D. Sharma, P. Kundu, S. Mahanty, R. N. Basu, J. Non-Cryst. Solids 354 (2008) 4081.

[188] V. A. C.Haanappel , V. Shemet, C. I. Vinke, W. J. Quadakkers, J. Power Sources 141 (2005) 102.

[189] B. Tiwari, A. Dixit, G. P. Kothiyal, Int. J. Hydrogen Energy 36 (2011) 15002.

[190] P. K. Ojha, S. K. Rath, T. K. Chongdar, N. M. Gokhale, A. R. Kulkarni, J. Power Sources 196 (2011) 4594.

[191] S. F. Wang, C. M. Lu, Y.C. Wu, Y. C. Yang, T. W. Chiu, Int. J. Hydrogen Energy 36 (2011) 3666.

[192] P. H. Larsen, F. W. Poulsen, R.W. Berg, J. Non-Cryst. Solids 244 (1999) 16.

[193] I. W. Donald, B. L. Metcalfe, L. A. Gerrard, J. Am. Ceram. Soc. 91 (2008) 715.

[194] A. Ananthanarayanan, G. P. Kothiyal, L. Montagne , G. Tricot, B. Revel, Mater. Chem. Phy.130 (2011) 880.

[195] H. Grussaute, L. Montagne, G. Palavit, Glastechnische Berichte Glass Sci. Technol. 73 (2000) 380.

[196] A. R. Boccaccini, B. Hamann, J. Mater. Sci. 34(1999) 5419.

[197] M. Goswami, G. P. Kothiyal, L. Montagne, L. Delevoye, J. Solid State Chem. 181 (2008) 269.

[198] A. Goel, D. U. Tulyaganov, M. J. Pascual, E. R. Shaaban, F. Munoz, Z. Lu, J. M. F. Ferreira, J. Non-Cryst. Solids 356 (2010) 1070.

[199] R. Martens, W. Muller-Warmuth, J. Non-Cryst. Solids 265 (2000) 167.

[200] K. J. D. Mackenzie, M. E. Smith, Multinuclear Solid-State NMR of Inorganic Materials, Pergamon, London, 2001.

[201] K. J. D. MacKenzie, T. Kemmitt, Thermochimica Acta 325 (1999) 5.

[202] J. B. Murdoch, J. F. Stebbins, I. S. E. Carmichael, Am. Mineral 70 (1985) 332.

[203] H. Grussaute, L. Montagne, G. Palavit, J. L. Bernard, J. Non-Cryst. Solids 263 (2000) 312.

[204] A. Ananthanarayanan, G. P. Kothiyal, L. Montagne, B. Revel, J. Solid State Chem. 183 (2010) 120.

[205] A. Stamboulis, R. G. Hill, R.V. Law, J. Non-Cryst. Solids 333(2004)101.

[206] K. T. Lee, B. P. Aswath, Mater. Sci. Eng. A 352 (2003) 1.

[207] A. Ananthanarayanan, G. P. Kothiyal, L. Montagne, B. Revel, J. Solid State Chem.183 (2010) 1416.

[208] B. C. Bunker, R. J. Kirkpatrick, R. K. Brow, G. L. Turner, C. Nelson, J. Am. Ceram. Soc. 74 (2005) 1430.

[209] J. F. Stebbins, S. Kroecker, S.K. Lee, T. J. Kiczenski, J. Non-Cryst. Solids 275(2000) 2425.

[210] A. R. Grimer, U. Haubenreisser, Chem. Phys. Lett. 99 (1983) 487.

[211] G. L. Turner, K. A. Smith, R. J. Kircpatrick, E. Oldfield, J. Magn. Reson. 70 (1986) 408.

[212] I. L. Mudrakovskii, V. P. Shmachkova, N. S. Kotsarenko, V. M. Mastikhin, J. Phys. Chem. Solids 47 (1986) 335.

[213] K. Sharma, G. P. Kothiyal, L. Montagne, F. Mayer, B. Revel, Int. J. Hydrogen Energy 37 (2012) 11360.

[214] A. M. Ferrari, C. Leonelli, G. C, Pellacani, C. Siligardi, J. Non-Cryst. Solids 315 (2003) 77.

[215] P. Alizadeh, V. K. Marghussian, J. Eur. Ceram. Society 20 (2000) 775.

[216] V. K. Marghussian, U. Balazadegan, B. Eftekhari-yekta, J. Eur. Ceram. Society 29 (2009) 39.

[217] M. Avrami, J. Chem. Phys. 7 (1939) 1103.

[218] N. P. Bansal, R. H. Doremus, J. Thermal Anal. 29 (1984)115.

[219] M. B.Volf, Chemical Approach to Glass, Elsevier, New York, 1984, 326.